A NOVEL CONTROLLER FOR SWITCHED RELUCTANCE MOTOR

Thesis

Submitted in partial fulfillment of the requirements for the degree of

DOCTOR OF PHILOSOPHY

by

ABDUL AHAD SHAIK

(03221019A)

DEPARTMENT OF
ELECTRICAL AND ELECTRONICS ENGINEERING
NATIONAL INSTITUTE OF TECHNOLOGY KARNATAKA
SURATHKAL, MANGALORE – 575025
May, 2013

DECLARATION

I hereby *declare* that the Research Thesis entitled "**A NOVEL CONTROLLER FOR SWITCHED RELUCTANCE MOTOR**" which is being submitted to the **National Institute of Technology Karnataka, Surathkal** in partial fulfillment of the requirements for the award of the Degree of **Doctor of Philosophy** in Electrical and Electronics Engineering is a *bonafide report of the research work carried out by me*. The material contained in this research thesis has not been submitted to any University or Institution for the award of any degree.

03221019A, Abdul Ahad Shaik

……

(Register Number, Name & Signature of the Research Scholar)

Department of Electrical and Electronics Engineering

Place: NITK, Surathkal
Date:

C E R T I F I C A T E

This is to *certify* that Research Thesis entitled "**A NOVEL CONTROLLER FOR SWITCHED RELUCTANCE MOTORS**" submitted by Abdul Ahad Shaik (Register Number: 03221019A) as the record of the research work carried out by him is *accepted as the Research Thesis submission* in partial fulfillment of the requirements for the award of **Doctor of Philosophy.**

Dr. Udaykumar R.Y
Research Guide
(Name and Signature
with Date and Seal

Chairman - DRPC
(Signature with Date and Seal)

Dedicated to...

MY BELOVED GRANDFATHER

Late Mr. SHAIK MASTAN ASHRAFI

.

ACKNOWLEDGEMENT

I would like to express my gratitude to all those who made it possible for me to complete this thesis.

I wish to express my whole hearted gratitude to the Management, Secretary ***Dr. Saqib Rasool Khan***, Nimra Educational Society, Hyderabad for granting me permission to pursue doctoral studies.

I am deeply indebted to my research supervisor Dr.Udaykumar R.Yeragatti, Professor, Department of Electrical and Electronics Engineering, NITK, Surathkal. He has always encouraged me to pursue my ideas, offered innumerable creative insights and guided me with unmatched wisdom. His stimulating suggestions and back-up helped me throughout the research work and writing of this thesis. It would not have been possible for me to complete this thesis within a short time without his encouragement, guidance and cooperation.

I would like to convey thanks to Director, National Institute of Technology, Surathkal and Prof. K. P. Vittal , Head of Electrical and Electronics Engineering Department for their support and encouragement during this research.

I am very thankful to thank members of Research Progress Assessment Committee, Late Prof. P. Durai Kannu, Dr. Debashish Jena and Dr A.C. Hedge for their support, guidance and helpful suggestions. Their guidance has served me well and I owe them my heartfelt appreciation.

It is indeed my pleasure to thank Prof. H. S. Y. Shastri, Department of Electrical and Electronics Engineering, NITK, Surathkal for his suggestions and guidance during my course of study at NITK.

I am profoundly grateful to all the teaching staff of the Department of Electrical and Electronics Engineering for providing me required facilities and constant encouragement and co-operation during my research work.

My thanks are due to Mr.Nagaraj Bhat, Foreman, Mr. Mahalinga Nayak, Foreman and all the non-teaching staff of the Department of Electrical and Electronics Engineering, NITK for their co-operation and support during my research and stay at NITK.

I am indeed indebted a lot to my dearest friend for her untiring and constant support without which my research work couldn't have been possible. Her consistent motivation throughout indeed is a source of inspiration for me in completing my research work.

My sincere thanks to all my colleagues other friends, my students who have extended their support from time to time in completing my thesis , and particularly who helped me in preparing my presentation slides with all animation , I am thankful to them from my bottom of my heart.

It wouldn't have been able to complete my thesis successfully if I hadn't had the support and the best wishes from my mother, father, sisters and brother during my research work, I owe a lot to them for having taken a lot of hardship, financial constraint and sacrifice throughout to enable me to carry out my education.

Finally, I thank Almighty God for Blessing me with Good health, Ability to work hard, un-wilting patience and guiding me at every step of my life.

Abdul Ahad Shaik

Abstract

Electrical drives are playing an important role in modern industries. In the last two decades an electrical drive named the Switched Reluctance Motor (SRM) drive is receiving considerable attention from industry in adjustable speed drives since it is characterized by robust construction, high operation reliability and efficiency. The successful application of SRM in automobiles depends on the proper motor design and overall cost of the drive which includes converter and controller costs. However, there have been inadequate design experience for SRM's as compared with more mature BLDC motors and induction motors, and applications are limited so far due to complex design procedure. Therefore, it is necessary to develop a set of design procedures for SRMs. Although the design principles of SRMs are available in different literatures; there is no clear idea in the basic design procedure. These procedures require extensive prior knowledge and experience in designing. The procedure outlined in this thesis requires only basic dimension data for SRM's. The empirical formulas are used for basic design and since it is difficult to accurately incorporate the saturation effect and the detailed geometrical information in the empirical formulas, the FEM was used for fine-tuning and validating the design. For dynamic behaviour of a SRM and for controller and converter design, the knowledge of the magnetization curves is very essential. Therefore this thesis discusses how the magnetic characteristics of SRMs are obtained by experimental, analytic and FEM. Thereafter a new method of finding the motor winding inductance at different rotor position using 3D FEM is carried out to validate the results as obtained by experimental method. The SRM drive consists of a power converter section that sequentially connects the motor phases independently and a control section that processes rotor position information form a position sensor and generates the phase excitation pulses. A new method to estimate the initial rotor position of the SRM at stand still and during running condition is proposed without the need of magnetisation curves. A pair of position sensors is used to detect the rotor positions and the output signals of the sensors are used as the basic triggering pulses for main switches. The proposed method was implemented by the simple microcontroller based systems. A known sensorless method of finding the rotor position is used to validate the correctness of the proposed method. The proposed method is implemented with the 8/6,1 kW,12000 RPM 8/6 SRM. The experimental results shows that the proposed rotor estimation technique provides good accuracy at different operating conditions

Keywords: *Design, split DC converter, position sensor, FEM, SRM, Novel controller.*

Table of Contents

Table of Contents

Table of Contents

Table of Contents

Table of Contents

List of Figures

List of Symbols

Symbol	Parameter(s)	Units
θ	Mechanical angular displacement or rotor position	Degrees
β_s	Stator pole arc	Degrees
β_r	Rotor pole arc	Degrees
N_s	Number of stator poles	
N_r	Number of rotor poles	
L_k	Inductance	Henry
$\frac{\partial L_k}{\partial \theta}$	Changing rate of self inductance with respect to rotor position	Henry/Degrees
$\frac{\partial L_k}{\partial i_k}$	Changing rate of self inductance with respect to phase current	Henry/Amperes
V_{dc}	DC Link Voltage	Volts
$\emptyset$	Magnetic flux	Webers
μ	Magnetic permeability	Henry/meter
Θ_{el},Θ_{mech}	Rotor position angle	Electrical & Magnetic degrees
Θ_{on}, Θ_{off}	Turn – on and Turn – off angle	Degrees
σ_a	Aligned saturation factor	
ω	Angular frequency	Radians/sec
A_s	Specific electric loading	Ampere.Cond/m
D	Bore diameter respectively inner stator diameter	mm
D_{sh}	Shaft diameter	mm
D_r, D_0	Rotor and stator outer diameter	mm
h_r, h_s	Height of the rotor and stator poles	mm
L_a, L_u	Aligned (maximum) and unaligned (minimum) phase inductance	Henry
l	Rotor length	mm
l_{eff}	Effective core length	mm
m	Number of simultaneously conducting phases	
mmf	Magnetomotive force	AmpereTurns
n	Rotor speed	RPM

List of Symbols

N, N_{ph}	Number of turns per pole; Number of turns per phase	
P_{Conv}	Converter losses	Watts
$\mathfrak{R}$	Reluctance	AT/Wb
t	Time	Sec
h_c	Stator Coil length	m

List of Tables

Chapter 1 Introduction

This chapter deals with general information about Switched Reluctance Motors, the history, literature review ,scope of thesis and the organization of thesis.

1.1 General

The Switched Reluctance Motor (SRM) drives have recently gained considerable attention among researchers due to several reasons. Firstly, stator can be easily manufactured as the stator windings are concentrated around the salient stator poles. Also the salient rotor poles are made up of steel laminations, without conductors or permanent magnets or cage. Due to this rotor structure, extremely high speed can be obtained as compared to rotors with magnets or windings. Secondly, the motor is cost-effective in comparison to conventional induction and synchronous motors, and also it is claimed to have a comparable or even higher efficiency over wide range of speed. Thirdly, due to unidirectional current requirement, the converter has a minimum number of switching devices compared to a conventional inverter-fed synchronous or induction motor drive and thereby greatly simplifying the design of power and control circuit. The other advantages include possible operations in high temperatures or in intense temperature variations. Also a high starting torque can be achieved without large inrush currents and the torque produced is independent of current direction. Therefore SRM is promising as an easy-to-manufacture, low priced, variable speed motor due to its very simple structure with reduced cost and the mechanical simplicity together with the recent advances in the power electronics components.

But, besides the above unique features and advantages, switched reluctance motor has certain disadvantages too. Some of these are acoustic noise and torque ripples, caused by a combination of the non-linear coupling between phase current, rotor position, overlap angle and proper machine design. These ripples are also responsible for part of the motor's noise problem. Improper machine design is also responsible for poor performance of the motor with respect to torque ripples. There are some more disadvantages associated with the control of the SRM. Rotor position is needed for excitation control. The rotor position information is essential for determining the switching instants for proper control of speed, torque, torque pulsations and controlling circuit design. A shaft position transducer is usually employed to

determine the rotor position. In inexpensive systems, the rotor position sensor consists of a magnetized ring with Hall Effect sensors or opto-interrupters with slotted disk that produce discrete signals with no information between the pulses. In more expensive systems, a large number of pulses per revolution can be obtained from a resolver or optical encoder. Alternatively, a large number of pulses can be obtained by phase-locking a high frequency oscillation to the pulses of discrete position sensors. Systems with such high resolution can work well down to the zero speed. However, these sensors add complexity and cost to the system. Moreover, electromagnetic interference and temperature effects tend to reduce the reliability of the system. In order to avoid these difficulties, some forms of indirect position sensing schemes are proposed in the past. The position sensing techniques depend on a number of factors and they have their own disadvantages. The recent research literature on SRM concerns the following major aspects: SR machine design and construction. SRM requires a complex controller on account of its non-linear characteristics. Accurate position sensing is required to achieve high performance for converter and controller circuit design. The work reported in this thesis addresses some of these aspects.

1.2 History of SRM

The concept of the Switched Reluctance Machine is actually very old, going back to the 19th century inventions called electromagnetic engines which were the forerunners of modern stepper motors. The switched reluctance motor is basically a stepper motor and has had many applications as both rotary and linear steppers. The idea of using the SR configuration in a continuous mode (on contrast to a stepper mode) with power semiconductor control is due primarily to (S.A. Nasar 1996; Lawrenson 1983). Previously, only thyristor power semiconductors were available for the relatively high-current, high-voltage type of control needed for SR machines. But the effective and efficient operation of SR machines has only recently been possible with the advancement of power electronic devices. With the falling prices of devices and its increasing popularity, switched reluctance is beginning to create a foothold in industry. In order to understand the operation of a SR machine, we can look at its name. The machine operates on the tendency for its rotor to move to a position where the reluctance is minimized. SR motors also go by another name i.e., Electronically Commutated Machines.

Chapter 1 Introduction

Till the publication (1989) of Millers' book on 'Brushless Permanent-Magnet and Reluctance Motor Drives', all the materials concerned related to SR motors were scattered in different conference proceedings and various journals. Miller gave a brief introduction of the different aspects of the motor and its controller in the book. The second book authored by Miller (1993) explains all the features of SR motor drive in more detail. This book depicts the qualitative aspects of SR motor in a very judicious manner without exaggerating the facts. Besides the potential of SR motor drives, the limitations are also well covered and that gives a good insight to a researcher about the state-of-the-art of this motor.

After the publication of Miller's book, a lot more work has been done on the various aspects of SR motor, like design, modeling, control, position/shaft sensor less operations, torque ripple minimization, acoustic noise reduction ,etc.

1.3 Review of literature

A number of studies have been published recently on switched reluctance motors (SRMs), as they are simple in construction and economical in comparison to synchronous and induction motors. This research has studied the various aspects of SRM like design for various applications including automobile applications etc., determination of performance parameters, magnetic characteristics like flux linkage characteristics, static torque characteristics and the analysis and design of the drive circuit. The present section provides a review of previous contributions and attempts made by several researchers working in the field of SRM drive. It addresses the basic approaches and techniques developed.

1.3.1 Significance of Machine Design and flux-linkage characteristics

The very nature of the machine demands that the development of the switched reluctance motor drives requires the design of the machine and control to go hand in hand unlike any other machine. While Lawrenson, P.J. et al.(1980) stands out in the development of the concepts of the machine as well as the fundamentals of control, the paper by Krishnan et al. (1988), stands out in the development of a design procedure from an analytical stand point because it helps equate the design of the machine to the design of other machines in terms of machine dimensions. There are a number of papers that heavily rely on the process of design solely based on finite element analysis. But as this work will demonstrate, the design of the machine is

rooted in the analytical relationships that govern the machine with finite element analysis being a tool for verification. Finite element analysis of switched reluctance machines had been described in detail first in (Arumugam et al.1985) and subsequently in a number of different papers. The design of the machine as described here is a step by step design process by applying the basic principles of electromagnetics; the other literatures on design are in (J.W. Finch et al. 1984; A. R .Miles et al. 1988; Arthur V. Radun et al.1995). An important requirement in control is flux linkage characteristic. The deeply saturated; doubly salient iron structure of the switched reluctance motor presents difficulties in developing an analytical method for predicting the flux linkage at different rotor positions. The flux-linkage being a rotor position and stator excitation dependent quantity, merely considering its values for the fully aligned and unaligned conditions of the stator and rotor poles for calculating the torque developed by the motor, will lead to erratic results. A simple analytical method for computing minimum and maximum inductances which is valid for realistic saturation is shown (Corda and Stephenson et al. 1979). This work was then extended (Krishnan et al. 2003) to include not only extreme, but also intermediate rotor positions. Methods for calculation of the fully aligned and unaligned inductances and flux linkages have been reported in the literature (Sharma et al.1999**).** An experimental set up for flux linkage determination has been reported in the literature (V. Ramanarayanan et al. 1996).

1.3.2 An Initial Rotor Position Estimation Method for SRM

The rotor position information is essential in SRM in order to generate the phase excitation pulses for optimum control of the motor. Typically mechanical devices such as opto interrupters with a slotted disc have been used to determine the shaft position, whereas isolated current sensors like current transformers or Hall Effect sensors have been used for current sensing (B. K. Bose et al.1986; T. J. E. Miller et al. 1988). However, due to poor resolution in the above techniques, resolvers or encoders are used to derive the shaft position in more sophisticated drives. But the use of these devices may lead to reliability problems in harsh environments or may become an important part of the overall drive system cost. Also, they increase the overall physical envelope of the motor. The difficulty in using these devices in many applications and the additional cost involved have led to the research in developing

indirect rotor position sensing schemes. Several indirect rotor position sensing schemes have also been proposed in the past. Papers on several techniques in this field have been published. (Lang, et al.1990) proposed state observers to determine the rotor position of the SRM. These observers, however, were very complicated to implement.

Another way to obtain the position information is to detect the phase current waveform and determine the position by calculating the phase inductance value from the changing rate of the phase current (Harris, W. D. et al.1990; MacMinn, S. R.et al. 1992). This method, however, requires injection of a diagnostic pulse to an inactive phase. This diagnostic pulse generates negative torque and reduces the performance of the drive system. Some researchers have used different approaches to estimate the rotor position of the SRM. (Ehsani, et al.1992; Ramani, K. R.et al.1996) proposed a linear inductance to time period converter in order to estimate the shaft position. Though this approach is good and direct, a modulated circuit is required. The modulated circuit is difficult to realize and easily polluted by the pulse width modulated (PWM) switching voltage as well. A sensorless method has been proposed by measuring a mutually induced voltage of an inactive phase of the SRM (Husain, I. et al. 1994). This is an effective way to estimate the shaft position of the SRM because it provides a clear relationship between the induced voltage and the rotor position. This method unfortunately has some disadvantages too. First, this method requires the design of a sample and hold circuit which is controlled by a synchronizing signal. The signal has to be synchronized with the PWM signals of the converter to detect whether the energized winding is operated in a conduction mode or in a free-wheeling mode. The circuit, therefore, is difficult to implement. Second, after the sample and hold circuit, the mutually induced voltage is related to the current command, the stator resistance, the mutual inductance, the self-inductance, and the rotor speed of the SRM. The proposed sensorless method in (Husain, I. et al.1994), therefore, has some limitations. For example, in a low speed control range, a three-dimensional table is required even under the assumption that the speed-dependent terms are negligible. The saturation effect of the SRM, which reduces the self and mutual inductances, is not considered. In addition, the proposed method can only be applied in a low speed range because the speed-dependent terms enlarge the estimated

position error as the motor speed is increased. There are other techniques, the waveform detection techniques (P. P. Acarnley et al.1985; Panda et al.1991), model-based estimator techniques (Lumsdaine et al.1990; Husain et al.1994), the flux/current method (Lyons et al. 1991) etc. The modulation encoding techniques of rotor position detection are based on extracting the periodically varying phase inductance in an encoded form by applying a high frequency carrier signal. The flux sensing method of is based on applying diagnostic pulses to an idle phase and integrating the voltage across the phase to obtain the phase flux. The method to estimate the initial rotor position of the SRM at the standstill condition using the machine parameter and by the simple microcontroller based system without the knowledge of magnetization curves has been reported in the literature (P. Jitkreeyarn et al.2007).

1.3.3 Conclusions

Hence, literature review reveals that today there are a number of different control schemes. It cannot be claimed that one particular motor design and controller is suitable for all types of applications. The position sensing techniques depend on a number of factors such as, the type of motor, the type of application, the type of converter used and the control strategy. The passive waveform detection techniques are well suited for low-cost, low-speed applications, but may not be suitable for high-resolution, high-performance drives. For high–resolution position sensing, computations become intensive and a signal processor becomes essential. This increases the cost of position sensing. Observer based methods and flux/current methods are examples of schemes that could be used for high-resolution position sensing. These methods are also suitable for position sensing at high-speeds, but high speed computational requirements tend to increase the cost of these types of indirect sensors even more. In this direction the study of designing a new in-expensive controller to find the rotor position is of interest in this thesis.

1.4 SCOPE OF THE THESIS

This thesis addresses some of these important issues associated with SRM. In spite of the mechanical and electrical simplicity offered by SRM, the design procedure is difficult due to salient pole structures of stator and rotor. The successful application of SRM in automobiles depends on the proper design of the motor and overall cost of the drive which includes converter and controller. However, there have been inadequate

design experience for SRM's as compared with more mature BLDC motors and induction motors, and applications are limited so far due to complex design procedure. Therefore, it is necessary to develop a set of design procedures for SRMs. Although the design principles of SRMs are available in different literatures; there is no clear idea in the basic design procedure. These procedures require extensive prior knowledge and experience in designing. The procedure outlined in this thesis requires only basic dimension data for SRM's. The empirical formulas are used for basic design and since it is difficult to accurately incorporate the saturation effect and the detailed geometrical information in the empirical formulas, the FEM was used for fine-tuning and validating the design. For dynamic behaviour of a SRM and for controller and converter design, the knowledge of the magnetization curves is very essential. Therefore this thesis discusses how the magnetic characteristics of SRMs are obtained by experimental, analytic and FEM. Thereafter a new method of finding the motor winding inductance at different rotor position using 3D FEM is carried out to validate the results as obtained by experimental method. The SRM drive consists of a power converter section that sequentially connects the motor phases independently and a control section that processes rotor position information form a position sensor and generates the phase excitation pulses. A new method to estimate the initial rotor position of the SRM at stand still and during running condition is proposed without the need of magnetisation curves. This method of determining the rotor position avoids complex circuitry, motor characteristics, huge mechanical mounting and technical computations. Also this thesis propose the design of a novel low cost controller circuit, which can be used for most of SRM topologies in a wide power and speed range and for several converter topologies.

A micro controller based platform is used for realizing the controller. A split-capacitor type of power converter is used with the state-of-the-art IGBT devices. The proposed controller is tested on a 1 kW, 4 phase, 8/6 pole SRM.

1.4.1 The objectives of the thesis are

In context to the questions discussed above the objectives of the thesis are as follows:

1) To design a 1 kW 8/6 4-phase SRM and fabricate a prototype , based on design procedure.
2) To build up a hardware setup for determination of flux linkage characteristics and motor inductance at different rotor positions and to carry out the flux linkages analysis using ANSOFT software to validate the results as obtained for experimental method
3) To develop a rotor position estimation algorithm and truth table at stand still and running condition based on machine geometry.
4) To design a controlling circuit based on the rotor position information
5) To implement the proposed control circuit using embedded micro controller.
6) To Integrate and implement the complete system and testing.

1.5 ORGANISATION OF THE THESIS

Chapter 1: Introduction

This chapter deals with general information about SRM, history, literature review and scope of the thesis.

Chapter 2: Construction, operating principle and basic control

The SRM is fundamentally different from the conventional a.c. or d.c. motors, both in terms of its construction and control requirements. Though the basic principle is well known, for the sake of totality these aspects are explained briefly in this chapter. After the constructional features and torque production principle are explained, the mathematical expressions comprising voltage, current, flux, instantaneous and average torque are derived. Unlike the conventional motors, SRM cannot run direct on line. The motor is always driven by a power converter. This chapter also addresses the control issues and variable of SRMs.

Chapter 3.Design and Steady State performance analysis of SRM

This chapter describes the design procedures used for switched reluctance motors in many applications. In this study process, empirical method, finite element method and analytical method have been applied. The empirical formulas as established by design experts yield a preliminary design. The finite element method accomplishes design

fine-tuning and validation. The analytical model as established by the generalized electrical machine theory enables a study of converter control and dynamic performance. A design procedure followed by analytical calculations of inductance in aligned and unaligned positions is discussed in detail. Analytical calculations of inductance at various positions of the rotor have also been discussed. The effects of various motor parameters on the design are investigated and finally Finite Element is used to predict design and performance parameters. Useful conclusions are drawn as to optimum configuration for switched reluctance motors

Chapter 4.Determination of flux-linkage characteristics of SRM

SR motor is characterized by its flux-linkage characteristics. Unlike the other motors, these characteristics are nonlinear functions of stator current and rotor position. Generally two approaches are followed to find out these characteristics: 1) Numerical approach following the finite element method; 2) Experimental method of direct measurement. In this thesis, the second approach has been adopted initially. A full set of static flux-linkage characteristics as a function of rotor position and current are measured experimentally. The obtained values have been validated with the ANSYS FEM method. The FEM analysis is carried out prove the correctness of the methodology. The experimental results values matches with the ANSOFT FEM Method

Chapter 5. Converters and Position Sensors of Switched Reluctance Motor

The SR motor drive circuits have been critically reviewed in this chapter. Comparison of the most common drive circuit's topologies has been held showing the major advantages and disadvantages of each topology together with its major field of applications. It is mentioned earlier that a shaft position sensors are necessary for SR motor drive and different sensing devices are discussed.

Chapter 6 Description of Experimental Setup, Hardware and Software

Different direct and indirect sensing methods are discussed. A novel algorithm to find out rotor position at stand still and during are running are explained. The experimental methods, test results and the block diagram of the experimental set-up are presented in detail. Finally the proposed method is validated using known indirect sensing method. Simulation results for an experimental prototype as well as experimental results are described in this chapter.

Chapter 7 Conclusions and Future Work

In this chapter, the various contributions are summarized. For an SR motor, issues like design, simulation and implementation of the controller are discussed. The proposed schemes are validated through experiments.

Chapter 2 Construction and Basic Control of SRM

In recent years SRM is receiving considerable attention for variable-speed drive applications. It's a simple construction due to the absence of magnets, rotor conductors and brushes. High system efficiency over a wide range of speeds make the SRM drive an interesting alternative to compete with permanent magnet brushless DC motor and induction motor drives. In this chapter the basic construction details, operation and basic control of Switched Reluctance Motor is discussed

2.1 Construction

The SRM is an electric machine that is characterized mainly by its constructive simplicity. It has salient poles on both stator and rotor and its magnetic core consists of laminated steel. It is a doubly salient, single excited motor. Each stator pole has a simple concentrated winding and there are no conductors of any kind on the rotor which makes the construction cheaper, reliable, and rugged. The schematic diagram of an SRM with eight stator and six rotor poles is shown in Fig.2.1. The stator windings on diametrically opposite poles are connected in series to form one stator phase. The rotor is also laminated. Thinner laminations of silicon steel are preferred in SRM as eddy current dominates the core losses due to higher commutating frequency compared to AC motor of comparable speed and rating. For very high speed application, cobalt-iron and variants are used for laminations (Miller, T.J.E 1993). The stator and rotor poles appear in pairs but are usually of unequal numbers. This is to avoid the eventuality of the rotor being in a state of producing no initial torque, which occurs when all the rotor poles are locked in with the stator poles. A unique feature of SRM is that it can be operated, even though with reduced power output, even when there is a loss of one of the phases. The choice of the number of poles and number of phases is not unique. Although the number of phases and the number of poles must be minimum to reduce the number of switching devices and the associated commutation, the torque capabilities will influence its selection. Different configurations have been studied and its influence on the performance has been reported (Miller, T.J.E 1993). In order to guarantee that the SRM can be started at any initial rotor position, and to get smooth torque capacity per revolution, SRM's with multi-phase as well as multi-rotor-pairs are developed. The number of stator and rotor poles is generally different. Some possible combinations are: $N_s = 6$, $N_r = 4$; $N_s = 8$,

N_r = 6; N_s = 12, N_r = 10, etc. These combinations ensure that the rotor is never in a position where the summation of the electromagnetic torque generated by each phase is zero. The larger the stator and rotor poles number, the less the torque ripple. By choosing a combination where there are two more stator poles than rotor poles, high torque and low switching frequency of the power converter can be achieved. Three phase 6/4 pole and four phase 8/6 pole configurations are popular among different configurations.

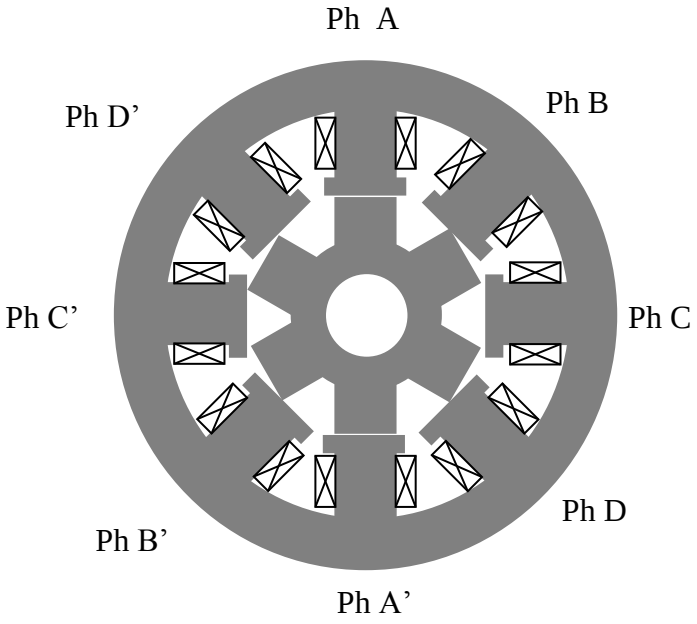

Fig.2.1 Cross section of a 8/6 SRM

2.2. Machine Topologies

SRM can offer a wide variety of aspect ratios and salient pole topologies. This means that each application is likely to be better suited to a specific SR topology. Therefore it is difficult to give an overview of which topology offers what advantage or disadvantage without resorting to sweeping statements

2.2.1 Single Phase Motor

These are the simplest SR motors with least connections between machine and electronics. The disadvantage lies in very high torque ripple and inability to start on at all angular positions. May be attractive for very high-speed applications, but starting problem may preclude their use. Fig.2.2 (a) represent a single phase SRM

2.2.2 Two Phase Motor

Stepping the air gap or providing symmetry in the rotor poles can overcome problems of starting compared with single phase machines. This machine may be of interest

where the cost of winding connections is important, but again high torque ripple may be detrimental. Fig.2.2 (b) represent a two phase SRM

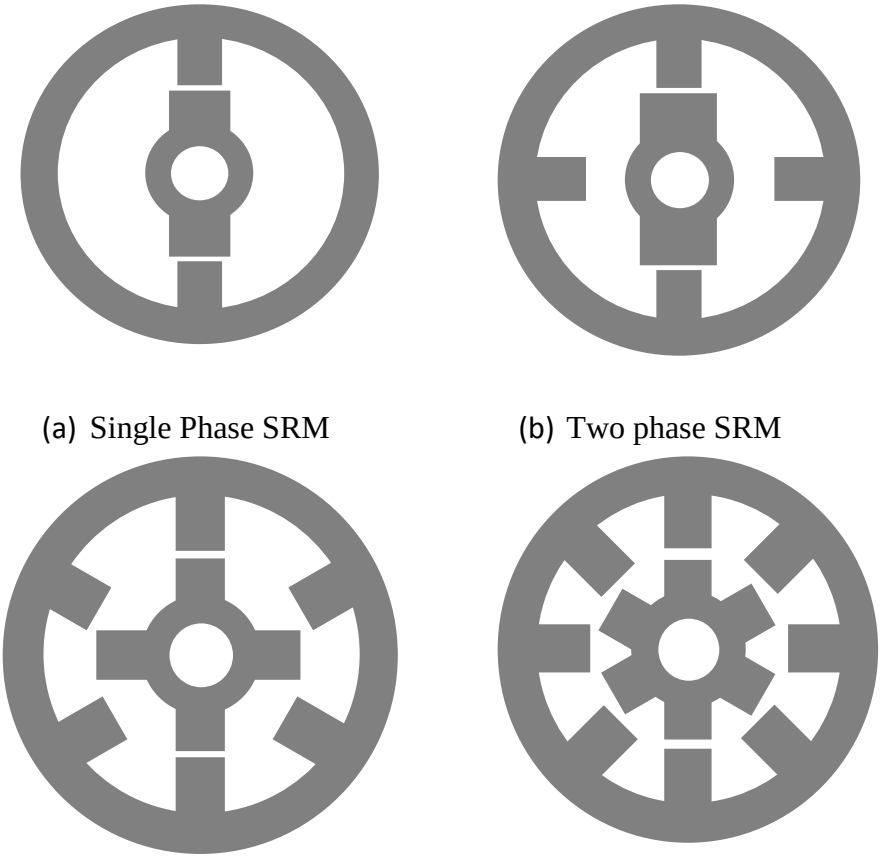

(a) Single Phase SRM (b) Two phase SRM

(c) Three Phase SRM (d) Four phase SRM

Fig.2.2 SRM Topologies

(a) Single Phase SRM (b) Two Phase SRM
(c) Three Phase SRM (d) Four Phase SRM

2.2.3 Three Phase Motor

This type of motors offers simplest solution to starting and torque ripple without resorting to high number of phases. Hence it this has been the most popular topology in its 6/4 forms. Fig.2.2 (c) represent a three phase SRM.

2.2.4 Four Phase Motor

Four phase motor may be popular for reducing torque ripple further, but the large number of power devices and connections probably limit four phases to a limited application field. Fig.2.2 (d) represents a Four Phase SRM. And the 5 and 6 phase motor can offer a better torque ripple reduction compared to 4 phases and 3 phases. Unlike conventional motors, SRM needs an electronic controller for their operations

since the switched reluctance drive is a type of brushless DC drive. Due to non-availability of fast switching power semiconductor devices, there were difficulties in commercializing SRM technology. Now with a new variety of power semiconductor devices such as MOSFETs and IGBTs being available easily there is a renewed interest in SRM. SRM uses a position sensor on the rotor together with power electronic switches to accomplish all the controls associated with a separately excited and fully controlled DC motor. Unlike more familiar brushless machines it needs neither current carrying circuits nor permanent magnets on the motor.

2.3. Principle of Operation

A typical motorized construction of SRM is given in Fig.2.3. The operating principle of SRM is such that the phase inductance is designed to vary almost linearly with the rotor angle.

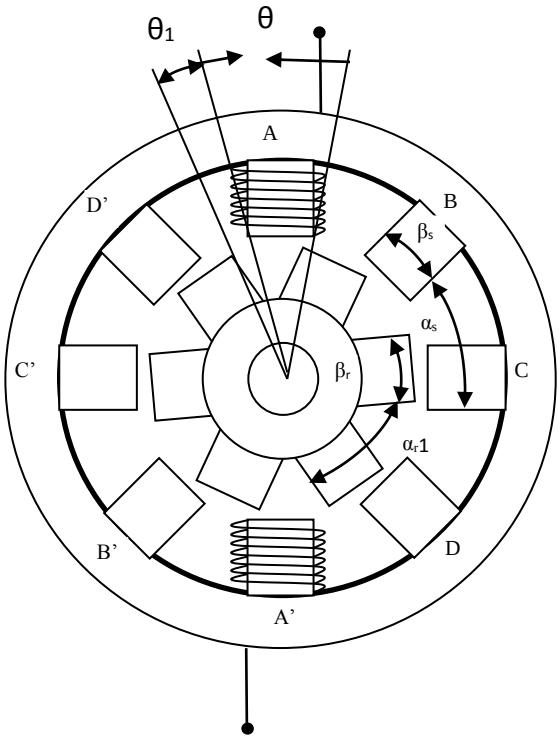

Fig.2.3 Motorized construction of SRM

Its operation can be explained by considering a working stroke for phase A while the rotor is at a standstill. A working stroke consists of energisation of the phase, achieved by forcing the current into it and, in its successive de-energisation achieved by zeroing the current. When phase A is energized, the nearest rotor pole pair is attracted towards the energized stator phase, as such an anticlockwise torque (in the

following assumed as positive) is exerted on the rotor, pulling the adjacent pair of rotor poles into alignment with phase A. This causes a rotation of SRM in the positive direction with conversion of electrical energy into mechanical energy. A series of working strokes commanding in sequence A, B, C, D, A, causes a continuous rotation of the SRM in the same direction.

2.4 Torque Development

Torque production in reluctance machines is achieved by the tendency of the rotor to move to a position where the inductance, and hence the magnetic field energy, of the excited winding is minimized (Krishnan, R. 2001; Miller, T.J.E 1993). An example of an 8/6 SRM is shown in Fig.2.3. This four-phase machine is denoted 8/6 because it has eight stator and six rotor poles. In the position shown, the resulting torque tends to rotate the rotor in anti clockwise direction towards the aligned position. If the rotor continues past the aligned position, due to its inertia, the attractive force between the poles produces a braking torque. To eliminate this negative torque, the current must be switched off while the poles are separating. The ideal current waveform is therefore a series of pulses synchronized with aligning rotor poles and stator poles. By exciting the stator windings of the different phases each time two rotor poles approach the appropriate stator poles, a continuous torque production and rotation of the rotor is achieved.

2.5 Circuit Equations

2.5.1 Voltage Equation

Voltage relations for a SRM are the same as for any other electrical machine. i.e., the voltage applied to the stator terminals equals the sum of a voltage drop due to resistive drop and the induced voltage due to flux linkage variations. Therefore, the voltage equation for the q^{th} phase of an SRM using Kirchhoff's voltage law is given below

$$v_q = R.\, i_q + \frac{\partial \varphi_q(\theta_q, i_q)}{\partial t} \qquad (2.1)$$

Where v_q = phase voltage ; i_q = phase current ; R = phase winding resistance; φ_q=flux linkages; θ_q= rotor position and t = time

Since φ_q is a function of θ_q , and i_q, equation (2.1) can be expanded using the partial

$$v_q = R.\,i_q + \frac{\partial \varphi_q(\theta_q, i_q)}{\partial \theta_q}\frac{\partial \theta_q}{\partial t} + \frac{\partial \varphi_q(\theta_q, i_q)}{\partial i_q}\frac{\partial i_q}{\partial t} \quad (2.2)$$

2.5.2 Inductance Profile

A crucial difference between the SRM (a doubly salient machine) and non salient machines lies in the fact that the dependence of flux linkage on the current does not vary sinusoidally with the rotor position. In general, it could be any periodic function of θ_q, (Miller, T.J.E 1993). Due to the symmetric location of the poles, the mutual inductance between phases can be neglected (S.K Panda. 1996). As a result, φ_q, is only a function of i_q, (in addition to the rotor position θ_q) and is not a function of any other winding currents. The flux linkage for a phase winding, φ_q, varies cyclically with the rotor position θ_q, and is a nonlinear function of the phase current i_q, when parts of the magnetic circuit become saturated. The relationship between the flux linkage and the winding inductance is $\varphi_q(\theta_q, i_q) = i_q L_q(\theta_q, i_q)$. It is essential for designing and building the SRM to recognise the dependence of the phase inductance on the instantaneous phase current as well as the rotor position. Under the commonly made assumption of magnetic linearity, the flux linkages of phase q would be

$$\varphi_q = L_q(\theta_q) i_q \quad (2.3)$$

where L_q is the phase inductance.

This equation (2.3) may be substituted into equation (2.2) to give equation (2.4)

$$v_q = R.\,i_q + L_q(\theta_q)\frac{\partial i_q}{\partial t} + i_q \frac{\partial L_q(\theta_q)}{\partial \theta_q}\frac{\partial \theta_q}{\partial t} \quad (2.4)$$

Since the term $\frac{\partial \theta_q}{\partial t}$ is the angular speed ω. Thus

$$v_q = R.\,i_q + L_q(\theta_q)\frac{\partial i_q}{\partial t} + i_q \omega \frac{\partial L_q(\theta_q)}{\partial \theta_q} \quad (2.5)$$

It is sometimes useful to reformulate equation (2. 4) as

$$\frac{\partial i_q}{dt} = \frac{v_q - R.i_q - i_q \frac{\partial L_q(\theta_q)}{\partial \theta_q}\frac{\partial \theta_q}{\partial t}}{L_q(\theta_q)} \quad (2.6)$$

or

$$\frac{\partial i_q}{dt} = \frac{1}{L_q(\theta_q)}\left[v_q - R.\,i_q - i_q \frac{\partial L_q(\theta_q)}{\partial \theta_q}\frac{\partial \theta_q}{\partial t}\right] \quad (2.7)$$

When voltage is applied to the winding, the rate at which the current builds up and the maximum value it attains, depends upon the relative positions of the poles at which the voltage is applied and the speed of the motor when it is applied. Assuming constant speed, then based on equation (2.7), it is desirable to switch the voltage on when $\frac{\partial L_q}{\partial \theta_q}$ is essentially zero, and when $L_q(\theta_q)$ is minimum. These conditions allow a very high rate of change of current; the current reaches the desired level quickly when $L_q(\theta_q)$ increases and $\frac{\partial L_q}{\partial \theta_q}$ becomes significant, $\frac{\partial i_q}{dt}$ decreases and may become negative if the motional emf $(i_q \omega \frac{\partial L_q(\theta_q)}{\partial \theta_q})$ overcomes$(v_q - R.i_q)$ .When the voltage is set to zero, the motional EMF forces the current to zero.

The actual shape of the current pulse is determined by the switching points and the magnitude of the voltage. This control scheme has been suggested by (Lawrenson, P.J et al 1980) and (Miller, T.J.E 1993).If the motional emf is insufficient to limit the current, then the voltage must be manipulated or chopped to keep the current within the machine and control constraints. It is seen that the performance of the machine is described in terms of the parameter $L_q(\theta_q)$. Assuming that $L_q(\theta_q)$ follows the trapezoidal current-independent variation. The idealized inductance profile over one rotor pole pitch is shown in Fig.2.4

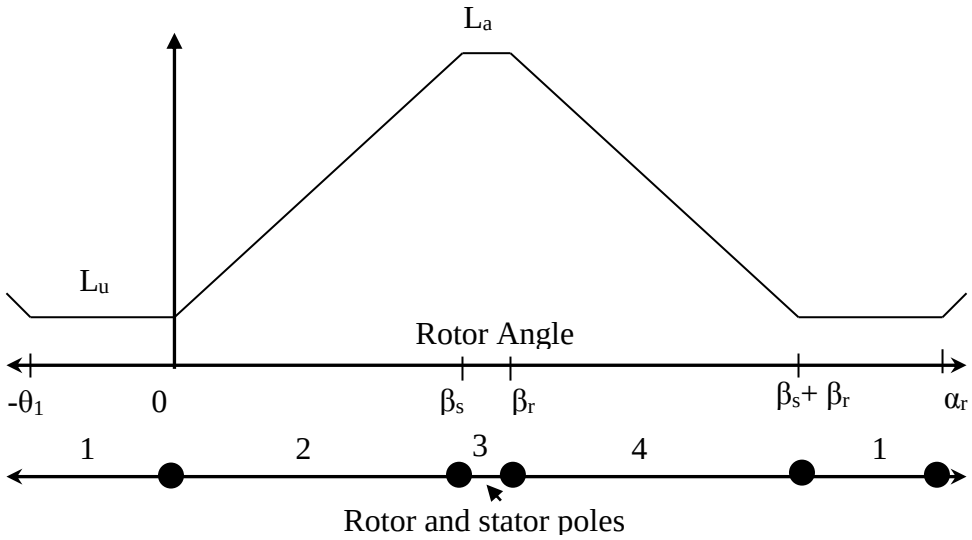

Fig.2.4 Inductance profile for one phase.

The structure of a four-phase SRM is depicted in Fig.2.3, where for simplicity; the coil of only one phase has been drawn. In Fig.2.4, four zones can be recongised along the pitch namely the zones from $-\theta_1$ to 0 from 0 to β_s , from β_s to β_r and from β_r to $\beta_s+\beta_r=\alpha_r-\theta_1$. In zone 1, (unaligned zone), the rotor pole does not face the stator pole and the inductance is minimum (L_u); in zone 2, there is a rise in the overlapping of the pole surfaces and the inductance increases. In zone 3 (aligned zone), the rotor pole faces the stator pole and the inductance is maximum (L_a). In zone 4, there is a shortage in the overlapping of the pole surfaces and the inductance decreases.

Inductance is a periodic function of θ with period α_r. The equation of the inductance profile for phase A can be approximated over a period by

$$L_A(\theta)=\begin{cases} L_u & -\theta_1 \le \theta \le 0 \\ L_u + K\theta & 0 \le \theta \le \beta_s \\ L_a & \beta_s \le \theta \le \beta_r \\ L_u - K(\theta-\beta_r-\beta_s) & \beta_r \le \theta \le \beta_s+\beta_s=\alpha_r-\theta_1 \end{cases} \quad (2.8)$$

and that of phase q by

$$L_q(\theta)=L_A\left[\theta-\frac{\alpha_r}{m}(k-1)\right] \quad (2.9)$$

where q is the number of phases, and K is the slope of the profile in the zone of increasing inductance, that is

$$K=\frac{L_a-L_u}{\beta_s} \quad (2.10)$$

The inductance profiles of phases for the SRM of Fig.2.3 are shown in Fig.2.5 (a). The Inductance profile of phases of an 8/6 SRM using equation (2.8) with the calculated inductance values using the analytical procedure (Krishnan, R. 2001) is shown in Fig.2.5 (b).

2.5.3 Instantaneous Torque Expression

The operation of the SRM is described by the voltage and torque equation of each phase. For convenience, let us write $L_q(\theta_q)$ as L_q. The voltage drop on the phase resistance R can be neglected as it is much less than the induced voltage. Assuming magnetic linearity, the phase voltage will be

$$v_q=L_q\frac{\partial i_q}{\partial t}+i_q\frac{\partial L_q}{\partial t} \quad (2.11)$$

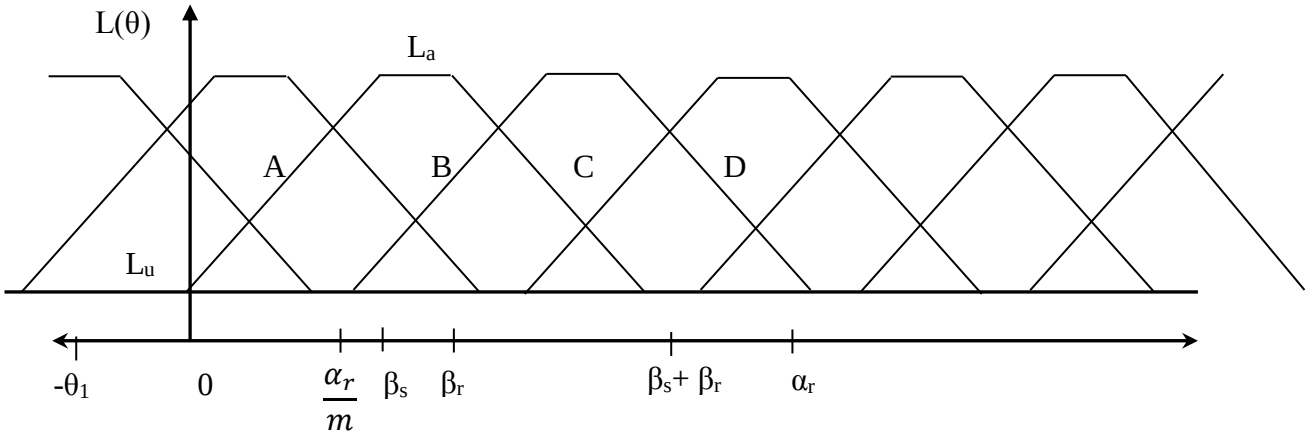

Fig.2.5 (a) Inductance profile of SRM phases

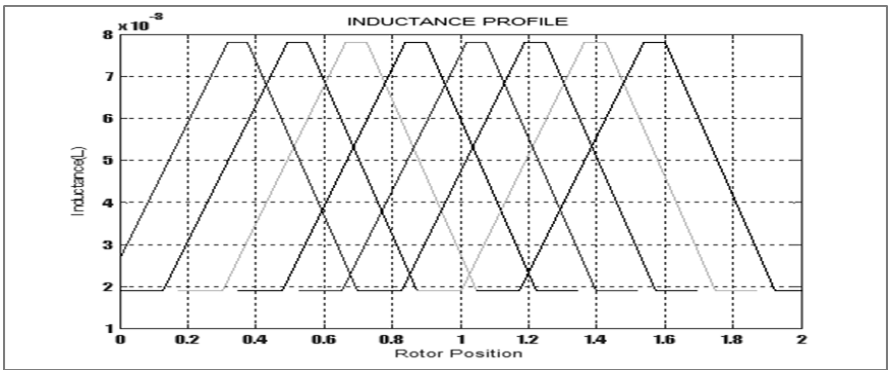

Fig.2.5 (b) Inductance profile of SRM phases of an 8/6 1 kW 4-phases SRM

The above equation may be rewritten as

$$v_q = L_q \frac{\partial i_q}{\partial t} + \frac{i_q}{2}\frac{\partial L_q}{\partial t} + \frac{i_q}{2}\frac{\partial L_q}{\partial t} \qquad (2.12)$$

The expression for the instantaneous power will be obtained by multiplying either side of equation (2.12) with i_q and is given as

$$v_q \times i_q = \left(L_q \frac{\partial i_q}{\partial t} + \frac{i_q}{2}\frac{\partial L_q}{\partial t} + \frac{i_q}{2}\frac{\partial L_q}{\partial t}\right) \times i_q$$

$$v_q \times i_q = \left[L_q i_q \frac{\partial i_q}{\partial t} + \frac{i_q^2}{2}\frac{\partial L_q}{\partial t}\right] + \frac{i_q^2}{2}\frac{\partial L_q}{\partial \theta}\frac{\partial \theta}{\partial t} \qquad (2.13)$$

The term in brackets may be rewritten as $\frac{\partial}{\partial t}(\frac{1}{2}L_q i_q^2)$ and the term $\frac{\partial \theta}{\partial t}$ is the motor speed and thus

$$v_q \times i_q = \frac{\partial}{\partial t}\left(\frac{1}{2}L_q i_q^2\right) + \frac{i_q^2}{2}\frac{\partial L_q}{\partial \theta}\omega \qquad (2.14)$$

The term $\frac{1}{2}L_q i_q^2$ is recognized as the increase in stored magnetic energy and the term $\frac{i_q^2}{2}\frac{\partial L_q}{\partial \theta}\omega$ as the power converted to mechanical work. But, the mechanical power developed per phase is

$$W_q = T_q \times \omega \tag{2.15}$$

where T_q is the torque developed per phase. Equating equation (2.15) with the second term in equation (2.14) we get

$$T_q = \frac{1}{2}\frac{\partial L_q}{\partial \theta} i_q^2 \tag{2.16}$$

Equation (2.16) shows that the instantaneous torque per phase, even with the simplifying assumptions, is a quadratic function of the phase current and is determined by the current injected into the phase winding and is positive in the rotor position interval at which the phase inductance is increasing as the rotor position θ increases. This torque is negative when the phase inductance is decreasing as θ increases and it is zero where the phase inductance is constant. Substituting equation (2.8) into equation (2.16) yields the instantaneous torque developed by phase A over the four sectors in Fig.2.4 respectively as

$$T_A(\theta) = \begin{cases} 0 & -\theta_1 \le \theta \le 0 \\ \frac{1}{2}Ki^2 & 0 \le \theta \le \beta_s \\ 0 & \beta_s \le \theta \le \beta_r \\ -\frac{1}{2}Ki^2 & \beta_r \le \theta \le \beta_s + \beta_s = \alpha_r - \theta_1 \end{cases} \tag{2.17}$$

where K is given by equation (2.10). The instantaneous torque developed by the motor is the sum of the instantaneous toques developed by the individual phases, i .e

$$T = \sum_{q=1}^{m} T_q = \frac{1}{2}\sum_{q=1}^{m} \frac{\partial L_q(\theta)}{\partial \theta} i_q^2 \tag{2.18}$$

For the SRM rotating in the positive direction, a motoring torque is therefore developed when the rotor travels along the zone of increasing inductance $\frac{\partial L}{\partial \theta} > 0$. No torque is developed when the rotor travels along the unaligned or the aligned zones $\frac{\partial L}{\partial \theta} = 0$. A braking torque is developed when the rotor travels along the zone of decreasing inductance $\frac{\partial L}{\partial \theta} < 0$. A more accurate analysis, including flux fringing and

saturable iron, would predict a torque pulse different from the one approximated by equation (2.16).To include flux fringing and iron saturation in the torque analysis, the magnetic fields must be numerically computed using a finite element methods (Krishnan, R. 2001; Miller, T.J.E 1993). From the equation (2.18), it is immediately understood that the generated torque is independent of the direction of current flow. Hence, unidirectional currents are generally used, thereby, greatly simplifying the design of the power converter.

A better understanding of the relationship between the phase inductance profile and the torque profile can be obtained from Fig.2.6 where the Fig.2.6 (a) shows the inductance variations of one typical phase and the corresponding torque profile according to equation (2.18) at constant current is shown in Fig.2.6 (b). At θ_0, the leading edges of the rotor poles meet the edges of the stator poles and the inductance starts a linear increase with rotation, continuing until the poles are fully overlapped at θ_1, when the inductance reaches its maximum value L_a. Ideally, $\theta_1 - \theta_0 = \beta_s$ (stator pole arc). From θ_1 to θ_2, the inductance remains constant at L_a through the region of complete overlap. Ideally, $\theta_2 - \theta_0 = \beta_r$ (rotor pole arc). From θ_2 to θ_3, the inductance decreases linearly to the minimum value L_u. Hence, $\theta_3 - \theta_0 = \beta_s + \beta_r$. From θ_3 to θ_4, the stator and rotor poles are not overlapped and the inductance remains constant at L_u. So, the rotor pole pitch $\alpha_r = \theta_4 - \theta_0$.

It is clear that for the motor to be able to start in one direction (forward) from any initial rotor position, the pole arcs must be chosen such that at least one of the phase windings are in a region of increasing inductance (or decreasing inductance for rotation in the reverse direction). Further, in order to produce a unidirectional forward motoring torque, the stator phase windings have to be sequentially energised such that the current pulse for a phase must coincide with the angular interval where the $\frac{\partial L}{\partial \theta}$ for that phase is positive. Similarly, a braking torque (generating mode) or reverse rotation (motoring in the reverse direction) is obtained when the current pulses coincide with the angular intervals where the respective is negative $\frac{\partial L}{\partial \theta}$. Therefore, a rotor position sensor is obviously required to start and stop the conduction various phases. When this motor is operated without feedback control and the phase currents

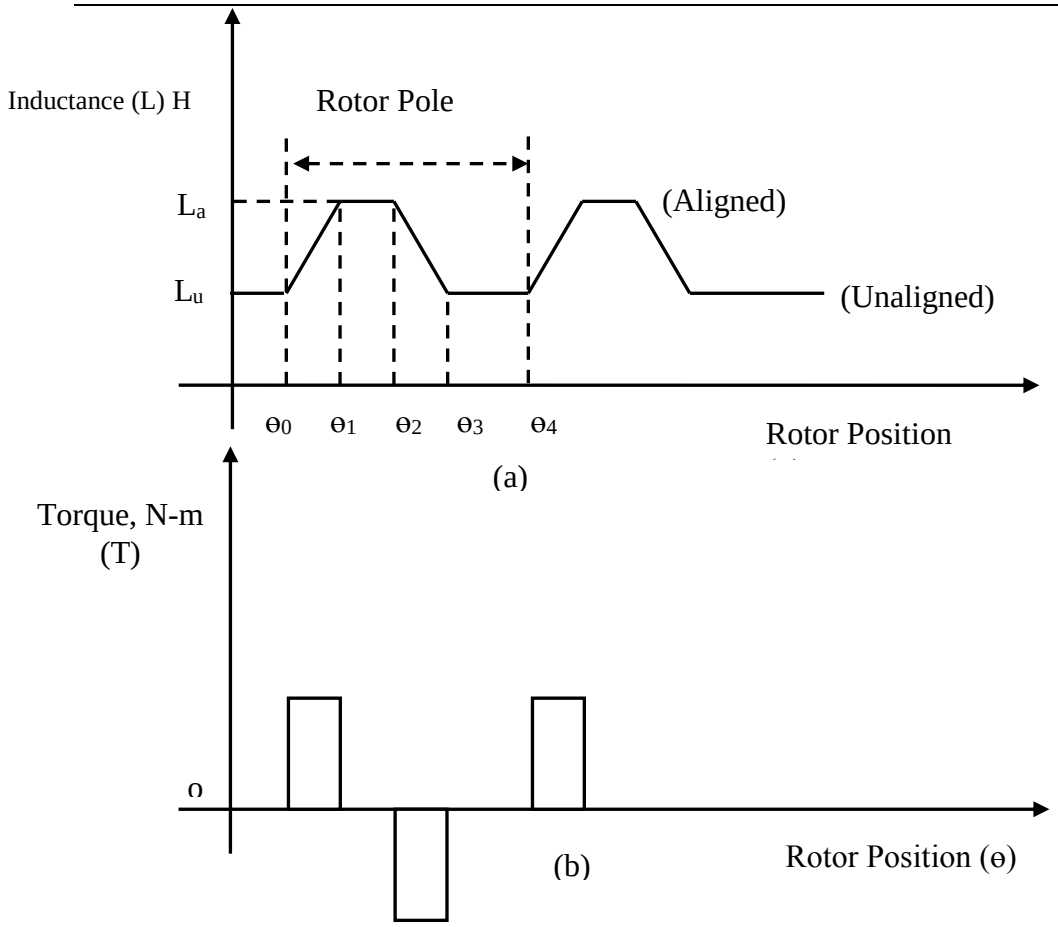

Fig.2.6
(a) Ideal variation of inductance of one stator phase as a function of rotor position.
(b) Corresponding variation of torque with constant current as a function of rotor position.

are switched on and off in sequence, the rotor will advance in steps of angle (called as step angle) φ, given by

$$\emptyset = \frac{360^0}{mN_r}$$

where m is the number of phases in the SRM and N_r is the number of rotor poles. For a four-phase SRM with six rotor poles, φ = 15˚.

2.5.4 Power Equation

The expression for the instantaneous power 'p' will be obtained by multiplying either side equation (2.12) with i_q and is given as

$$P_q = \left[L_q i_q \frac{\partial i_q}{\partial t} + \frac{i_q^2}{2}\frac{\partial L_q}{\partial t}\right] + \frac{i_q^2}{2}\frac{\partial L_q}{\partial \theta}\frac{\partial \theta}{\partial t} \qquad (2.19)$$

2.5.5 Equivalent Circuit

Fig. 2.7 illustrates the equivalent circuit for one phase of the SRM

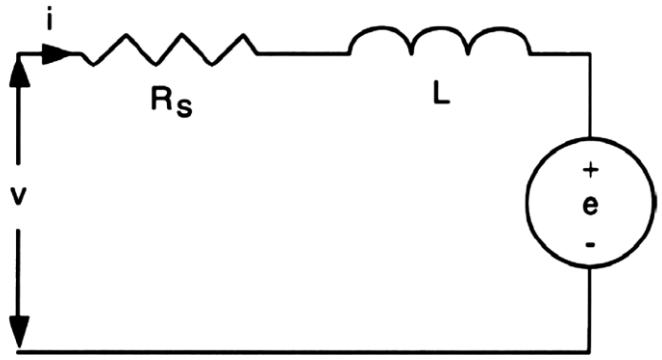

Fig.2.7 Single phase equivalent circuit of SRM

2.6 Performance characteristics-Flux Linkage Characteristics

As the machine is doubly salient and prone for saturation, the flux-linkage in SRM is a function of rotor position and current. The nature of flux-linkage performance characteristics for different rotor positions is explained below.

2.6.1 Aligned position

When any rotor pole pair aligns exactly with the stator poles of a phase, that phase is said to be in aligned position. Fig.2.8 (a) illustrates the aligned position for phase A. In the Fig.2.8 (a), the stator poles A and A' forming the phase A of SRM are aligned with the rotor poles. In this position, the magnetic circuit will have minimum reluctance due to the small air gap. The magnetic circuit, exhibits considerable degree of saturation in this position and the nature of the flux-linkage characteristics is shown by curve 3 in Fig.2.9.

2.6.2 Unaligned position

When inter polar axis of the rotor aligns with the stator poles of a phase, that phase is said to be in an unaligned position. In Fig.2.8 (c) the phase A which is obtained by connecting the stator poles A and A' is in an unaligned position. The nature of the flux-linkage characteristics is as shown by curve 1 in Fig.2.9. The rotor of an SRM is said to be at the aligned position with respect to a fixed phase, if the current reluctance has the minimum value; and the rotor is said to be at the unaligned position with respect to a fixed phase if the current reluctance reaches its maximum value; otherwise the rotor is said to be at the intermediated position shown by curve 2 in

Fig.2.9. In this position, the magnetic circuit will have high reluctance owing to large air gap and it is not susceptible for saturation as in the aligned position.

2.6.3 Intermediate position

Any position between the unaligned and aligned position is an intermediate position. An intermediate position is illustrated in Fig.2.8 (b) for phase A. For intermediate position of the rotor, the flux-linkage characteristics will be between the unaligned and aligned positions. The nature of the flux-linkage characteristics for intermediate positions is shown in Fig.2.9 by the curves between the curves 1 and 2. The flux-linkage characteristics do not change appreciably for few degrees near the unaligned positions and also for few degrees near the aligned position. As a circuit concept and to make certain preliminary analysis, the inductance of the phase winding is helpful. The nature of unsaturated inductance profile of the machine is as shown in Fig.2.4. For a given rotor position, the unsaturated inductance is given by the slope of the flux-linkage characteristics in the linear portion. As the flux linkage characteristics do not change appreciably for few degrees near unaligned position, the inductance of the winding remains nearly constant. The slope of the flux linkage characteristics in the unsaturated region starts increasing, as the rotor position approaches the aligned position. Therefore, inductance starts increasing as the rotor approaches the aligned position and it reaches maximum value at aligned position. Hence the inductance profile shows a positive slope after the initial constant inductance intervals up to aligned position.

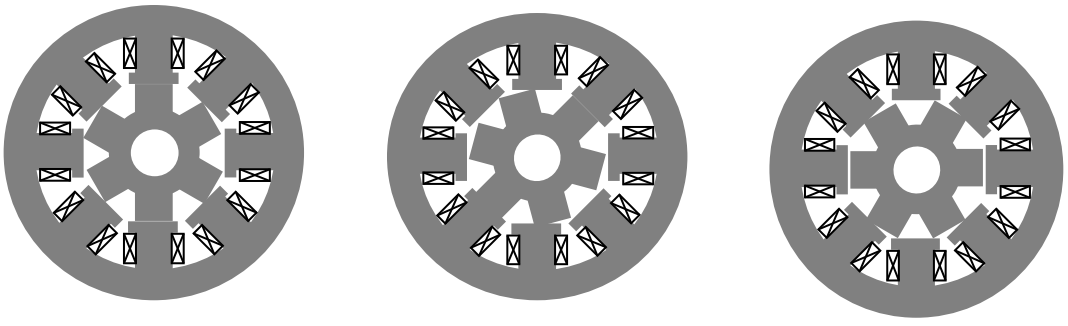

(a) (b) (c)

Fig.2.8 Illustration of different rotor position
(a) Aligned position (b) Intermediate position (c) Unaligned position

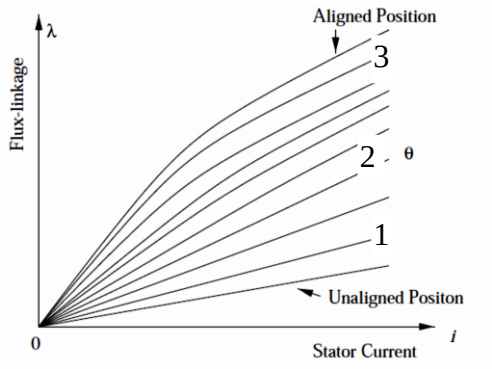

Fig.2.9 Flux linkage characteristics 8/6 SRM

2.7 Features and Industrial Applications of the SRM

Simple construction is a prime feature of the SRM. SRM eliminate rotor windings, permanent magnets (PMs), brushes, and commutator. With no rotor winding, the rotor is basically a piece of steel (and laminations) shaped to form salient poles. The absence of brushes provides long life. The absence of permanent magnets and rotor winding reduces the cost. Besides, SR motors have some other attractive advantages that make it favorable for various industrial applications.

2.7.1 Advantages

1. Simple and robust structure. There are no windings on the rotor of the machine and hence it is inherently less expensive. High torque-to-inertia ratio. It has high starting torque without the problem of in-rush currents and its power density is comparable to that of an induction machine. Maximum operating speed and maximum rotor temperatures are higher when compared to other machines of similar ratings. Each phase winding of the SRM is independent of the other phase windings and this makes the machine highly reliable. Motor torque is independent of the phase current polarity. Thus, the converter for the SRM drive requires only one switch per phase. It has inherent four-quadrant operation. It has a wide constant torque/power region in the torque-speed characteristics. It has high efficiency throughout the entire torque-speed range.

2.7.2 Disadvantages

Although there are many inherent structural advantages, the doubly-salient structure and non-ideal switched square wave winding current give the SRM higher torque ripple, and thus lead to the generation of higher vibration and acoustic noise. In addition, the rotor position and current dependent winding nonlinear inductance makes its torque and dynamic behaviour highly nonlinear. Moreover, analysis of vibration behaviour is also difficult to perform accurately.

1. **Need for position sensing**

As mentioned above, for smooth SR motor rotation, current switching between phases must occur at precise angular points. Traditionally, the rotor position is measured with some mechanical angle transducers mounted on the rotor shaft. However, these sensors not only increase cost and size to the motor, but also are a major source of unreliability. Therefore, sensorless control is required to make the motor truly practical in many applications. Sensorless operation involves measuring motor characteristics at the drive and then using sophisticated calculations to derive the required position data.

2. **High torque ripple, Acoustic Noise and Vibrations**

In dealing with the mechanical vibration and acoustic noise problems of an SRM, there have been much previous literatures (Cameron, D.E., Lang, J.H., and Umans, S.D 1992; Lovatt, H.C., and Stephenson, J.M 1997) concerning their origin, exploration and reduction. The studies in (Miller, T.J.E 2002; Krishnan R., and Vijayraghavan, P 1998) show that the sources of acoustic noise can be basically classified into four categories, namely magnetic, mechanical, aerodynamic and electronic. Among these, it is shown that the radial attractive force between stator and rotor is the dominant one, particularly for the case in which the de-energisation occurs at the aligned rotor position. In making performance evaluation, it was found that vibration measurement can be used as an alternative to acoustic noise (Lovatt, H.C., and Stephenson, J.M 1997). Basically, the existing solutions for vibration and acoustic noise reduction can be achieved via the motor design (Colby, R.S., Mottier, F.M., and Miller, T.J.E 1996 ; Cai, W., Pillay, P., Tang, Z., and Omekanda, A 2001) and the converter control. Some typical previous research areas of the former topic are: (i) the use of thicker back-iron, wherein the trade-off between noise and power

density must be considered; (ii) applying an axial preload to reduce bearing noise; (iii) dynamic rotor balancing to eliminate noise due to rotor unbalance; (iv) the adoption of a slightly larger air gap; and (v) suitable core laminations; in (Gabsi, M., Camus, F., Loyau, T., and Barbry, J.L 1999; Cai, W., Pillay, P., Tang, Z., and Omekanda, A 2001) the finite-element method is used for computer-aided analysis and design.

As to the converter control approaches, there exist three key tunable parameters, namely the turn-on angle, the turnoff angle and the current shape. In the previous research reported in (Fahimi, B., Suresh, G., Rahman, K.M., and Ehsani, M 1998) the optimised current profile including turn-on and turnoff angles is generated using an artificial neural network to yield performance compromise between acoustic noise, efficiency and average torque. As generally recongised, winding current-tail shaping is an effective means, which has been accomplished via voltage smoothing, and two stage and three-stage commutation control (Cameron, D.E., Lang, J.H., and Umans, S.D 1992 ; Michaelides, A., and Pollock, C 1996 ; Pollock, C., and Wu, C.Y 1997; Krishnan, R., and Vijayraghavan, P 1998). Random PWM (RPWM) switching control (Blaabjerg, F., and Pedersen, J.K 1993; Im, Y.C., Kim, K.H., Na, S.H., Kim, H.D., and An, J.H 1998) and random turn-on and turn-off angles (Boukhobza, T., Gabsi, M., and Grioni, B 2001) have also been studied recently. However, owing to limited success, the optimisation of the key parameters in random switching schemes needs to be studied more deeply (Blaabjerg, F., and Pedersen, J.K 1993), Accordingly, vibration reduction using random frequency PWM (RFPWM) with harmonic spectrum shaping is presented

In (Ahn, J.W., Park, S.J., and Lee, D.H (2004)) a hybrid excitation method was presented. Overlap excitation is employed to reduce the rapid change of radial MMF, and a C-damp converter is added to reduce the decrease in efficiency. In (Ha, K.H., Kim, Y.K., Lee, G.H., and Hong, J.P (2004),prediction and experimental transfer function estimation of the vibration caused by the magnetic force are presented, and accordingly a vibration reduction control strategy is proposed. Intuitively, minimisation of ripple torque is a direct means, and this type of research is reported in (Cailleux, H., Pioufle, B.L., Multon, B., and Sol, C 1993; Stephenson, J.M., Hughes, A., and Mann, R. 2001), In (Cailleux, H., Pioufle, B.L., Multon, B., and Sol, C 1993),the ripple torque reduction is achieved via torque nonlinear control, associated

with a suitable phase commutation strategy. In (Lovatt, H.C., and Stephenson, J.M. (1997), the current waveforms are optimised using computer search techniques to yield ripple free torque. In (Stephenson, J.M., Hughes, A., and Mann, R. 2001) torque ripple minimisation is obtained by optimum harmonic current injection, and in (Stephenson, J.M., Hughes, A., and Mann, R. 2002) the same authors developed the online simplex optimisation technique to set the injected current harmonics, and it has been verified to be effective in reducing steady-state torque ripple. Each approach described above possesses its advantages and limitations in implementation and effectiveness

2.7.3 Applications

1. General purpose industrial drives.
2. Application –Specific drives: compressors, fans, pumps, centrifuges.
3. Domestic drives: food processors, washing machines, vacuum & cleaners.
4. Electric vehicle application, aircraft applications and servo-drive.

2.8 Control Strategies

The key to effectively control the SRM lies in the ability to control two parameters: how much of the current flows to the phase winding and when the current flows with respect to the rotor position. The ideal waveform of the phase current for maximum production of motoring torque is a controlled current pulse flowing during the increasing inductance period only. However, this type of current waveform is difficult to produce in all practical circumstances primarily due to the inductance of the stator phase winding and the back EMF. This is explained as follows

Using equation (2.5), we have

$$v_q = R.i_q + L_q(\theta_q)\frac{\partial i_q}{\partial t} + i_q\omega\frac{\partial L_q(\theta_q)}{\partial \theta_q}$$

The term $i_q\omega\frac{\partial L_q(\theta_q)}{\partial \theta_q}$ is the motional EMF (back EMF) and, as expected, it increases with the motor speed ω. At low speed, the back EMF and the term Ri_q are small in value, therefore, the current can build up quickly when the inductance is low. Once the current reaches the desired value, the current will continue to rise unless the phase voltage is switched off. Therefore, the current magnitude should be regulated for proper control of speed and torque. The different controlling mode used for SRM to regulate phase current depends upon the motor speed. For example for high speeds,

angle control mode and for lower speeds chopping mode (Miller, T.J.E 1993; Lawrenson, P.J. 1980).These two modes of control are briefly discussed in the following sections.

2.8.1 Angle control mode

This mode of control can be explained with inductance profile as reference which is shown in Fig.2.11. In this mode of control, the phase is excited at an angle θ_0 near the unaligned position and it is switched off at the commutation angle θ_c which will be less than the angle corresponding to aligned position. Assuming two switches per phase type of converter shown in Fig.2.10. The two switches are switched on at θ_0 and are switched off at θ_c. When the speed of the motor is sufficiently high, the nature of voltage, and the flux-linkage waveforms will be as shown in Fig.2.11 [b-c]. When the phase is excited at θ_0, neglecting the residual flux, its flux-linkage can be written as

$$\varphi = \int (v - iR)dt \quad \text{(In Simple form)} \tag{2.20}$$

Neglecting the drop in the switches and the iR drop the flux linkage raises linearly up to commutation angle θ_c. At turn off instant corresponding to commutation angle, the switches S_1 and S_2 are switched off and the diode D_1 and D_2 starts conducting freewheeling current. The diodes D_1 and D_2 continue to conduct till the extinction angle θ_q, where the current and flux linkage becomes zero.

As the applied voltage to the phase winding is negative during the freewheeling period, the flux-linkage during this period is governed by

$$0 = \varphi_c + \int_{\theta_c}^{\theta_q} (-v - iR)dt \tag{2.21}$$

Neglecting the iR, drop the flux-linkage linearly falls to zero. At turn on, the current rises at a constant rate as the inductance is nearly constant around the unaligned position. As the rotor advances and comes to the position for which the inductance of phase winding starts increasing, the positive slope of the inductance profile generates back EMF which will oppose the applied voltage. Therefore, the resultant voltage reduces and rate of rise of current decreases. The magnitude of the back EMF depends

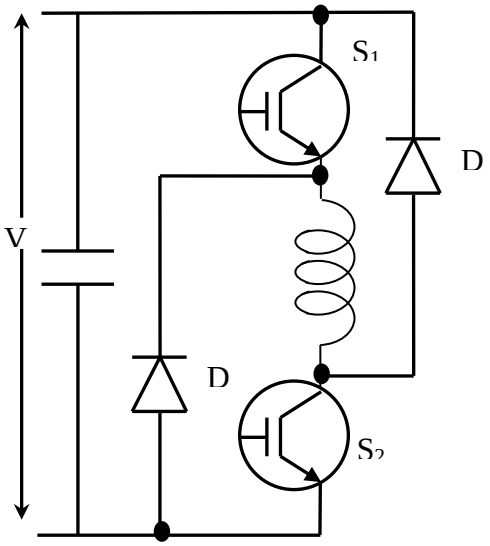

Fig.2.10 One leg of a converter with two switches per phase

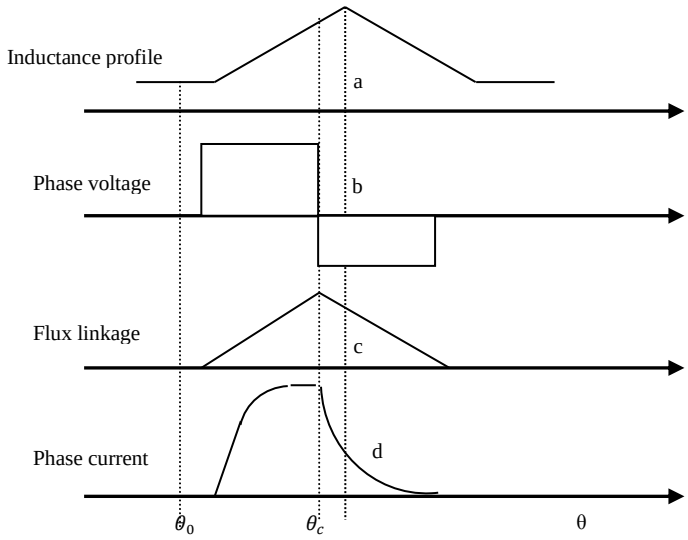

Fig.2.11 Angle control mode (back emf < phase voltage)

on the speed. Fig.2.11 [d] shows a typical current waveform for which the back emf is less than the applied voltage. The change in slope of the current after the initial rise is clear from the Fig.2.11 [d]. After crossing the commutation angle, the applied voltage reverses and the current starts falling rapidly. At the aligned position, the back emf reverses so that instead of augmenting the negative applied terminal voltage, it reduces it. Therefore, the rate of fall of current decreases. The current produces a positive torque till aligned position and produces negative torque after crossing

aligned position. Hence to reduce the negative torque the commutation angle must precede the aligned position by several degrees. The torque developed by the motor is controlled by controlling the turn on angle.

Fig.2.12 shows the typical waveform of phase voltage, flux-linkage, and current along with the inductance profile, for the speed at which the back emf is higher than the applied voltage. In this case, the current starts falling after the rotor moves into the rising inductance profile region as the resultant voltage becomes negative due to

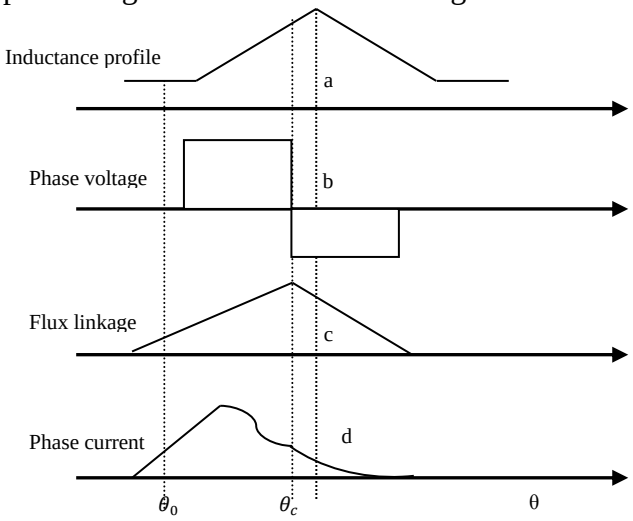

Fig.2.12 Angle control mode (back emf > phase voltage)

increased back EMF. The turn on angle is advanced in this case and it is before unaligned position. For higher torque, the turn on angle may even start at the previous falling inductance zone. Although it is simpler to have fixed turn off angle, in angle control mode, it calls for variable turn off angle for certain optimum performance strategy.

2.8.2 Chopping control

At low speeds, the back emf is low and the rotor takes longer time to move through the positive torque producing region. If the phase is turned on near unaligned region, the current can go to very high values by the time it reaches the aligned position. Therefore at low speeds, the phase current is controlled by chopping. The reference current for chopping depends on the torque requirement. With PWM current control (current chopping) of the SRM, assuming that each phase of the SRM can be independently controlled, there are two PWM current control strategies except for single pulse operation: Hard chopping mode and soft chopping mode. In the hard

chopping mode, both phase transistors (S_1 and S_2 in Fig.2.10) are driven by the same pulsed signal: the two transistors are switched on and off at the same time. It increases

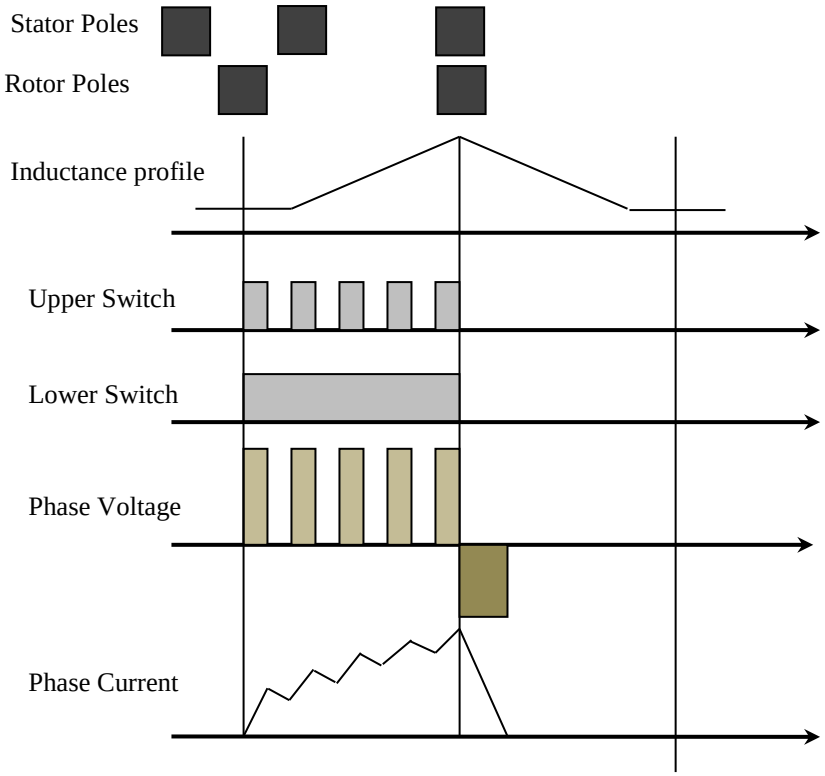

Fig.2.13 Soft chopping

the current ripple by a large factor. In contrast, in the soft chopping mode, the low side transistors is left on during phase conduction period and the high side transistors (S_1 in Fig.2.10) is chopped according to the pulsed signal. It allows not only control of the current but also a minimization of the current ripple. In low speed operation, the commutation angle can be close to the aligned position as de-fluxing can be accomplished within very few degrees. Fig.2.13 shows typical waveform of switching signals, phase voltage, and the current along with the idealised inductance profile, for soft chopping mode of control.

Fig.2.14 shows typical waveform of switching signals, phase voltage, and the current along with the idealised inductance profile, for hard chopping mode of control

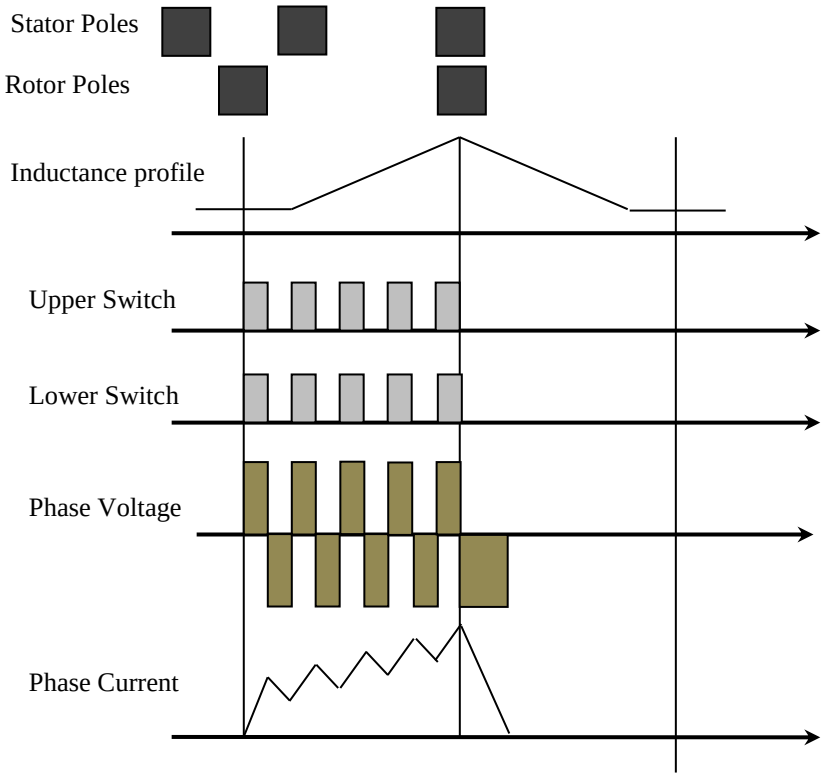

Fig.2.14 Hard chopping

2.9 Conclusions

The SRM drives for industrial applications are of recent origin. In this chapter brief introduction to SRM and its principle of operation are discussed. Key to an understanding of any machine is its torque expression, which is derived from first principles. The variation of motor winding inductance as a function of rotor position is explained in detailed. The implications of machine operation and its salient features are inferred from the torque expression. Various configurations of the SRM, including single-phase machines, are also discussed in detailed

The concept of control from the machine characteristics of inductance vs. rotor position for a fixed excitation is discussed in this chapter. The variables of control

such as advance rise and commutation angles are recognized and their dependence on machine inductance and speed, are discussed.

Chapter 3 Design of SRM

This chapter presents the design of a low power, 4-phase SRM that will be used to verify the design procedure and process for an automobile application. A 2D /3D model of the SRM is created using the results obtained from the design calculation. Finite element analysis (FEA) shows the expected characteristics of the designed SRM. The designed SRM is constructed and results from FEA match the performance of the experimental motor. The design procedure and FEA is used to predict the performance and design of a 4-phase, 1kW SRM designed for an automobile.

The design of SRM starts with the empirical formulae as obtained from the earlier design knowledge and extracted from the technical literatures available in (P. J. Lawrenson 1980; M.R. Harris and T.J.E. Miller 1989; N.N. Fulton and J.M. Stephenson 1988; L. Chen and Y. Zhou 1993; J. Faiz and J.W. Finch 1993; Krishnan, R 2001., Arumugam, R., Lindsay, F.F 1998).This includes the selection of various coefficients related to the motor geometry, magnetic and electric properties such as number of poles, rotor and stator pole arcs, core length, bore diameter, back iron thickness, number of turns in each phase, air gap.Certain references such as (Krishnan, R. 2001) do have a design procedure outlined but this does require a lot of background knowledge to implement. The procedure outlined in (Krishnan, R. 2001) also depends on some variable parameters, which requires intense design experience in SRM. Krishnan, R. (2001) develops an output equation similar to the output equation developed for induction machines and d.c. machines. This process requires extensive preceding knowledge and experience in designing switched reluctance machines. This thesis attempts to modify the design procedure described in Krishnan, R. (2001) to fit a manufacturer's needs while helping a machine manufacturer with no background in SRM design to build and test prototypes. With the selection of dimension and design results, a procedure to calculate the inductance in the aligned and unaligned position is as well required. This was firstly reported by (Corda, J. and Stephenson, J.M 1979) and many methods have been outlined by different authors including (Radun, A. 1999). The problems with this former stuff are the lack of transparency between the assumptions that are made and resulting equations. Therefore procedure outlined here allows the designers to use first

principles thus making it portable to different configurations of switched reluctance motors. The development here follows the procedure outlined in Krishnan, R. (2001) with more flux paths. Additionally, there is an attempt to calculate inductance in various intermediate positions of the rotor between the aligned and unaligned portions with varied success. Although, there are some significant errors caused by the assumptions made, the process can still be used as a rough analytical tool .The finite element method accomplishes final design fine-tuning verification and validation. Finite element method analysis was used by Dawson to determine the magnetic characteristics of an SRM Finite element analysis is used to obtain magnetic characteristics of machines by considering the saturation effect and by affixing the stator pole shoes. Method of modeling SRM is described and static analysis results are presented for SRM with three different stator pole arc sizes. Finally, the methods of inductance calculations in ANSOFT MAXWELL are discussed in detailed.

3.1 Design Procedure for a SRM

The successful applications of SRMs in automobiles depend highly on the proper design of the motors. However, there have been inadequate design experience and standards for SRM's as compared with more mature brushless dc motors and induction motors, due mainly to the limited applications so far and the complex design process of SRMs. Therefore, it is necessary to develop a set of design procedures for SRM's based on the existing design experience and the available design tools.

This section presents the procedures for the design of a switched reluctance motor in automobile applications. For the design of the SRMs, empirical method, finite element method and analytical method have been applied. The empirical formulas as established by design experts give way a preliminary design. The finite element method accomplishes design fine tuning and validation of preliminary design. The analytical method as established by the generalized electrical machine theory enables a study of converter control and dynamic performance

3.1.1 Design by Empirical Method

The design starts with the empirical formulas as obtained from the previous design experience and extracted from the technical publications **(**Arthur V. Radun 1985; A. R. Miles 1991; J. Faiz and J.W. Finch 1993; Krishnan, R., Arumugam R., Lindsay,

F.F 1998; Krishnan, R. 2001)**.** This involves the selection of various coefficients related to the motor geometry, magnetic and electric properties.

3.1.1.1 Machine Specification

The design specifications for the SRM comprise the required power output "P_{hp}" in h.p., motor speed N_r in rpm, allowable peak phase current i_p in amps, and available dc supply voltage V_{dc} in volts for the system. Knowing the speed and power output will automatically fix the torque to be developed by the machine as,

$$T_{req} = \frac{P_{hp} \text{ x } 745.6}{2\pi\left(\frac{N_r}{60}\right)} = \frac{P_{kw}}{2\pi\left(\frac{N_r}{60}\right)} \text{N. m} \quad (3.1)$$

Where P_{kw} is the power output in watts

3.1.1.2 Frame Size Selection

When the design procedure of a SRM is started, a good starting point as regards the physical dimensions of the machine would be a comparison with an equivalent induction motor [IEC71]. A comparison with an equivalent induction motor will fix the frame size of the SRM to be designed. This is advantageous as in many applications a SRM may be used to replace other machines. The IEC standards fix dimensions for all electrical machines made internationally according to the International Standards Organization (ISO) regulations and for machines made in the United States according to National Electrical Manufacturers Association (NEMA) regulations. During the progression of the design, if the machine size is found to be too large or too small, a different frame size can be used. The preliminary selection of frame size automatically fixes the outer diameter of the stator. Practically, the outer diameter of the stator is fixed as follows:

$$D_0 = (\text{FrameSize} - 3) \text{ x } 2 \text{ mm} \quad (3.2)$$

where the Frame Size is given according to the IEC recommendations [IEC71]. The 3 mm subtraction is used in industry to account for the foot of the machine, which is used for mounting.

3.1.1.3 Pole Selection.

Usually, the designer determines a common number of stator and rotor poles N_s and N_r and deviates from this fixed value only for very special applications because then converter configurations and feedback devices can be standardized. There are many possible combinations for the number of poles resulting in different phase numbers.

The choice of the number of phases mainly depends on the desired application and their required properties as it has been explored in detail by (T.J.E Miller 1991). Generally, it is preferred to have the ratio between N_s and N_r is a non integer. Based on this guideline, the stator and rotor pole combinations common in industrial designs are given below.

Table 3.1 Typical Stator and Rotor Pole Combination

	Poles					
Stator Poles, N_s	4	6	8	10	12	12
Rotor Poles , N_r	2	4	6	8	8	10

There are many possible combinations for the number of poles. This thesis primarily focuses on the popular combination of 8 stator and 6 rotor poles, also commonly known as the 8/6 machine. This machine has the advantage of lesser torque ripple than the other common combination of 6 stator and 4 rotor poles (6/4 machine) and has the disadvantage of using more switches in the converter, two extra terminals and higher core losses because of higher switching losses.

3.1.1.4 Air gap

To maintain balanced phase currents and minimize acoustic noise, the SRM needs a uniform air gap. The machine also requires a small air gap to maximize specific torque output and minimize the volt-ampere requirement in the converter. A small air gap decreases the minimum reluctance in the zone of stator-rotor-pole-overlapping and therefore increases the achievable torque. Nevertheless, the bending of the shaft and the expansion of the material with increasing temperature must be considered during design in addition to manufacturing tolerances. So, the air gap should be chosen in such a way that the machine works reliable under common operating conditions in every operating point. In practical, typical values of the air gap length are in the range of

$0.2 \leq l_g \leq 0.6\text{mm}$,

depending on the machine size and the properties of the application.

3.1.1.5 Stator and Rotor Pole Angle Selection

The stator and rotor pole angle selection forms a crucial part of the design process. There are many guidelines to be followed during the selection process. The standard design normally has the stator pole arc angle β_s smaller than the rotor pole angle β_r. The constraints on the values of pole arc angles are as follows

1. The stator pole arc angle is less than the rotor pole arc angle, i.e., $\beta_s < \beta_r$.
2. The effective torque zone is lesser than the stator pole angle β_s but greater than the stroke angle ε. The stroke angle is defined as

$$\varepsilon = \frac{2\pi}{\frac{N_s}{2} N_r} \tag{3.3}$$

In an 8/6 machine the stroke angle is $\varepsilon=15^0$.

If $\beta_s < \varepsilon$, then there may be some positions in the machine from where the machine may not start.

3.1.1.6 Output Equation

The output equation relates the bore diameter, length, speed, magnetic and electric loading to the output of a machine. In general, the conventional machines are designed starting from the output equation. A similar development of the output equation for the switched-reluctance motor will make its design systematic. Moreover, the experience of the machine designers can be effectively used in the design of these new machines, as they could use the commonality between these and the conventional machines. While the output equation of the switched-reluctance motor will be significantly different from that of the conventional machine, the emphasis here is placed on their similarities.

Fig.3.1 shows a schematic of an 8/6 SRM. Fig.3.2 shows the flux linkages versus current characteristics of the switched-reluctance motor for the unaligned and perfectly aligned position of the stator and rotor poles. Unaligned position of the stator and rotor poles means that the center of the stator pole is in between the two rotor poles.

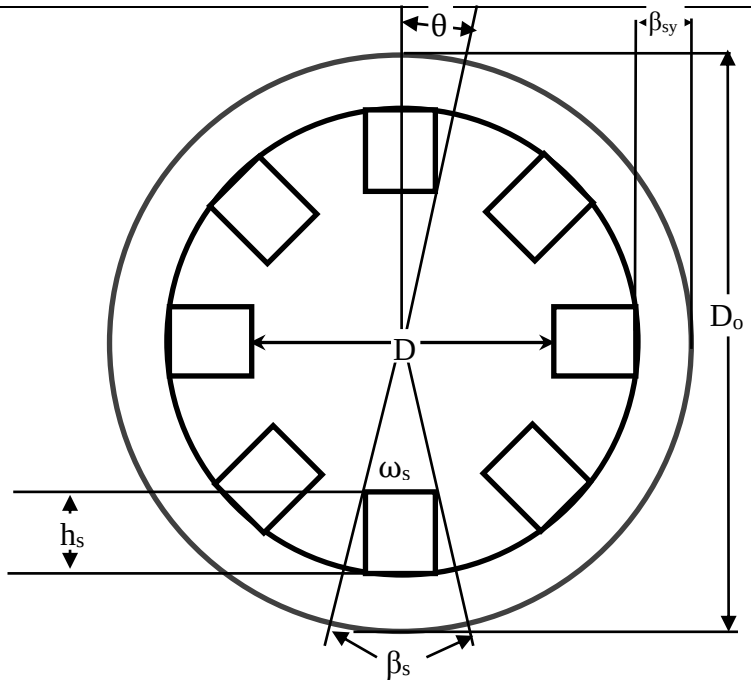

Fig.3.1 (a) Stator Schematic of a 8/6 SRM

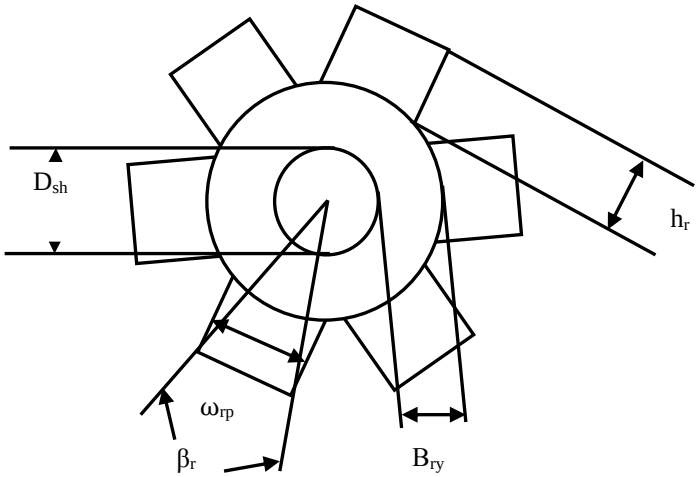

Fig.3.1 (b) Rotor Schematic of a 8/6 SRM rotor

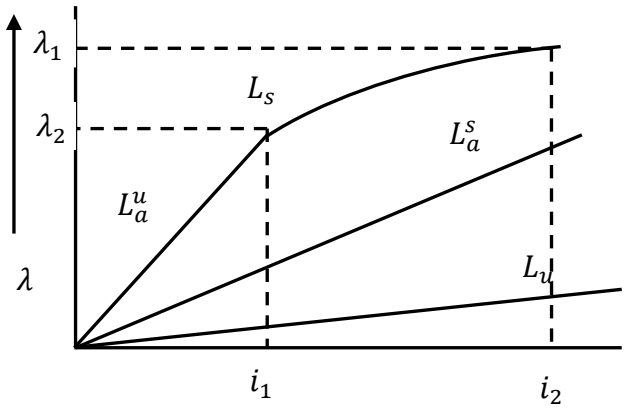

Fig.3.2(a) Flux linkages versus current for different values of rotor positions

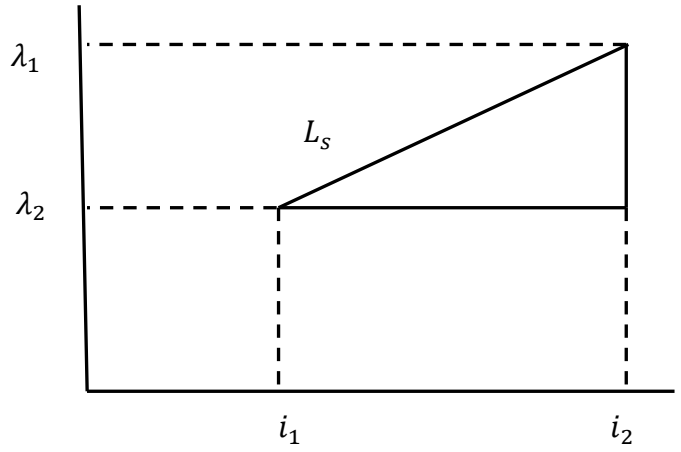

Fig.3.2 (b) Aligned Saturated Condition

(a) Voltage Equation per phase

$$V = \frac{d\lambda}{dt} = \frac{\lambda_a - \lambda_u}{t} \quad (3.4)$$

λ_a is the aligned flux linkage; λ_u is the unaligned flux linkage

λ = Flux linkage = Nϕ Weber turns. Where N is the number of turns and ϕ is the magnetic flux in Weber's and β_s is the angle of the stator pole arc. The time taken for the rotor to move from aligned position to unaligned position,

$$t = \frac{\beta_s}{\omega_m} \quad , \quad (3.5)$$

Where ω_m is the rotor speed in radians /second.

From Fig.3.2 (a) it is seen that when stator current increases, flux linkage also increases and it saturates at point c and then it comes to L_s at which it will be steady. L_s is the saturated inductance slope.

In the Fig.3.2(b) dotted lines indicates the aligned saturated condition. The motor is already in saturation from starting, on increasing stator current, flux linkage will increase. Flux linkage increases indefinitely correspondingly to the stator

σ_s is constant,

$$\sigma_s = \frac{L_a^s}{L_a^u} \quad (3.6)$$

L_a^s is the aligned saturated inductance and L_a^u is the unaligned unsaturated inductance.

$$\sigma_u = \frac{L_a^u}{L^u} \quad (3.7)$$

L_u is the unaligned inductance in Henrys.

From equation (3.4)

$$V=\frac{\lambda_a-\lambda_u}{t} \quad (3.8)$$

Where, $\lambda = L \times i$,

$\lambda_a=L_a^s \times i$,

$\lambda_u=L_u \times i$,

$$\frac{\lambda_a-\lambda_u}{t}=\frac{(L_a^s-L_u)i}{t}$$

$$V=\frac{(L_a^s-L_u)i}{t}$$

$$=\frac{L_a^s i}{t}\left[1-\frac{L_u}{L_a^s}\right]$$

$\frac{L_u}{L_a^s}$ is a constant.

$$\sigma_s \times \sigma_u = \frac{L_a^s}{L_a^u} \times \frac{L_a^u}{L^u}=\frac{L_a^s}{L^u}$$

$$V=\frac{L_a^s i}{t}\left[1-\frac{1}{\frac{L_a^s}{L_u}}\right]$$

$$V=\frac{L_a^s i}{t}\left[1-\frac{1}{\sigma_s\sigma_u}\right] \quad (3.9)$$

Magneto motive force, M.M.F = N x i in Ampere Turns (AT)

$$T_{ph} \times i = MMF = N \times i \quad (3.10)$$

The flux linkage in the aligned position in terms of flux and number of turns

$$T_{ph} \times \emptyset = \lambda = L \times i \quad (3.11)$$

L is aligned saturated inductance in Henry.

i.e. $\lambda = L_a^s \times i$, where i is rms value of the current through the phase

i.e. $L_a^s = \frac{(T_{ph} \times \emptyset)}{i}$

Substituting La^s in (3.9), we have

$$V=\frac{L_a^s i}{t}\left[1-\frac{1}{\sigma_s\sigma_u}\right]$$

$$=\frac{T_{ph} \times \emptyset \times i}{i \times t}\left[1-\frac{1}{\sigma_s\sigma_u}\right]$$

$$V=\frac{T_{ph} \times \emptyset}{t}\left[1-\frac{1}{\sigma_s\sigma_u}\right] \quad (3.12)$$

Flux, ϕ = B x Area where B is the flux density

$$= B \times \beta_s \times \frac{D}{2} \times L \quad (3.13)$$

where β_s is the angle in degrees, $\frac{D}{2}$ is the bore radius, ϕ is the flux density and L is the stack length

$$V=\frac{T_{ph} \times B \times \beta_s \times D/2 \times L}{t}\left[1-\frac{1}{\sigma_s \sigma_u}\right]$$

On substituting $t=\frac{\beta_s}{\omega_m}$ we have

$$V=\frac{T_{ph} \times B \times \beta_s \times D/2 \times L}{\frac{\beta_s}{\omega_m}}\left[1-\frac{1}{\sigma_s \sigma_u}\right]$$

$$V=\omega_m \times T_{ph} \times B \times D/2 \times L\left[1-\frac{1}{\sigma_s \sigma_u}\right] \quad (3.14)$$

where, ω_m is the rotor speed in rad/sec

(b) Specific Electric Loading: A_s

$$A_s = \frac{\text{Stator Current} \times \text{No.of Conductors}}{\pi \times D} \quad (3.15)$$

Conductors per phase is = 2 x T_{ph}

$$A_s = \frac{2T_{ph} i \times m}{\pi D} \quad (3.16)$$

m is the number of phases excited at a time. For 8/6 SR motor m=1

(c) Duty Cycle Constant

K_d is the duty cycle constant.

$$K_d = \frac{\theta_i \times q \times N_r}{360} = \frac{15^0 \times 4 \times 6}{360} = 1 \quad (3.17)$$

where θ_i is the current conduction angle in this case 15°, q is the number of the phases given by $\frac{N_s}{2}$, N_s is the number of stator poles, N_r is the number of rotor poles.

Here q = 4

(d) Power Equation

We know power developed per phase as

$$P_d = V \times i = V \times i \times m \quad (3.18)$$

where V is the voltage and i is the rms current, m is the number of phases conducting at a time and m =1 in this case. If K_e is the efficiency of the motor and K_d is the duty cycle constant then

$$P_d = K_e \times K_d \times V \times i \times m \quad (3.19)$$

Substituting $V=\omega_m x\, T_{ph}\, x\, B\, x \frac{D}{2} x\, L\left[1-\frac{1}{\sigma_s \sigma_u}\right]$ in above we get,

$$P_d = K_e\, K_d\ \omega_m\, T_{ph}\, B\ \times \frac{D}{2}\, x\, L\left[1-\frac{1}{\sigma_s \sigma_u}\right] im$$

Substituting for i

$$=K_e K_d\ \omega_m\, T_{ph}\ B \times \frac{D}{2}\, x\ L\left[1-\frac{1}{\sigma_s \sigma_u}\right]\frac{A_s \pi Dm}{2T_{ph} m}$$

$$P_d = K_e K_d \omega_m B \frac{D^2}{2}\ A_s\left[1-\frac{1}{\sigma_s \sigma_u}\right]\frac{\pi L}{2}$$

ω_m is the motor speed and $\omega_m=\frac{2\pi N_r}{60}$; N_r is the rated rotor speed in rpm.

Substituting ω_m, we have,

$$P_d = K_e K_d \frac{2\pi N_r}{60} B \frac{D^2}{2}\ A_s\left[1-\frac{1}{\sigma_s \sigma_u}\right]\frac{\pi L}{2}$$

Power equation in watts is

$$P_d = K_e\, K_d\ B\ \frac{D^2}{2}\ A_s\left[1-\frac{1}{\sigma_s \sigma_u}\right]\frac{2\pi^2 N_r L}{120}$$

where K_d and K_e are duty cycle and efficiency of the motor and are unity, B is the flux density under the stator pole in Tesla. Flux density in Tesla i.e. Weber/ meter ^{2}

$$K_2 = \left[1-\frac{1}{\sigma_s \sigma_u}\right]$$

K_2 is a constant varying from 0.65 to 0.75

And $K_1=\frac{\pi^2}{120}$

$$P_d = K_e K_d K_1 K_2 B A_s D^2 L N_r \qquad (3.20)$$

D & L we have to calculate Power/Phase and total power is same in the case of SRM.

3.1.1.7 Selection of Dimensions

(i) Diameter and Length

Here the stack length is assumed to be as the multiple or submultiples of rotor bore diameter.

$$L = KD$$

which on substitution in the output power equation in:

$$P_d \propto K_2 D^3 \qquad (3.21)$$

In general, the rated operating point, the range of K_2 is given by:

$$0.65 < K_2 < 0.75 \quad (3.22)$$

The values of B for the aligned position can be taken as the maximum allowable for the core material. The specific electric loading in ampere conductors per meter is usually in the range of:

$$25{,}000 < A_s < 90{,}000 \quad (3.23)$$

The duty cycle K_d can be assumed to be 1.

For stack length $L = K \times D$

For non-servo applications the range of K can be

$$0.25 < K < 0.7 \quad (3.24)$$

For servo applications it's usually the range given by

$$1 < k < 3 \quad (3.25)$$

(ii) Number of Turns

The number of turns T_{ph} is calculated as described earlier for a given current. The size is chosen such that the available winding space should be filled. The resulting current density is calculated and checked against the maximum permissible value. For a given specific electric loading and bore diameter it can be seen that the product of T_{ph} and 'i' is a constant

(iii) Stator Back Iron Thickness

The stator back iron thickness, β_{sy} is determined on the basis of maximum flux density in it and by the additional factor of vibration minimization to reduce acoustic noise.

If ω_{sp} is the pole width given in terms of pole arc as follows:

$$\omega_{sp} = D \sin\left(\frac{\beta_s}{2}\right) \quad (3.26)$$

Then the back iron thickness has to be minimum of $0.5\omega_{sp,}$ Thus to consider of mechanical robustness and minimization of vibration it could have a value in the range of:

$$\omega_{sp} > \beta_{sy} > 0.5\omega_{sp} \quad (3.27)$$

(iv) Stator coil Dimensions

The stator coil dimensions given by its width, ω_c and length ,$h_{c,}$ emerge from the area of cross –section of the conductor a_c, determined the current density and the number of turns per phase , T_{ph} .Let ω_{cs} is the width or gap to be left between two adjacent

coils in a slot at the bore including the slot liners. Stator coil area, in terms of number of turns and area of cross-section of the conductor is given by:

$$h_c \omega_c = \frac{a_c T_{ph}}{2} \quad (3.28)$$

$$\omega_c = \frac{\pi D}{2P_s} - \left(\frac{1}{2}\right)\left\{\frac{D}{2} \times \beta_s + \omega_{cs}\right\} \quad (3.29)$$

and from this ,

$$h_c = \frac{a_c T_{ph}}{2\omega_c}. \quad (3.30)$$

(v) Stator Pole Height

The minimum stator pole height is approximately, equal to the coil height, but the coil has to be held in place and for that a small space is required near the pole face. The coil seating at the root of the pole is not usually tight fitting; so, some additional space is lost which must be accounted for to calculate the stator pole height. So, by taking this into consideration all these factors,

The pole height of the stator is given by:

$$h_{c<} h_s < 1.4 h_c \quad (3.31)$$

(vi) Outer Diameter of Stator Lamination

$$D_0 = D + 2\beta_{sy} + 2h_s \quad (3.32)$$

(vii) Rotor Back Iron Thickness

The rotor back iron thickness, β_{ry} is based on structural integrity and operational flux density. It need not be as much as the thickness of stator back iron and neither has to be equal to the minimum value equal to stator pole width.

The rotor back iron thickness in terms of stator pole width is

$$0.5\omega_{sp} < \beta_{ry} < 0.75\omega_{sp} \quad (3.33)$$

(viii) Rotor pole Height:

For an air gap length of l_g, rotor back iron thickness and rotor shaft diameter the rotor pole height is given by:

$$h_r = \left[\frac{D - 2l_g - D_{sh} - 2\beta_{ry}}{2}\right] \quad (3.34)$$

where D_{sh} is the rotor shaft diameter

(ix) Stack Length (L):

$$L = K \times D \quad (3.35)$$

where K = 0.25 to 0.7

(x) Stator Back Iron Thickness (β_{sy}):

$$\omega_{sp} > \beta_{sy} > 0.5\omega_{sp} \quad (3.36)$$

where ω_{sp} is the stator pole width. $\omega_{sp} = D \sin\left(\frac{\beta_s}{2}\right)$ where β_s is the stator pole arc

(xi) Thermal consideration:

The thermal capability of the motor is one of the important characteristics. The thermal capability is determined by the losses in the machine, the available surface area for cooling and additional cooling arrangements provided by a fan or a blower or water- or liquid-circulated cooling.

3.1.2 Preliminary Design Calculation

$$P_d = K_e K_d K_l K_2 B A_s D^2 L N_r \quad (3.37)$$

Substituting known values as

$K_e = 1;\ K_d = 1$

$K_l = \frac{\pi^2}{120};\ K_2 = 0.65\ to\ 0.75$

B=$\frac{\mu_0 Ni}{l_g}$ where μ_0 is permittivity of free space =4π x 10^{-7}

N is the number of turns per pole=155, l_g is the air gap between the stator and rotor=0.23mm, i is the rms current through the phase=3A. Substituting the above values in the above equation we get

B=2.54 Tesla

L=K x D; K=0.25 to 0.7; $N_r = 12000$

$$P_d = \frac{1 \text{ x } 1 \text{ x } \pi \text{ x } 0.71 \text{ x } 0.4 \text{ x } 2.54 \text{ x } 2 \text{ x } 310 \text{ x } 3 \text{ x } D^2 \text{ x } N_r}{120}$$

$=35.1128 D^2 N_r$

$P_d = Total\ Power = 1000\ watts$

$$D^2 = \frac{1000}{35.1128 \text{ x } N_r} = 23.73 \times 10^{-4}$$

$D = (23.73 \times 10^{-4})^{\frac{1}{2}}$

$=0.048713$ m

$A_s =$ Specific Electric Loading

$$A_s = \frac{2T_{ph}im}{\pi D} \quad (3.38)$$

m is the number of phases excited at a time now we take m=1, T_{ph} is the number of turns per phase =310; i = 3A and D=48.71 mm ; Substituting the values we have

$A_s = 12154.71$

(i) Stator Pole height

If h_s is the stator pole height then

$h_c < h_s < 1.4h_c$

$h_c = \frac{a_c T_{ph}}{2\omega_c}$,where $\omega_c = \frac{\pi}{2}\frac{D}{p_s} - \frac{1}{2}\left\{\frac{D}{2} \text{ x } \beta_s + \omega_{cs}\right\}$

$= \frac{\pi r^2 x310}{2x5x10^{-3}}$

$= \frac{\pi x\left(0.23x10^{-3}\right)^2 x310}{2x5x10^{-3}}$

= 5.152 mm

5.152 mm < h_s < 7.213mm (3.39)

(ii) Outer Dimension of Stator Lamination (D_0)

$D_0 = D + 2\beta_{sy} + 2h_s$

= 48.7 + 2 x 8.80 + 2 x 7.213

= 80.726mm

(iii) Rotor Back Iron Thickness (b_{ry})

$\omega_{sp} = 8.87$

$0.5\omega_{sp} < \beta_{ry} < 0.75\omega_{sp}$ (3.40)

4.435mm< β_{ry} < 6.653mm

Since the sizing procedure described in the preceding section does not include the saturation effect of the motor, the preliminary dimensions, however could only serve as approximate design. Further quantitative analysis, such as electromagnetic performance evaluation and electromechanical dynamic simulation, are necessary for fine tuning the preliminary design. However, these detailed analysis could be realized if the magnetization data ψ ,i θ of the motor is available, therefore there are two methods to predict the ψ ,i θ characteristics, i.e analytical approach or FE numerical technique, The later is explain first in the next section, as it takes into a account the fringing effect and non linearity of the motor during the computation of the magnetic distribution

3.1.3 Design by Finite Element Method

Accurate and reliable modeling of the electrical systems is essential in performance prediction and verification of the systems (Zhang, Y., X. Wei, and E. Li 2004). The Finite Element Method can be one of the best choices for providing realistic and precise model. Also, 3D-FEM has advantages over 2D in many applications modeling for example the skew effect, end ring effect and some other practical issues such as motor length are missed in two dimensional analyses. This method considers the geometric and magnetic of the motor to solve for the magnetic field distribution in and around the motor. Moreover, machine parameters such as flux density, flux linkage, coil inductance and torque can be achieved from resulted magnetic field.

The SRM modeling under normal and abnormal conditions is complicated in comparison with the ac or dc machines because of operating in nonlinear region. Therefore, in this section a three dimensional finite (Arumugam, R., Lowther, D.A., Krishnan, R. and Lindsay, J.F.1985; Parreira, B., S. Rafael, A.J. Pires, P.J. Costa Branco, 2005) is being employed to assess the magnetic field distribution in and around the motor. In order to present the operation of the motor and to determine the motor parameters at different positions of the rotor, the field solutions are obtained. There are two common methods for solving magnetic field problems one utilizes magnetic vector potential **A** and the other one employs electric vector potential **T**. From the poison's equation the relationship for magnetic vector potential and current density is given by

$$\nabla^2\vec{\mathrm{A}} = -\mu \mathrm{J} \tag{3.41}$$

The partial differential equation for the magnetic vector potential is given by;

$$-\frac{\partial}{\partial \mathrm{x}}\left(\gamma\frac{\partial\vec{\mathrm{A}}}{\partial \mathrm{x}}\right)-\frac{\partial}{\partial \mathrm{y}}\left(\gamma\frac{\partial\vec{\mathrm{A}}}{\partial \mathrm{y}}\right)-\frac{\partial}{\partial \mathrm{z}}\left(\gamma\frac{\partial\vec{\mathrm{A}}}{\partial \mathrm{z}}\right)=\mathrm{J} \tag{3.42}$$

where,J and A are the current density and magnetic vector potential. Equation (3.42) is replaced with energy functional given by

$$F\left(\vec{A}\right)=\frac{1}{2}\int\left(\frac{\nabla\bar{\mathrm{A}}.\nabla\bar{\mathrm{A}}}{\mu}+\bar{\mathrm{A}}.\mathrm{J}\right)\mathrm{dV} \tag{3.43}$$

and equation (3.43) can be expanded as

$$F\left(\vec{A}\right)=\frac{1}{2}\iiint_{\alpha}\left[\gamma\left(\frac{\partial\vec{A}}{\partial x}\right)^2+\gamma\left(\frac{\partial\vec{A}}{\partial y}\right)^2\gamma\left(\frac{\partial\vec{A}}{\partial z}\right)^2\right]d\alpha-\iiint_{\alpha}J\ \bar{\mathrm{A}}\mathrm{d}\alpha \tag{3.44}$$

where, α is the problem region of integration. The field analysis has been performed using an **ANSYS ANSOFT MAXWELL** package which is based on the variational energy minimization technique to solve for the electric vector potential. In this method, electric vector potential known as T - Ω formulation in their **T** defined by;

$$\vec{J} = \nabla \times \vec{T} \tag{3.45}$$

from the Maxwell's equation we have

$$\nabla \times \vec{H} = \vec{J} = \nabla \times \vec{T} \tag{3.46}$$

Then

$$\nabla \times (\vec{H} - \vec{T}) = 0 \tag{3.47}$$

Since the vector ($\vec{H}$ -$\vec{T}$) can be expressed as the gradient of a scalar i.e

$$\vec{H} = \vec{T} - \nabla\Omega \tag{3.48}$$

where, Ω is a magnetic scalar potential

And since

$$\nabla \times \vec{E} = -\frac{\partial \vec{B}}{\partial t} \tag{3.49}$$

Then

$$\nabla \times \vec{E} = \nabla \times \left[\left(\frac{1}{\sigma}\right)\nabla \times \vec{T}\right] = -\frac{\partial \vec{B}}{\partial t} = -\mu_o \mu_r \frac{\partial \vec{H}}{\partial t}$$

$$= -\mu_o \mu_r \frac{\partial}{\partial t}(\vec{T} - \nabla\Omega)$$

$$= -\mu_o \mu_r \frac{\partial \vec{T}}{\partial t} - \nabla \frac{\partial \Omega}{\partial t} \tag{3.50}$$

which finally reduces to the following two scalar equations

$$\nabla^2 \vec{T} - \mu\sigma\left(\frac{\partial \vec{T}}{\partial t}\right) = -\mu\sigma\nabla\left(\frac{\partial \Omega}{\partial t}\right) \tag{3.51}$$

$$\nabla^2 \Omega = 0 \tag{3.52}$$

3.1.4. Modelling of SRM.

In this section, finite element analysis is used to obtain magnetic characteristics of machines by considering the saturation effect and by affixing the stator pole shoes. Method of modeling SRM is described and static analysis results are presented for SRM with three different stator pole arc sizes.

The Information of the SR motor under test in this section is shown in Fig.3.3 and Table 3.2 respectively. The stator and rotor cores are made up of non-oriented silicon

steel laminations and, each phase winding consists of 155 turns/ pole. Table 3.3 shows the conditions of analysis.

Table 3.2 8/6 SR motor dimensions

Parameter		Value
Number of Phases	:	4
Number of turns per pole (approx)	:	155
Rated output power (kW)	:	1
Rated Current (A)	:	18
Rated Voltage (V)	:	72 V dc
Rated speed (RPM)	:	12000
Rotation	:	bidirectional
Shaft diameter (mm)	:	17
Stator outer diameter(mm)	:	90

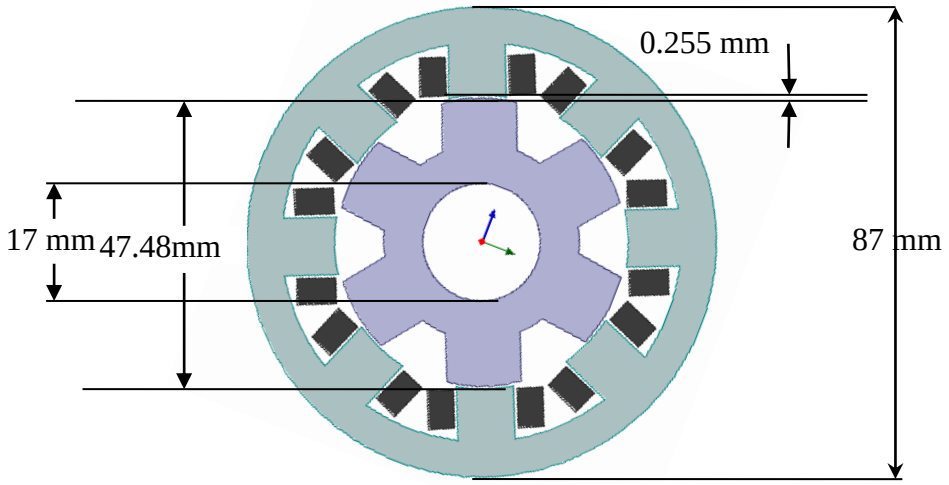

Fig.3.3 Analytical Model

Using the analytical model as shown in Fig.3.3, the calculation is carried out by three dimensional magnetic field analysis. The 2-dimensional FE model with mesh densities of SR motor with unequal pole arcs of stator and rotor used in the simulation are shown in Fig.3.4 and Fig.3.5 respectively. The intricate geometry of SRM has, however, posed precision problems in its field computation. Mainly, for those finite

elements located at the machine gap. Air gap has a higher degree of changing the magnetic quantities.

Table 3.3 Conditions of Analysis

Number of nodes	35033
Shape of element	Triangle
Excitation phase of coil	:One phase Only
Excitation current	:10 A
Analysis of range	:0~30/60 degrees

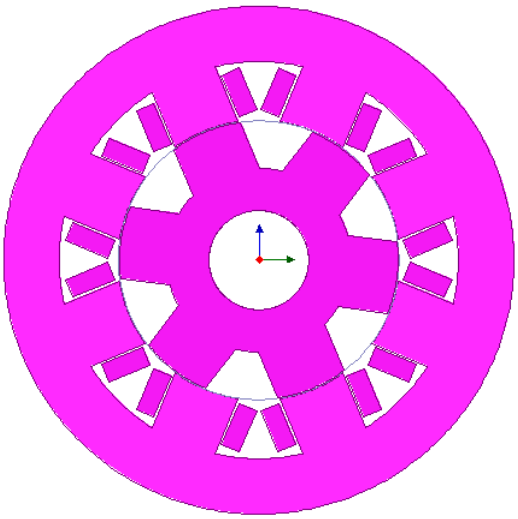

Fig.3.4 8/6 SRM 2D-FEM model assembly.

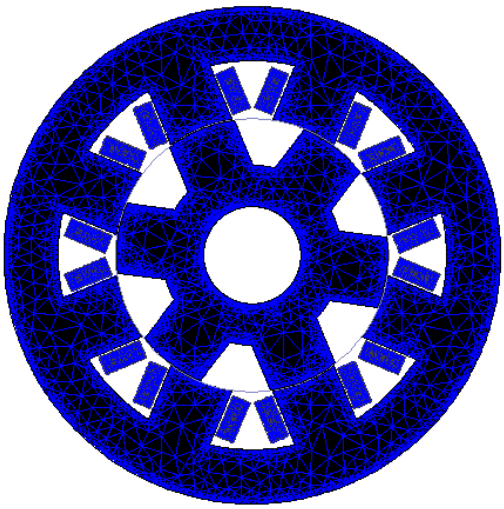

Fig.3.5 2-D Finite elements mesh density for the SRM.

3.1.4.1 Calculation of static torque and Inductance:

Static analysis is carried out after the modeling and applying of boundary conditions to motor. So one of the stator phases for example phase “A” is excited. Since the pole number of rotor is 6, the magnetic circuit becomes the same after rotating 60 degrees, when only one phase is excited. In additions, the stator salient pole and rotor salient pole repeat facing condition and non-facing conditions for the interval of rotation 30 degrees. It is possible to obtain the inductance of the 360 degrees rotation by using calculated inductance of the 30 degree rotation, if such geometric symmetry is utilized. Then, non-facing condition of stator salient pole and rotor salient pole is defined as “0” degrees and the rotor is made to rotate 30 degrees of the facing

condition. For each 2 degrees, the inductance and static torque of one phase are calculated and calculation of self inductance can be obtained by the following relation

$$L(\theta) = \frac{\lambda(\theta)}{i}, \quad i = \text{constant} \tag{3.53}$$

Also average torque can be calculated by

$$T_{avg} = \frac{1}{\tau}\int_0^{\tau} T(\theta)\partial\theta \tag{3.54}$$

where $\tau = \frac{\pi}{6}$; for 8/6 SRM and T(θ) is the torque at position θ

Equation (3.54) in discrete format can be written as

$$T_{avg} = \frac{1}{n}\sum_{j=1}^{n} T(j) \tag{3.55}$$

Where n is the number of steps that rotor rotates from unaligned to aligned positions and T(j) is the calculated torque in j^{th} stage.

Fig.3.6 (a) show the inductance L (θ) in rotor position calculated using equation (3.53) and reluctance torque T (θ) is calculated using the equation (3.55). Fig. 3.6 (b) shows static torque T (θ) in rotor position.

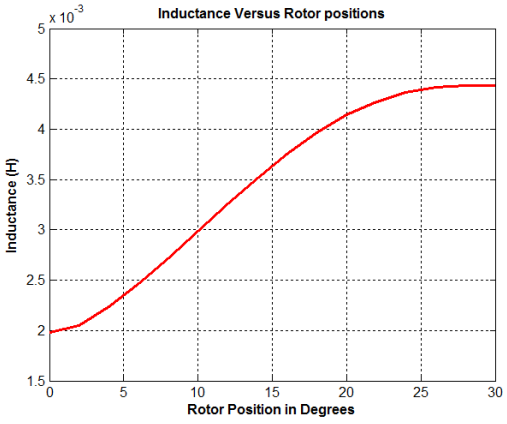

Fig.3.6(a) Calculated results of inductance with I=18A(Rated Current)

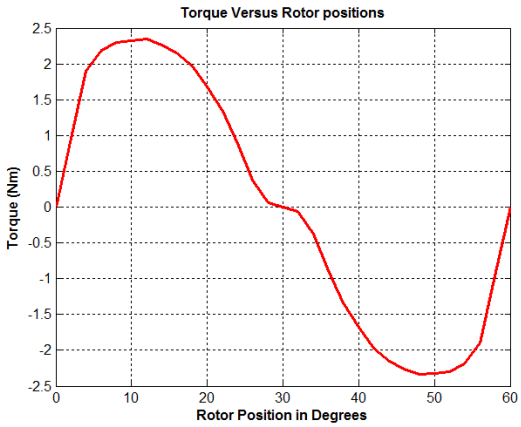

Fig.3.6 (b) Calculated results of static torque with I=18A(Rated Current)

T (θ) of the positive direction is obtained regardless of the current direction, if the exciting current is flowing when L (θ) increases, because T (θ) is proportional to the derivate for the rotor position of the inductance. In short , the rotor keeps rotating in the positive direction, because the torque of the positive direction is obtained at every excitation, when winding is continued to be excited in the position where the gradient of L(θ) become positive direction

3.1.4.2 Magnetization Curves:

The current excitations per stator pole are selected to be from 1.5 A to 18 A in order to investigate the saturation effect, to calculate the torque characteristics and flux linkages under various current excitation levels. The range of rotor position angles is from ‘0’at the rotor stator unaligned position to ‘30’ aligned position. This range allows the study on the rotor positions of the entire SRM control cycle

Fig.3.7 shows magnetization curves for different current excitations. In unaligned position air gap then reluctance is maximum and saturation don’t occur, so flux linkage is linear function of current. But saturation in magnetization curves happen , when the overlap between the corners of stator and rotor poles is very negligible; therefore, the focusing of flux in the corners causes saturation (Fig.3.8) and the linear relation between the current and flux linkage to be destroyed, which is true even for low excitation currents. Second, whenever the overlapped poles are closer to align position, yokes are saturated (Fig.3.9) at high currents and have tendency toward flux linkage to be limited in a maximum limit. Static Torque Characteristics with different current excitations is shown in Fig.3.10

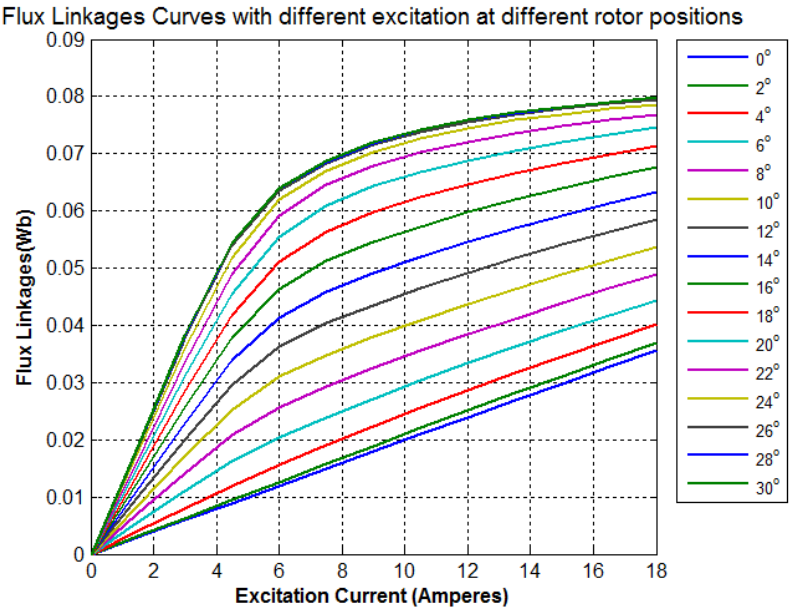

Fig.3.7 Magnetization curves of SRM with different excitation

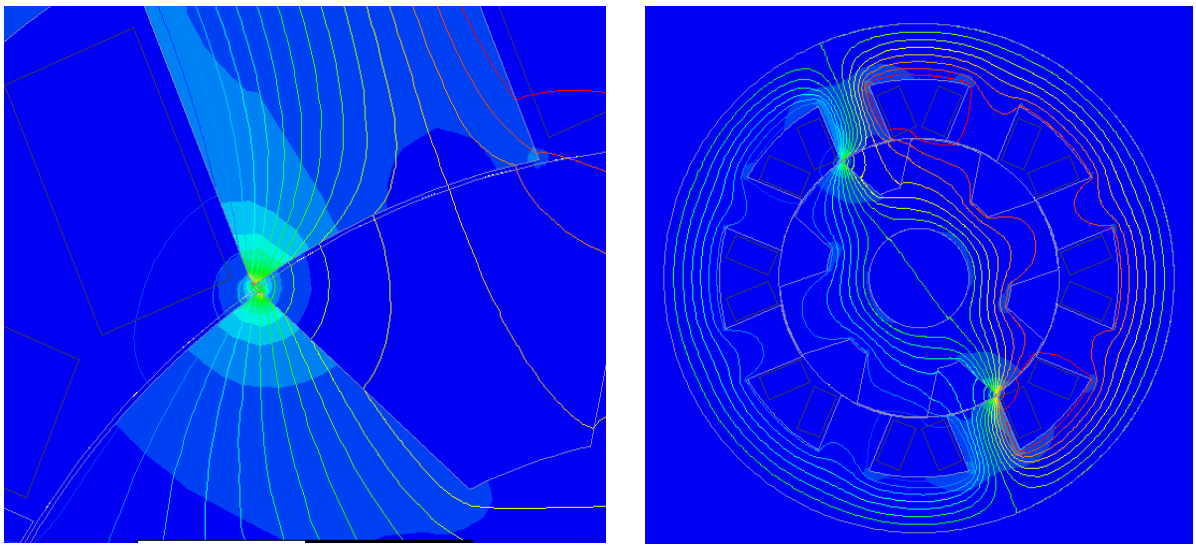

Fig.3.8 Permeability of basic SRM at the beginning of overlapping between stator and rotor poles (Un Aligned) with excitation current of 1.5 A

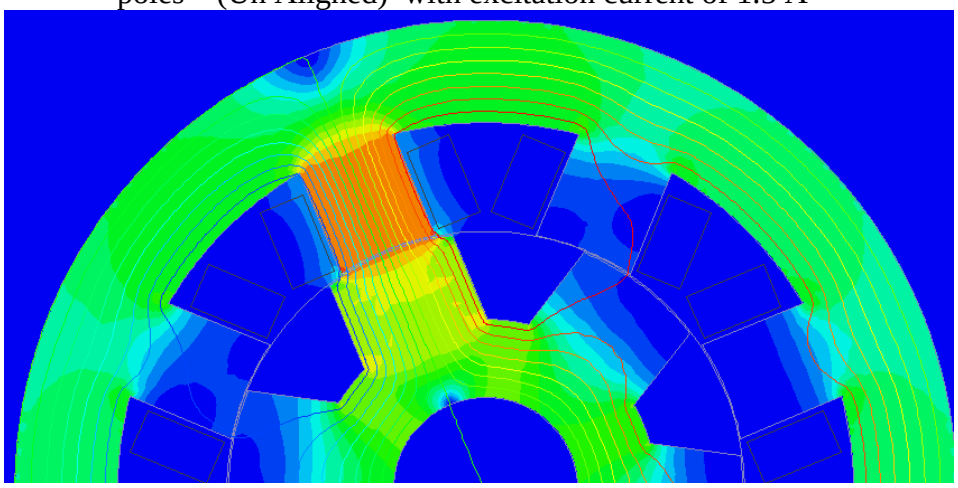

Fig.3.9 Flux distribution of basic SRM when both stator and rotor are overlapped poles (Completely Aligned) with energised phased carry excitation current of 50A

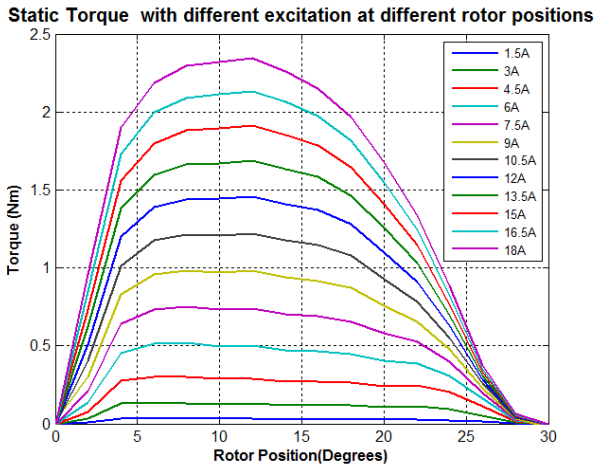

Fig.3.10 Static Torque Characteristics with different current excitations

3.1.4.3 Effect of Stator pole widths:

In this section, flux linkage, inductance and torque produced by switched reluctance motor are analyzed by introducing stator design modification such as variation in stator pole width.

Let βs be the stator pole arc and βr the rotor pole arc. For sensitivity study of the stator pole arc on SRM inductance, flux linkages and static torque by keeping other design parameters, stator pole arc sizes are chosen in three values i.e βs =22.5°, βs =30°and βs =37.5° as shown in Fig.3.11

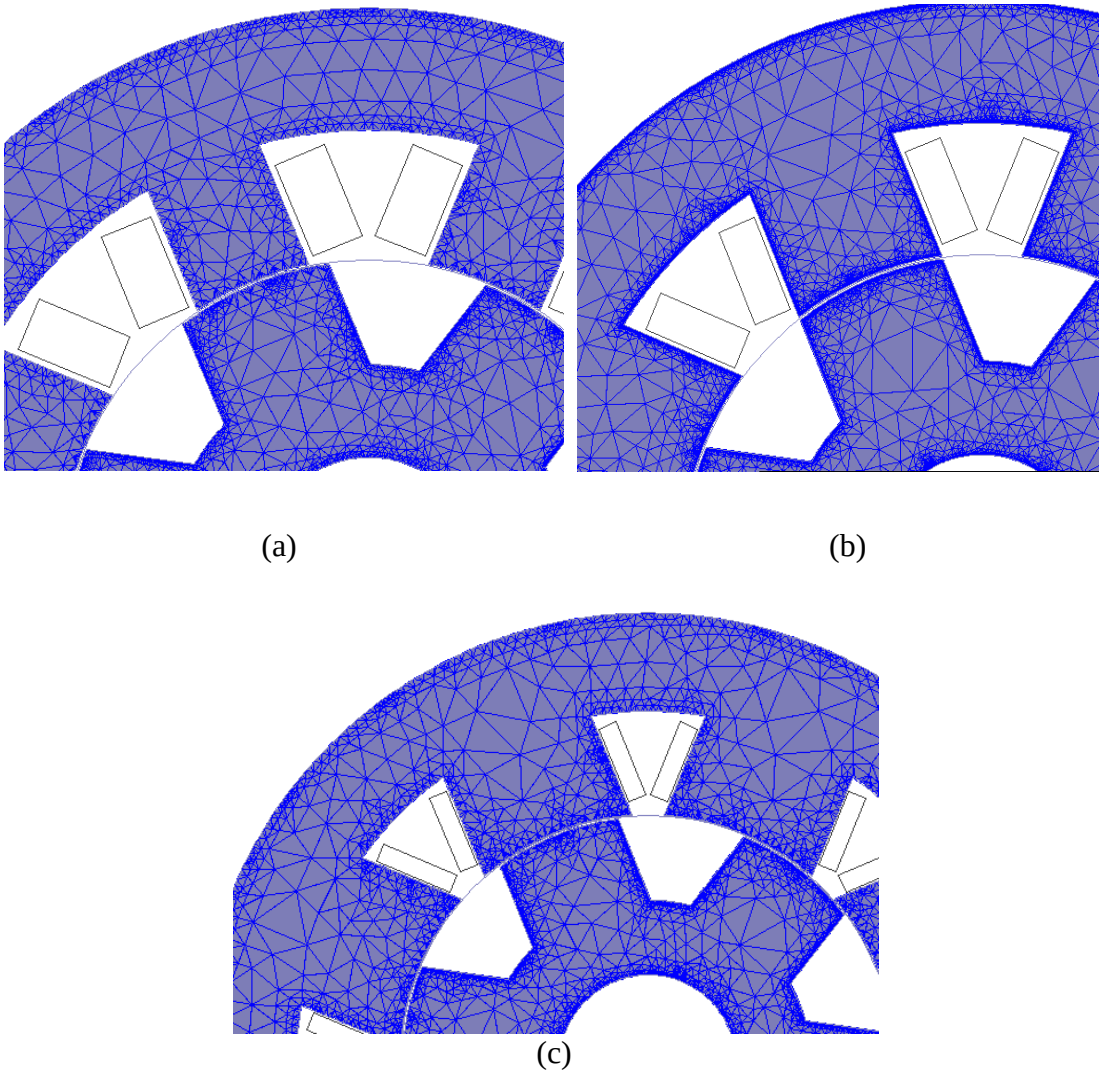

(a) (b)

(c)

Fig.3.11 Meshing of stator and rotor poles (a) βs =22.5° (b) βs =30° (c) βs =37.5°.

Using magnetization curves and with a given excitation current, inductance is calculated in each rotor position. Also, static torque profiles can be obtained by using

magnetization curve data. Magnetization curves for three stator pole geometry of SRM are shown and compared in Fig.3.12 for aligned and unaligned positions

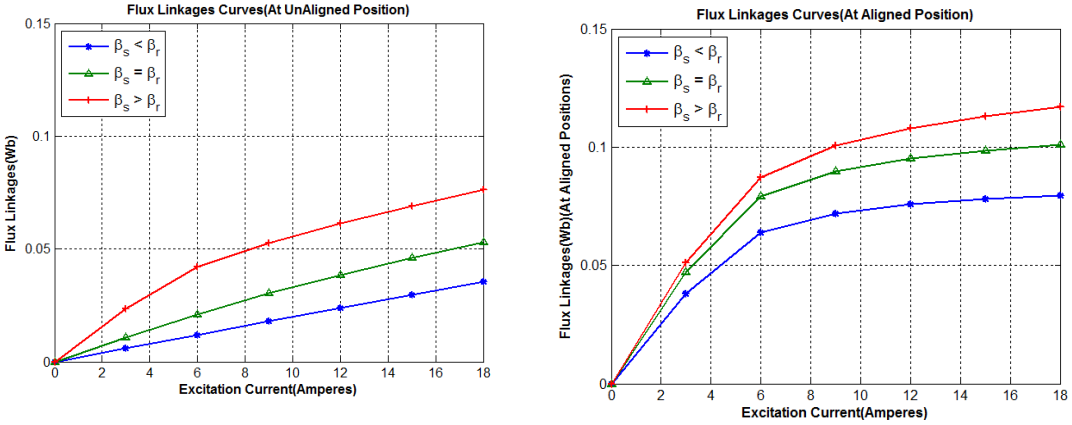

(a) Un Aligned position (b) Aligned position

Fig.3.12 Magnetization curves of SRM (βs =22.5°, βs =30°, βs =37.5°)

By comparing the characteristic curves in Fig.3.12 it is observed that by affixing the pole shoes to stator poles, flux linkage has increased where this increase is more notable in regions between unaligned to aligned positions and it's in aligned position negligible, but pole shoes approximately have less effect on unaligned position which is due to high reluctance between stator and rotor under this condition.

The reasons for the increase in flux linkage, by affixing pole shoes, can be accounted for by shortening the flux route between stator and rotor poles, and because of this, route reluctance decreases (specially from unaligned to a position that stator and rotor start to overlap). Flux linkage of phase A vs. rotor position (βs =22.5°) for different excitation currents is Fig.3.13. Other phases will have similar curves. For state of βs =22.5° (βr > βs) with an increase in current excitation, flux linkage of unaligned position has negligible increase. However flux linkage by closing the aligned position has a notable increase. Also, because of more increase in current limit, saturation effect limiting the flux linkage in environs of aligned position is seen well as in Fig.3.13

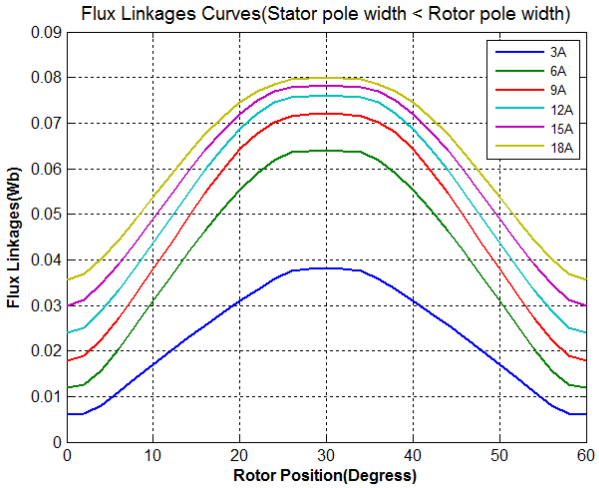

Fig.3.13 Flux linkage vs. rotor position for βs =22.5° (βs < βr).

(a) Inductance Profiles:

Inductance profiles of SR motor with βr > βs, βr = βs, βr < βs are shown in Fig.3.14 for different current excitation values. With attention to each of the inductance profiles, it's completely clear that for different excitation currents at closing the unaligned position (until θ=2° for βr > βs and until θ=1° for βr = βs and θ=5° for βr < βs), inductance has equal values, approximately

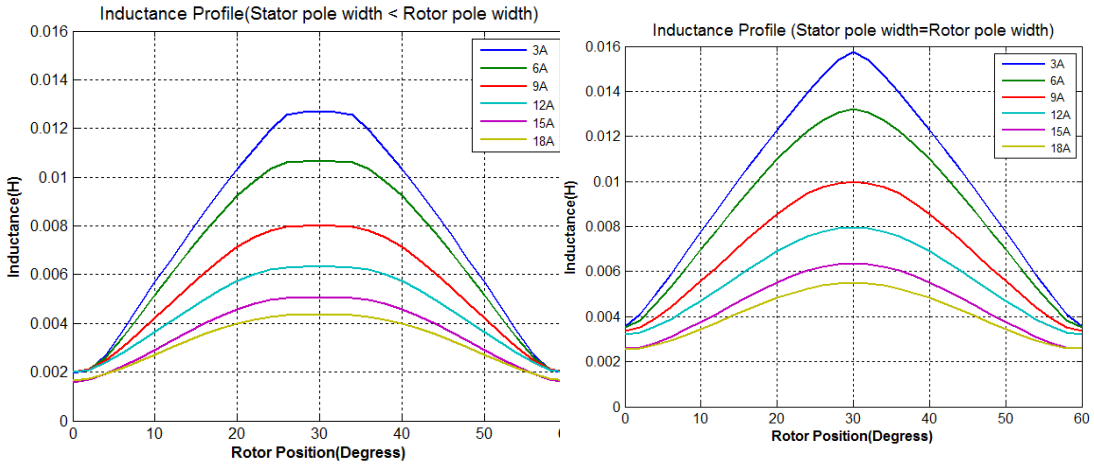

(a) (b)

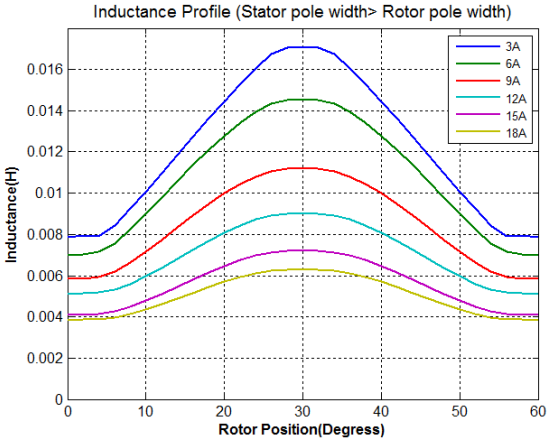

(c)

Fig.3.14 Inductance vs. rotor position for (a) βs =22.5 ° (βs < βr)
(b) βs =30° (βs = βr) , (c) βs =37.5° (βs > βr)

Also, inductance profiles have nearly linear part for low values of excitation currents and in case of increasing the excitation current (by starting the overlap between stator and rotor and by reasons of saturation) the value of aligned inductance (L_{max}) has reduced. To take into consideration the inductance profiles of Fig.3.15, it seems clear that pole shoes affect inductance profiles and cause them to increase a modest. Also, in the regions that overlap is started between stator and rotor (with a few degrees of difference between three states of motor), rising slope of inductance is substantial because these regions have much effect on production of flat torque (low torque ripple).

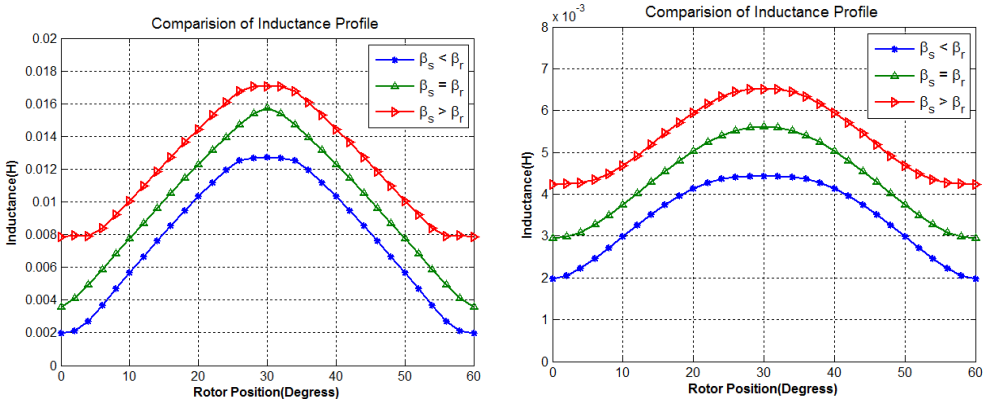

(a) (b)

Fig.3.15 Comparing Inductance profiles for three states of SRM with excitation currents of (a) I=3A. (b) I=18A

In Table 3.4 maximum inductance per minimum inductance ratio value for different current values is presented for SRM with βr > βs, βr = βs and βr < βs, which explains how much the static analysis for a given current the ratio of $\frac{L_{max}}{L_{min}}$ in three different stator pole sizes has near values toward each other. Modifications should be undertaken to maintain this almost the same ratio to avoid any reduction in the static torque per ampere. According to Table 3.4, it seems that the values of $\frac{L_{max}}{L_{min}}$ ratio are reduced by increasing the β_s for higher current values. So an upper limit should come into account. If for value of β_s the increase continues, this will lead to a larger decrease in the static torque per ampere, at the cost of which, torque ripple minimization should not be expectant.

Table 3.4: Ratio of $\frac{L_{max}}{L_{min}}$ for various currents

Excitation Current(A)	$\frac{L_{max}}{L_{min}};\ \beta_r > \beta_s$	$\frac{L_{max}}{L_{min}};\ \beta_r = \beta_s$	$\frac{L_{max}}{L_{min}};\ \beta_r < \beta_s$
3	6.4119	4.4014	2.1676
6	5.3673	3.7654	2.0790
9	4.0139	2.9640	1.9161
12	3.1751	2.4674	1.7635
15	3.1751	2.4674	1.7635
18	2.6199	2.1379	1.6378

(b) Static torque Profiles:

From the foundation reluctance torque, positive torque is generated when each phase is excited during the rising of inductance, and vice versa (negative torque is produced by falling of inductance). Static torque relevant to stator poles of βr > βs, βr = βs, βr < βs for different current excitation is shown in Fig.3.16.

Comparison of static torques for current values of 3A and 18A for three stator pole arcs are shown clearly in Fig.3.17 with great value of stator pole arc size, torque profile is improved. So the maximum torque is allowed to remain the same for more positions of rotor. On the other hand, by increasing stator pole arc, inductance profile is modified and therefore with attention to torque profile in Fig.3.17, position and inductance rising slope is not similar to the three states and by the reasons of its role on production of torque, rising slope of βr < βs is desired than other states. By affixing pole shoes to stator poles, the possibility of using firing angles (turn on angle)

near the unaligned position increases. Pole arc sizes for stator (following it, pole shoes) depend on some parameters like the value of torque ripple and requested average torque which has an upper limit because of leakage reasons.

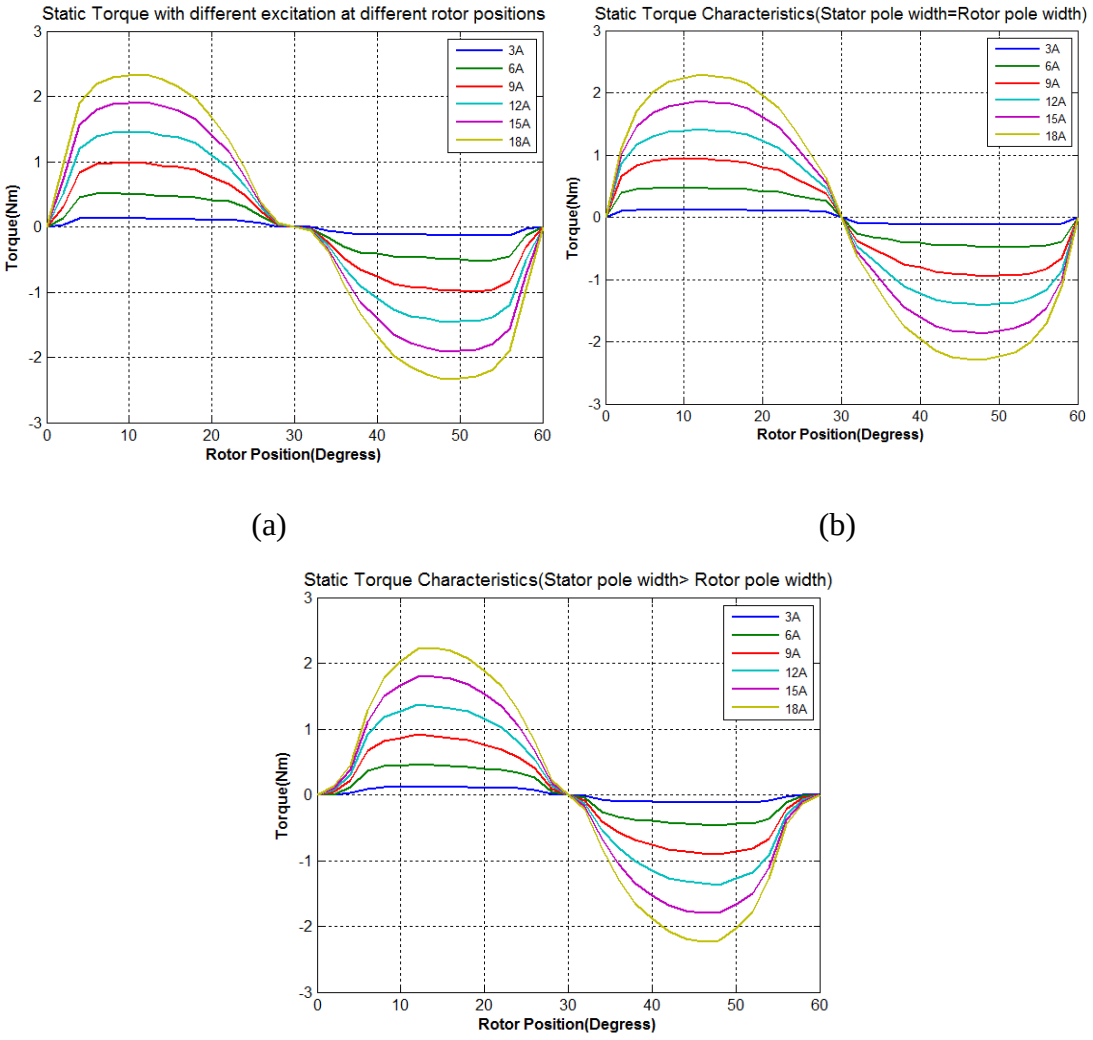

(a) (b)

(c)

Fig.3.16 Static torque vs. rotor position for (a) βs =22.5° (βs < βr) (b) βs =30° (βs = βr) ,(c) βs =37.5° (βs > βr).

Conclusions:

In the above section, processing the static modeling of 8/6 SRM with three different stator pole arcs sizes is described. The result of static analysis, including inductance, flux linkage, and static torque vs. rotor position for various current excitations by considering saturation effect in three states of motor different stator pole widths are investigated. The effect of the increase in stator pole arcs is presented for improving SRM performance.

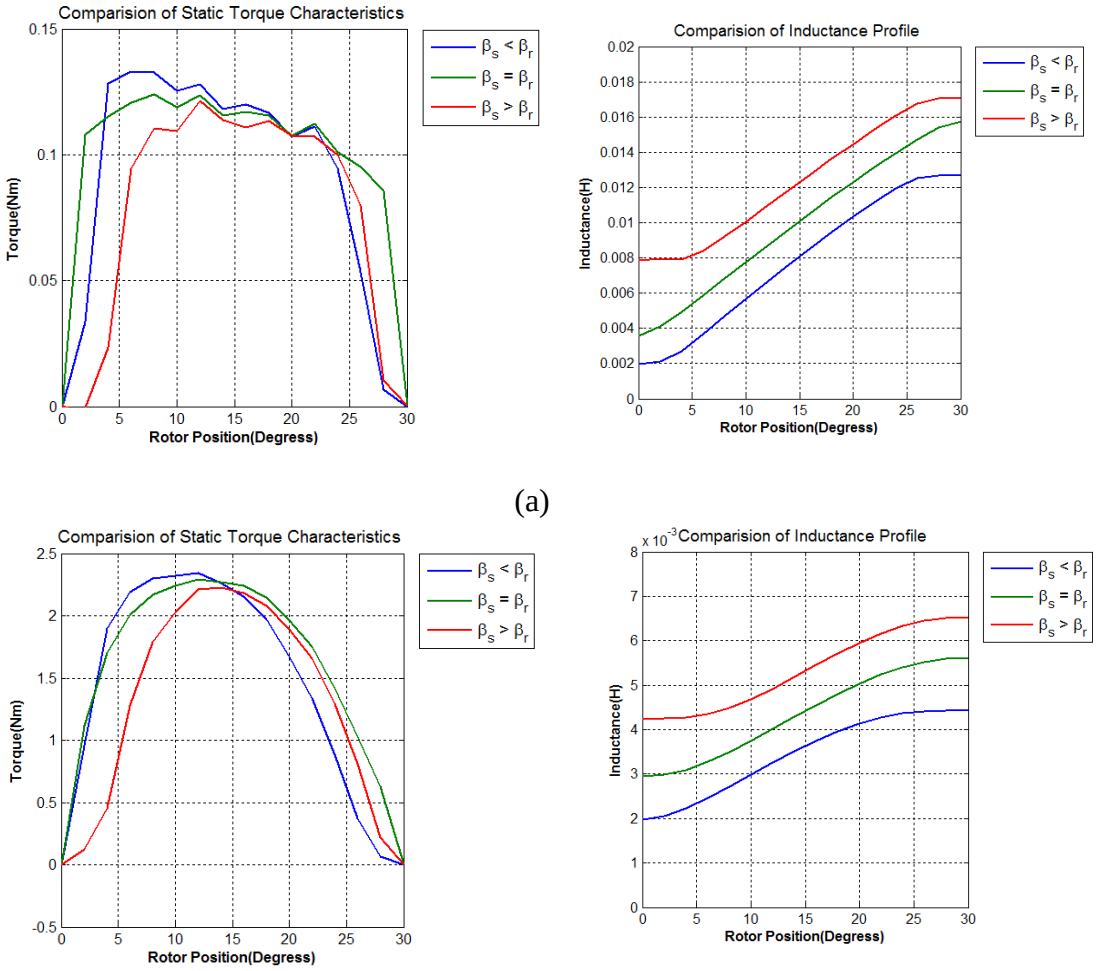

Fig.3.17 Static torque and Inductance vs. rotor position for (a) I=3A. (b) I=18A.

3.1.4.4 Effect of Air gap:

In this section, torque produced by switched reluctance machine is analyzed by introducing rotor design modification such as variation in air gap.

Flux linkages, inductance profiles and static torque characteristic characteristics of SR motor with βr > βs, βr = βs, βr < βs for current excitation of 12 A and air gap lg=0.25mm, 0.5mm and 0.75mm are shown in Fig.3.18

It clearly shows the strong influence on the maximum torque as well as the flat torque range on the characteristics. Hence the machine with the smallest air gap length, subject to acceptable manufacturing tolerances, will produce the highest average torque. The torque ripples can be slightly reduced by growing air gap length.

However, the original air gap length of l_g=*0.25mm* and therefore the rotor outer diameter remain unchanged due to manufacturing tolerances.

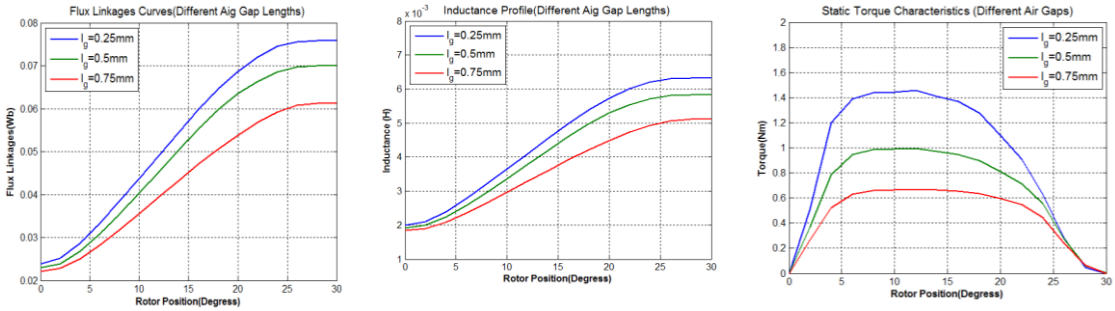

(a) Stator pole width < Rotor pole width

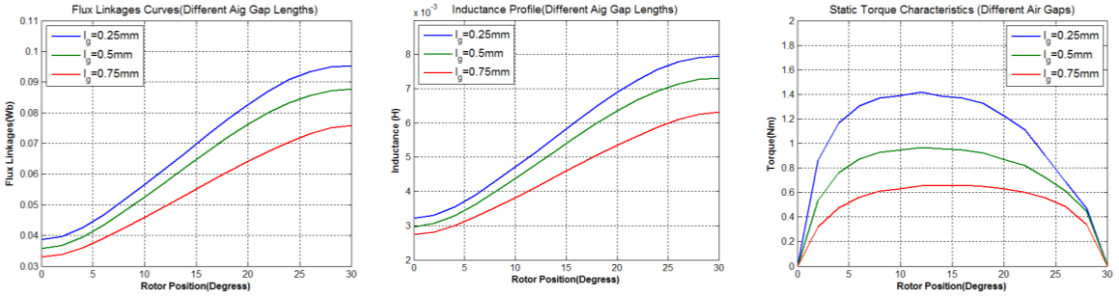

(b) Stator pole width =Rotor pole width

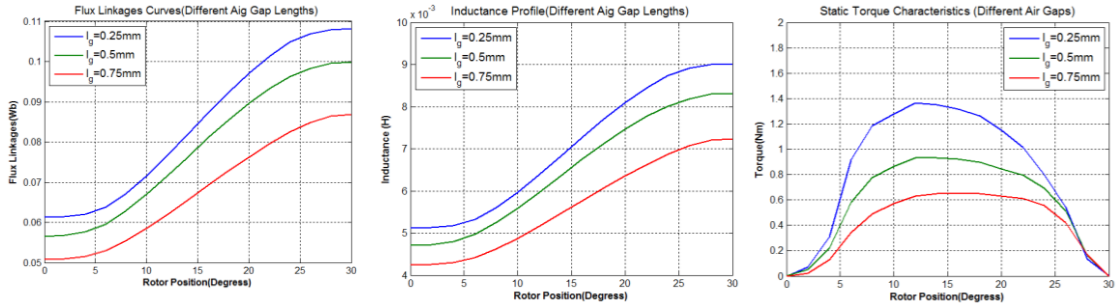

(c) Stator pole width>Rotor pole width

Fig.3.18 Performance curve of SR motor for different air gaps

3.1.4.5. Effect of Stack Length (Motor Length):

In this section, torque produced by switched reluctance machine is analyzed with different stack lengths.

flux linkages, inductance profiles and static torque characteristic characteristics of SR motor with βr > βs, for current excitation of 3 A and Stack lengths , L=20mm, L=40mm,L=60mm and L=80mm are shown in Fig.3.19.

In this section, processing the static modeling of 8/6 SRM with three different stator pole arcs sizes is described. It is observed that, with the increase in stack length, static

torque increases due to the increase in flux density, as the area of the pole core increases, due to increase in stack length.

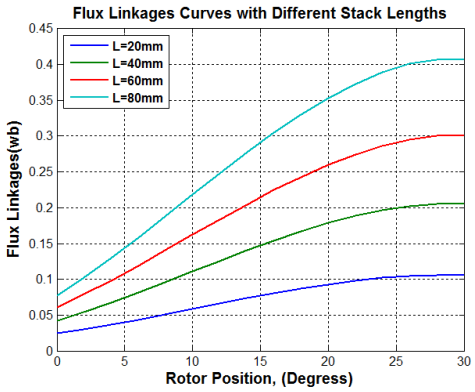

(a)Flux Linkage Curves

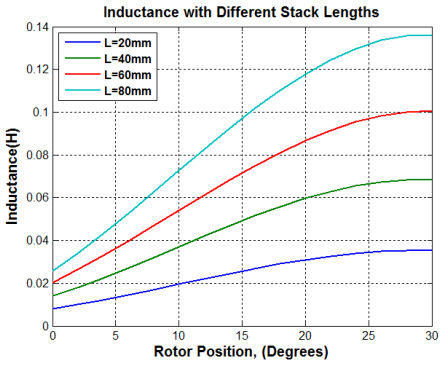

(b)Inductance Profile

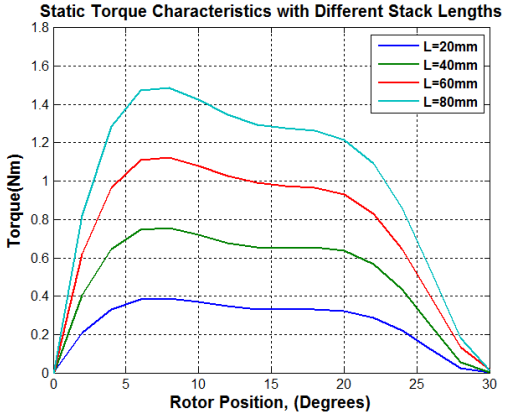

(c)Static Torque Characteristics

Fig.3.19 Performance curves of SR motor for different Stack Lengths

3.1.4.6 Summary:

The finite element geometries based on the preliminary design in are modified to include the variations in air-gap, stator pole, rotor pole widths and stack lengths. The total current excitations per stator pole are selected to be 1.5 A, to 18 A, in order to investigate the saturation effect, to calculate the torque characteristics and flux linkages under various current excitation levels. The range of rotor position angles is from 0" at the rotor stator aligned position to 30". This range allows the study on the rotor positions of the entire SRM control cycle. These comparative studies lead to the selection of several preferred SRM geometries. The final selection of SRM geometry is based on an investigation into the torque generation under the converter control, which requires the evaluations of SRM flux linkage and inductance

3.1.5 FEM Model of SR Motor

From the values obtained from the basic equations derived from the output equations, and other parameter, a FEM based SRM is designed. As per the requirement for automobile application, fine tuning of the basic design structure is carried using FEM. The FEM based SRM model is shown in Fig.3.20. Fig.3.20(a) represents stator design, Fig.3.20 (b) represents rotor design Fig.3.20 (c) represents both stator and rotor design. Fig.3.20 (d) represents 3-dimensional transparent view of stator & rotor structures

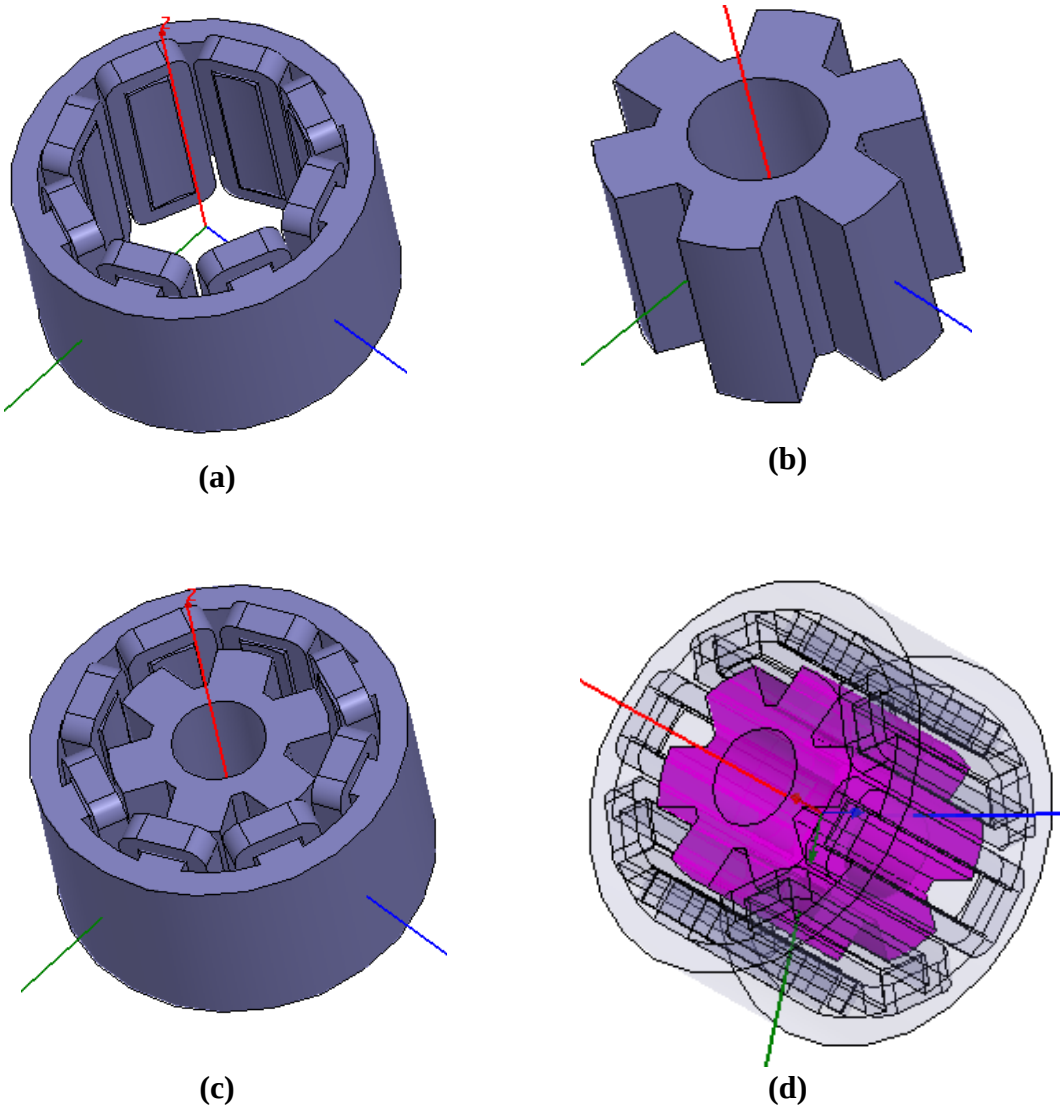

Fig.3.20 FEM Model
a) Designed Stator, b) Designed Rotor, c) Both Stator &Rotor
d) 3-dimensional view of stator & rotor

3.2 Motor Construction.

The first step in the construction of the SRM is to find an appropriate method to support the stator and rotor. For this motor an old inductor motor frame is used to house the SRM and provide the bearings for the rotor. Fig.3.21 shows the final designed SRM in the old motor frame.

Fig.3.21 Experimental SRM

Spark erosion wire cutting is used to cut out the stator and rotor stacks from non grain oriented silicon sheet steel. The accuracy of the cutting is within 0.04mm. The stator stack is held together by two aluminium cups that aligned and centered the stator stack in the middle of the motor casing. Fig.3.22 shows the fully completed stator and stator housing and the aluminium cups are visible within the motor frame. The rotor stack was clamped over the nonmagnetic stainless steel shaft by a stainless steel nut at one side, and a flange on the other.

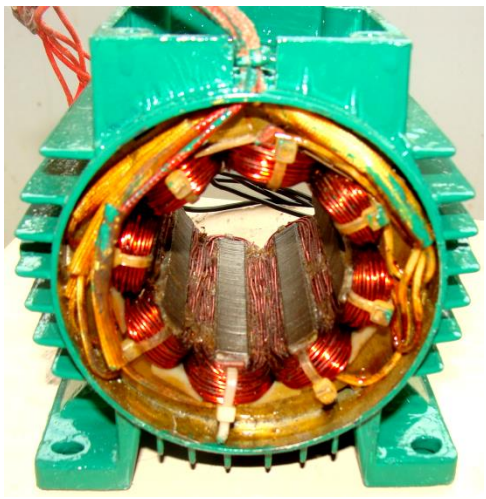

Fig.3.22 Stator and stator housing

Fig.3.23 shows a photograph of the rotor and shaft. The flange that clamps the rotor stack over the shaft is visible and it has a larger size compared to the bearings internal

Fig.3.23 Rotor and shaft

The location of the bearings in this design depends on the end housing of the motor case. The rotor position is determined by using an optical encoder disk that is placed on the outer of the end housing. Only the wires from the sensor can be seen in Fig.3.23 and Fig.3.24 show the complete motor accessories

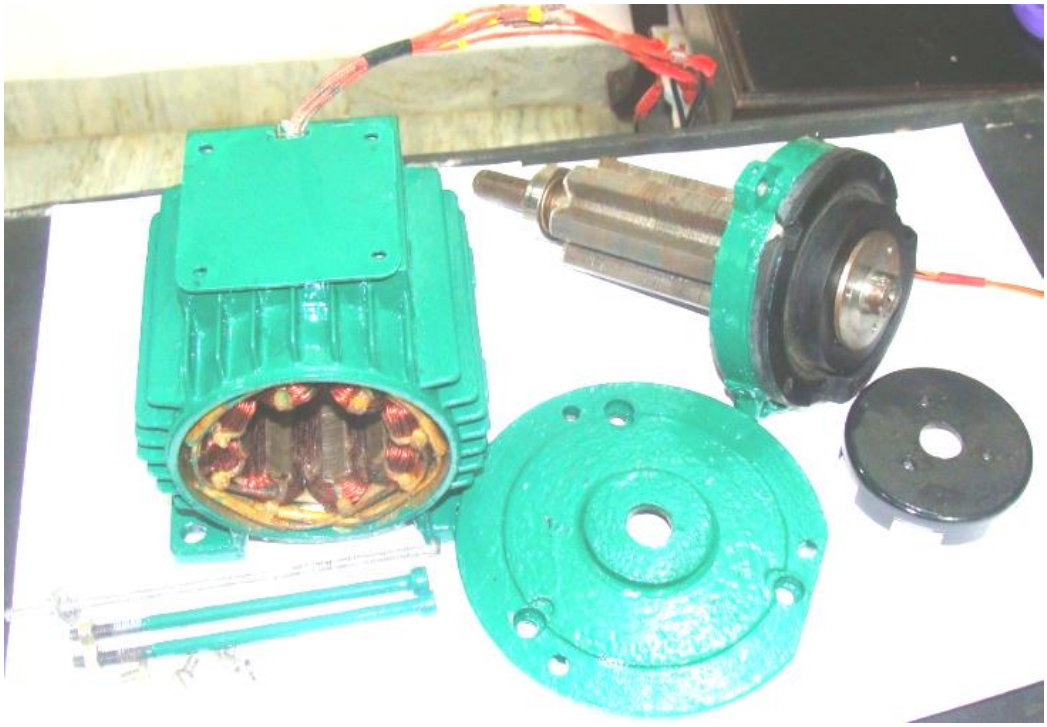

Fig.3.24 Complete Motor

3.2.1 Motor Dimensions:

Each stator pole is 10.5 millimeters in width and has a radius of curvature of 27.5 degrees. The stator inner diameter is 48 millimeters. The stator back iron diameter is 9.5 millimeters. The rotor outer diameter is 47.5 millimeters .The rotor poles are slightly larger with a width of 11 millimeters and a radius of curvature of 30 degrees. The rotor stack length is 80mm. The rotor shaft diameter is 17 mm. The case of the machine is circular with a side length of 90mm. The stack length is 80 mm. Note that in this position the rotor poles are completely unaligned with respect to the main stator poles. Then excitation of the main stator poles at this time will generate an air gap torque turning the rotor

3.3 Design Verification

The design verification process for SRM is carried out using analytical procedure, finite element analysis and experimental verification. The analytical part of the verification finds the performance of the motor through its flux linkage vs. current vs. rotor position characteristics derived using a magnetic equivalent circuit approach. The finite element analysis is carried out for the fine tuning of the preliminary motor design. Based on the empirical formulae and FEM, a prototype is built and tested. A strong correlation between the analytical, finite element and experimental results assures confidence in the engineering analysis and the design method adopted and also enables confidence in scaling of the machine.

3.4 Analytical Inductance calculation

The basic design of an SRM using the output equation is verified from the flux linkages vs. current characteristics for both the aligned and unaligned positions. Before going to verify the design analytically, the derivation for the flux linkages calculation and hence the values of the inductances at different rotor position are discussed in the present section .The evaluation of aligned flux linkages are accurate, the same cannot be used for the unaligned values. The leakage fluxes and the path of the mutual flux, complicate accurate estimation of the unaligned flux linkages and unaligned inductance. Finite element analysis techniques have been used to estimate accurately the unaligned flux linkages and inductance.

The variation in the motor winding inductance as a function of rotor position is discussed in detailed in chapter 2, section 2.5.2. The aligned position corresponds to the center of the stator and rotor poles coinciding, and the unaligned position with the midpoint of the interpolar rotor gap facing the stator pole.

3.4.1 Calculation of aligned Inductance.

A certain stator pole flux density is assumed, giving a stator pole flux by multiplying with the stator pole cross section area. The flux densities in other machine parts are derived from the machine geometry and the assumed stator pole flux density. From the flux densities in various machine parts and the B-H characteristic (Fig.3.25) of the lamination material, the corresponding magnetic field strengths are obtained. Given the magnetic field strengths and the length of the flux path in each part, their product gives the magneto-motive force mmf. The mmfs for various parts are likewise obtained, and for the magnetic equivalent circuit and stator excitation the AMPERE'S circuital law is applied.

The derivation of inductance is much simpler for the stator and rotor pole aligned positions than for unaligned positions. The flux lines, about 90 to 98%, pass the air gap between the stator and rotor. There is a small flux due to leakage between adjacent poles. The fringing is not very significant and can be accounted for, if necessary. The flux plot of the 8/ 6 SRM is shown in Fig.3.26.

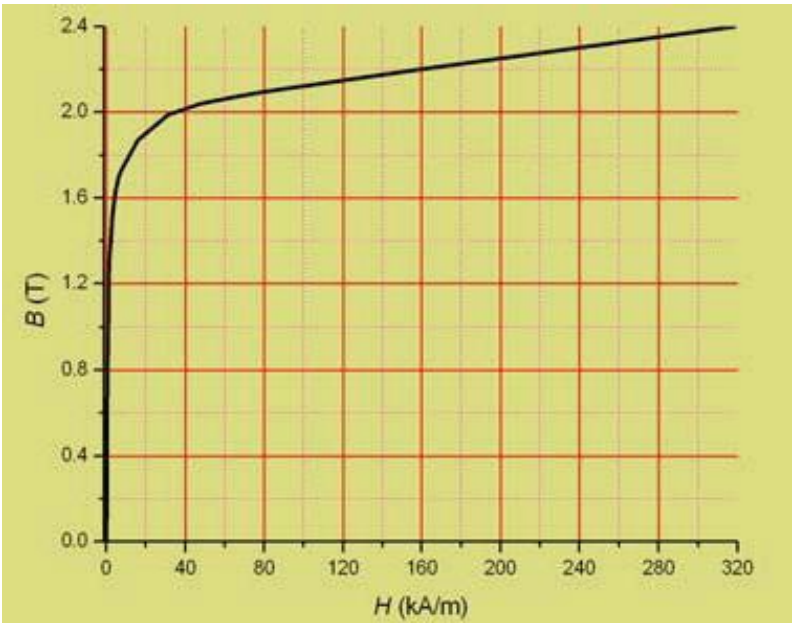

Fig.3.25 Steel B-H curve of 1010

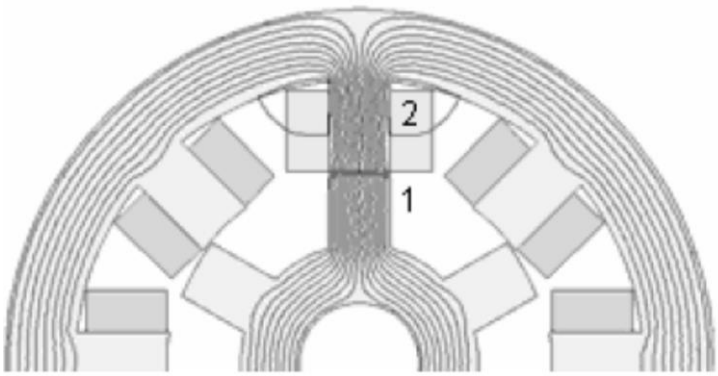

Fig.3.26 Two flux path for calculation of aligned inductance

Neglecting leakage and stacking factor, the stator pole area A_s can be written as,

$$A_s = \frac{D}{2} L\beta_s \quad (3.56)$$

The flux in the stator pole φ is given by

$$\varphi = B_s A_s \quad (3.57)$$

The flux in the yoke $\emptyset_y$ is given by

$$\emptyset_y = \frac{\emptyset}{2} = \frac{B_s A_S}{2} \quad (3.58)$$

Assuming that the yoke flux density B_y is half the stator flux density B_s, the yoke flux

$$\emptyset_y = B_y A_y = \frac{B_s}{2} A_Y \quad (3.59)$$

Comparing (3.58) and (3.59), the area of the yoke A_y can be set as,

$$A_y = A_s \quad (3.60)$$

The yoke area is the product of back iron thickness C and the stack length L. Therefore, the back iron thickness is obtained as,

$$C = \frac{A_y}{L} \quad (3.61)$$

The stator pole height h_s is given by,

$$h_s = \frac{D_0}{2} - C - \frac{D}{2} \quad (3.62)$$

The rotor pole area A_r is given by,

$$A_r = \left(\frac{D}{2} - g\right) L\beta_r \quad (3.63)$$

The rotor pole flux density B_r is given by,

$$B_r = \frac{B_S A_S}{A_r} \quad (3.64)$$

The area of the rotor core A_{rc} is given by,

$$A_{rc} = L\left(\frac{D}{2} - g - h_r - \frac{D_{sh}}{2}\right) \quad (3.65)$$

where g is the length of the air-gap and h_r is the height of the rotor pole. The length of g is kept as small. The rotor core carries half the flux and is limited to a flux density of approximately 80% of the maximum value. Hence,

$$\emptyset_{rc} = \frac{\emptyset}{2} = \frac{B_s A_S}{2} \quad (3.66)$$

The rotor core flux density B_{rc} can be written as,

$$\emptyset_{rc} = B_{rc}A_{rc} = 0.8B_s A_{rc} \quad (3.67)$$

Comparing (3.66) and (3.67), the area of the rotor core is calculated as,

$$A_{rc} = \frac{A_s}{1.6} \quad (3.68)$$

The height of the rotor pole h_r is obtained from (3.65) as,

$$h_r = \frac{D}{2} - g - \frac{D_{sh}}{2} - \frac{A_{rc}}{L} \quad (3.69)$$

The average area of A_g is calculated as,

$$A_g = \frac{A_s + A_r}{2} = \frac{L}{2}\left(\beta_s \frac{D}{2} + \beta_r\left(\frac{D}{2} - g\right)\right) \quad (3.70)$$

The reluctance of the air gap is given by,

$$\mathfrak{R}_g = \frac{2I_g}{\mu_0 A_g} \quad (3.71)$$

The permeance of the air gap is calculated as,

$$P_a = \frac{\mu_0 A_{airgap}}{I_{airgap}} \quad (3.72)$$

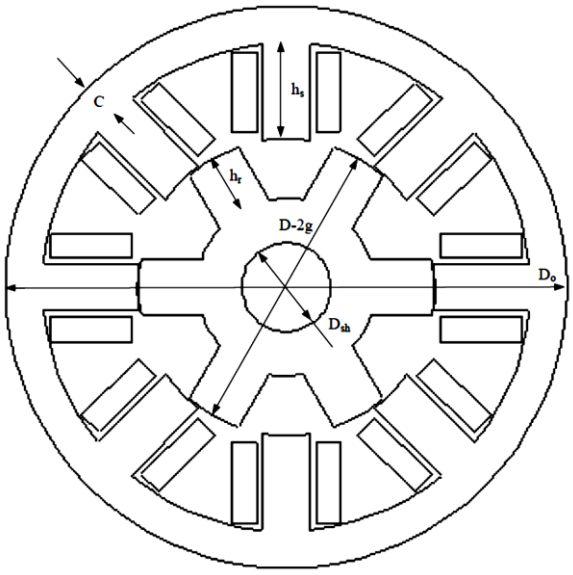

Fig.3.27 Constructional view of 8/6

The mean path lengths of various sections are given as follows:

$$l_s = h_s + \frac{C}{2} \tag{3.73}$$

$$l_g = g \tag{3.74}$$

$$l_r = h_r + \left(\frac{\frac{D}{2} - g - h_r - \frac{D_{sh}}{2}}{2}\right) = \frac{D}{4} - \frac{g}{2} + \frac{h_r}{2} - \frac{D_{sh}}{4} \tag{3.75}$$

$$l_{rc} = \pi\left(\frac{\frac{D}{2} - g - h_r - \frac{D_{sh}}{2}}{2} + \frac{D_{sh}}{2}\right) = \pi\left(\frac{D}{4} - \frac{g}{2} + \frac{h_r}{2} - \frac{D_{sh}}{4}\right) \tag{3.76}$$

The mean length l_y for a circular yoke SRM which is shown in Fig 3.27

$$l_y = \pi\left(\frac{D_0}{2} - \frac{C}{2}\right) \tag{3.77}$$

Using the B-H characteristics for the material used for the laminations, the magnetic field intensity in Ampere-turns per meter for each portion of the machine except the air-gap is obtained. The magnetic field intensities in the stator pole, stator yoke, rotor pole and rotor core are designated as H_s, H_y, H_r and H_{rc}, respectively. The flux density in the air-gap B_g is given by,

$$B_g = \frac{A_s B_s}{A_g} \tag{3.78}$$

The magnetic field intensity of the air-gap H_g is calculated as,

$$H_g = \frac{B_g}{4\pi \times 10^{-7}} \tag{3.79}$$

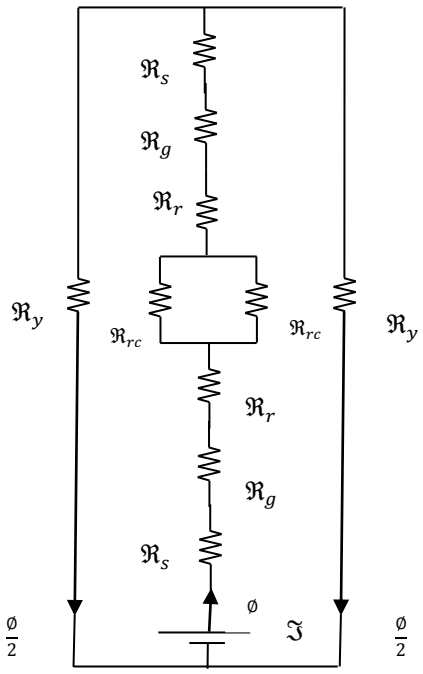

Fig.3.28 Magnetic Circuit of the SRM

The magnetic circuit of the SRM is shown in Fig.3.28. The reluctances of the stator pole, yoke, rotor pole, rotor core and air-gap are represented by $\mathfrak{R}_s$, $\mathfrak{R}_y$, $\mathfrak{R}_r$, $\mathfrak{R}_{rc}$ and $\mathfrak{R}_g$ respectively.

The lumped parameter $\mathfrak{R}_L$ in Fig. 3.29 is obtained as

$$\mathfrak{R}_L = 2\left(\mathfrak{R}_s + \mathfrak{R}_g + \mathfrak{R}_r\right) + \frac{\mathfrak{R}_{rc}}{2} \tag{3.80}$$

The reluctance $\mathfrak{R}$ in a particular section can be represented as

$$\mathfrak{R} = \frac{H.l}{BA} = \frac{H.l}{\emptyset} \tag{3.81}$$

Where, H is the magnetic field intensity, l is the mean path length in the section, B is the flux density in the section, A is the area of the section and $\emptyset$ is the flux in the section. For the magnetic circuit in Fig.3.28, the magnetic circuit equation can written as; the magnetic circuit equation of aligned inductance can be written as,

$$\mathfrak{I}_{aligned} = T_{ph} i = \mathfrak{R}_L \emptyset = 2\left(H_S I_S + H_r I_r\right) + \frac{B_g A_g}{P_a} + H_{rc} I_{rc} + H_y I_y \tag{3.82}$$

Now, the total ampere-turns $\mathfrak{I}$ required for the machine operation at full load can be calculated. It is also know that $\mathfrak{I} = T_{ph} i$.Since the peak current i_p is assumed initially , the turns per phase T_{ph} can be calculated.The aligned inductance at maximum current is calculated as,

$$L_{aligned} = \frac{T_{ph}\emptyset}{i} = \mathfrak{I}\frac{B_s A_s}{i_p^2} \tag{3.83}$$

The effects of leakage can also be calculated. The area of the leakage track is assumed as, $A_f = \frac{3h_s}{4} L$ (3.84)

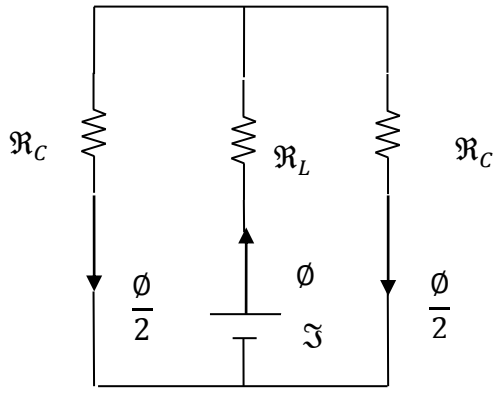

Fig.3.29 Simplified Magnetic Circuit of the SRM

The length is approximately calculated as,

$$l_f = \frac{3h_s}{4}\frac{\pi}{2} \tag{3.85}$$

The yoke area is obtained from (3.61)

$$A_y = CL \tag{3.86}$$

The area of the stator pole is given as

$$A_{sf} = \frac{3h_s}{4}L \tag{3.87}$$

The length of the path in the stator is calculated as,

$$l_s = \frac{1}{2}\frac{3h_s}{4} + \frac{C}{2} \tag{3.88}$$

The yoke length is approximately,

$$l_y = \frac{1}{2}\frac{3h_s}{4} \tag{3.89}$$

The reluctance of the leakage tube is given by,

$$\Re_f = \frac{l_f}{\mu_0 A_f} \tag{3.90}$$

The permeance of the air gap is calculated as,

$$P_f = \frac{1}{\Re_f}$$

The magnetic circuit equation of leakage tube can be written as,

$$\Im_f = \frac{1}{2}\frac{3}{4}T_{ph}i = \Re_L \emptyset = H_s l_s + \frac{B_s A_{sf}}{P_f} + H_y l_y \tag{3.91}$$

The inductance of the leakage tube is then calculated as,

$$L_{af} = \Im_f \frac{B_{smin} A_{sf}}{i_p^2} \tag{3.92}$$

The leakage inductance above is calculated for one track. There are 4 such tracks as can be seen in Fig.3.30. The total aligned inductance is therefore given by,

$$L_a = L_{aligned} + 4L_{af} \tag{3.93}$$

3.4.2 Calculation of unaligned position inductance

The best way to determine the minimum inductance is to plot the equiflux lines for a test machine in the completely unaligned position and calculate the lengths of the equiflux lines in the air gap and then account for the paths in the iron sections, as proposed in (Krishnan, R. 2001). Fig.3.30 shows the equiflux lines in the unaligned position of a 4-phase 8/6 SRM, obtained by FEM computation.

Track 1: To calculate the length l_1 and area A_1, consider Fig.3.31. The area of the track at the stator pole is calculated as,

$$A_{1s}=\frac{\beta_s}{4}\frac{D}{2}L \quad (3.94)$$

The arc subtended by half the rotor pole is given by,

$$\frac{\beta_r}{2}\left(\frac{D}{2}-g\right) \quad (3.95)$$

The angle θ_2 is given by,

$$\theta_2=\frac{\beta_r\left(\frac{D}{2}-g\right)}{\left(\frac{D}{2}-g-h_r\right)}$$

The rotor pole pitch is defined as

$$\theta_{rp}=\frac{2\pi}{N_r} \quad (3.96)$$

The angle θ_3 is calculated as,

$$\theta_3=\frac{\theta_{rp}}{2}-\theta_2 \quad (3.97)$$

The area of the track at the rotor core is calculated,

$$A_{1r}=2\left(\frac{D}{2}-g-h_r\right)\theta_3 L \quad (3.98)$$

The average area of the air gap A_1 calculated as,

$$A_1=\frac{A_{ls}+A_{lr}}{2}=\frac{l}{2}\frac{\beta_s}{4}\frac{D}{2}L+\left(\frac{D}{2}-g-h_r\right)\theta_3 L \quad (3.99)$$

The length of the air gap is given as,

$$l_1=\frac{D}{2}-g-h_r \quad (3.100)$$

The length of the path through the stator and yoke are given by (3.73) and (3.77). The area of the rotor core and yoke is given by (3.65) and the length of the path through the rotor core is given by (3.76).

The reluctance of track 1 in the air gap is given by

$$\mathfrak{R}_1=\frac{2l_l}{\mu_0 A_l}$$

(3.101)

The permeance of track 1 is calculated as,

$$P_1=\frac{l}{\mathfrak{R}_l} \quad (3.102)$$

Using the B-H characteristics of the material used for the laminations, the magnetic field intensity in Ampere-turns per meter for each portion of the

machine except the air-gap is obtained. The magnetic field intensities in the stator pole, stator yoke, and rotor pole and rotor core are designated as H_s, H_y, H_r and H_{rc}, respectively.

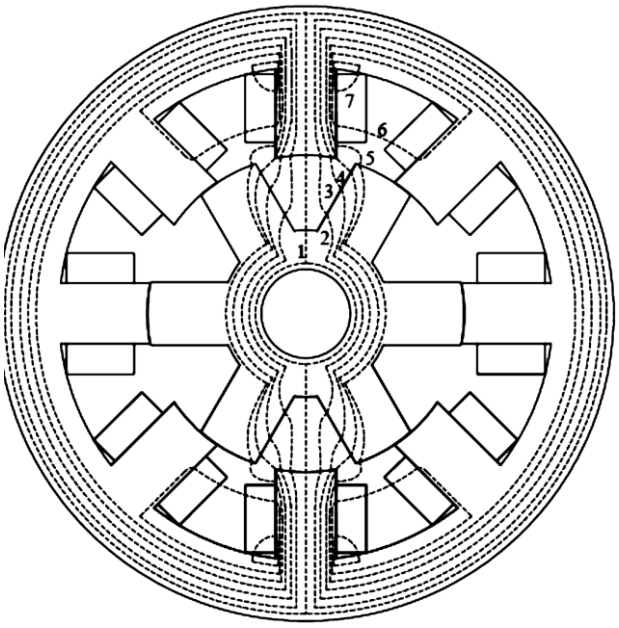

Fig.3.30 Identification of 7 flux tracks for analytical calculation of Unaligned inductance

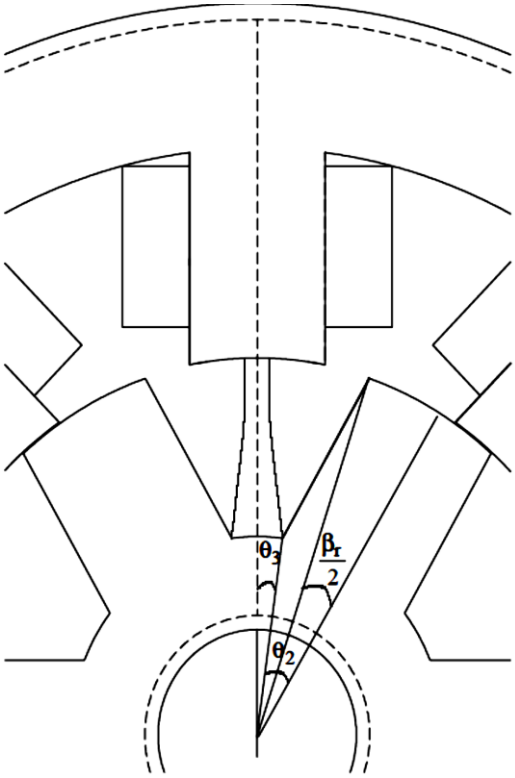

Fig.3.31 Track 1 calculations

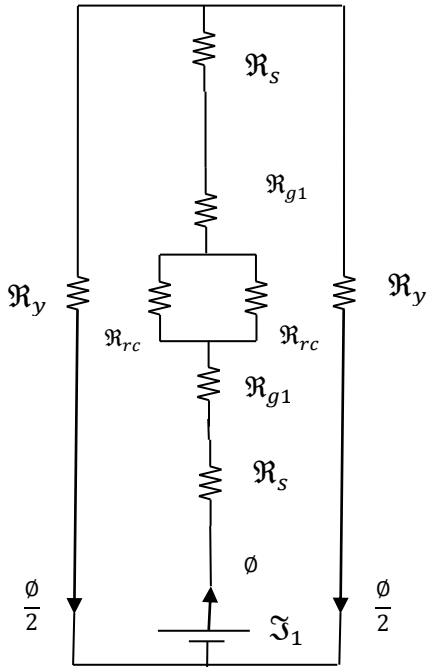

Fig.3.32 Reluctance circuit for Track 1

Referring to Fig.3.32, the magnetic circuit equation of track 1 can be written as,

$$\Im_l = T_{ph} i = \Re_L \phi + \frac{\Re_c \varphi}{2} = 2(H_s l_s) + \frac{B_s A_{Is}}{P_l} + \frac{H_{rc} I_{rc}}{2} + \frac{H_y l_y}{2} \quad (3.103)$$

The unaligned inductance of track 1 is then calculated as,

$$L_{u1} = \Im_l \frac{B_{smin}\, A_{ls}}{i_p^2} \quad (3.104)$$

Track 2: To calculate the length l_2 and area A_2, consider Fig.3.33. The area of the track at the stator pole is calculated as,

$$A_{2s} = \frac{\beta_s}{4} \frac{D}{2} L \quad (3.105)$$

The area of the track at the rotor pole is calculated,

$$A_{2r} = \frac{h_r}{2} L \quad (3.106)$$

The average area of A_2 is calculated as,

$$A_2 = \frac{A_{2s} + A_{2r}}{2} = \frac{L}{2}\left(\frac{\beta_s}{2} \frac{D}{2} + \frac{h_r}{2}\right) \quad (3.107)$$

The angle θ_1 is assumed to be $\frac{\beta_s}{4}$. The Length AB is calculated as $x_1 = \frac{D}{2} \sin \theta_1$. The length OA is given by $y_1 = \frac{D}{2} \cos \theta_1$. Consider point B has the coordinates as,

$$(x_1, y_1) = \left(\left(\frac{D}{2}\right)\sin\left(\frac{\beta_s}{4}\right), \left(\frac{D}{2}\right)\cos\left(\frac{\beta_s}{4}\right)\right) \quad (3.108)$$

The angle θ_4 is calculated as,

$$\theta_4 = \frac{\frac{\beta_r}{2}\left(\frac{D}{2} - g\right)}{\left(\frac{D}{2} - g - \frac{3}{4}h_r\right)} \quad (3.109)$$

The angleθ_5 is calculated as,

$$\theta_5 = \frac{\theta_{rp}}{2} - \theta_4 \quad (3.110)$$

The point C is given in coordinate form with respect to point O as,

$$(x_2, y_2) = \left(\left(\frac{D}{2} - g - \frac{3h_r}{4}\right)\sin\theta_5, \left(\frac{D}{2} - g - \frac{3h_r}{4}\right)\cos\theta_5\right) \quad (3.111)$$

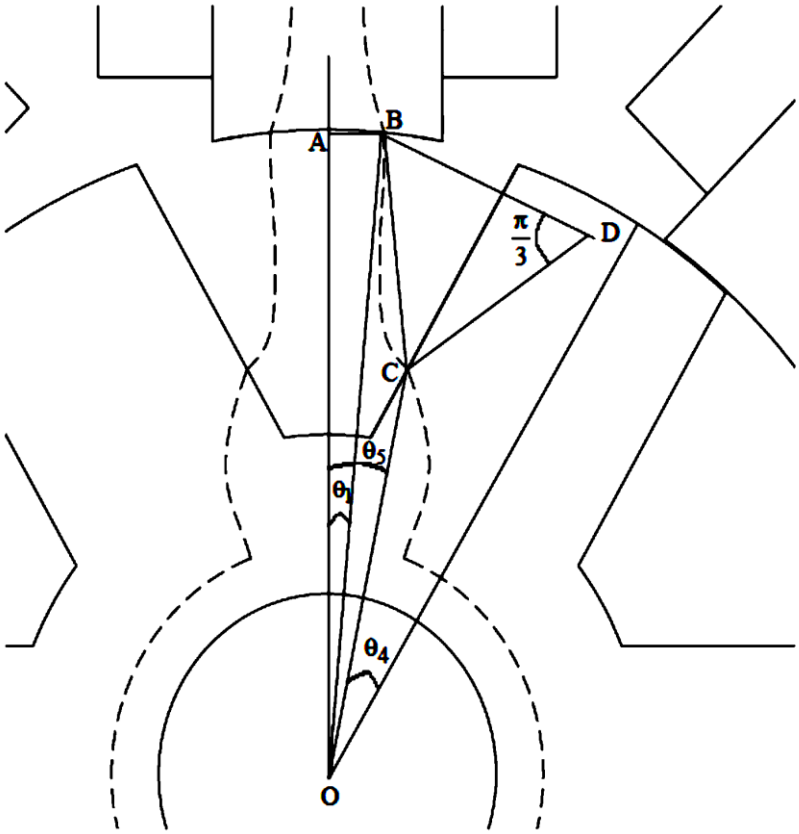

Fig.3.33 Track 2 Calculations

The linear distance between the points B and C, is assumed to be on one side of an equilateral triangle and forms the radius of the arc formed by track 2. From (3.108) & (3.111), this length is given as follows,

$$l_{x2} = \sqrt{(x_2 - x_1)^2 + (y_2 - y_1)^2} \quad (3.112)$$

The length of the track is given by,

$l_2 = l_{x2}\frac{\pi}{3}$ (3.113)

The area of the yoke and rotor core is given by (3.86) & (3.65).The length of the path through the stator and yoke are given by (3.73) and (3.77). The length of the path through the rotor core is given by,

$$l_{rc}=\frac{2}{3}\pi\left(\frac{\frac{D}{2}-g-h_r-\frac{D_{sh}}{2}}{2}+\frac{D_{sh}}{2}\right)=\frac{2}{3}\pi\left(\frac{D}{4}-\frac{g}{2}-\frac{h_r}{2}+\frac{D_{sh}}{4}\right) \quad (3.114)$$

The length of the path through the rotor,

$l_r = \frac{h_r}{4}$ (3.115)

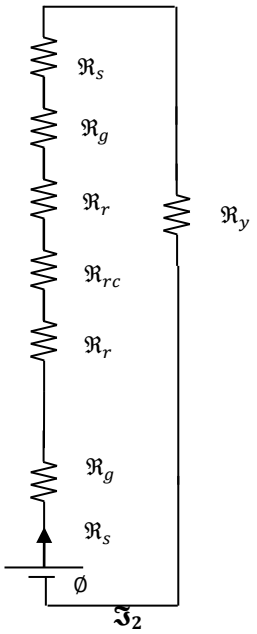

Fig.3.34 Equivalent reluctance circuits of Track 2

The reluctance of track 2 in the air gap is given by,

$\Re_2 = \frac{2l_2}{\mu_0 A_2}$ (3.116)

The permeance of track 2 is calculated as,

$P_2 = \frac{l}{\Re_2}$ (3.117)

Referring to Fig.3.34, the magnetic circuit equation of track 2 can be written as

$$\Im_2 = T_{ph}i = R_L\emptyset = 2(H_sI_s + H_rI_r) + \frac{B_sA_{2s}}{P_2} + H_{rc}I_{rc} + H_yI_y \quad (3.118)$$

The unaligned inductance of track 2 is then calculated as,

$$L_{u2}=\Im_2 \frac{B_{s\,min} A_{2s}}{i_p^2} \quad (3.119)$$

Track 3: To calculate the area A_3 and length l_3, consider Fig.3.35. The area of the track at the stator pole is calculated as,

$$A_{3s}=\frac{3}{4}\frac{\beta_s}{8}\frac{D}{2}L \quad (3.120)$$

The area of the track at the rotor pole is calculated,

$$A_{3r}=\frac{h_r}{4}L \quad (3.121)$$

The average area of A_3 is calculated as,

$$A_3=\frac{A_{3s}+A_{3r}}{2}=\frac{L}{2}\left(\frac{3}{4}\frac{\beta_s}{8}\frac{D}{2}+\frac{h_r}{4}\right) \quad (3.122)$$

The angle θ_1 is assumed to be

$$\theta_1=\frac{27\beta_s}{64} \quad (3.123)$$

The Length AB is calculated as $x_1=\frac{D}{2}\sin\theta_1$.The length OA is given by $y_1=\frac{D}{2}\cos\theta_1$.Consider point B has the coordinates as

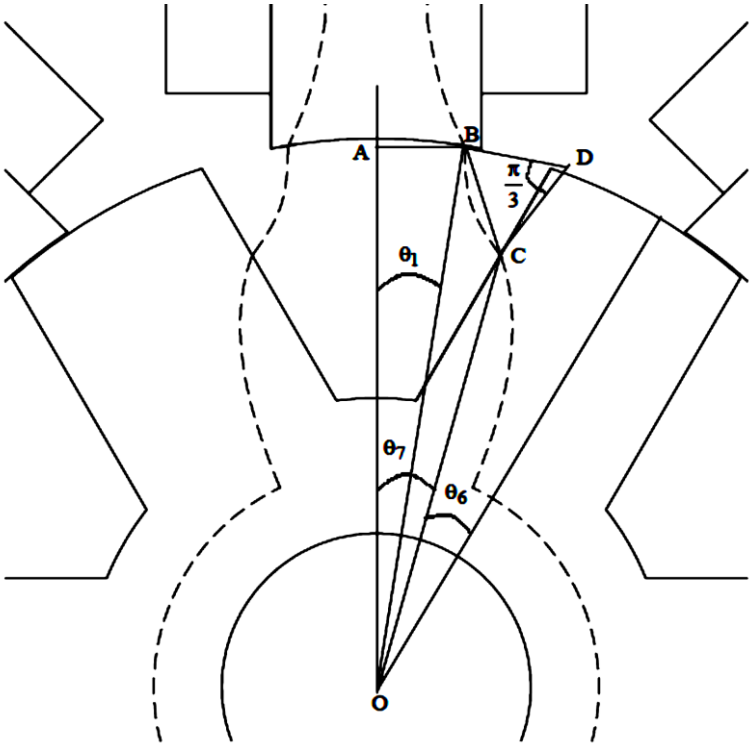

Fig. 3.35 Track 3 Calculations

The point B has the coordinates as,

$$(x_1, y_1) = \left(\left(\frac{D}{2}\right)\sin\left(\frac{27\beta_s}{64}\right), \left(\frac{D}{2}\right)\cos\left(\frac{27\beta_s}{64}\right)\right) \quad (3.124)$$

The angle θ_6 is given by,

$$\theta_6 = \frac{\frac{\beta_r}{2}\left(\frac{D}{2}-g\right)}{\left(\frac{D}{2}-g-\frac{3}{8}h_r\right)} \quad (3.125)$$

The angle θ_7 is calculated as,

$$\theta_7 = \frac{\theta rp}{2} - \theta_6 \quad (3.126)$$

The point C is given in coordinate form with respect to point O as

$$(x_2, y_2) = \left(\left(\frac{D}{2} - g - \frac{3h_r}{8}\right)\sin\theta_7, \left(\frac{D}{2} - g - \frac{3h_r}{8}\right)\cos\theta_7\right) \quad (3.127)$$

The linear distance between the points B and C, is assumed to be one side of an equilateral triangle and forms the radius of the arc formed by track 3. From (3.124) &(3.127) this length is given by

$$l_{x3} = \sqrt{(x_2 - x_1)^2 + (y_2 - y_1)^2} \quad (3.128)$$

The length of the track is given by,

$$l_3 = l_{x3}\frac{\pi}{3} \quad (3.129)$$

The area of the yoke and rotor core is given by (3.86) & (3.65) respectively. The length of the path through the stator, yoke and rotor core are given by (3.73), (3.77) and (3.114) respectively. The length of the path in the rotor is calculated as,

$$l_r = \frac{h_r}{2} + \frac{h_r}{8} = \frac{5h_r}{8} \quad (3.130)$$

The reluctance of track 3 in the air gap is given by,

$$\Re_3 = \frac{2l_3}{\mu_0 A_3} \quad (3.131)$$

The permeance of track 3 is calculated as,

$$P_3 = \frac{1}{\Re_3} \quad (3.132)$$

Referring to Fig.3.34, the magnetic circuit equation of track 3 can be written as,

$$\Im_3 = T_{ph}i = \Re_L \emptyset = 2(H_s l_s + H_r l_r) + \frac{B_s A_{3s}}{P_3} + H_{rc} l_{rc} + H_y l_y \quad (3.133)$$

The unaligned inductance of track 3 is then calculated as,

$$L_{u3} = \Im_3 \frac{B_{smin} A_{3s}}{i_p^2} \quad (3.134)$$

Track 4: To calculate the area A_4 and length l_4, consider Fig.3.35. The area of the track at the stator pole is calculated as,

$$A_{4s}= \frac{1}{4}\frac{\beta_s}{8}\frac{D}{2}L + \frac{1}{4}\frac{h_s}{4}L \quad (3.135)$$

The area of the track at the rotor pole is calculated,

$$A_{4r} = \frac{h_r}{4}L \quad (3.136)$$

The average area of A_4 is calculated as,

$$A_4 = \left(\frac{A_{4s}+A_{4r}}{2}\right) = \frac{L}{2}\left(\frac{1}{4}\frac{\beta_s}{8}\frac{D}{2} + \frac{1}{4}\frac{h_s}{4} + \frac{h_r}{4}\right) \quad (3.137)$$

Track 4 can be assumed to be a straight line between points B and C. The angle θ_1 is assumed to be,

$$\theta_1 = \frac{\beta_s}{2} \quad (3.138)$$

The length AB is calculated as $x_1 = \frac{D}{2}\sin(\theta_1)$ .The length OA is calculated as $y_1 = \frac{D}{2}\cos(\theta_1)$ .Considering that point B has the coordinates as

$$(x_1, y_1) = \left(\left(\frac{D}{2}\right)\text{Sin}\left(\frac{\beta_s}{2}\right), \left(\frac{D}{2}\right)\cos\left(\frac{\beta_s}{2}\right)\right) \quad (3.139)$$

The angle θ_8 is given by,

$$\theta_8 = \frac{\frac{\beta_r}{2}\left(\frac{D}{2} - g\right)}{\left(\frac{D}{2} - g - \frac{1}{8}h_r\right)} \quad (3.140)$$

The angle θ_9 is calculated as,

$$\theta_9 = \frac{\theta_{rp}}{2} - \theta_8 \quad (3.141)$$

The point C is given in coordinate form with respect to point O as,

$$(x_2, y_2) = \left(\left(\frac{D}{2} - g - \frac{1}{8}h_r\right)\sin\theta_5, \left(\frac{D}{2} - g - \frac{1}{8}h_r\right)\cos\theta_5\right) \quad (3.142)$$

From (3.124) and (3.127), the linear distance between the points B and C, is given as follows,

$$l_4 = \sqrt{(x_2 - x_1)^2 + (y_2 - y_1)^2} \quad (3.143)$$

The area of the yoke and rotor core is given by (3.86)& (3.65). The length of the path through the stator, yoke and rotor core are given by (3.73), (3.77) and (3.114) respectively.

The length of the path in the rotor is calculated as,

$$l_r = \frac{3h_r}{4} + \frac{h_r}{8} = \left(\frac{7}{8}\right)h_r \quad (3.144)$$

The reluctance of track 4 in the air gap is given by,

$$\mathfrak{R}_4 = \frac{2l_4}{\mu_0 A_4} \tag{3.145}$$

The permeance of track 4 is calculated as,

$$P_4 = \frac{1}{\mathfrak{R}_4} \tag{3.146}$$

Referring to Fig.3.34, the magnetic circuit equation of track 4 can be written as,

$$\Im_4 = T_{ph} i = \mathfrak{R}_L \emptyset = 2(H_s l_s + H_r l_r) + \frac{B_s A_{4s}}{P_4} + H_{rc} l_{rc} + H_y l_y \tag{3.147}$$

The unaligned inductance of track 4 is then calculated as,

$$L_{u4} = \Im_4 \frac{B_{smin} A_{4s}}{i_p^2} \tag{3.148}$$

Track 5: To calculate the area A_5 and length l_5, consider Fig.3.37. The area of the track at the stator pole is calculated as,

$$A_{5s} = \frac{3}{4}\frac{h_s}{4} L \tag{3.149}$$

The area of the track at the rotor pole is calculated,

$$A_{5r} = \frac{\beta_r}{8} L \left(\frac{D}{2} - g\right) \tag{3.150}$$

The average area of A_5 is calculated as,

$$A_5 = \frac{A_{5s} + A_{5r}}{2} = \frac{L}{2}\left(\frac{3}{4}\frac{h_s}{4} + \frac{\beta_r}{8}\left(\frac{D}{2} - g\right)\right) \tag{3.151}$$

Track 5 can be assumed to be an arc centered at the point D. The length AO is assumed to be,

$$y_1 = \frac{D}{2}\cos\frac{\beta_s}{2} + \frac{5h_s}{32} \tag{3.152}$$

The length AB is equal to

$$x_1 = \frac{D}{2}\sin\left(\frac{\beta_s}{2}\right) \tag{3.153}$$

The angle θ_1 can be calculated from (3.152) and (3.153) as,

$$\theta_1 = \tan^{-1}\left(\frac{x_1}{y_1 - \left(\frac{D}{2} - g - h_r\right)}\right) \tag{3.154}$$

The angle θ_2 is assumed to be,

$$\theta_2 = \frac{\pi}{N_r} - \frac{7\beta_r}{16} \tag{3.155}$$

The length CE is given by,

$$y_2 = \left(\frac{D}{2} - g\right)\cos(\theta_2) - \left(\frac{D}{2} - g - h_r\right) \tag{3.156}$$

The length DE is given by,

$$x_2 = \left(\frac{D}{2} - g\right)\sin(\theta_2) \quad (3.157)$$

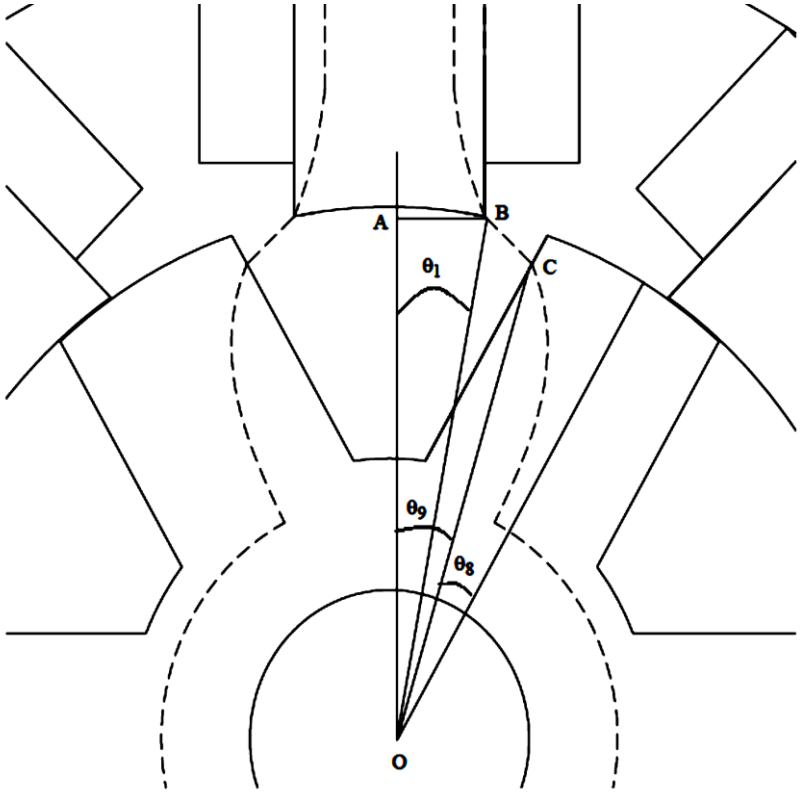

Fig.3.36 Track 4 Calculations

The angle θ_3 can be calculated from (3.156) and (3.157) as,

$$\theta_3 = \tan^{-1}\left(\frac{y_2}{x_2}\right) \quad (3.158)$$

The angle θ_4 is obtained from (3.154) and (3.155) as

$$\theta_4 = \frac{\pi}{2} - \theta_1 - \theta_3 \quad (3.159)$$

The length DB is given by

$$r_1 = \frac{x_1}{\sin(\theta 1)} \quad (3.160)$$

The length CD is given from (3.156) and (3.157) as

$$r_2 = \sqrt{x_2^2 + y_2^2} \quad (3.161)$$

The length of the flux track is approximately given from (3.159) – (3.161) as,

$$l_5 = \frac{r1+r2}{2}\theta_4 \quad (3.162)$$

The area of the yoke and rotor core is given by (3.86) & (3.65). The lengths of the track through the yoke and rotor core are given by (3.77) and (3.114) respectively. The length of the track in the rotor is calculated as,

$l_r=h_r$ (3.163)

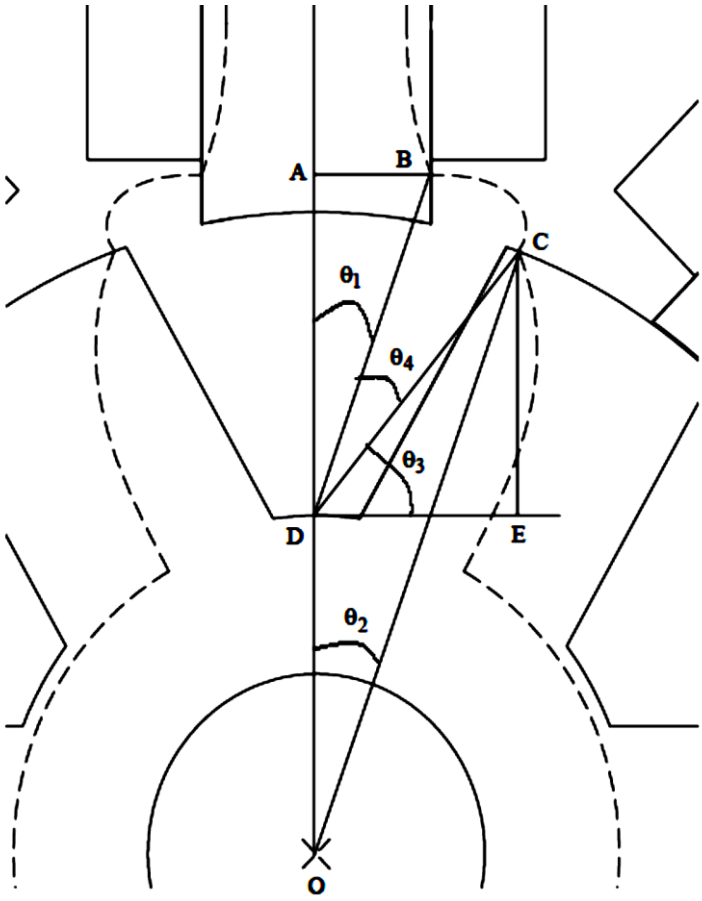

Fig.3.37 Track 5 Calculations

The length of the track in the stator is calculated as,

$$l_s = h_s + \frac{C}{2} - \frac{3}{8}\frac{h_s}{4} \quad (3.164)$$

The reluctance of track 5 in the air gap is given by,

$$\mathfrak{R}_5 = \frac{2l_5}{\mu_0 A_5} \quad (3.165)$$

The permeance of track 5 is calculated as,

$$P_5 = \frac{1}{\mathfrak{R}_5} \quad (3.166)$$

Referring to Fig.3.34, the magnetic circuit equation of track 5 can be written as,

$$\Im_5=T_{ph}i=\Re_L\emptyset = 2(H_s l_s+H_r l_r)+\frac{B_s A_{5s}}{P_5}+H_{rc}l_{rc}+H_y l_y \quad (3.167)$$

The unaligned inductance of track 5 is then calculated as,

$$L_{u5}= \Im_5 \frac{B_{smin}A_{5s}}{i_p^2} \quad (3.168)$$

Track 6: To calculate the area A_6 and length l_6, consider Fig.3.38. The area of the track is calculated as,

$$A_6= \frac{h_s}{4}L \quad (3.169)$$

Track 6 can be assumed to be an arc centered at the center of the shaft. The length AO is assumed to be,

$$Y_1= \frac{D}{2}\cos\frac{\beta_s}{2}+\frac{3h_s}{8} \quad (3.170)$$

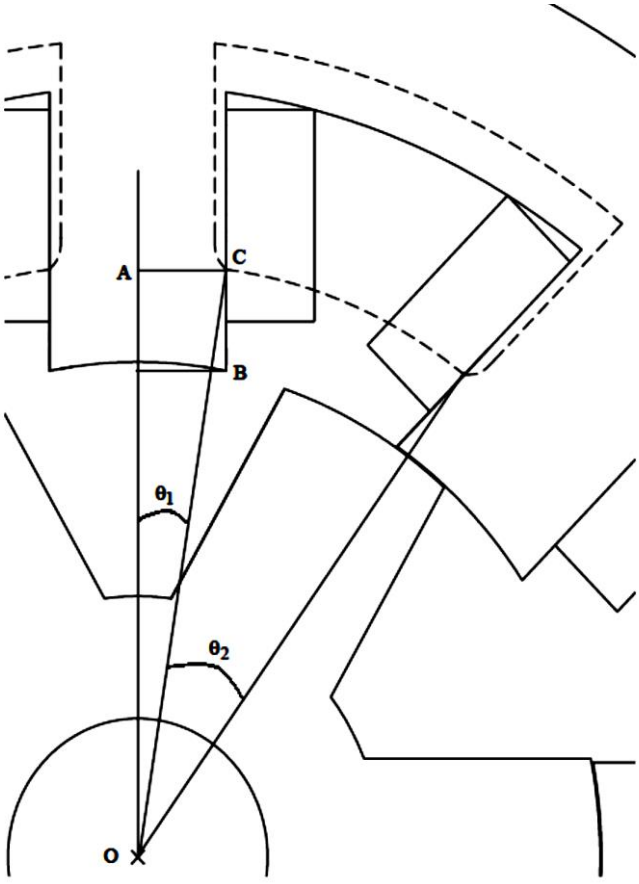

Fig.3.38 Track 6 Calculations

The length AB is defined in (3.153).

From (3.153) and (3.170), The angle θ_1 can be calculated as,

$\theta_1 = \tan^{-1}\left(\frac{x_1}{y_1}\right)$ (3.171)

The angle θ_2 is assumed to be,

$\theta_2 = \frac{2\pi}{N_s} - 2\theta_1$ (3.172)

The length CO is given from (3.153) and (3.171) by

$r_1 = \frac{x_1}{\sin(\theta_1)}$ (3.173)

The length of the track is given from (3.172) and (3.173) by,

$l_6 = r_1\,\theta_2$ (3.174)

From the yoke area given in (3.86).The stator pole area is equal to the air gap area. Therefore,

$A_{6s} = A_6 = \frac{h_s}{4}L$ (3.175)

The length of the track in the stator is calculated as,

$l_s = \frac{h_s}{2} + \frac{1}{2}\frac{h_s}{4} + \frac{C}{2}$ (3.176)

The yoke length is given by,

$l_y = \frac{\pi}{4}\left(\frac{D_0}{2} - \frac{C}{2}\right)$ (3.177)

The reluctance of track 6 in the air gap is given by,

$\Re_6 = \frac{l_6}{\mu_0 A_6}$ (3.178)

The permeance of track 6 is calculated as,

$P_6 = \frac{1}{\Re_6}$ (3.179)

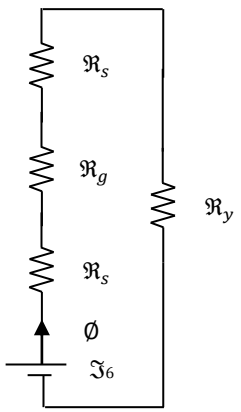

Fig.3.39 Magnetic Circuit for Track 6

Referring to Fig.3.39, the magnetic circuit equation of track 6 can be written as,

$\Im_6 = \frac{1}{2}\frac{3T_{ph}i}{4} = \Re_L\emptyset = 2(H_s l_s) + \frac{B_s A_6}{P_6} + H_y l_y$ (3.180)

The unaligned inductance of track 6 is then calculated as,

$$L_{u6} = \Im 6 \frac{B_{smin} A_6}{i_p^2} \quad (3.181)$$

Track 7: To calculate the area A_7 and length l_7, consider Fig.3.38. The area of the track is calculated as,

$$A_7 = \frac{h_s}{2} L \quad (3.182)$$

Track 7 is assumed to be an arc centered about point B. The length is approximately calculated as,

$$l_7 = \frac{h_s}{4} \frac{\pi}{2} \quad (3.183)$$

The stator area is equal to the air gap area. Therefore

$$A_{7s} = \frac{h_s}{2} L \quad (3.184)$$

From the yoke area given (3.86).The length of the track in the stator is calculated as,

$$l_s = \frac{1}{2} \frac{h_s}{2} + \frac{C}{2} \quad (3.185)$$

The yoke length is approximately,

$$l_y = \frac{1}{2} \frac{h_s}{2} \quad (3.186)$$

The reluctance of track 7 in the air gap is given by,

$$\Re_7 = \frac{l_7}{\mu_0 A_7} \quad (3.187)$$

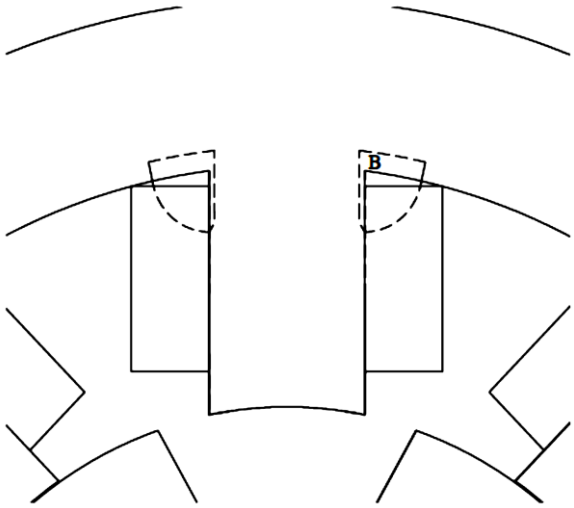

Fig.3.40 Track 7 Calculations

The permeance of track 7 is calculated as,

$$P_7 = \frac{1}{\Re_7} \quad (3.188)$$

Referring to Fig.3.41, the magnetic circuit equation of track 7 can be written as,

$$\Im_7 = \frac{1}{2}\frac{T_{ph}i}{2} = \Re_L \emptyset = H_s l_s + \frac{B_S A_7}{P_7} + H_y l_y \quad (3.189)$$

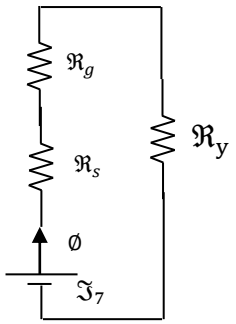

Fig.3.41 Reluctance Circuit for Track 7

The unaligned inductance of track 7 is then calculated as,

$$L_{u7} = \Im_7 \frac{B_{smin} A_S}{i_p^2} \quad (3.190)$$

The total unaligned inductance is given by,

$$L_u = L_{u1} + 2(L_{u2} + L_{u3} + L_{u4} + L_{u5}) + 4(L_{u6} + L_{u7}) \quad (3.191)$$

3.4.3 Calculation of intermediate position Inductance

There are primarily two areas to be considered while calculating the inductance at different positions. The areas can be identified as the portion where the rotor and stator poles are not overlapping and the portion where the stator and rotor poles are overlapping. Assuming that $\theta = 0^0$ is the completely unaligned position and $\theta = 30^0$ is the completely aligned position the inductances can be calculated as follows

Zone: 1 $\quad 0 \leq \theta \leq \frac{\pi}{N_r} - \left(\frac{\beta_s + \beta_r}{2}\right)$

The flux tracks are identified as shown in Fig.3.42.

Track 1: Considering Fig.3.42, the centre of the shaft has the xy coordinates of (0,0), and the stator pole is divided into five equal angles of $\frac{\beta_s}{5}$ .The angle θ_1 is assumed to be $\frac{2\beta_s}{5}$. The length AB as $x_1 = \frac{D}{2}\sin(\theta_1)$.The length OA is calculated as $y_1 = \frac{D}{2}\cos(\theta_1)$

Considering that point B has the

$$(x_1, y_1) = \left(\left(\frac{D}{2}\right)\sin\left(\frac{2\beta_s}{5}\right), \left(\frac{D}{2}\right)\cos\left(\frac{2\beta_s}{5}\right)\right) \quad (3.192)$$

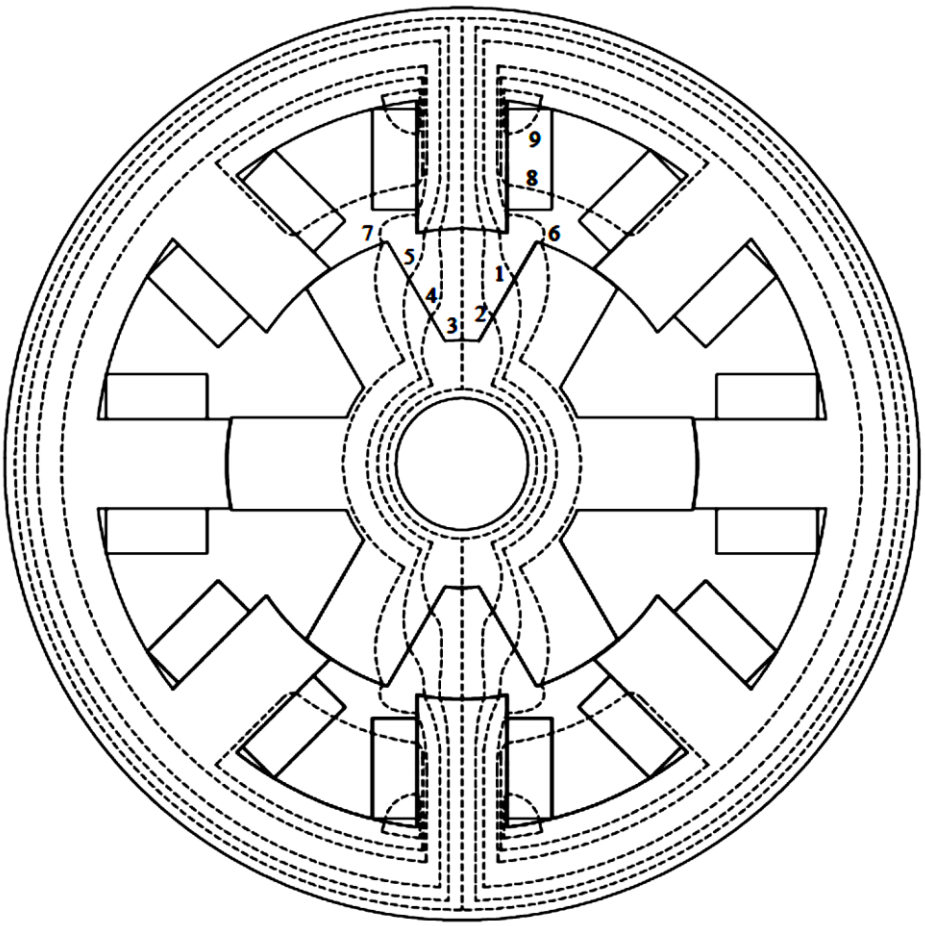

Fig.3.42 Identification of flux tracks in Zone I

Consider that the rotor is moving towards the stator, the length of the track in the air gap is constantly changing as is the area. The angle θ_5 is calculated as, coordinates as

$$\theta_5 = \frac{\theta_{rp}}{2} - \frac{\beta_r}{2} - \theta \tag{3.193}$$

The coordinates of point C is given as,

$$(x_2, y_2) = \left(\left(\frac{D}{2} - g - h_{elu}\right)\sin\theta_5, \left(\frac{D}{2} - g - h_{elu}\right)\cos\theta_5\right) \tag{3.194}$$

where,

$$h_{e1u} = \frac{h_r}{6}\left(1 - \frac{\theta}{2\left(\frac{\theta_{rp}}{2} - \frac{\beta_s + \beta_r}{2}\right)}\right) \tag{3.195}$$

The linear distance between the points B and C, is assumed to be on one side of an equilateral triangle and forms the radius of the arc formed by track 1.

If this length is given from (3.181) and (3.183) ,

$$l_{x1} = \sqrt{(x_2 - x_1)^2 + (y_2 - y_1)^2} \tag{3.196}$$

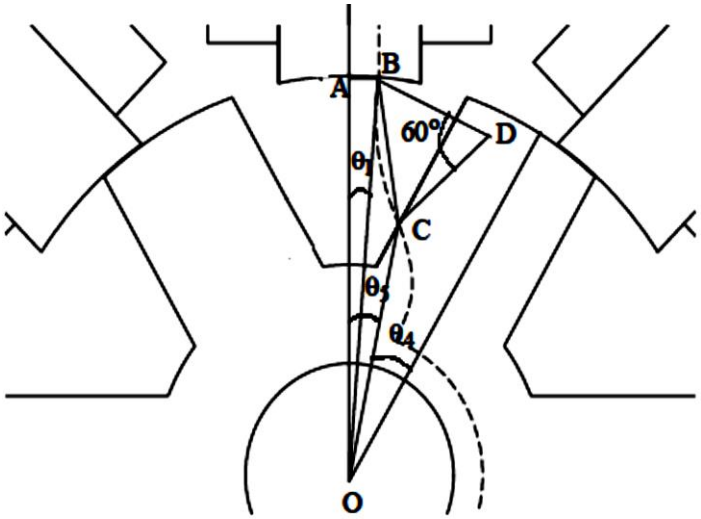

Fig.3.43 Track 1 and 2 Calculations

The length of the track is given by,

$$l_1 = l_{x1}\frac{\pi}{3} \tag{3.197}$$

The rotor area varies from $L\frac{h_r}{3}$ when $\theta = 0^0$ to $L\frac{h_r}{6}$

When $\theta = \left(\frac{\theta_{rp}}{2} - \frac{\beta_s+\beta_r}{2}\right)$ Therefore

$$A_{1r} = L\frac{h_r}{3}\left(1 - \frac{\theta}{2\left(\frac{\theta_{rp}}{2} - \frac{\beta_s+\beta_r}{2}\right)}\right) \tag{3.198}$$

The area of the track is calculated as,

$$A_1 = \frac{1}{2}(A_{ls} + A_{lr}) \tag{3.199}$$

where the area of the stator pole is given by

$$A_{1s} = \frac{D}{2}\frac{\beta_s}{5}L \tag{3.200}$$

The length of the track through the rotor is given as,

$$l_r = h_r - h_{e1u} \tag{3.201}$$

The length of the path through the stator, yoke and rotor core is given by (3.73), (3.77) and (3.114), respectively. The area of the yoke and rotor core is given by (3.86) & (3.65). The reluctance of the air gap of track 1 in the upper portion is given as,

$$\Re_1 = \frac{l_l}{\mu_0 A_l} \tag{3.202}$$

The above calculations are valid for the track passing in the upper portion of the stator. In the lower portion, the pole is moving away from the excited portion. This is similar to the effects experienced by track 5 in the upper portion. Therefore, Track 5 calculations are performed next.

Track 5: Considering Fig.3.44. The point B_5 has the coordinates as,

$$(x_1, y_1) = \left(-\left(\frac{D}{2}\right)\sin\left(\frac{2\beta_s}{5}\right), \left(\frac{D}{2}\right)\cos\left(\frac{2\beta_s}{5}\right)\right) \quad (3.203)$$

The angle θ_5 is calculated as ,

$$\theta_5 = \left(\frac{\theta_{rp}}{2} - \frac{\beta_r}{2}\right) + \theta \quad (3.204)$$

The coordinates of point C is given as,

$$(x_2, y_2) = \left(\left(\frac{D}{2} - g - h_{e5u}\right)\sin\theta_5, \left(\frac{D}{2} - g - h_{e5u}\right)\cos\theta_5\right) \quad (3.205)$$

where,

$$h_{e5u} = \frac{h_r}{6}\left(1 + \frac{\theta}{2\left(\frac{\theta_{rp}}{2} - \frac{\beta_s+\beta_r}{2}\right)}\right) \quad (3.206)$$

The linear distance between the points B and C, is assumed to be on one side of an equilateral triangle and forms the radius of the arc formed by track 5. If this length is given , $l_{x5} = \sqrt{(x_2 - x_1)^2 + (y_2 - y_1)^2}$

The length of the track is given by,

$$l_5 = l_{x5}\frac{\pi}{3} \quad (3.207)$$

The rotor area varies from L $\frac{h_r}{3}$ when $\theta = 0^0$ to L $\frac{h_r}{2}$ when $\theta = \left(\frac{\theta_{rp}}{2} - \frac{\beta_s+\beta_r}{2}\right)$.

Therefore

$$A_{5r} = L\frac{h_r}{3}\left(1 + \frac{\theta}{2\left(\frac{\theta_{rp}}{2} - \frac{\beta_s+\beta_r}{2}\right)}\right) \quad (3.208)$$

The area of the track is calculated as,

$$A_5 = \frac{1}{2}(A_{5s} + A_{5r}) \quad (3.209)$$

Where the area of the stator pole remains the same as track 1 and is given by,

$$A_{5s} = L\frac{\beta_s}{5}\frac{D}{2} \quad (3.210)$$

The length of the track through the rotor is given as,

$$l_r = h_r - h_{e5u} \quad (3.211)$$

The length of the path through the stator, yoke and rotor core is given by (3.73), (3.77) and (3.114), respectively.

The area of the yoke and rotor core is given by (3.86) & (3.65). The reluctance of the air gap of track 5 in the upper portion is given as,

$$\mathfrak{R}_5 = \frac{l_5}{\mu_0 A_5} \tag{3.212}$$

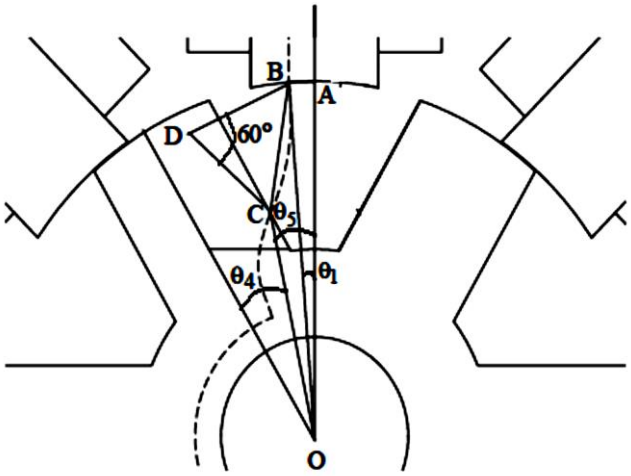

Fig.3.44 Track 4 and 5 Calculations

The combined reluctance for track 1 is given by,

$$\mathfrak{R}_{1,5} = \mathfrak{R}_1 + \mathfrak{R}_5 \tag{3.213}$$

The permeance of track 1 is calculated as,

$$P_1 = \frac{1}{\mathfrak{R}_{1,5}} \tag{3.214}$$

Using the B-H characteristics for the material used for the laminations, the magnetic field intensity in ampere-turns per meter for each portion of the machine except the air-gap is obtained. The magnetic field intensities in the stator pole, stator yoke, and rotor pole and rotor core are designated as H_s, H_y, H_r and H_{rc} respectively.

The magnetic circuit equation of track 1 can be written as,

$$\mathfrak{I}_1 = T_{ph}i = 2(H_s l_s + H_r l_r) + \frac{B_s A_{ls}}{P_l} + H_{rc} I_{rc} + H_y I_y \tag{3.215}$$

Since the LHS is known, the RHS can be calculated initially by setting $B_s = B_{max}$. If the RHS is greater than the LHS, the value of the stator flux density can be reduced and the other flux densities can be calculated at this reduced value and the magnetic field intensities can be calculated. This process is repeated till the RHS equals the LHS and the stator flux density are obtained as B_{smin}.

The inductance of track 1 is then calculated as,

$$L_{u1} = \Im_1 \frac{B_{s\,min} A_{ls}}{i_p^2} \quad (3.216)$$

Obviously, Track 5 has the exact same inductance and the procedure need not be repeated.

Therefore,

$$L_{u5} = L_{u1} \quad (3.217)$$

Track 2: Considering Fig. 3.43, since track 2 has a similar shape as track 1, the center of the shaft has the xy coordinates of (0,0). The angle θ_1 is assumed to be $\frac{\beta_s}{5}$

The length of AB is calculated as

$$x_1 = \frac{D}{2}\sin(\theta_1) \quad (3.218)$$

The length of OA is calculated as

$$y_1 = \frac{D}{2}\cos(\theta_1) \quad (3.219)$$

Considering that point B has the coordinates as,

$$(x_1, y_1) = \left(\left(\frac{D}{2}\right)\sin\left(\frac{\beta_s}{5}\right), \left(\frac{D}{2}\right)\cos\left(\frac{\beta_s}{5}\right)\right) \quad (3.220)$$

The angle θ_5 is calculated as,

$$\theta_5 = \frac{\theta_{rp}}{2} - \frac{\beta_r}{2} - \theta \quad (3.221)$$

The coordinates of point C is given as,

$$(x_2, y_2) = \left(\left(\frac{D}{2} - g - h_{e2u}\right)\sin\theta_5, \left(\frac{D}{2} - g - h_{e2u}\right)\cos\theta_5\right) \quad (3.222)$$

Where,

$$h_{e2u} = \frac{h_r}{2}\left(1 - \frac{\theta}{2\left(\frac{\theta_{rp}}{2} - \frac{\beta_s + \beta_r}{2}\right)}\right) \quad (3.223)$$

The linear distance between the points B and C, is assumed to be one of the sides of an equilateral triangle and forms the radius of the arc formed by track 2. If this length is given from (3.220) and (3.222) ,

$$l_{x2} = \sqrt{(x_2 - x_1)^2 + (y_2 - y_1)^2} \quad (3.224)$$

The length of the track is given by,

$$l_2 = l_{x2}\frac{\pi}{3} \quad (3.225)$$

The rotor area can be calculated as,

$$A_{2r} = h_r L - A_{lr} \quad (3.226)$$

where A_{1r} is the rotor area for that particular position calculated for path 1 in (3.198). The area of the track is calculated as,

$$A_2 = \frac{1}{2}\left(L\frac{\beta_s}{5}\frac{D}{2} + A_{2r}\right) \quad (3.227)$$

The length of the path through the rotor is given as,

$$l_r = h_r - h_{e2u} \quad (3.228)$$

The length of the path through the stator, yoke and rotor core is given by (3.73) (3.77) and(3.114), respectively. The area of the stator pole, yoke and rotor core is given by (3.86), (3.65) & (3.114), respectively. The reluctance of the air gap of Track 2 in the upper portion is given as,

$$\Re_2 = \frac{l_2}{\mu_0 A_2} \quad (3.229)$$

The above calculations are valid for the track passing in the upper portion of the stator. In the lower portion, the pole is moving away from the excited portion. This is similar to the effects experienced by track 4 in the upper portion. Therefore, Track 4 calculations are performed next.

Track 4: Considering that point B has the coordinates as

$$(x_1, y_1) = \left(-\left(\frac{D}{2}\right)\sin\left(\frac{\beta_s}{5}\right), \left(\frac{D}{2}\right)\cos\left(\frac{\beta_s}{5}\right)\right) \quad (3.230)$$

The angle θ_5 is calculated as,

$$\theta_5 = \frac{\theta_{rp}}{2} - \frac{\beta_r}{2} + \theta \quad (3.231)$$

The coordinates of point C is given as,

$$(x_2, y_2) = \left(\left(\frac{D}{2} - g - h_{e4u}\right)\sin\theta_5, \left(\frac{D}{2} - g - h_{e4u}\right)\cos\theta_5\right) \quad (3.232)$$

Where,

$$h_{e4u} = \frac{h_r}{2}\left(1 + \frac{\theta}{2\left(\frac{\theta_{rp}}{2} - \frac{\beta_s + \beta_r}{2}\right)}\right) \quad (3.233)$$

The linear distance between the points B and C, is assumed to be as one of the sides of an equilateral triangle and forms the radius of the arc formed by track 4. If this length is given from (3.230) and (3.232) as follows,

$$l_{x4} = \sqrt{(x_2 - x_1)^2 + (y_2 - y_1)^2} \quad (3.234)$$

The length of the track is given by,

$$l_4 = l_{x4}\frac{\pi}{3} \quad (3.235)$$

The rotor area can be calculated as,

$$A_{4r} = h_r L - A_{5r} \quad (3.236)$$

The area of track is calculated as $A_4 = \frac{1}{2}\left(L\frac{\beta_s}{5}\frac{D}{2} + A_{4r}\right)$

The length of the path through the rotor is given as,

$$l_r = h_r - h_{e4u} \quad (3.237)$$

The reluctance of the air gap of path 4 in the upper portion is given as,

$$\Re_4 = \frac{l_4}{\mu_0 A_4} \quad (3.238)$$

The combined reluctance for path 2 is given by,

$$\Re_{2,4} = \Re_2 + \Re_4 \quad (3.239)$$

The permeance of track 2 is calculated as,

$$P_2 = \frac{1}{\Re_{2,4}} \quad (3.240)$$

The magnetic circuit equation of track 2 can be written as,

$$\Im_2 = T_{ph} i = 2(H_s l_s + H_r l_r) + \frac{B_s A_{2s}}{P_2} + H_{rc} l_{rc} + H_y l_y \quad (3.241)$$

The inductance of track 2 is then calculated as,

$$L_{u2} = \Im_2 \frac{B_{s\,min} A_{2s}}{i_p^2} \quad (3.242)$$

Obviously, track 4 has the exact same inductance and the procedure need not be repeated.

Therefore,

$$L_{u4} = L_{u2} \quad (3.243)$$

Track 3: Considering Fig.3.31, the area of the track at the stator pole is calculated as,

$$A_{3s} = \frac{\beta_s}{5}\frac{D}{2}L \quad (3.244)$$

The angle θ_2 is given by,

$$\theta_2 = \frac{\frac{\beta_r}{2}\left(\frac{D}{2} - g\right)}{\left(\frac{D}{2} - g - h_r\right)} \quad (3.245)$$

The angle θ_3 is calculated as,

$$\theta_3 = \frac{\theta_{rp}}{2} - \theta_2 \quad (3.246)$$

The area of the track at the rotor core is calculated,

$$A_{3rc}= 2\left(\frac{D}{2} - g - h_r\right)\theta_3\ L \tag{3.247}$$

The average area of A3 is calculated as,

$$A_3=\frac{A_{3s}+A_{3rc}}{2}=\frac{1}{2}\frac{\beta_s}{5}\frac{D}{2}L + \left(\frac{D}{2} - g - h_r\right)\theta_3 L \tag{3.248}$$

The length of the air gap is given as,

$$l_3=\frac{D}{2} - g - h_r \tag{3.249}$$

The area of the stator pole is given as

$$A_{3s}= \frac{\beta_s}{5}\frac{D}{2}L \tag{3.250}$$

The length of the path through the stator, yoke and rotor core is given by (3.73), (3.77) and (3.76), respectively. The area of the yoke is given by (3.86). As the rotor moves, although the shape of the track changes, the length and the area of the path is assumed to be same without too much error in the calculations

The reluctance of the air gap of track 3 is given as,

$$\mathfrak{R}_3= \frac{2l_3}{\mu_0 A_3} \tag{3.251}$$

The permeance of track 3 is calculated as,

$$P_3 = \frac{1}{\mathfrak{R}_3} \tag{3.252}$$

The magnetic circuit equation of track 3 can be written as,

$$\mathfrak{I}_3=T_{ph}i=2(H_s l_s) + \frac{B_s A_{3s}}{P_3} + \frac{H_{rc} l_{rc}}{2} + \frac{H_y l_y}{2} \tag{3.253}$$

The unaligned inductance of track 3 is then calculated as,

$$L_{u3}= \mathfrak{I}_3 \frac{B_{smin} A_{3s}}{i_p^2} \tag{3.254}$$

Track 6: To calculate the area A_6 and length l_6, consider Fig.3.37. The area of the track at the stator pole is calculated as

$$A_{6s}= \frac{h_s}{4} L \tag{3.255}$$

The area of the track at the rotor pole is calculated,

$$A_{6r}= \frac{\beta_r}{4} L \left(\frac{D}{2} - g\right) \tag{3.256}$$

The average area of A_6 is calculated as,

$$A_6=\frac{A_{6s}+A_{6r}}{2} \quad (3.257)$$

Track 6 can be assumed to be an arc centered at the point D.

The length OA is assumed to be

$$y_1=\frac{D}{2}\cos\left(\frac{\beta_s}{2}\right)+\frac{h_s}{8} \quad (3.258)$$

The length AB is obtained in (3.153).The angle $\theta_1$is calculated as can be calculated from (3.153) and (3.207)

$$\theta_1=\tan^{-1}\left(\frac{x_l}{y_l-\left(\frac{D}{2}-g-h_r\right)}\right) \quad (3.259)$$

The angleθ_2 is assumed to be

$$\theta_2=\frac{\pi}{N_r}-\frac{3\beta_r}{8}-\theta \quad (3.260)$$

The length CE is given by

$$y_2=\left(\frac{D}{2}-g\right)\cos(\theta_2)-\left(\frac{D}{2}-g-h_r\right) \quad (3.261)$$

The length DE is given by

$$x_2=\left(\frac{D}{2}-g\right)\sin(\theta_2) \quad (3.262)$$

The angle θ_3 can be calculated as

$$\theta_3=\tan^{-1}\left(\frac{y_2}{x_2}\right) \quad (3.263)$$

The angle θ_4 is obtained from (3.259) and (3.263) as,

$$\theta_4=\frac{\pi}{2}-\theta_1-\theta_3 \quad (3.264)$$

The length DB is given from (3.153) and (3.259) as,

$$r_1=\frac{x_1}{\sin(\theta_1)} \quad (3.265)$$

The length CD is given from (3.261) and (3.262) as,

$$r_2=\sqrt{x_2^2+y_2^2} \quad (3.266)$$

The length of the flux path is approximately given from (3.244)-(3.266) as,

$$l_6=\frac{r_1+r_2}{2}\theta_4 \quad (3.267)$$

The area of the yoke and rotor core is given by (3.86) and (3.65)

The length of the path in the rotor is given by (3.163). The length of the path in the stator is calculated as,

$$l_s=h_s+\frac{C}{2}-\frac{l}{2}\frac{h_s}{4} \quad (3.268)$$

The reluctance of the air gap of path 6 in the upper portion is given as,

$$\mathfrak{R}_6 = \frac{l_6}{\mu_0 A_6} \tag{3.269}$$

The above calculations are valid for the track passing in the upper portion of the stator. In the lower portion, the pole is moving away from the excited portion. This is similar to the effects experienced by track 7 in the upper portion. Therefore, track 7 calculations are performed next.

Track 7: To calculate the area A_7 and length l_7, consider Fig.3.37. The area of the track at the stator pole is calculated as,

$$A_{7s} = \frac{h_s}{4} L \tag{3.270}$$

The area of the track at the rotor pole is calculated,

$$A_{7r} = \frac{\beta_r}{4} L\left(\frac{D}{2} - g\right) \tag{3.271}$$

The average area of A_7 is calculated as,

$$A_7 = \frac{A_{7s} + A_{7r}}{2} \tag{3.272}$$

Track 7 can be assumed to be an arc centered at the point D. The length AO is given (3.258) and the length AB is given by (3.153). The angle θ_1 can be calculated by (3.259). The angle θ_2 is assumed to be

$$\theta_2 = \frac{\pi}{N_r} - \frac{3\beta_r}{8} + \theta \tag{3.273}$$

The length CE is given by,

$$y_2 = \left(\frac{D}{2} - g\right)\cos(\theta_2) - \left(\frac{D}{2} - g - h_r\right) \tag{3.274}$$

The length DE is given by,

$$x_2 = \left(\frac{D}{2} - g\right)\sin(\theta_2) \tag{3.275}$$

The angle θ_3 can be calculated as,

$$\theta_3 = \tan^{-1}\left(\frac{y_2}{x_2}\right) \tag{3.276}$$

The angle θ_4 is obtained from (3.259) and (3.275) as,

$$\theta_4 = \frac{\pi}{2} - \theta_1 - \theta_3 \tag{3.277}$$

The length DB is given by (3.265).

The length CD is given from (3.274) and (3.275) as,

$$r_2 = \sqrt{x_2^2 + y_2^2} \tag{3.278}$$

Length of the flux track is approximately given from (3.265), (3.277) and (3.278) by,

$$l_7 = \frac{r_1+r_2}{2}\theta_4 \quad (3.279)$$

The length of the track in the rotor is calculated from (3.163). The length of the track in the stator is calculated from (3.268).

The reluctance of the air gap of track 7 in the upper portion is given as,

$$\Re_7 = \frac{l_7}{\mu_0 A_7} \quad (3.280)$$

The combined reluctance for track 6 is given by,

$$\Re_{6,7} = \Re_6 + \Re_7 \quad (3.281)$$

The permeance of track 6 is calculated as,

$$P_6 = \frac{1}{\Re_{6,7}} \quad (3.282)$$

The magnetic circuit equation of track 6 can be written as,

$$\Im_6 = T_{ph} i = \Re_L \emptyset = 2(H_s l_s + H_r l_r) + \frac{B_s A_{6s}}{P_6} + H_{rc} l_{rc} + H_y l_y \quad (3.283)$$

The unaligned inductance of track 6 is then calculated as,

$$L_{u6} = \Im_6 \frac{B_{s\,min} A_{6s}}{i_p^2} \quad (3.284)$$

Obviously, track 7 has the exact same inductance and the procedure need not be repeated.

Therefore,

$$L_{u7} = L_{u6} \quad (3.285)$$

Track 8: To calculate the area A_8 and length l_8, consider Fig.3.38. The area of the track is calculated as,

$$A_8 = \frac{h_s}{2} L \quad (3.286)$$

Track 8 can be assumed to be an arc centered at the center of the shaft.

The length AO is assumed to be,

$$y_1 = \frac{D}{2}\cos\left(\frac{\beta_s}{2}\right) + \frac{h_s}{2} \quad (3.287)$$

The length AB is given by (3.153). The angle θ_1 can be calculated from (3.153) and (3.287) as,

$$\theta_1 = \tan^{-1}\left(\frac{x_1}{y_1}\right) \quad (3.288)$$

The angle θ_2 is assumed to be,

$$\theta_2 = \frac{2\pi}{N_s} - 2\theta_1 \quad (3.289)$$

The length CO is given from (3.153) and (3.288) as,

$$r_1 = \frac{x_1}{\sin(\theta_1)} \quad (3.290)$$

The length of the track is given from (3.289) and (3.290) as,

$$l_8 = r_1\theta_2 \quad (3.291)$$

The area of the stator core is given by,

$$A_s = \frac{h_s}{2} L \quad (3.292)$$

The length of the path through the stator,

$$l_s = \frac{h_s}{2} + \frac{C}{2} \quad (3.293)$$

The length of the path through the yoke is given by (3.177). The magnetic circuit equation of track 8 can be written as,

$$\Im_8 = \frac{1}{2}\frac{3T_{ph}i}{4} = \Re_L \emptyset = 2(H_s l_s) + \frac{B_s A_8}{P_8} + H_y l_y \quad (3.294)$$

The unaligned inductance of track 8 is then calculated as,

$$L_{u8} = \Im_8 \frac{B_{s\,min} A_g}{i_p^2} \quad (3.295)$$

Track 9: To calculate the area A_9 and length l_9, consider Fig.3.40. The area of the track is calculated as,

$$A_9 = \frac{h_s}{4} L \quad (3.296)$$

Track 9 is assumed to be an arc centered about point B. The length is approximately calculated as,

$$l_9 = \frac{h_s}{8}\frac{\pi}{2} \quad (3.297)$$

The stator and yoke area remain same as above. The length of the path in the stator is calculated as,

$$l_s = \frac{1}{2}\frac{h_s}{4} + \frac{C}{2} \quad (3.298)$$

The yoke length is approximately,

$$l_y = l_s \quad (3.299)$$

The magnetic circuit equation of track 9 can be written as,

$$\Im_9 = \frac{1}{2}\frac{T_{ph}i}{2} = \Re_L \emptyset = H_s l_s + \frac{B_s A_9}{P_9} + H_y l_y \quad (3.300)$$

The unaligned inductance of track 9 is then calculated as,

$$L_{u9}= \Im_9 \frac{B_{s\,min} A_9}{i_p^2} \quad (3.301)$$

The total inductance at a position θ in area I is given by,

$$L_{u\theta} =(L_{u1} + L_{u2} + L_{u3} + L_{u4} + L_{u5} + L_{u6+} L_{u7}) + 4(L_{u8} + L_{u9}) \quad (3.302)$$

Zone II: $\frac{\pi}{N_r} - \left(\frac{\beta_s+\beta_r}{2}\right) < \theta < \frac{\pi}{N_r} - \left(\frac{-\beta_s+\beta_r}{2}\right)$

The flux tracks are identified as follows:

Track 1: This track is considered to be a track that encompasses the overlap area. Therefore the area of the track is given by

$$A_1=L\frac{D}{2}\left(\theta - \frac{\pi}{N_r} + \left(\frac{\beta_s+\beta_r}{2}\right)\right) \quad (3.303)$$

The length of the air gap is given by,

$$l_1 = g \quad (3.304)$$

The area of the stator core is given by,

$$A_{1s} = A_1 \quad (3.305)$$

The length of the path through the stator, yoke, rotor and rotor core is given by (3.73) ,(3.77),(3.163) and (3.76) The area of the yoke and rotor core is given by (3.86) and (3.65)

The area of the rotor core is given by

$$A_{lr}=A_l \quad (3.306)$$

The reluctance of track 1 is calculated as,

$$\Re_1=\frac{2l_l}{\mu_0 A_l} \quad (3.307)$$

The permeance of track 1 is,

$$P_1=\frac{l}{\Re_1} \quad (3.308)$$

The magnetic circuit equation of track 1 can be written as,

$$\Im_1=T_{ph}i=2(H_s l_s+ H_r l_r) +\frac{B_s A_l}{P_l} + \frac{H_{rc} l_{rc}}{2} + \frac{H_y l_y}{2} \quad (3.309)$$

The inductance of track 1 is then calculated as,

$$L_{a1}= \Im_1 \frac{B_{s\,min} A_l}{i_p^2} \quad (3.310)$$

Track 2: To calculate the length l_2 and area A_2, consider Fig.3.45. The area of the track at the rotor pole is calculated and is assumed to be equal to the track area,

$$A_2=L\frac{D}{2}\left(\beta_r-\theta+\frac{\pi}{N_r}-\left(\frac{\beta_s+\beta_r}{2}\right)\right) \quad (3.311)$$

Track 2 can be assumed to be an arc centered at the point D.

The angle θ_2 is assumed to be,

$$\theta_2=\frac{\left(\beta_r-\theta+\frac{\pi}{N_r}-\left(\frac{\beta_s+\beta_r}{2}\right)\right)}{2}+\frac{\beta_s}{2} \quad (3.312)$$

The length CE is given by,

$$y_2=\left(\frac{D}{2}-g\right)\cos(\theta_2)-\left(\frac{D}{2}-g-h_r\right) \quad (3.313)$$

The length DE is given by,

$$x_2=\left(\frac{D}{2}-g\right)\sin(\theta_2) \quad (3.314)$$

The angle θ_3 can be calculated from (3.313) and (3.314) as,

$$\theta_3=\tan^{-1}\left(\frac{y_2}{x_2}\right) \quad (3.315)$$

The length CD is given from (3.313) and (3.314) as,

$$r_2=\sqrt{x_2^2+y_2^2} \quad (3.316)$$

The angle$\theta 1$ is assumed as,

$$\theta_1=\frac{\beta_s}{2} \quad (3.317)$$

The angle θ_4 is obtained from (3.315) and (3.317) as,

$$\theta_4=\frac{\pi}{2}-\theta_1-\theta_3 \quad (3.318)$$

The length of the flux path is approximately given from (3.316) and (3.318) by,

$$l_2=r_2\theta_4 \quad (3.319)$$

The reluctance of track 2 is calculated as,

$$\Re_2=\frac{2l_2}{\mu_0 A_2} \quad (3.320)$$

The permeance of track 2 is

$$P_2=\frac{l}{\Re_2} \quad (3.321)$$

The yoke and rotor core area are given by (3.86).

The stator pole area and the rotor pole area are given by,

$$A_{2s}=A_{2r}=A_2 \quad (3.322)$$

The length of the path in the rotor is calculated from (3.163). The length of the path in the stator is calculated approximately as,

$$l_s = h_s + \frac{C}{2} - \left(\frac{D}{2} - g\right)(\theta_2) \quad (3.323)$$

The magnetic circuit equation of track 2 can be written as,

$$\Im_2 = T_{ph} i = \Re_L \emptyset = 2(H_s l_s + H_r l_r) + \frac{B_s A_2}{P_2} + \frac{H_{rc} l_{rc}}{2} + \frac{H_y l_y}{2} \quad (3.324)$$

The inductance of track 2 is then calculated as,

$$L_{a2} = \Im_2 \frac{B_{s\,min} A_2}{i_p^2} \quad (3.325)$$

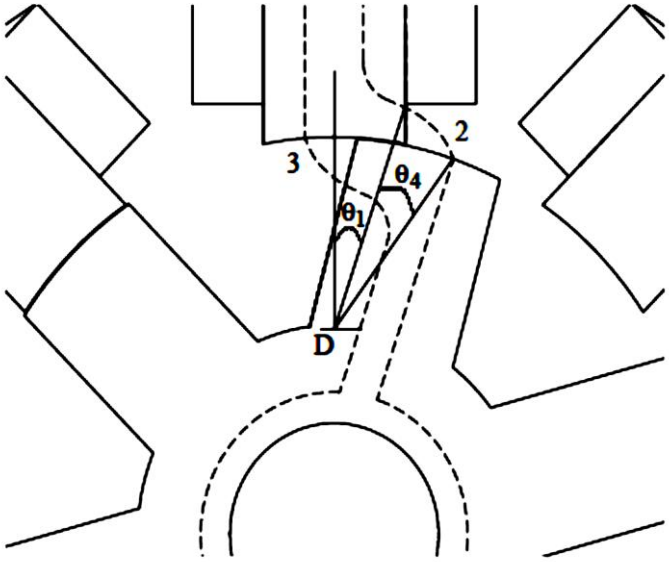

Fig.3.45 Track 2 and Track 3 calculations in the overlap region

Track 3: To calculate the area A_3 and length l_3, consider Fig.3.45. The area of the track at the rotor pole is calculated and is assumed to be equal to the track area,

$$A_3 = L\frac{D}{2}\left(\beta_s - \theta + \frac{\pi}{N_r} - \left(\frac{\beta_s + \beta_r}{2}\right)\right) \quad (3.326)$$

Track 3 can be assumed to be an arc similar to the arc in track 1 of zone 1. The coordinate of the corner of the rotor pole is given by

$$(x_1, y_1) = \left(\left(\frac{D}{2} - g\right)\sin\left(\frac{\pi}{N_r} - \theta - \frac{\beta_r}{2}\right), \left(\frac{D}{2} - g\right)\cos\left(\frac{\pi}{N_r} - \theta - \frac{\beta_r}{2}\right)\right) \quad (3.327)$$

The varying point on the stator pole has the coordinates as,

$$(x_2, y_2) = \left(\left(\frac{-D}{2}\sin\left(\frac{\theta - \left(\frac{\pi}{N_r} - \frac{\beta_s + \beta_r}{2}\right)}{2}\right)\right), \frac{D}{2}\cos\left(\frac{\theta - \left(\frac{\pi}{N_r} - \frac{\beta_s + \beta_r}{2}\right)}{2}\right)\right) \quad (3.328)$$

The arc length can be considered to be,

$l_{x3}=\sqrt{(x_2-x_1)^2+(y_2-y_1)^2}$ (3.329)

The length of the track is approximately given by,

$l_3=l_{x3}\frac{\pi}{2}$ (3.330)

The area of the stator pole and rotor pole are given as,

$A_{3s}=A_{3r}=A$ (3.331)

The yoke and rotor core areas and the length of the path through the stator, yoke and rotor core are given by (3.86), (3.65), (3.73), (3.77) and (3.76), respectively.

The length of the path through the rotor,

$l_r=h_r-l_{x3}$ (3.332)

The reluctance of track 3 is calculated as,

$\mathfrak{R}_3=\frac{2l_3}{\mu_0 A_3}$ (3.333)

The permeance of track 3 is,

$P_3=\frac{l}{\mathfrak{R}_3}$ (3.334)

The magnetic circuit equation of track 3 can be written as,

$\Im_3 = T_{ph}i = 2(H_s l_s+H_r l_r) + \frac{B_s A_3}{P_3} + \frac{H_{rc} l_{rc}}{2} + \frac{H_y l_y}{2}$ (3.335)

The unaligned inductance of track 3 is then calculated as,

$L_{a3}=\Im_3 \frac{B_{s\,min} A_3}{i_p^2}$ (3.336)

The tracks 4 and 5 are assumed to be similar to tracks 8 and 9 from zone I.

The total inductance at a position θ in zone II is given by,

$L_{a\theta}=(L_{a1}+L_{a2}+L_{a3})+4(L_{u4}+L_{u5})$ (3.337)

Zone III: $\frac{\pi}{N_r}-\left(\frac{-\beta_s+\beta_r}{2}\right)\leq\theta<\frac{\pi}{N_r}$ **;**Zone III can be assumed to be the area where the rotor and stator are completely overlapping. The calculation of the inductance in this position is described by the aligned inductance

3.5 Calculation of Motor winding inductances:

$A_s=\frac{D}{2}L\beta_s=\frac{48.71\times10^{-3}}{2}$ x 90 x 10^{-3} x $\frac{21\pi}{180}=7.77$ x 10^{-4}m^2

The flux in the stator pole $\varnothing$ is given by

$\varnothing=B_s A_s=2039.62$ x 10^{-6}Wb

The flux in the yoke $\emptyset_y$ is given by

$\emptyset_y = \frac{\emptyset}{2} = \frac{B_s A_s}{2} = 1019.81 \times 10^{-6} Wb$

The area of the yoke A_y can be set as,

$A_y = A_s = 803 \times 10^{-6} m^2$

The back iron thickness C is obtained as,

$C = \frac{A_y}{L} = 8.92 \times 10^{-3} m$

The stator pole height h_S is given by,

$h_S = \frac{D_o}{2} - C - \frac{D}{2} = 7.08 mm$

The rotor pole area A_r is given by,

$A_r = \left(\frac{D}{2} - g\right) L\beta_r = 871 \times 10^{-6} m$

The rotor pole flux density B_r is given by,

$B_r = \frac{B_s A_s}{A_r} = 2.34 T$

The area of the rotor core A_{rc} is given by,

$A_{rc} = \frac{A_s}{1.6} = 3.43 \times 10^{-4} m$

The height of the rotor pole h_r is calculated as,

$h_r = \frac{D}{2} - g - \frac{D_{sh}}{2} = 9.55 mm$

Neglecting leakage and fringing, the air-gap area can be approximately written as,

$A_g = \left(\frac{D}{2} - \frac{g}{2}\right)\left(\frac{\beta_r + \beta_s}{2}\right) L = 1.27 \times 10^{-3} m$

The flux density in the air-gap B_g is given by,

$B_g = \frac{A_s B_s}{A_g} = 1.606 T$

The magnetic field intensity of the air-gap H_g is calculated as,

$H_g = \frac{B_g}{4\pi \times 10^{-7}} = 1278014.193 AT/m$

The magnetic field intensities in the stator pole, stator yoke, rotor pole and rotor core are designated as H_s, H_y, H_r and H_{rc}, respectively are obtained from the BH characteristics of the stator core and rotor core material,

By using the above equations the values of $l_s, l_g, l_r, l_{rc}, l_y$ are calculated and by substituting all these values in the above equation , we have the aligned inductance , The aligned saturated inductance at maximum current neglecting leakage, as,

$L_{aligned} = \frac{T_{ph}\emptyset}{i_p} = \frac{\Im B_s A_s}{i_p^2}$=7.64mH.

$L_a = L_{aligned} + 4L_{af}$ = 8.11mH

Similarly using the equations described in section (3.4.2), the unaligned inductance can be calculated as, L_u is 1.49 mH. The aligned inductance including leakage is calculated as La is 8.11 mH

3.6 Experimental set up for motor winding inductance measurements:

Design Verification

A satisfactory control strategy can be developed if true knowledge of motor winding inductance and the flux-linkage characteristics of the machine are available. Hence knowledge of actual flux linkage versus current profiles is essential for design verification and performance prediction of switched reluctance motors

3.6.1 Experimental Set up:

To verify the main winding inductance of SRM, the circuit shown in Fig.4.1 (Chapter 4) is used. .In order to limit the peak value of current through the motor winding a resistance of known value is connected in series with the main winding and a switch (an electronic switch). A DC pulse voltage is applied to this combination consisting of external resistance and the motor phase winding, and current through this series combination is allowed to reach steady state current. The circuit can be treated as simple series RL, and the current rises exponential. The raise in current is decided by the time constant of the circuit. When the circuit is switched off, the current starts decaying. From this decay rate of current, it is possible to determine the time constant of the RL circuit, hence from this; the inductance of the motor winding can be calculated. The main winding resistance was taken into account since the main winding was not a pure inductor. Each phase winding resistance of the motor was measured separately from a experimental set up and it was approximately 0.66 Ω per phase

Table 3.5 Inductance versus Current

I(A)	$I_{measured}$(A)	63.2%of $I_{measured}$(A)	$\tau = \frac{L}{R}$	L(mH)
1	0.99	0.632	1.5	1.22
2	2.06	1.3	2.25	1.94
3	3.05	1.927	2.5	2.02
4	4.07	2.572	2.33	1.92
5	5.02	3.172	1.09	0.78

Table 3.6 Inductance versus the rotor positions

Rotor Position (Degrees)	Inductance(mH)	Rotor Position (Degrees)	Inductance(mH)
0	1.21		
2	1.47	24	7.07
4	1.56	26	6.98
6	1.69	28	6.39
8	2.66	30	5.74
10	3.70	32	4.81
12	5.52	34	3.26
14	5.61	36	2.98
16	6.18	38	1.69
18	7.29	40	1.57
20	8.15	42	1.46
22	9.34	44	1.21

3.6.2 Experimental Results

Fig.3.46 (a) shows the single pulse view decay of the current. From this plot, the amplitude of the current was measured and then 63.2 % value of the current was determined and found on the curve. This point was then shifted to the axis for a marker, and then time cursors were used to determine the time between the points where the current first started to decay to the point when it reaches the 63.2 % value. This value of time is equal to the time constant of the RL circuit. Table 3.5 shows the time constants and inductances for DC currents ranging from one ampere to five Amperes. Table 3.6 gives the inductance of the motor winding at different rotor positions Fig.3.46 (b) shows Inductance Profile of a single phase from the experimental results.

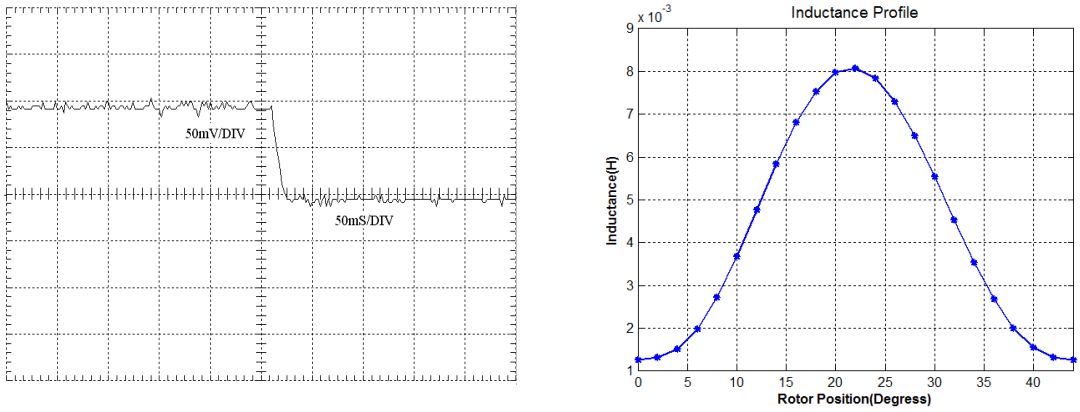

(a) (b)

Fig.3.46 (a) Expanded Inductance Measurements at 2Amp DC
(b) Inductance Profile from the experimental results

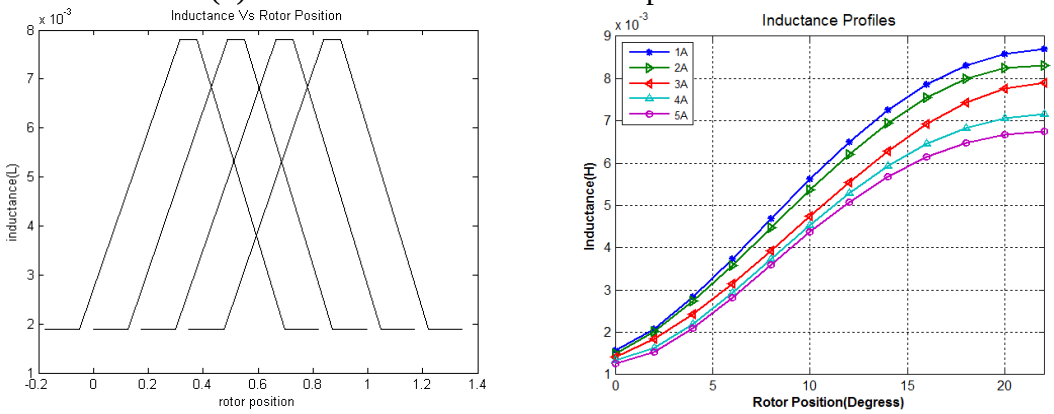

(a) (b)

Fig.3.47
(a) Inductance Profiles for Specific DC Currents from simulation results
(b) Inductance Profiles for Specific DC Currents from Experimental Results and Interpolation

Also, a measurement was taken for an unaligned inductance value. A small current of 3 A was passed through the setup while the rotor shaft was held at the unaligned position of 0 degrees. The same procedure as the one described in Section 3.6.1 was followed. The inductance value calculated was 1.21 mH. Fig.3.47 (a) shows Inductance Profiles for Specific DC Currents from simulation results. Fig.3.47 (b)

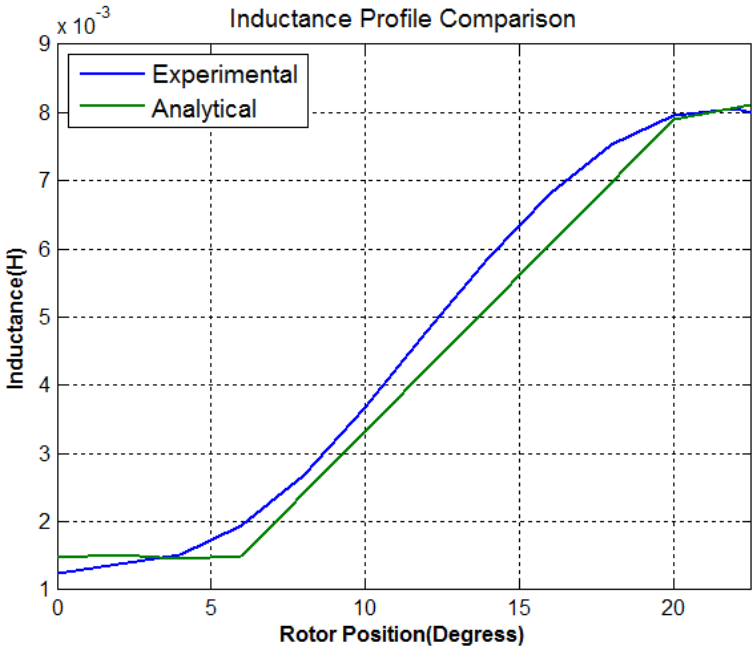

Fig.3.48 Comparison of analytical inductance calculation and FEA results at rated current

presents the measured results for inductance profiles at currents ranging from one Ampere to five Amperes DC. It can be seen that the measured results for five Amperes does correspond to the analytical results for five Amperes with some slight error. The peak inductance for the analytical results is approximately 8.11 mH while the experimental value is approximately 9.33 mH. The unaligned position analytical result is approximately 1.49 mH, while the experimental result is approximately 1.21mH. The error is high, but it is still acceptable. From the shape of the inductance profile from the analytical analysis and the measured inductance points for aligned and unaligned positions, it was possible to extract the other inductance curves at different currents. As the current is decreased, the inductance rises. Also, it can be noted that the unaligned inductance does not vary much with decreasing current.

3.6.3 Inductance Calculation Comparison

The inductance of a phase is calculated analytically using the procedure described in section 3.4.1 and 3.4.2. A very good correlation is seen in Fig.3.78 between the results especially at the unaligned and aligned position

Table: 3.7 Inductance Calculation Comparisons;

	Analytical Results	Experimental Results
Aligned Inductance	8.11 mH	8.34 mH
Un Aligned Inductance	1.49 mH	1.57 mH

3.7 Summary

This chapter covers the design procedure of an 8/6 switched reluctance motor from the first principles. A step-by-step design procedure of SRM is discussed in detailed. No major assumptions are made in the design although a few assumptions are made in the analysis section of the design procedure. It differs from some of the sources cited in the procedure of designing the machine, which is simplified for a person with basic knowledge to attain. The procedure is perceptive and it may be argued that there is no major contribution. But an intensive literature search did not reveal the procedure followed although it may be claimed that other sources may follow the same procedure but did not document them. Distinct references such as (Krishnan, R. 2001) do have a design procedure outlined. This process requires extensive prior knowledge and experience in designing switched reluctance machines. The procedure outlined in this thesis requires only basic dimension data for Switched Reluctance motors.

Since it is difficult to accurately incorporate the saturation effect and the detailed geometrical information in the empirical formulas, the finite element method was used for fine-tuning and validating the design. Torque characteristics, flux and flux linkages of SRMs are calculated by FEM for various stator current excitations and rotor position angles. Inductance of a stator winding was also evaluated by FEM. Incorporating the FEM-calculated parameters and the analytical model enables the study into the dynamic performance of an SRM under the converter control. A 8/6 1 kW 4 phase prototype SRM has been developed as an example of the design process and this prototype is designed keeping in view of automobile applications

The analytical calculation of the unaligned inductance in this chapter follows the basic principles of electromagnetic and does not rely on any previous sources whose documentation is hard to verify. The procedure outlined in this thesis is easy to follow and while it has approximately the same error as in other methods when compared to

the finite element analysis, the value tends to be higher than the finite element analysis value which is a positive as far as machine design is concerned since the analytical output torque would be calculated to be lower than the finite element value or the actual measured value in the machine. This would lead to a slight overdesign of the machine that would be perfectly acceptable rather than designing a machine that would not produce the required output torque.

The design verification using analytical procedure and experimental methods are also explained in detail. The experimental setup for determining the motor winding inductance at different rotor positions is discussed in detailed. These verification techniques have their own advantages and disadvantages in design verification. Moreover, it is observed that verification of the design either using analytical procedure or experimental method gave slightly similar results.

.

Chapter 4 Determination of flux-linkage characteristics of SRM

Determination of the magnetic characteristics is a key point to the optimizing design or control strategy evaluation in a SR motor. The SR motor drive performance is strongly dependent on its design and control. Therefore, the motor mathematical model and its accuracy are the important issues. And the most important factor for all SRM models is constituted by the flux linkage versus current characteristics calculation, which can be through analytically, via numerical field analysis by employing usually the finite element method (FEM), or by combining the analytic and numeric calculations and other by experimental approach.

In particular, the SRM phase magnetization characteristics vary strongly as a function of the excitation current and rotor position. Therefore, numerical methods must be used for the calculation of the magnetic field and for the prediction of the SRM magnetization characteristics.A number of previous literatures is available on the magnetic characteristic models and experimental approaches. A set of analytical expressions has been proposed or (Krishnan, R. 2001) for flux-linkage model design. The magnetization curves model can also be obtained by finite-element analysis (Parreira, B., S. Rafael, A.J. Pires, P.J. Costa Branco 2005) . Although general expressions are achieved in the former models, many details of the machine geometry and structure are required for both models mentioned above and being also a time consuming task. Although the FEM was a time-consuming and difficult method in the past, with contemporary high speed computers with large memory, the method can be used properly in analysis of electric machines. In addition, various commercial finite-element packages such as ANSYS have been so far developed for this purpose There are, at least, two methods to obtain flux- linkage characteristic for experimental purposes:

- Simulation approach, using finite-element models or lumped parameter based calculation or even polynomial functions as a look-up table based model (Rahman M.F. et al 2002)
- Experimental approach using the direct measurement or deriving the flux-linkage characteristic from the measured phase voltage and current and after search for the adjusted analytical functions (Xiang-Dang Xue, K. W. E. Cheng, and S. L. Ho 2002).

The former approach generally requires less expense and time in comparison to the second one. Nevertheless, due to faults in the machine processing plus simplifications concerning simulations methods, the real SRM could present different features from the simulation model. For these reasons, In the present chapter we started with the experimental tests in order to determine the real machine characteristic and afterwards - simulation approach, using finite-element models for verification analysis is carried out. Finite element method analysis was used by Dawson to determine the magnetic characteristics of an SRM. In the present chapter measurement of magnetic characteristics of SRM by experimental , analytical and FEM are discussed. A new way of finding motor magnetising characteristics using 3-D ANSOFT FEM is carried out to validate the correctness of the measured and calculated resutls

4.1 Characteristics of Regular SRM

The requirement for finding the performance characteristics of the SRM is to generate the magnetization curves. On the other hand, these SRM characteristics depend on numerous factors (G.S,Buja, M.I.Valla 1994) namely machine structure (number of phases, number of stator and rotor poles, stator and rotor poles arcs), magnetic properties of the laminations, converter topology (P. Lobato, A. J. Pires, J.A. Dente 2003; David A. Torrey 2002). Due to the non-linear magnetization of the iron and to the variable air gap, the flux-linkage of phase j, Ψ_j is a nonlinear function of the stator phase current i_j and rotor angular position θ

$$\Psi_j = \Psi_j(i_j, \theta) \tag{4.1}$$

This complex function can be obtained by finite-element field computation using the machine geometry and properties or experimental measurement on the real machine or by analytical procedure. Each method presents advantages or drawbacks in terms of accuracy, computation time, problem definition time, etc.

4.1.1 Analytical Procedure

Various analytical methods have been developed over the years for predicting the magnetization curves of switched reluctance motors. (Miller, T.J.E. *et* al.1990) presents an efficient analytical model, based on flux-linkage against current. The model avoids the concept of inductance and includes all the significant electromagnetic and dynamic characteristics, being very suitable for automated

computer calculations and performance analysis. The drawback is that several correction factors have to be introduced in order to improve accuracy. Hence, these correction factors are derived from two or three points on pre-existing magnetization curves determined either by measurements or calculated by finite element methods.

(Krishnan, R. 2001) develops a procedure for analytically deriving the machine characteristics given the motor dimensions and excitation conditions along with the number of turns per phase are given. Even though the calculation of the flux-linkage appears to be simple, data generation for their calculation is a complex process.

(Vujicic, V. et al. 2000) presented a simple non-linear model for the switched reluctance motor which is very convenient for use in the earlier stage of SRM design, to minimize the time required for finding the optimal configuration. The model produces accurate torque shape for a given current and accurate flux-linkage-current relation. As in Miller's paper, the drawback of the method is that it requires a minimum of pre-calculated or measured input data.

Although the analytical formulation is very tentative, the calculation time involved in solving the equation system is large and may take several hours of computing time. The main difficulty of this method occurs when rotor and stator pole begins to overlap.

4.1.2 Finite element analysis

The Finite Element Method (FEM) of the magnetic field inside electric machines became popular in the 1980's. Every electromagnetic problem can be represented using Maxwell's partial differential equations, the constitutive equations (material behaviour) and the appropriate boundary conditions in space and time. An analytical solution in closed form can be obtained only for simple geometries and linear material behaviour. Technical applications involve non-linear materials and complex geometries, so that the electric or magnetic field has to be calculated numerically. (R. Belmans 1994) suggests that every finite element calculation contains three steps: pre-processing, solving and post-processing. The finite element method transforms the partial differential equations in a set of algebraic equations. This set of algebraic equations is solved using specific

numerical techniques. This computation step is called solving. Depending on the problem specifics, the program solver that can handles this part of the analysis is chosen between various well-known techniques like successive substitution .The finite element method allows the designer to specify all possible structural details as well as material characteristics. The material models used in the finite element software are often approximative of the real material behaviour. The data used for these models come from measurements representing the material as it is before assembly into the machine. Iron is the key material in designing and analyzing the electric machine, but the relevant material effects such as an isotropic permeability, frequency dependent hysteresis and iron losses, an isotropic magnetostriction etc. are hard to capture in a sufficiently simple material model. An accurate measurement is also very difficult to make, since these effects influence each other. The SR motor operates in modes resulting in high levels of magnetic saturation, and this leads to the widespread use of the finite element method as a means of predicting flux-linkage characteristics. FEM is usually applied for steady-state performance computation. The technique demands the knowledge of the relationships of motor output variables to motor dimensions, number of poles, number of turns per phase, excitation current, and current conduction angle. The skills of the user and his capability of correctly defining the nature of the problem is an important prerequisite for the accuracy of the results obtained using finite elements.

The FEM analysis of SRM can be done using 2-D or 3-D solvers. Two-dimensional solvers cannot give accurate magnetization curves because of the significant influence of end effects in partially aligned positions. A more accurate result is obtained by using a three dimensional solvers. However there are no important differences between the results obtained by applying a 2-D or a 3-D FEM solver on the SRM. Most of the authors have used 2-D FEM computation, adding correction factors to compensate the errors.

4.1.3 Experimental measuring methods

There are two experimental methods that can be used to measure such curves either directly or indirectly, direct and indirect method.

4.1.3.1 Indirect Method:

The indirect method consists in the determination of magnetization curves using the static torque curves. From the measurement of the static torque characteristic, the complete set of flux-linkage characteristics may be calculated. The accurate determination of the static torque curves is not easy, as any mechanical misalignment leads to large errors in the calculations. The static torque curves are insufficient to reconstruct the magnetization curves. Therefore, the knowledge of one value of flux-linkage by some other means is absolutely necessary.

4.1.3.2 Direct Method

In case of direct method the coil is energized either by an AC source or a DC source and steady state current in case of AC excitation is measured and transient current response in case of DC excitation is recorded.

(a) Sinusoidal Excitation Voltage to the SRM phase:

In the first case, a sinusoidal voltage at different positions of the locked rotor supplies the SRM phase. The supply source can be an adjustable transformer. The resulting RMS current is measured, and knowing the winding resistance, the flux-linkage can be calculated. This method has two error sources: distortion of the applied voltage (due to the non-ideal source) and distortion of the resulting current (due to magnetic saturation).

(b) DC Excitation Voltage to the SRM phase:

This method is the most communally used. It consists in applying a step voltage to one SRM phase and the rate of rise of the current is measured. The winding resistance has to be measured before each test, allowing accounting for the influence of the temperature rise. Before each test, any offset has to be removed. Such offsets can be introduced by the iron core remnant flux density.

Chapter 4 Determination of flux-linkage characteristics of SRM

Using the processed data the flux linkage characteristics are calculated at different rotor positions, some of the direct methods are outlined in this section

(a) Bridge method

The flux-linkage characteristics can be obtained by inductance measurement by using suitable AC bridge method. In this method, the inductance of a phase is measured with different DC bias for different rotor positions. The flux-linkage characteristics are obtained by integration. This approach has been used earlier for other conventional machines to account for saturation. In this method, the accuracy of the result gets affected by the errors associated with bridge measurements and the non - sinusoidal phase currents with DC bias.

(b) Rising Current method

When one of the phases of SRM is energized with a voltage pulse with all other phases open and with its rotor held in position, its voltage equation is given by

$$v(t) = Ri(t) + \frac{d\varphi}{dt} \tag{4.2}$$

where *v(t)* is the phase voltage, R is the phase resistance, and *i(t)* is its current. As all the other phases are kept open, the flux-linkage of the phase winding will not be affected due to the mutual inductance between the phases. Neglecting the mutual inductance between the coupled conducting parts of the motor, the total flux-linkage of the phase winding can be considered to be due to its current, *i(t).* Therefore, the flux-linkage can be computed as,

$$\varphi(\mathrm{t}) = \int [\mathrm{v}(\mathrm{t}) - \mathrm{i}(\mathrm{t})]\mathrm{dt} \tag{4.3}$$

For any given rotor position, the flux-linkage can be computed for different values of current using equation (4.3). By moving the rotor to a set of equally spaced intervals between unaligned and aligned position and repeating the same procedure a set of flux-linkages, the current with rotor position as a parameter can be obtained.

(c) Falling current method

For any given rotor position, the flux-linkage can also be obtained by allowing the current decays to zero after establishing the desired steady state current keeping all other phases open. The current oscillogram is taken and the flux-linkage is obtained from the following equation.

$$0 = \varphi(t) + \int_0^{t_1} -i(t)Rdt \tag{4.4}$$

where $\varphi(t)$ is the flux-linkage of the phase winding with the steady state current and t_1 is the time at which the current reaches zero. In this method, the accuracy of the result will be affected by the drop in the freewheeling diode in addition to other errors

(d) High frequency method

High frequency voltage can be impressed on the winding fixing the rotor in the desired position mechanically. The reactance of the winding is determined from the voltage and the current measurements. The inductance is determined from reactance. As the inductance of the phase winding is a function of current, the experiment is repeated with different DC bias to estimate inductance with saturation. The flux-linkage characteristics can be obtained by integration. This method works well when the magnetic circuit is unsaturated. But with saturation, the current waveform will not be sinusoidal and it reduces the accuracy of measurement. Errors can also occur due to inter-turn capacitance and eddy currents.

4.2. Experimental Set up and Methods: Magnetic curves measurement

An experiment was designed such that the magnetisation curves of the tested SRM could be measured at discrete rotor positions from the fully unaligned position ($\pm$ 30) to the fully aligned position (30^0). Due to the symmetry of the motor's structure, negligible phase interaction (mutual coupling) was assumed. The manufacturing data of the switched reluctance motor under investigation are shown in Table 4.1

Table 4.1 The Information of the SRM under test

Number of phases	:4
Number of stator/rotor poles	:8/6
Number of turns per phase [approx.]	:310
Rated output power	:1 kW
Rated current	:18 A
Rated Voltage	:76 V
Rated Speed	:12000 RPM
Rotation	:Bi-directional
Shaft diameter	:17mm
Stator outer diameter	:87mm

Fig 4.1 illustrates the experimental setup for measuring magnetisation characteristics of the tested SRM. The motor was firmly installed on a test bed. As mentioned before, the flux-linkage is a non-linear function both of winding current and rotor position, when energizing one SRM winding at a certain position, the rotor has to be fixed at that position; otherwise the rotor rotates due to the excitation except at the aligned position. For this an indexing head on frontal shaft of SRM is attached with a resolution of 1/6 th of a degree to lock the rotor in position against high torque produced during the experiment. The voltage supply used for the SRM phase winding is a Lead-Acid battery. The phase winding resistance is usually very small for the SRM tested in this thesis, which is apt to be the serious factor limiting the use of regular power supply. For such case where resistance is small, the voltage across the SRM will not remain constant throughout the measurement period due to poor regulation of power supply. For this purpose a set of 12 V, 18 A lead acid battery is used. Depending on the resistance of the SRM winding and the peak current required during the test, two or more batteries can be used in series. The two electrical variables $v\ (t)$ and $i\ (t)$ needed are to be measured. The phase current is measured using a current probe. A two-channel DSO is used for voltage measurement. The

voltage and current waveforms were visualized and recorded using a digital oscilloscope.

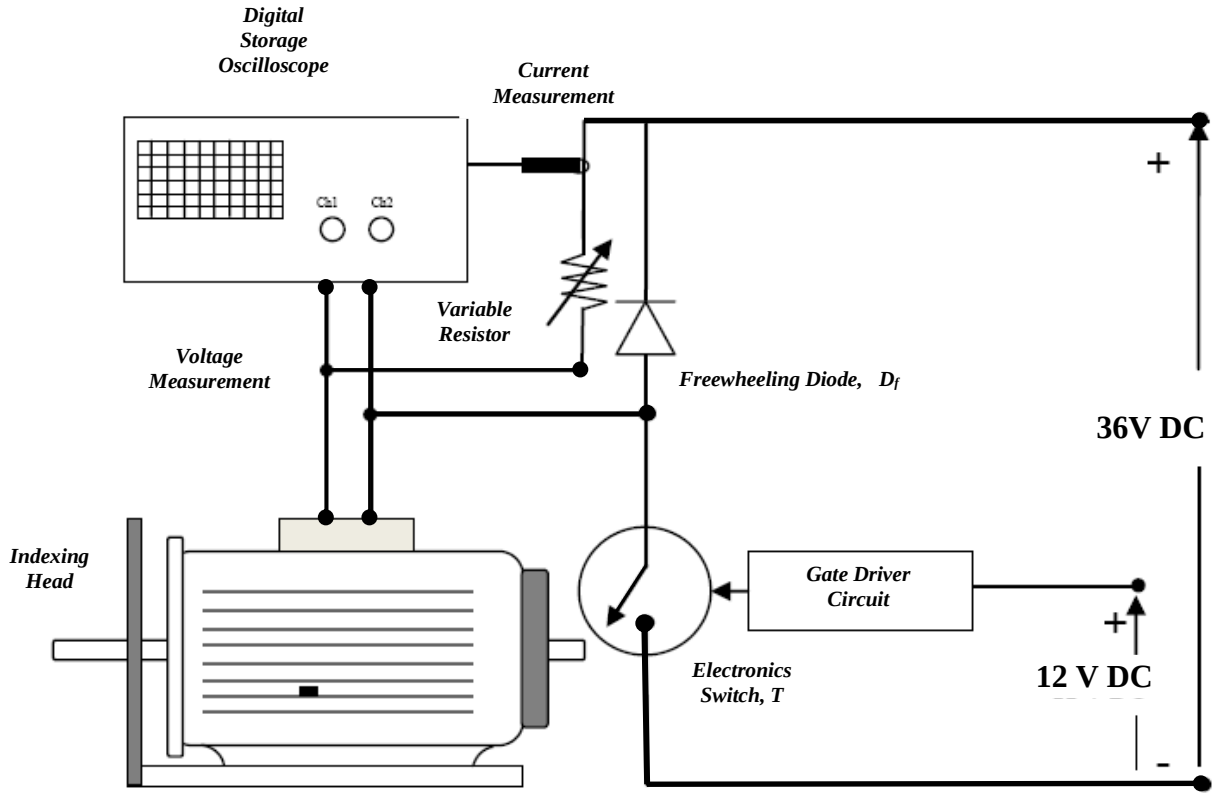

Fig.4.1 Experiment set up to determination of Flux Linkage Characteristics

The method is based on the instantaneous terminal voltage equation of a switched reluctance motor and the equation pertaining are given by equation (4.2) and (4.3).

The measurement algorithm consists of five steps described as follows:

- Scale and remove any offsets from the voltage and current waveform
- Lock the rotor to a known position
- Apply a step voltage pulse to the phase winding by closing the T switch
- Record voltage and current waveforms data
- Remove any vertical offset by opening the switch "T" and prepare the next measurement.

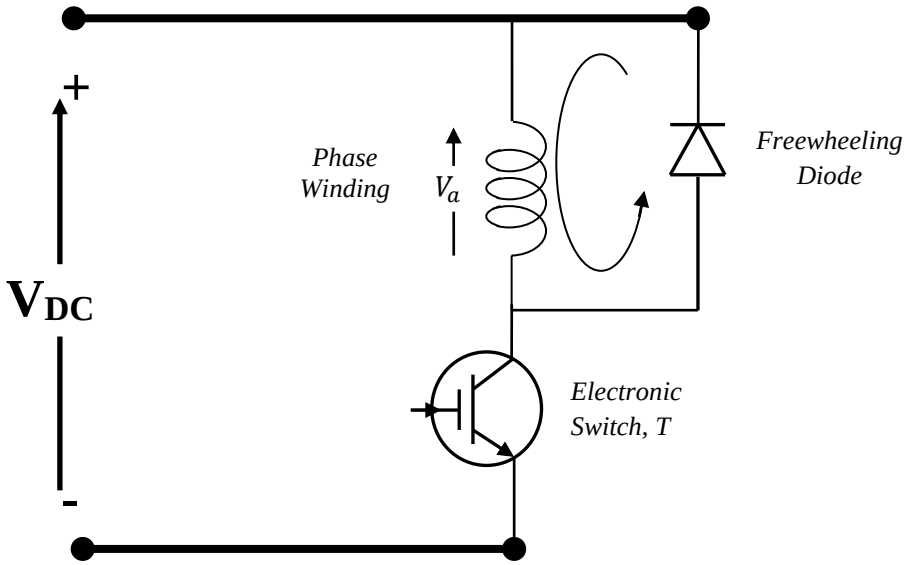

Fig.4.2 Measurement circuit

Fig. 4.2 shows the schematic diagram for the measurement of the phase winding flux-linkage. The measurement circuit consists of one switch and a freewheeling diode. Keeping all other phases open, any one of the phases of the motor is connected to a DC source through an electronic switch T. By locking the rotor mechanically into the preset position, the switch T is turn-on, and a constant voltage pulse is applied to the phase winding. The duration of the voltage pulse is made sufficiently large to make the current reaches nearly to 20 to 30% more than the estimated peak current. Once the current reaches such value, the electronic switch is turned off and the current is diverted through the freewheeling diode. The current rise (transient response) and the voltage fall during the switch on time are captured. The variation of the phase resistance with temperature and the influence of the voltage drop across the diode, effect the correct evaluation of the time constant. This effect can be minimized using a large external resistor connected in series with the winding.

A digital storage oscilloscope is used to capture the phase voltage and phase current. The data is loaded to a PC and processed in Matlab®. Fig.4.3 shows the captured phase voltage and phase current at a particular rotor position. In this thesis, a steady phase current of 15 A has been aimed, and a step voltage of 36 V has applied to the winding. Inspecting the behaviour of the phase current, the variations in phase inductance with respect to the rotor position can easily be identified. The slope of the

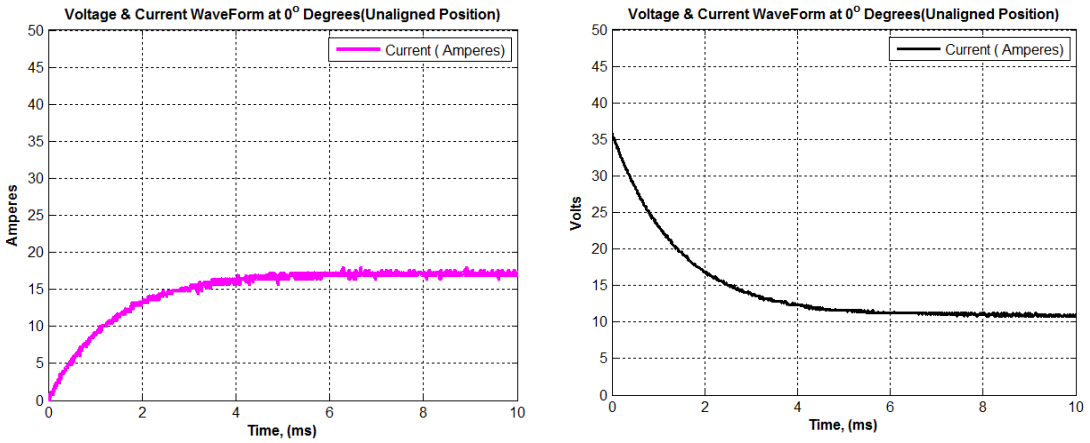

(a) Voltage and Current Wave forms at Unaligned position

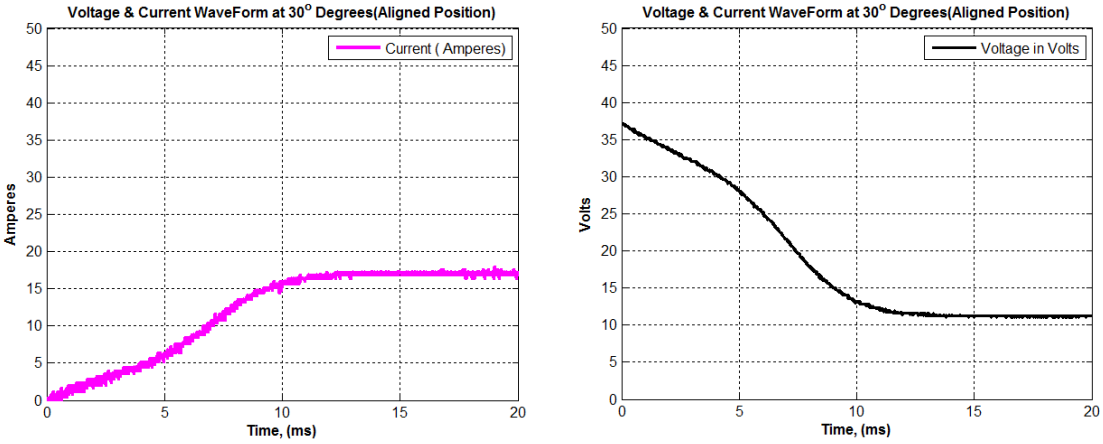

(b) Voltage and Current Wave forms at Aligned position

Fig.4.3 Measured Voltage and Current Waveforms

phase current is higher at unaligned position, suggesting a lower inductance compared to the aligned rotor position. Post-processing consists multiplying the current waveform by the phase resistance and subtract the resistive voltage drop from the voltage waveform, and finally to obtain the flux-linkage value by integrating the difference [$v(t) - i(t)R$]. The flux-linkage at different current levels (up to 15A) is computed using equation 4.2. For computation the data is transferred to the computer and numerical integration is performed. The experiment is repeated for every 2^0 of displacement of the rotor from the unaligned position to the aligned position (30 degrees). For an 8/6 SRM, the rotor pole pitch is 30^0 and hence the test should be conducted for fifteen discrete rotor positions. Fig.4.4 shows the flux-linkage

characteristics with respect to the current for different rotor positions from the experimental results.

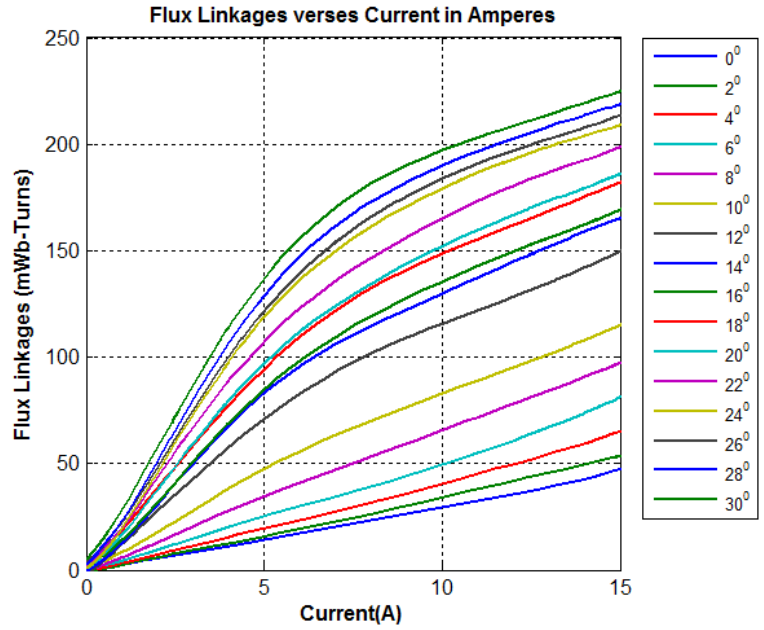

(a)

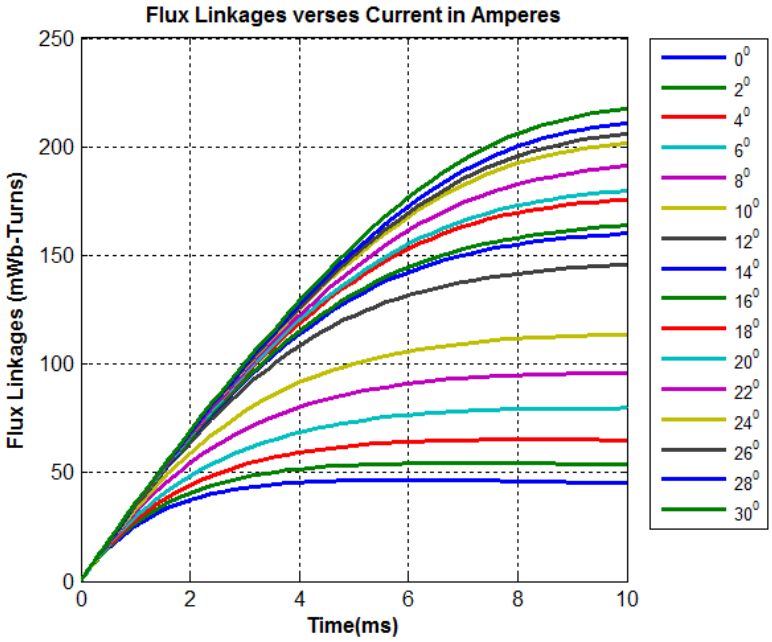

(b)

Fig.4.4 Measured flux linkage characteristics (a) with different excitations (b)with respect to time

Fig.4.4 clearly presents the two distinct effects of saturation. When the rotor is near the aligned position, the flux is higher and the bulk effect begins. At this position, the phase inductance is at its maximum as the magnetic reluctance of the flux is at its

lowest. Non-linear effect of the magnetic circuit starts at around 5A. The unaligned curve is straight because of the large air-gap in this position. In the unaligned position, the phase inductance is at its minimum. The saturation of the unaligned curve is less sharp due to the larger leakage flux in this position.

As seen from Fig.4.4, the flux-current curve at each rotor position is not smooth enough. Various interpolation routines were tried in an attempt to remove the skew from the data. A powerful Matlab® tool has been used to smooth the magnetization curves by polynomials in least-square sense. The test bench used for the magnetic characteristics is shown in Fig.4.5.

Fig.4.5 Test bench for flux linkage curves

The phase inductance is also an important circuit concept making the control of switched reluctance motor more compatible for control system. The classical definition of inductance is the ratio flux-linkage / current (ψ/i). The specific non-linearity of SRM circuit suggests a three dimensional dependence of the phase inductance to current and rotor position. At the unaligned position, the slope of the magnetization curve is constant, being equal to the ratio ψ/i for any point of the magnetic curve. This suggests that at this position for any value of the current, the phase inductance is constant (L_u). As the motor moves for a constant phase current, the inductance rises till its maximum value (La) corresponds to the aligned position

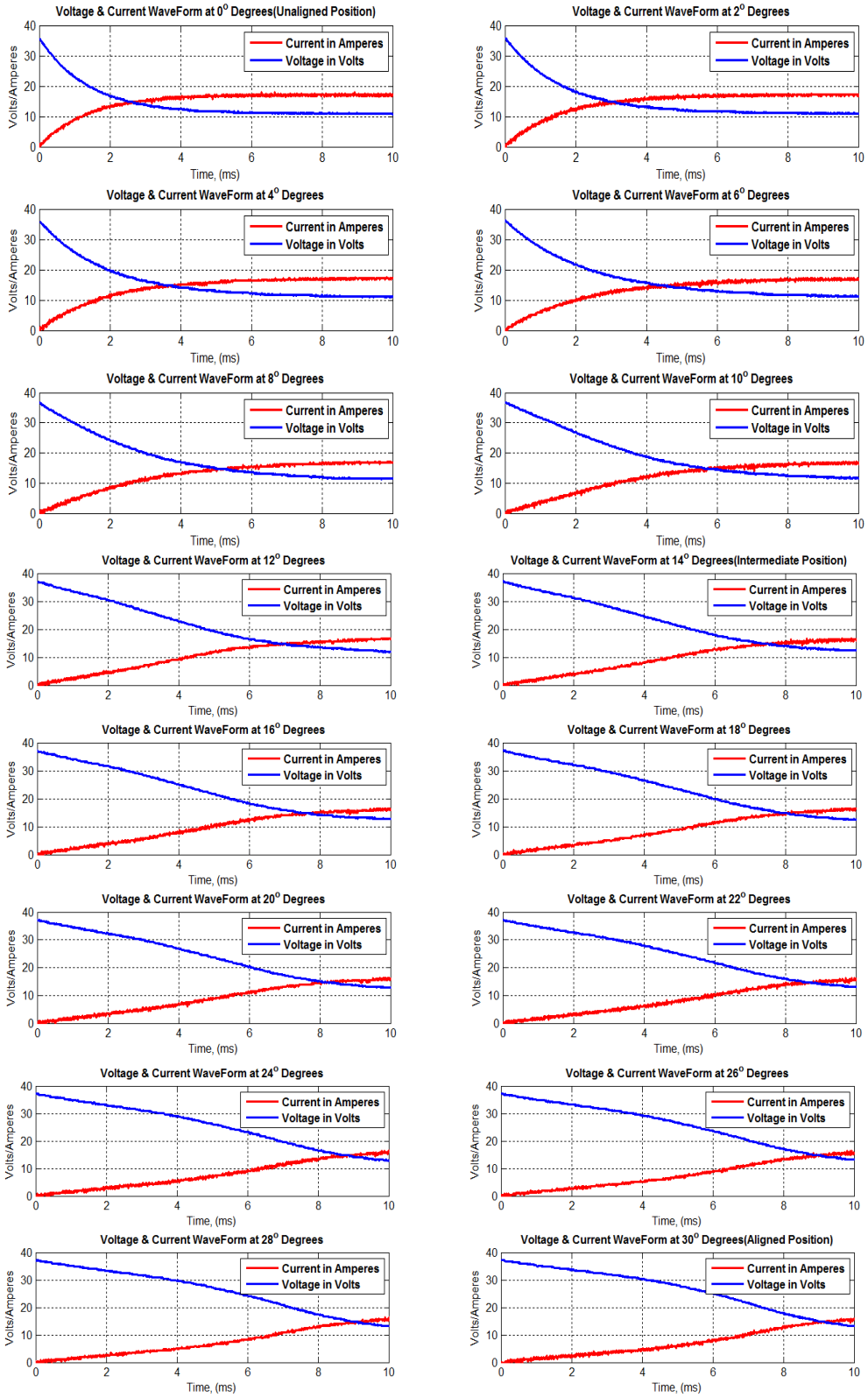

Fig.4.6 The phase voltages and phase current at different rotor positions

These curves are symmetric in space with a periodicity equal to the rotor pole-pitch. The procedure to find out the motor winding inductance at different rotor position was explained in chapter 3 in section 3.6.The phase voltages and phase currents at different rotor positions is given in Fig.4.6

4.3 Finite Element Verification and Analysis of the Prototype

The motor configuration and specifications used in this study are shown in Fig.4.7 and Table 4.2, respectively. In Ansoft Maxwell/3D Simulator related to the parameters given in Table 4.2. Firstly 8/6 pole base structure rotor SRM's geometrical model is obtained. Fig.4.7 shows the dimensional model of SRM realized in a Simulator. The finite element mesh is constructed with about 30008 mesh elements and is shown in Fig.4.8. The finite element model is constructed with a moving air-gap that allows the calculation of the parameters for the movement of the rotor by 60^{o} for a given current in each simulation. This allows simulations to be conducted for each current rather than each current and each position thereby speeding the entire verification procedure.

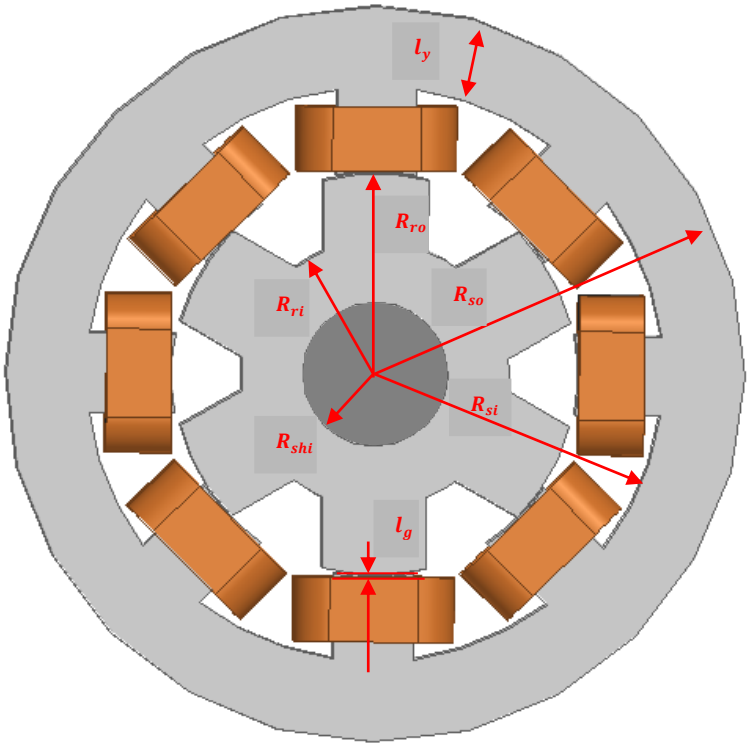

Fig. 4.7 Geometrical model of 8/6 pole SRM

Table 4. 2. Electrical and geometrical parameters of a prototype SRM

Symbol	Explanation	Dimension(mm)
R_{ri}	Rotor Inner Diameter	17
R_{ro}	Rotor Outer Radius	47.5
R_{so}	Stator Outer Radius	87
R_{si}	Stator Inner Radius	48
l_y	Stator yoke length	9
l_g	Air gap	0.25
l_{stk}	Stack length	80
n_s	Stator pole number	8
n_r	Rotor pole number	6
m	Phase number	4
N	Winding number per phase	310

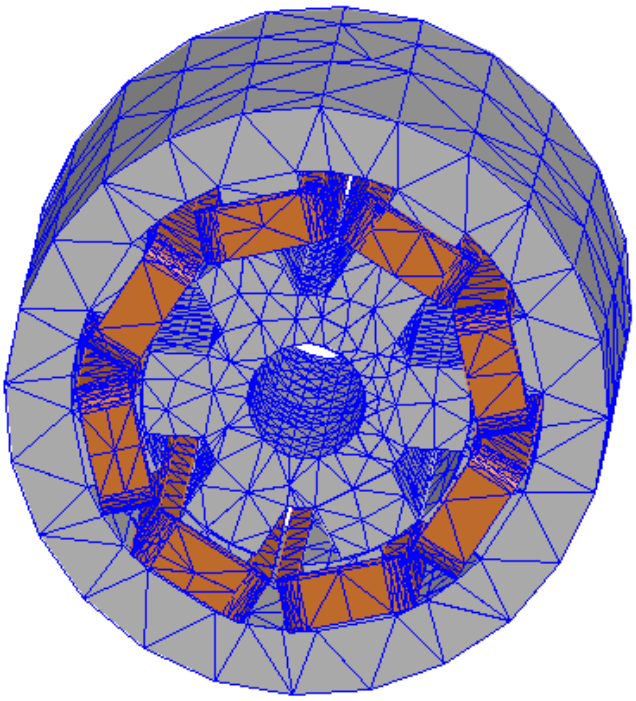

Fig. 4.8 3-D Finite elements mesh density for the SRM.

The stator and rotor cores are made up of non-oriented silicon steel laminations and also, each phase winding consists of 310 turns.

4.3.1 Numerical Results and Analysis

The proposed 3D-finite element method is employed to evaluate the performance of the motor at three states, unaligned, intermediate and aligned position.

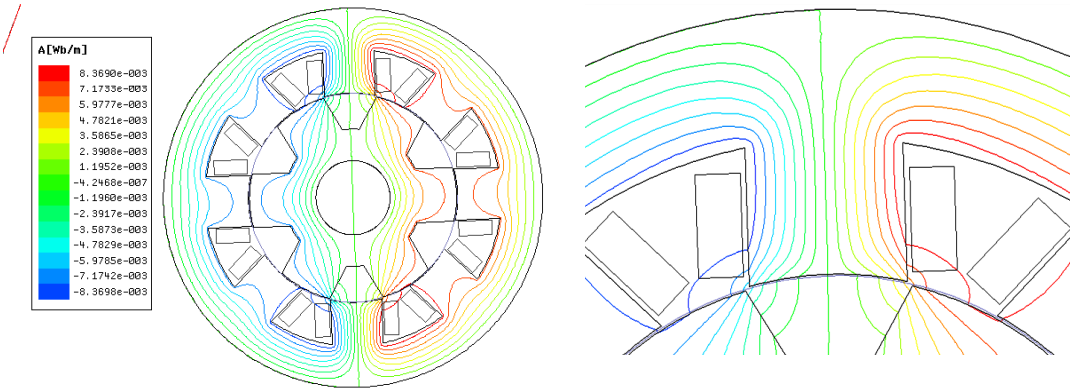

(a) Unaligned position (0^o Degrees)

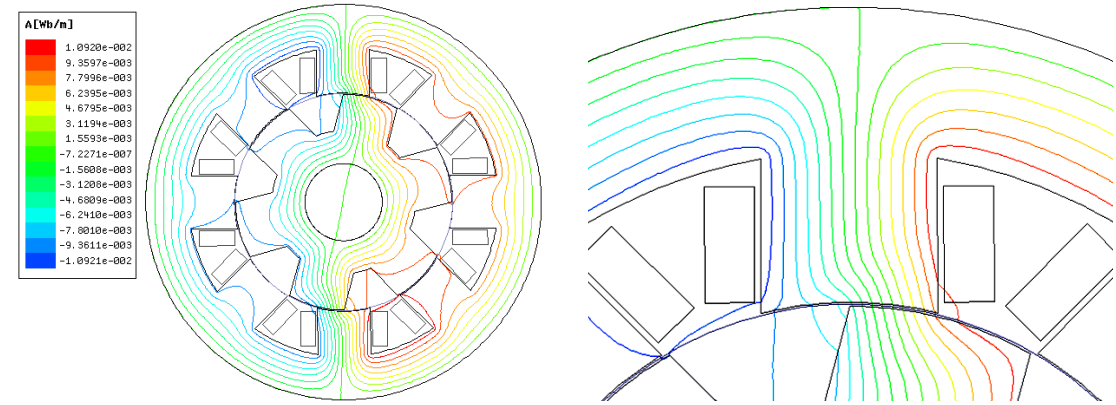

(b) Intermediate position 15^0 Degrees

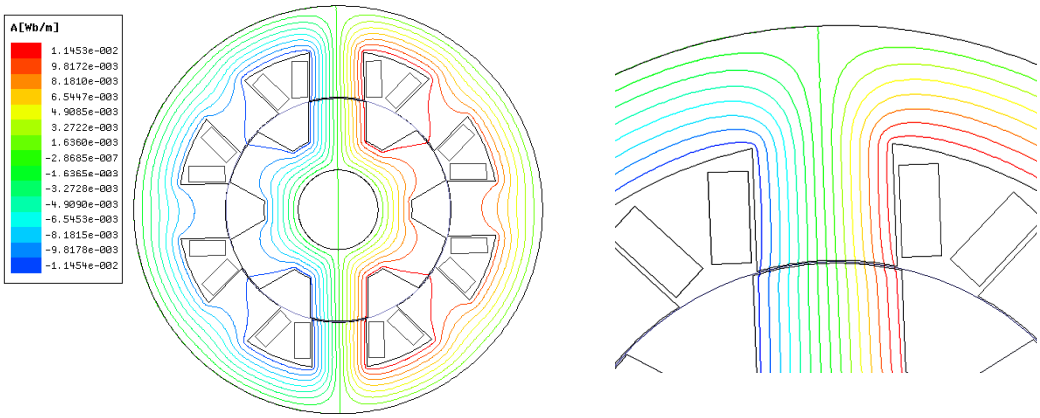

(c) Aligned Position 30^0 Degrees

Fig.4.9 SRM's Field distribution at different rotor positions for a phase excitation current of 15 Amperes

Once the system is fully designed, the last task is to burden the system with constraints, such as physical loadings or boundary conditions. The load for SRM is given as the current in ampere (A) passing through the conductor windings for

specified rotor position. The current is varied from 0 A to 15 A for the rotor positions from 0 °-90 ° with respect to the excited pole of the stator.

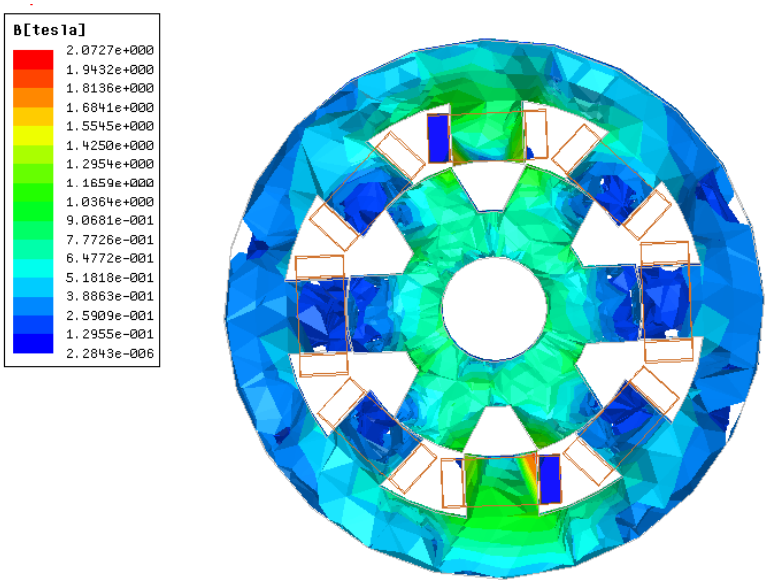

(a) Magnetic flux density distribution

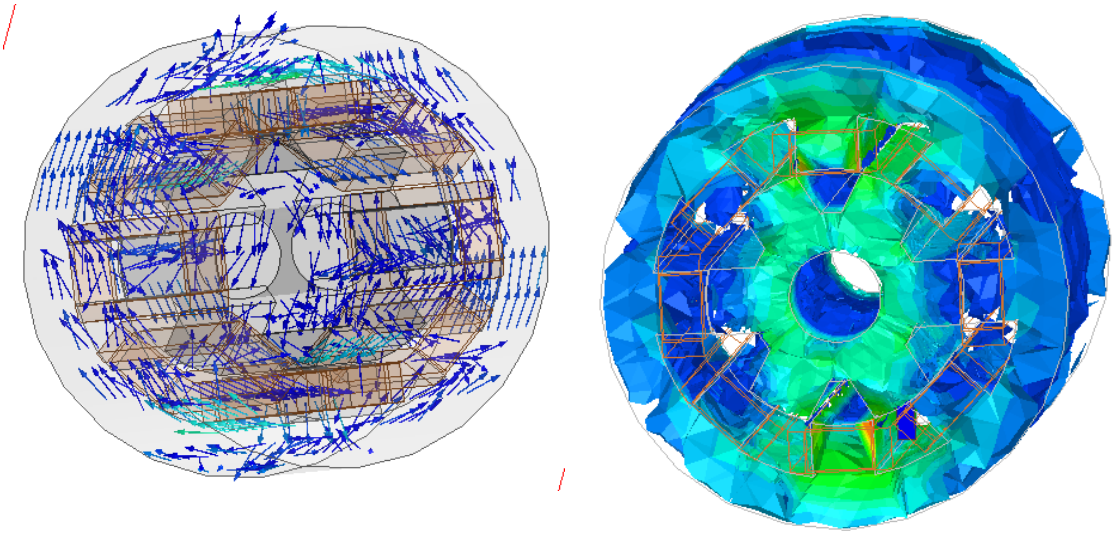

(b)Magnetic flux vectors in Stator and Rotor Surfaces

(c) 3- D View

Fig.4.10 Magnetic flux density distribution/Flux Vectors on SRM's stator and rotor surfaces at overlapping(Unaligned Position, $\theta=0^{o}$) Position with phase excitation current of 10 A

0° position specifies the reference as the rotor pole in about align with the excited stator pole. This step specifies the type of analysis required to be performed and the parametric values to be known as the output at the end of the simulation.

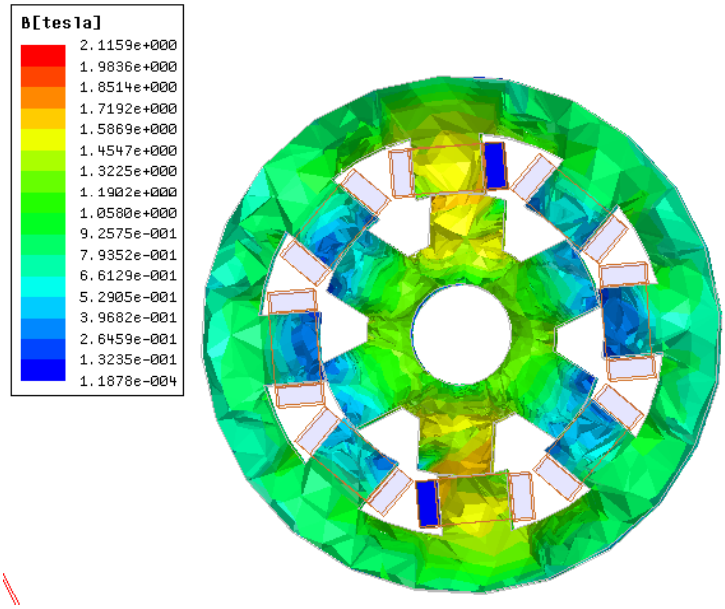

(a) Magnetic flux density distribution

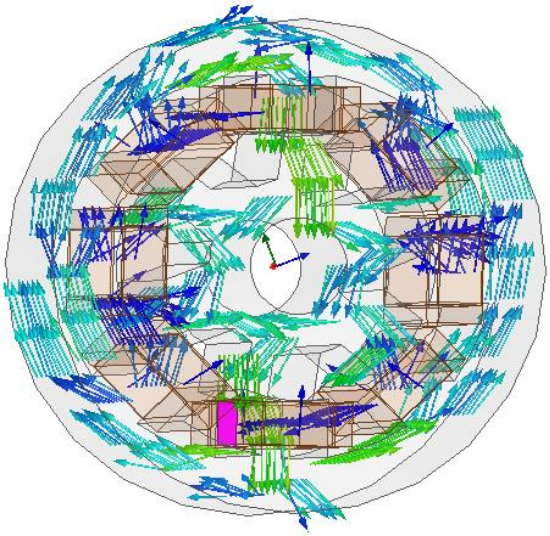

(b)Magnetic flux vectors in Stator and Rotor Surfaces

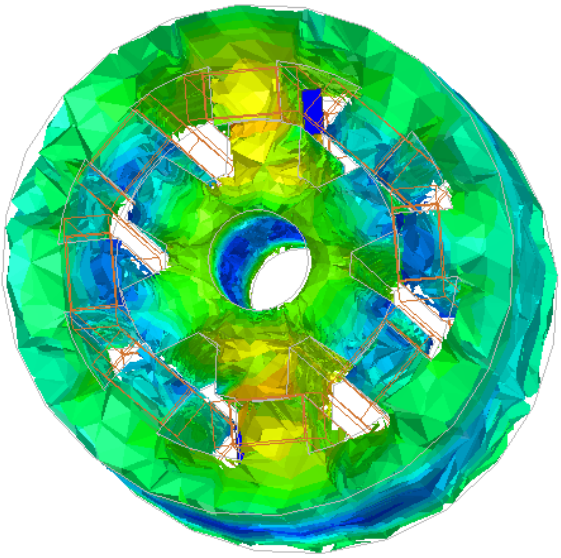

(c) 3- D View

Fig.4.11 Magnetic flux density distribution/Flux Vectors on SRM's stator and rotor surfaces at overlapping(Intermediate positions, $\theta=15^{o}$) Position with phase excitation current of 10 A

After the solution has been obtained, there are many ways to present ANSOFT results, to be chosen from many options such as tables, graphs and contour plots. The flux linkage values, Flux and field distribution pattern are obtained in the form of graphs and contours. For analysis and comparison proposes the rotor positions

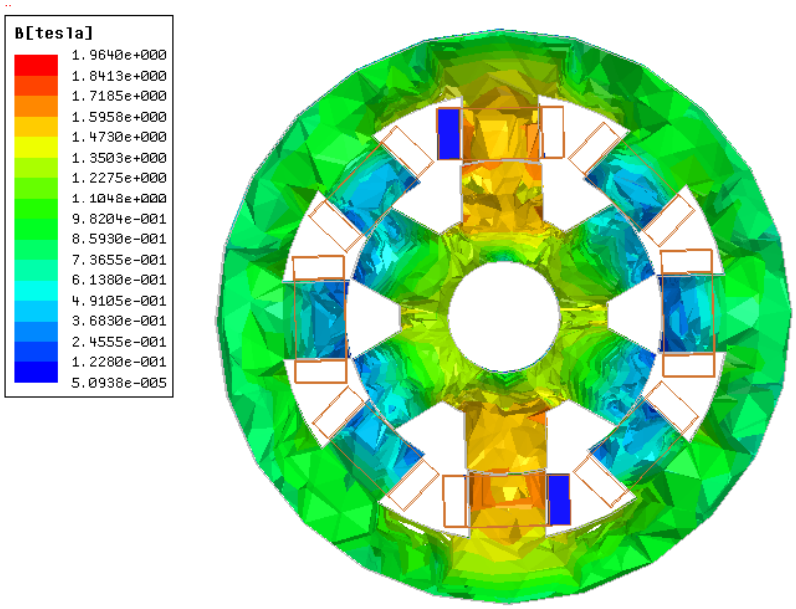

(a) Magnetic flux density distribution

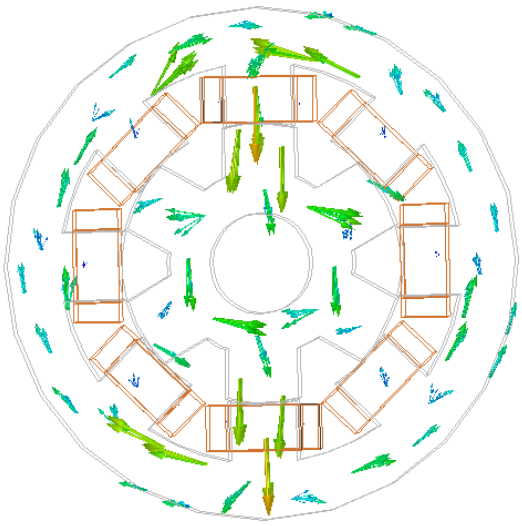

(b)Magnetic flux vectors in Stator and Rotor Surfaces

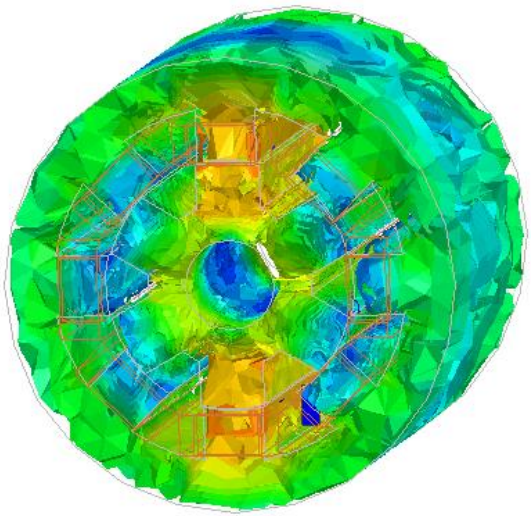

(c)3-D View of Magnetic Flux Density

Fig.4.12 Magnetic flux density distribution/Flux Vectors on SRM's stator and rotor surfaces at overlapping(Aligned Position, $\theta=30^{o}$) Position with phase excitation current of 10 A

selected were identical to those measured in the experimental tests. The magnetic field distribution as calculated by the finite element method is shown in Fig.4.9 for the different rotor positions for a phase excitation current of 15 A

Fig.4.10 shows the assumed distribution in the tip sections of a rotor and a stator pole just prior to the beginning of overlap. The tip sections experience higher magnetic fields than the other parts of the iron core. It is assumed that the flux density in these regions equals the maximum value for the iron core material. In this model, the area subjected to local saturation is approximated by the (shaded) parallelograms on the stator and rotor poles shown in Fig.4.10. The two areas are assumed to be equal for a fixed rotor position. Local saturation is assumed to be present at all non overlapping rotor positions and at small overlap lengths for overlap angles in the range $\varepsilon \leq .03\Phi$ where Φ is the rotor pole pitch and **c** is the overlap angle (Lawrenson, P. J. et al 1980), while Fig.4.11 shows the magnetic flux density distribution on SRM's stator and rotor core surface, at intermediate position; It is observed that the maximum flux density is 2.115 T. In Fig 4.12 Magnetic flux density distributions on SRM's stator and rotor core surfaces at full overlapping $\theta=30^{o}$ (Aligned Position) positions is shown. It is seen that maximum B is 1.96 T and saturation has started at coincidence part of the stator and rotor poles.

4.3.2 Flux linkage Characteristics- Verification

The method of flux linkage calculation by external circuit coupled to FE is used to determining, comparing and verifying the obtained flux linkage characteristics by experimental analysis. For this reason, basic SRM modelled and coupled to external circuit (Fig. 4.13) which one phase of motor is modelled by stranded coil in order for flux linkage calculation. Voltage sources and external resistor values are chosen so that in steady state, current value of 18 A flows in modelled phase. By doing the static analysis of circuit coupled to FE domain and for every 2 mechanical degrees of rotation from unaligned to aligned position, flux linkage are obtained as a function of current and rotor position, are shown in Fig.4.15

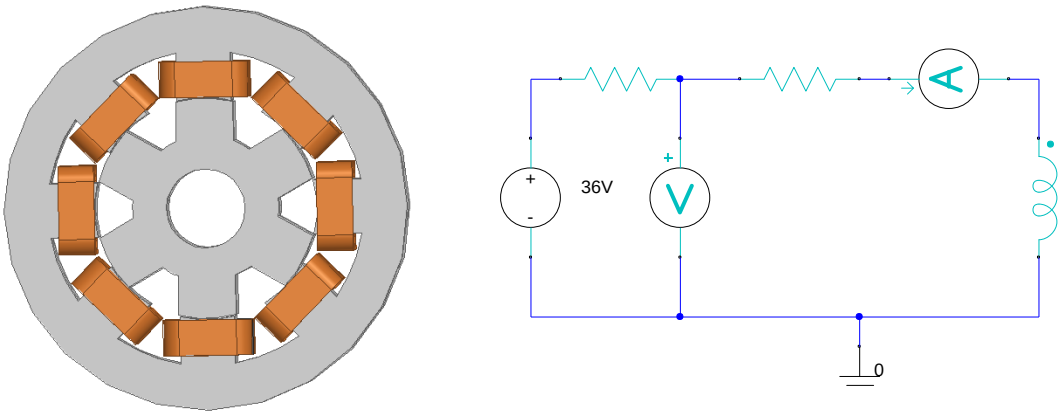

Fig.4.13 Model of basic SRM coupled to external circuit for verifying the Flux Linkages

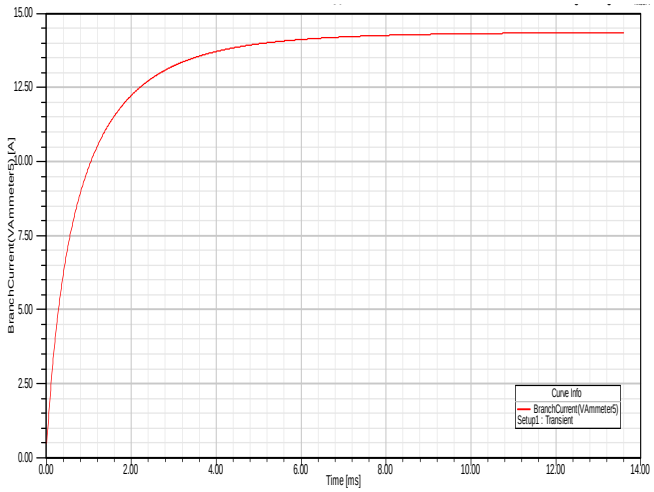

Fig. 4.14 (a) Calculated current profile at Unaligned Position

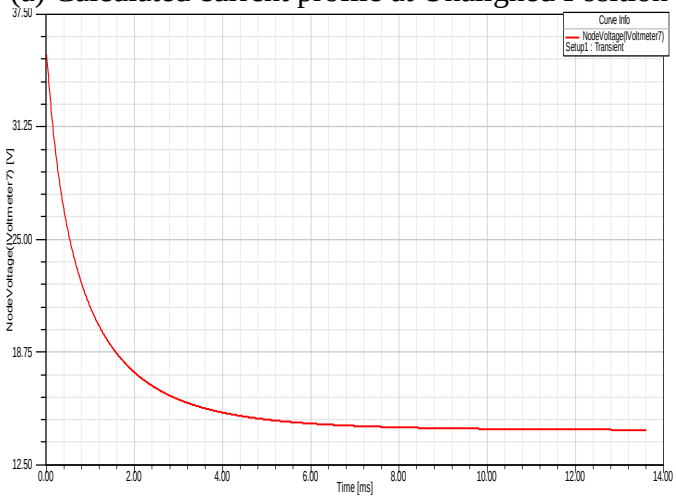

Fig.4.14 (b) Calculated voltage profile at Unaligned Position

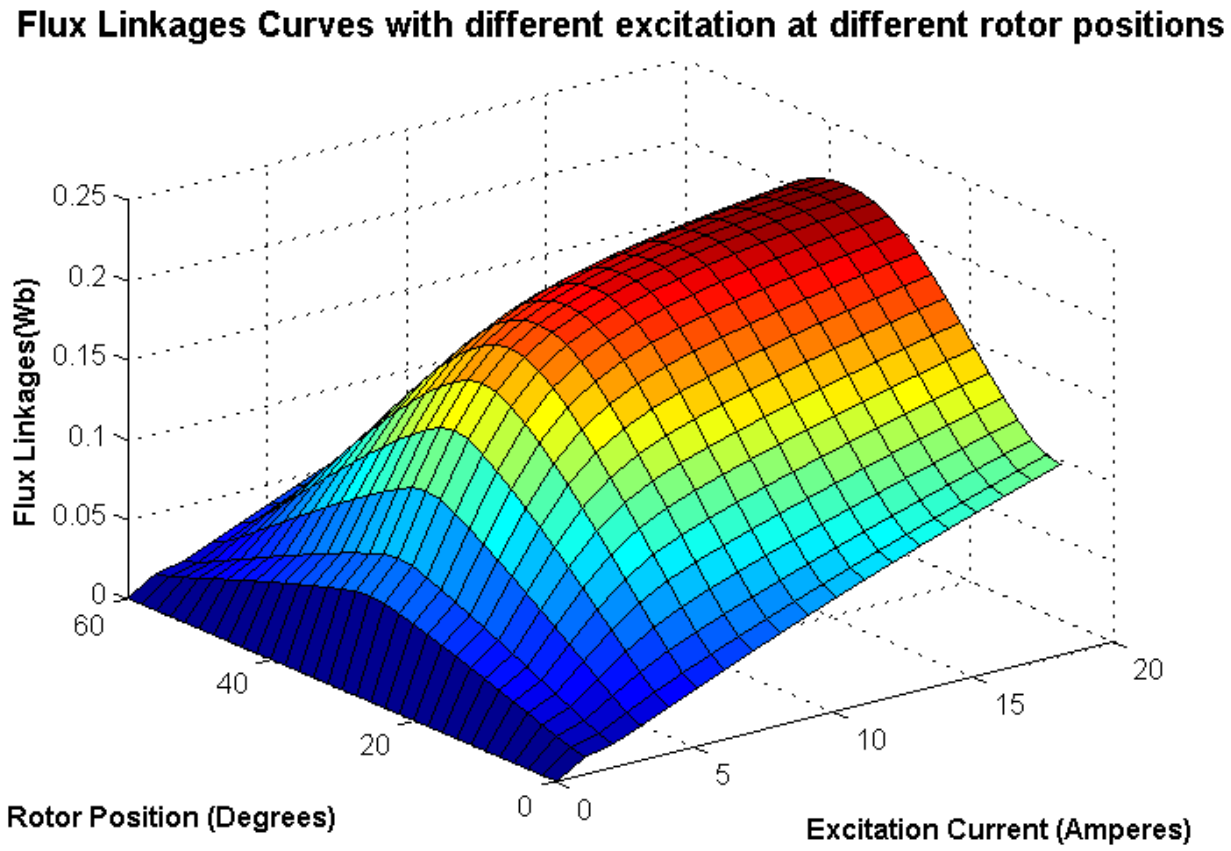

Fig.4.15 Flux-linkage characteristic as a function of current and rotor position

The experimentally measured values of transient voltages and currents at unaligned, intermediate and aligned positions are compared with those values obtained through Finite Element Analysis (FEA) in ANSOFT. Fig.4.14 (a) and Fig.4.14 (b) show the plot of transient voltage and currents versus time obtained through FEA for unaligned position.

The FEM and experimentally measured magnetization curves of the 8/6 SRM are shown in Fig.4.16 for the selected rotor positions. FEM curves and experimental curves are represented and compared. Both curves show a good accuracy when

compared with the experimental one; nevertheless the experimental curves are generally closer to the FEM magnetization curves as rotor position tends to the unaligned position (linear region). However in rotor positions revealing strong saturation, the model presents an acceptable accuracy.

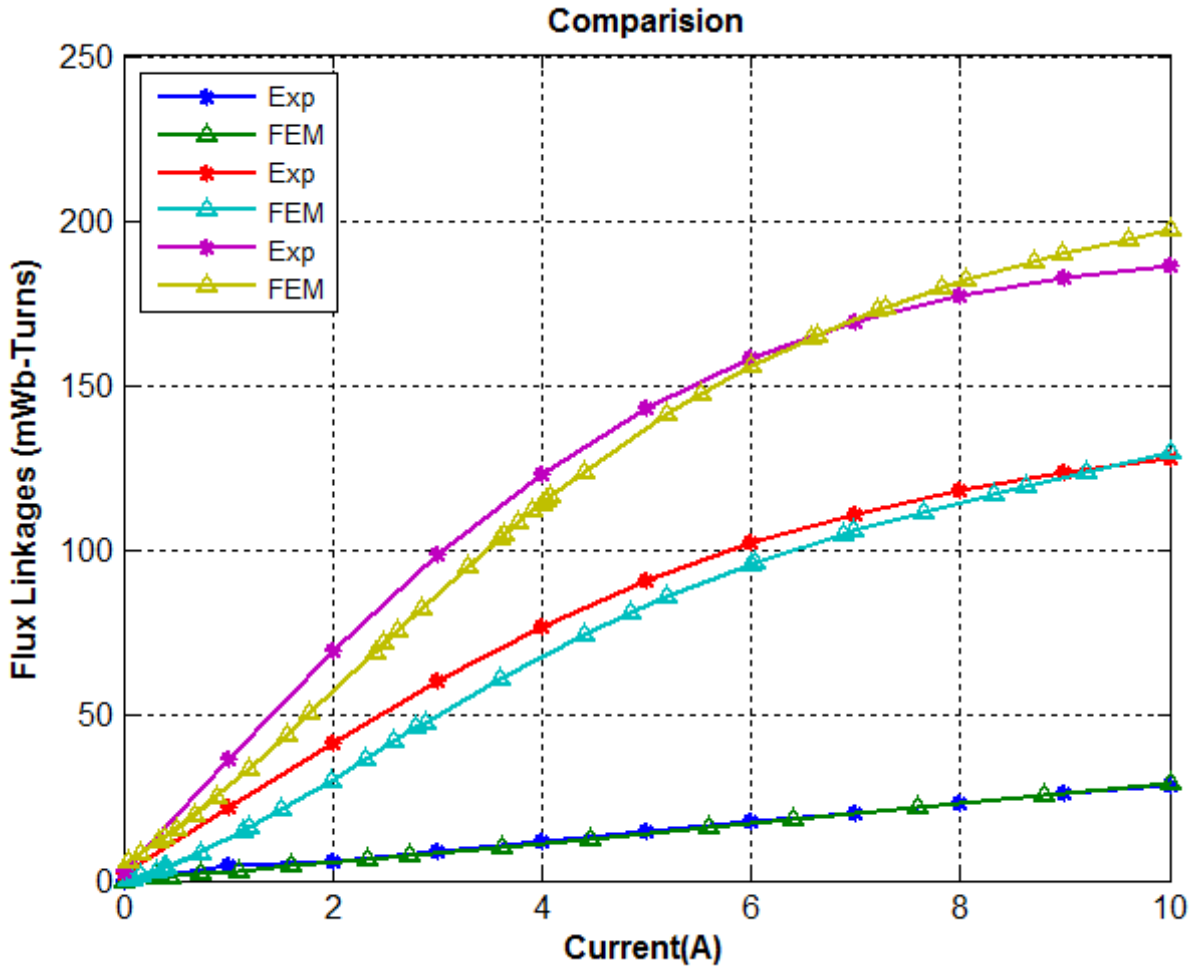

Fig.4.16 Comparison of flux-linkage characteristic as a function of current and rotor position

4.4 Summary

This chapter discussed how the magnetic characteristics of SRM are obtained by experimental and FEM analysis. For proper design of converter & control system and performance analysis of the SR motor, the knowledge of accurate flux linkage characteristics is necessary.

The flux linkage and inductance profile of the SR motor is depends on the rotor position and phase current and the family of the flux linkage characteristics (for different rotor positions) will have to be determined as accurately as possible for proper controller design. Since the SRM is non-linear in nature, estimation and calculation of these flux linkage characteristics and Inductance are very difficult.

Different measurement techniques of flux-linkage characteristics have been described (Krishnan, R. 2001) in this chapter. A simplified experimental set for the determination of flux linkage characteristics of SR motor has been presented.

This method involves in applying a step voltage application to one SRM phase and the rate of rise of current is measured. Despite the present drawbacks of the method, the accuracy of the measured parameters concludes that the direct method is recommended.

The measurement scheme is based on the digital data processing using a digital storage oscilloscope to record voltage and current waveforms with the rotor locked into various known positions.

The data is loaded to a PC and processed in Matlab®. The accurate knowledge of the motor's characteristics obtained can enable the motor's performance to be predicted correctly. The obtained values have been validated with the ANSYS FEM method.

The FEM analysis is carried out prove the correctness of the methodology. The experimental results values matches with the ANSOFT FEM Method.

The small variations between the two methods can be further minimized by properly defining a library of materials that composes the object (or project) being modelled, which includes thermal and mechanical properties.

It means that the presented method could be employed for the SRM design procedure to predict its performances and also to design the controller.

Chapter 5 Converters and Position Sensors of Switched Reluctance Motor

5.1 Introduction

In this chapter we are going to discuss the features of power converters circuits in switched reluctance motor drives and the various converter topologies used along with the merits, demerits and application of each topology and also about position sensors.

5.2 Features of the Power Switching Circuits

The essential features of the power switching circuit for each phase of S R motor are comprised of two parts

1. A controlled switch to connect the voltage source to the coil windings to build up the current
2. An Alternative path for the current to flow when the switch is turned off, since the trapped energy in the phase winding can be used in the other strokes. In addition, this protects the switch from the high current produced by the energy trapped in the phase winding.

5.3 Various Converter Topologies for S R Motor

It is essential before considering the different topologies of S R motor drives circuits to introduce the following features of the motor which give it an attractive advance over other types of AC machines; and effects the design of the drive circuit, these features are:

1. The torque in a SRM is independent of the polarity of the phase excitation current, which means only one switch per phase winding is required to energize or de-energize this phase.
2. There is always one switch connected in series with a phase winding, which makes the SR motor self protected against shoot –through faults.
3. The phases of the SR motor are electrical and magnetically independent, which allows separate control of current and torque for each phase, and also allows possible operation of the machine in case of one phase winding failure, although with reduced output power.
4. The mutual coupling between phases in a S R motor can be neglected; this also gives an advance for independent phase and torque control.

5. The phase inductance of the S R motor varies with the rotor position in either a non linear profile.

The previous facts about the S R motor explain the expected function of the drive circuit for this type of AC machines, which could be concluded in three tasks; first, is to divert current into the phase only in the positive gradient period of its inductance profile. Secondly, is to shape the energizing current of each phase, including its amount and its rise and fall times, of course less rise and fall times are desired to maximize the torque productivity during motoring operation. Third task is to provide a path for the stored magnetic energy in the phase winding during the commutation period, otherwise it will result in excessive voltage stress across the phase winding, hence across the semiconductor switching element leading to its failure, this energy could be free wheeled, or returned to the DC source either by electronic of electromagnetic means.

There are several topologies suggested to achieve the above function of the drive circuit. These topologies are well classified in based on the number of switches used to energize and commutate each phase (A. Consoli, A. Testa, N. Aiello, F. Gennaro, and M. Lo Presti (2001))

5.3.1. An Introduction to Converter Topology

Since the torque in S R motor drives is independent of the excitation current polarity, the S R motor requires only one switch per phase winding. This is contrary to the ac motor drives where at least two switches per phase are required for current control. Moreover, the windings are not in series with the switches in ac motor drives, leading to irreparable damages in shout –through faults. The S R motor drives always have a phase winding in series with a switch.

In case of a shoot- through faults, the inductance of the winding limits the rate of rise in current and provides time to initiate protective relaying to isolate the faults. The phases of the S R motor are independent and, in case of one winding failure, uninterrupted operation of the motor drive operation is possible, although with reduced output. Some configuration of converters used in S R motor drives are presented and discussed in thesis the comparisons of these converter topologies .

While many of these configuration have been known for some time, the rest are emerging form research laboratories

5.4 Converter Configurations

The mutual coupling between phases is negligible in S R motor. This give complete independence to each phase winding for control and torque generation . While this features is advantageous , a lack of mutual coupling requires a careful handling of the stored magnetic field energy, The magnetic field energy has to be provided with a path during commutation of a phase; other wise , it will result in excessive voltage across the windings and hence on the power semiconductor switches leading to their failure. The manner in which this energy is handled gives way to unique but numerous converter topologies for S R motor drives. The energy could be free wheeled, partially converting it to mechanical/electrical energy and partially dissipating it in machine windings. Another option is to return it to the dc source either by electronics or electromagnetic means. All these options have given way to power converter topologies with q, (q+1), 1.5q, and 2q switch topologies, where q is the number of machine phases. A two stage converter configuration which does not fit categorization bsed on the number of phases is also included

Fig. 5.1 gives an overview of power converters used for SRM. One note that in the different converters analyzed below, the power switch is represented as a transistor. However, in industrial applications, there may be other switches like IGBTs, Thyristors or may be MOSFETs. Furthermore, auxiliary circuitry such as snubbers, voltage spike suppressors, di/dt limiters, RC protective components, etc. are not represented. All converter topologies assume that a dc voltage source is available for their inputs. The DC source may be from batteries or mostly a rectified AC supply with a filter to provide a DC input source to the SRM converters. Besides a controlled rectifier, an uncontrolled rectifier could also be used to provide constant dc voltage at the bank capacitor terminals. However, adjustable voltage provides greater flexibility in variable speed reluctance drives. Detailed description of such DC sources may be found in standard power electronics textbooks (Krishnan, R. 2001).

5.5 Power Converter for Switched Reluctance Motors

Since the torque in S R motor drives is independent of the excitation current polarity, the S R motor drives requires only one switch per phase winding, Moreover , unlike the ac motor drives, the S R motor drives always have a phase winding in series with a switch. Thus in case of a shoot through fault, the inductance of the winding limits the rate of rise in current and provides time to initiate the protection. Furthermore, the phases of SR motor are independent and, in case of one winding failure, uninterrupted operation is operation. Following are some configuration of converter used in SR motor drive

5.6 Classification of Power Converter for Switched Reluctance Motor

5.6.1 Eight Switch (Asymmetric Bridge) Bridge Converter

The most versatile SRM converter topology is the classic bridge converter topology shown in Fig.5.2, suitable for powering a 4-phase machine. Note that this asymmetric bridge converter requires 2q power switches and 2q diodes for a q-phase converter. The asymmetric bridge converter provides the maximum control flexibility, fault tolerance capability and efficiency, with a minimum of passive components and is therefore one of the most popular converter topology. Firstly, consider phase "*a"*. The voltage applied to the phase winding is $+V_{dc}$ when the upper and lower transistors T_{aH} and T_{aL} are on. Phase current i_a then increases through both switches. If one transistor is off while the other is still on, the winding voltage will be zero. Phase current then slowly decreases by freewheeling through one transistor and one diode. When both transistors are off, the phase winding will experience $-V_{dc}$ voltage. Phase current then quickly decreases through both diodes. By appropriately coordinating the above three switching states, phase current of the SRM can be controlled. The main advantages of the asymmetric bridge converter are the independent control of each motor phase and the relatively low voltage rating of the inverter components Fig.5.3 shows the operational waveforms of the asymmetrical bridge converter. During the current control phase, the top switch is kept on as long as the phase is to be on and the bottom switch is turned on and off accordingly (Vukosavic, S, 1991: Krishnan, R. 2001:T.J.E.Miller1993).

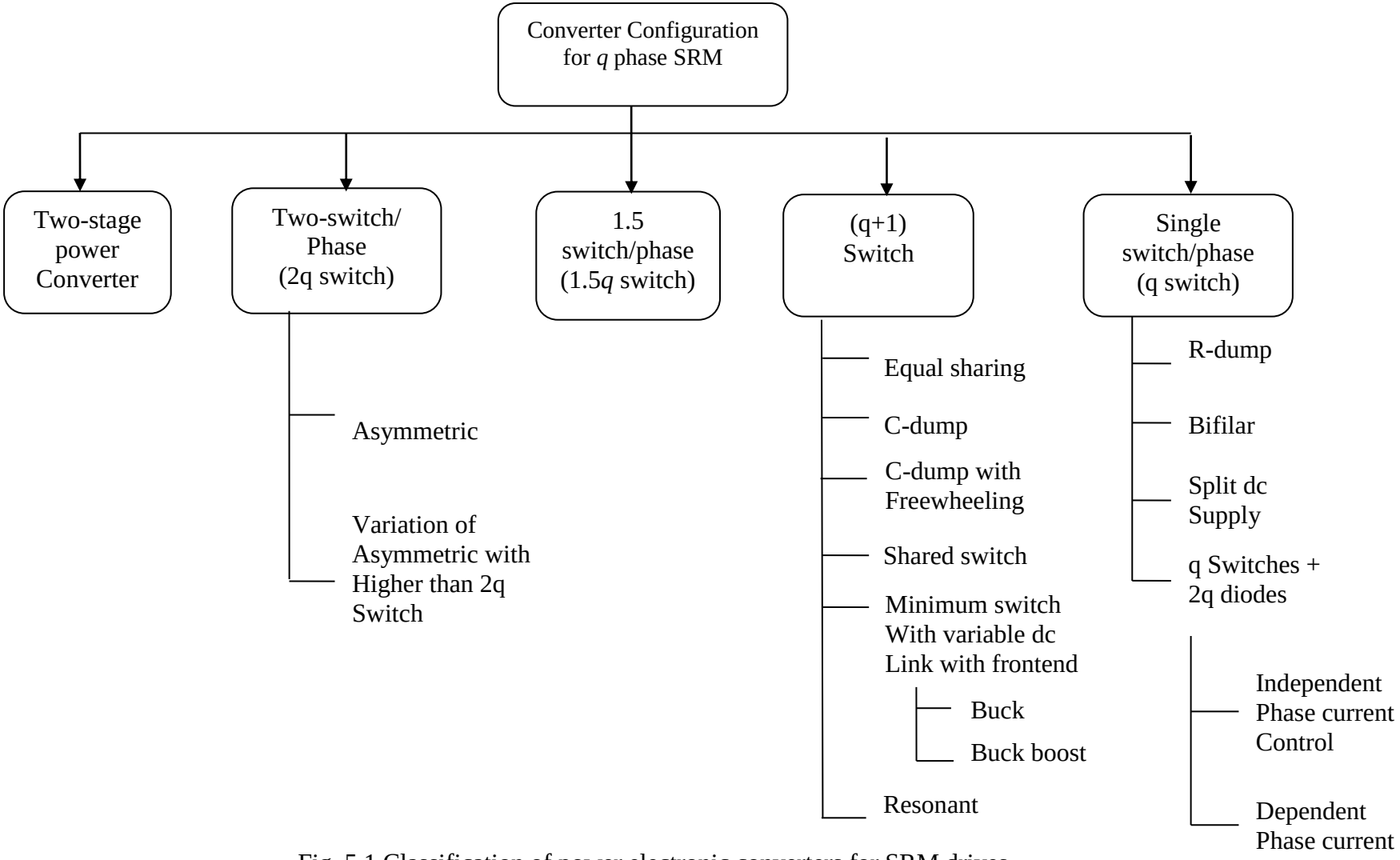

Fig .5.1 Classification of power electronic converters for SRM drives

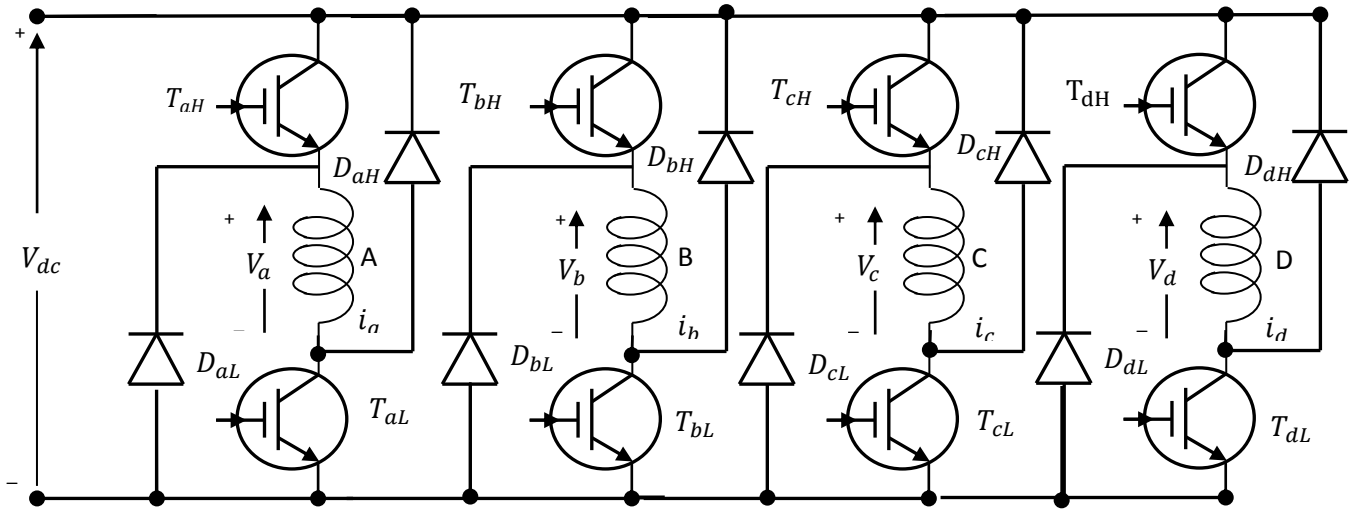

Fig.5.2 Asymmetric half-bridge converter

Advantages

1. Complete freedom to apply voltages $+V_{dc}$, 0 or $-V_{dc}$ to the phase.
2. Two or even three phases can be turned on regardless of the currents in other phases thereby allowing for negative torque to be instantly generated for changing the direction of rotation.
3. If one switch is damaged, the drive can still function at reduced power levels with just three phases.

Disadvantages

1. 8 switches and 8 diodes are required for the converter.
2. 8 switches under normal circumstances would require 8 gate drive power supplies and 8 gate drive circuits.
3. Size of the drive as well as cost increases.

5.6.2 Six switch converter

The six switch converter shown in Fig.5.4 has four phase switches and a common upper switch for phases "a" and "c" and a common upper switch for phases "b" and "d". If phase "a" is to be operated, switches T_{acH} and T_{aL} and diodes D_{aH} and D_{acL} form a circuit similar to the eight switch converter. The operational modes are identical to that of the eight switch converter

Advantages

1. 2 lesser diodes and switches when compared to the eight switch converter.
2. Only 3 power supplies are required for the gate drive circuits.

3. Complete freedom to apply voltages $+V_{dc}$, 0 or $-V_{dc}$ to the phase.

Disadvantages

1. Phases "a" and "c" or phases "b" and "d" cannot be turned on simultaneously. When changing direction of the machine, the reference speed should be set to zero till all machine currents are zero and only then negative speed can be commanded. In this respect, the freedom of operation is more limited than the eight switch converter.

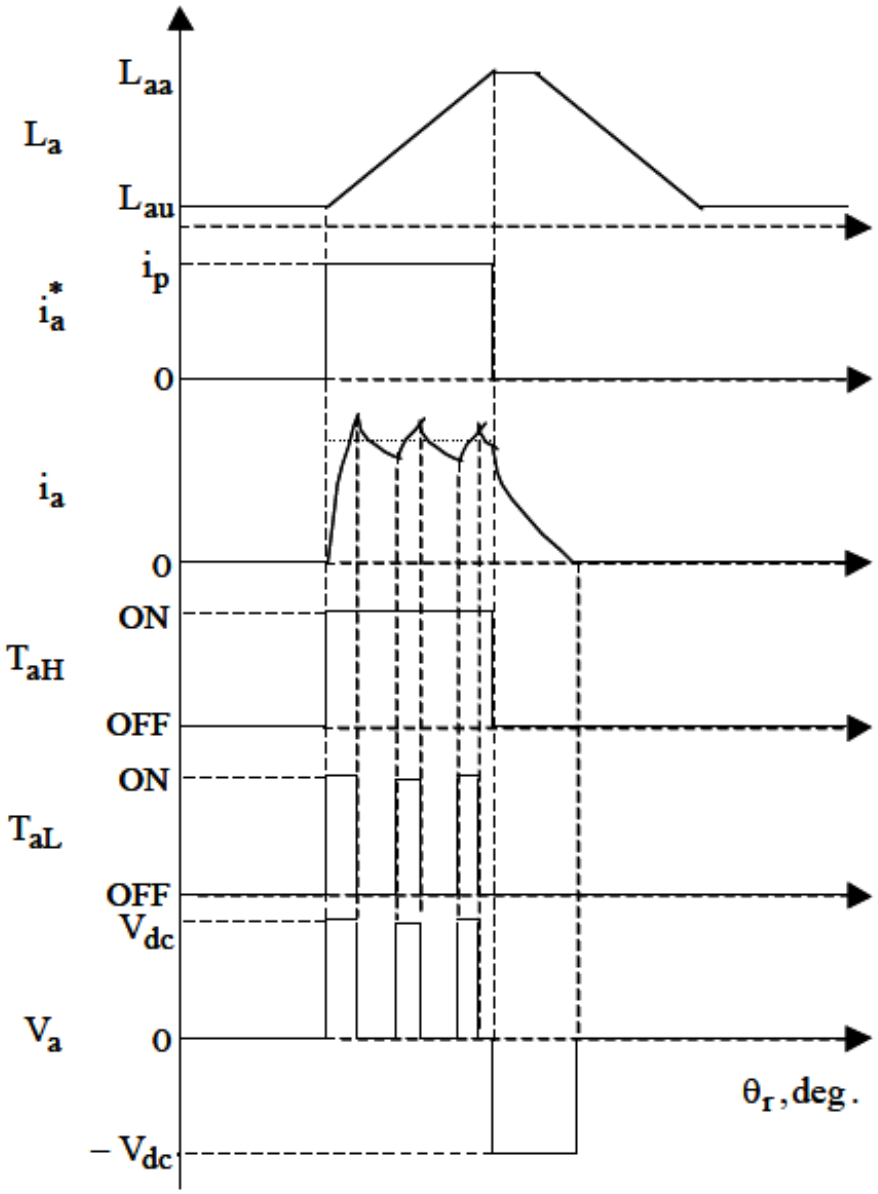

Fig.5.3 Operational waveforms of the asymmetrical bridge converter

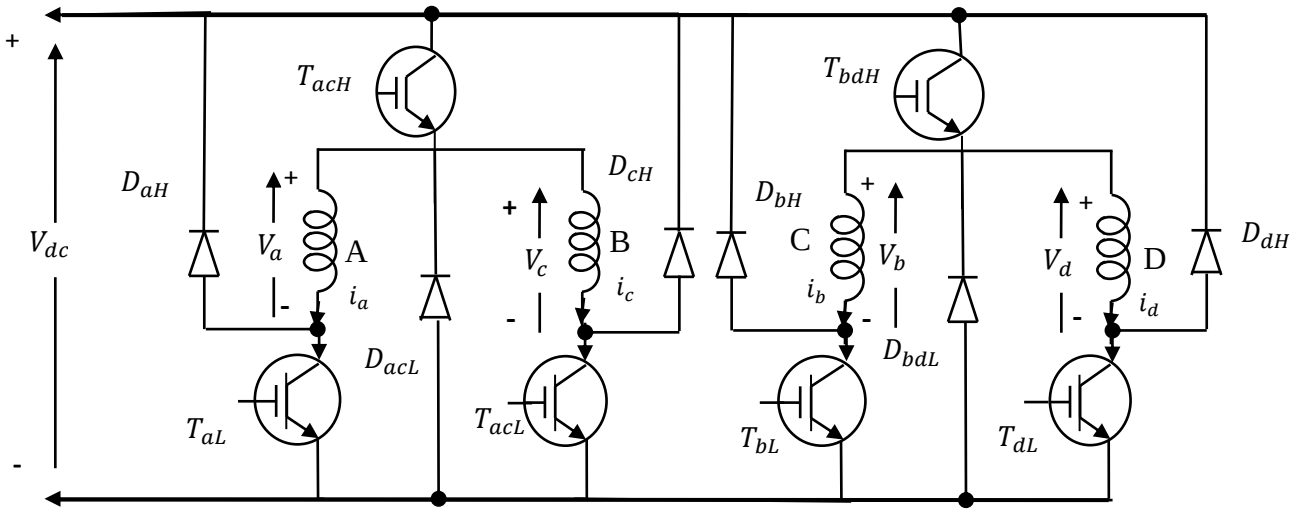

Fig.5.4 Six switch converter

5.6.3 Single-Switch-per-phase Converters

Single-switch-per-phase converters are appealing due to their compactness of converter package and hence a possible reduction in their cost compared to other converters. They also have the disadvantage of being unable to apply zero voltage across the machine phase during current conduction. Such an operational constraint increases the circulation of energy between the machine and DC link, resulting in higher losses and reduced system efficiency. Also, the rate of change of the voltage is doubled during current control, which causes insulation deterioration and increased acoustic noise in the machine. In spite of many shortcomings, a large number of single-switch-per-phase converter topologies have been proposed and tested. They have selective advantages that may suit an application. These converter topologies are described in this section. In this present section some of the single switch converters which are widely used are discussed in brief. An overall view about the construction and basic operating principle are also discussed.

5.6. 3.1 R-Dump

The R-dump converter configuration with one transistor and one diode per phase of the SRM is shown in Fig.5.5. When T_1 is turned off, the current freewheels through D_1, charging Cs, and later flows through the external resistor R. This resistor partially dissipates the energy stored in phase A. This has the disadvantage that the current in phase A will take longer to extinguish compared to recharging the source. The energy,

in addition, is dissipated in a resistor, thus reducing the overall efficiency of the motor drive.(R. Krishnan and P.N. Materu 1993)

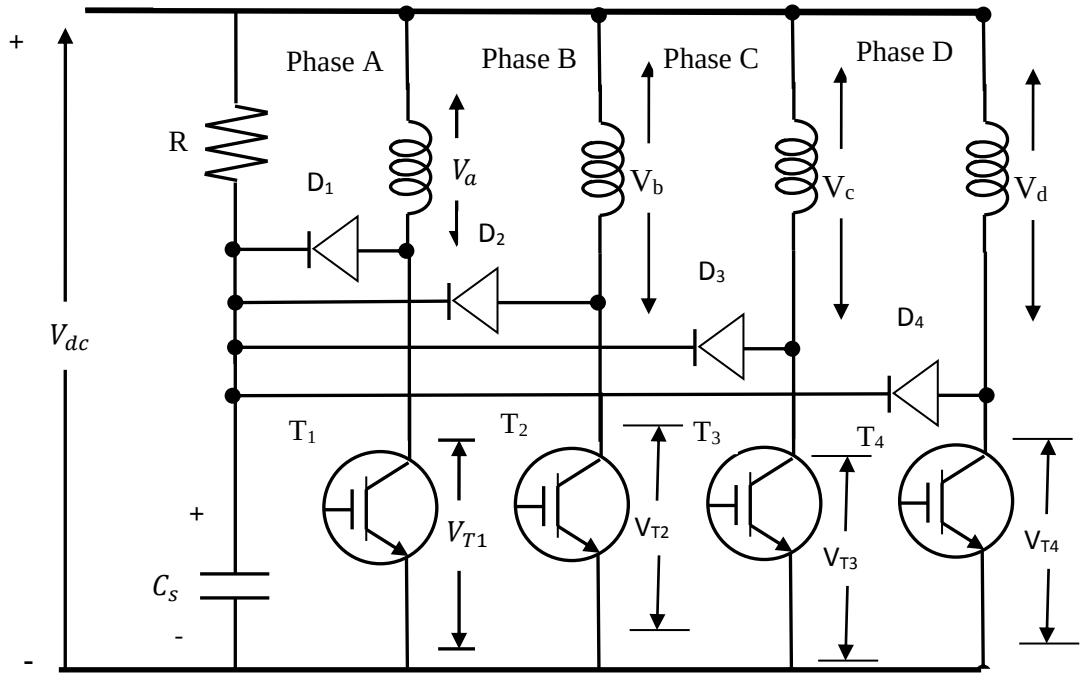

Fig.5.5 R-dump Converter for SRM with freewheeling path

The selection of R not only determines the power dissipation but also the switch voltage. A lower value of R increases the fall time of the current. If the current comes under the negative slope region of the phase inductance, negative torque will be generated, decreasing the average motoring torque. A high value of R increases the voltage drop across the winding and hence across T_1. Fig 5.6 shows the operational wave forms of R dump converter.

5.6.3.2 Bi-Filar Type Converter

Fig.5.7 shows a bifilar converter configuration with one transistor and one diode per phase but regenerating the stored magnetic energy to the source. This is achieved by having a bifilar winding with the polarity as shown in the Fig. 5.7. When the phase-A current is turned off by removing the base drive signal to T_1, the induced EMF in the winding is of such polarity that D_1 is forward biased. This leads to the circulation of current through D_1, the bifilar secondary winding, and the source thus transferring energy from the machine winding to the source. The various timing waveforms of the circuit are shown in Fig.5.8. During current turn-off, the applied voltage across the

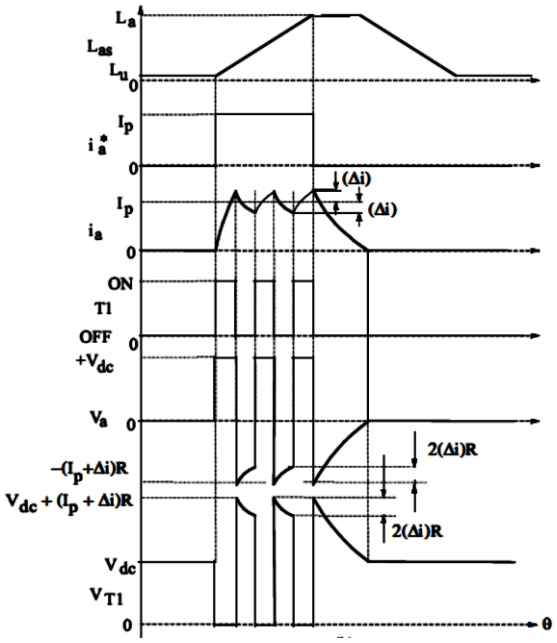

Fig.5.6 Operational wave forms of R dump converter

bifilar secondary winding is equal to the DC link voltage. The voltage reflected into the main winding is dependent upon the turn's ratio of the windings. The main disadvantage of this drive is that the SRM needs a bifilar winding and such a form of winding is not economical for large motors. Also, the bifilar windings require additional slot volume, reducing the power density of the SRM.

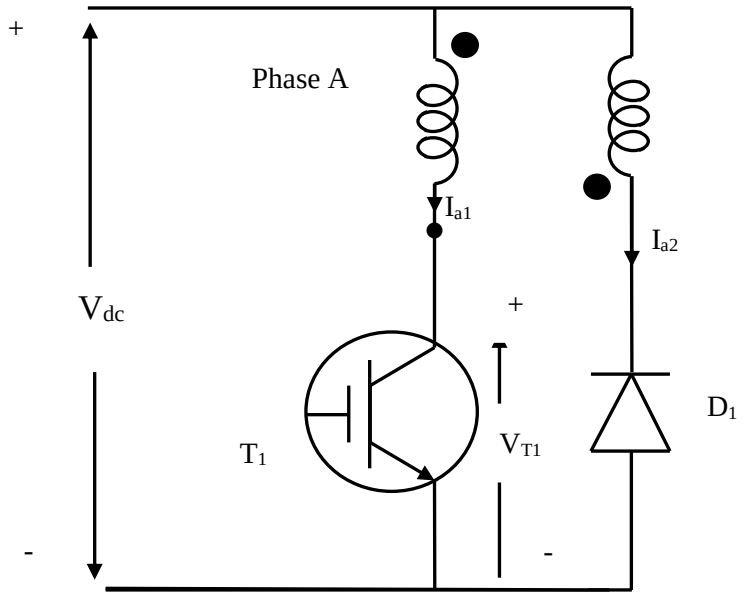

Fig.5.7 Converter for an SRM with bifilar windings

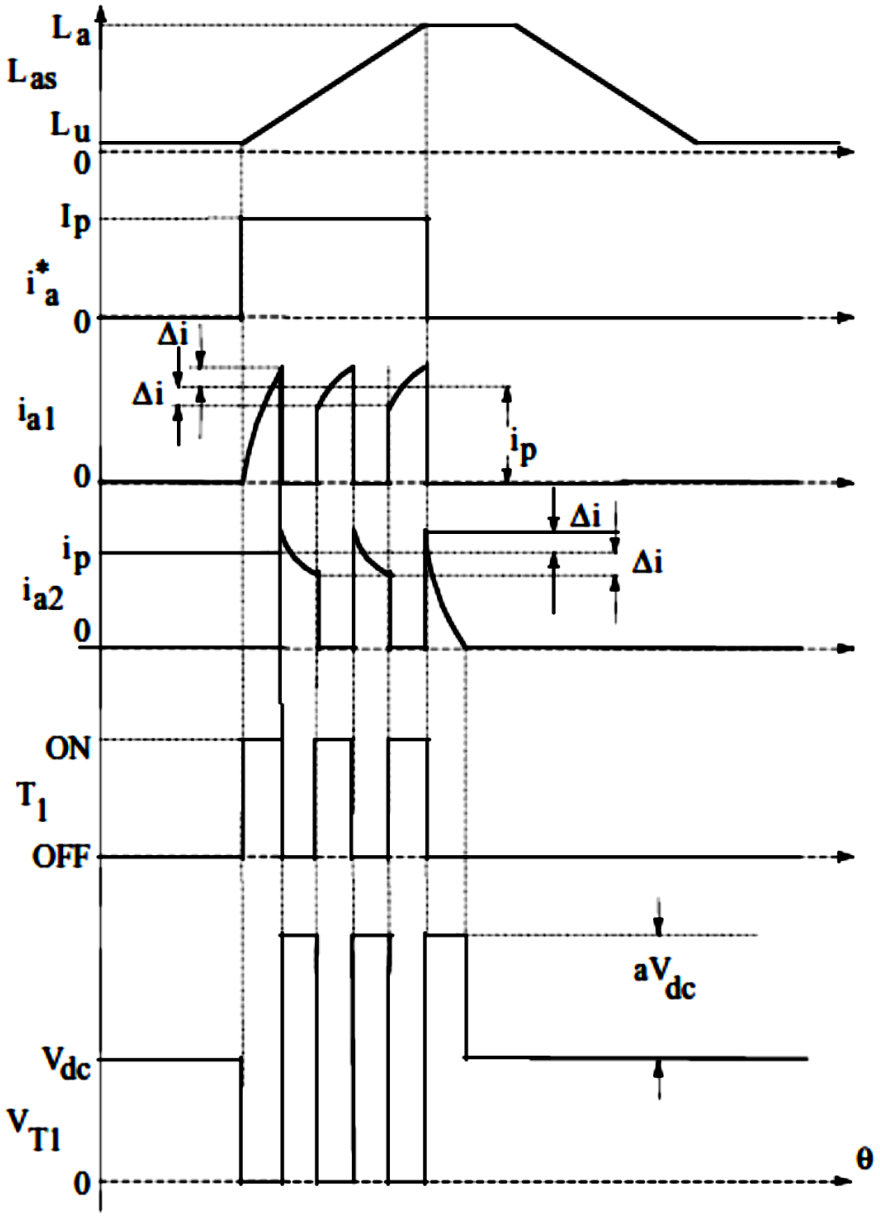

Fig.5.8 Operational waveforms of bifilar converter

5.6. 3.3 Split DC Supply Converter

A split DC supply for each phase allows freewheeling and regeneration, as shown in Fig.5.9. This topology preserves one switch per phase; its operation is as follows. Phase A is energized by turning on T_1. The current circulates through T_1, phase A, and capacitor C_1. When T_1 is turned off, the current will continue to flow through phase A, capacitor C_2, and diode D_2. In that process, C_2 is being charged up and hence the stored energy in phase A is depleted quickly. Similar operation follows for phase B(Hong-Je Ryoo, Won-Ho Kim, Geun- Hie Rim, Wook Kang, Ji-Ho Park and

Ching-Yuen Won 1998). The detailed analysis of the converter is discussed in next chapter. Split dc converter is used along with 8/6 SRM for testing the new controller designed in this thesis.

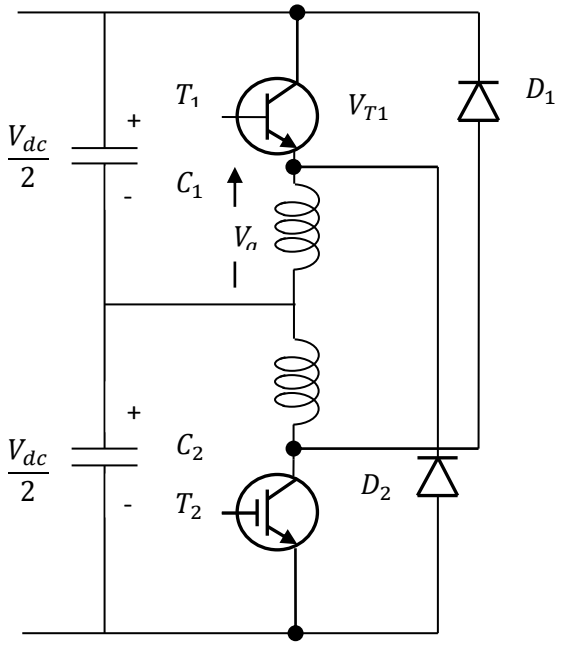

Fig.5.9 Converter for SRM with split dc supply

5.6. 3.4 q-Switches and 2q- Diodes Converters

This is another single-switch-per-phase converter configuration. The q -Switches and 2q- Diodes Converter (modified single-switch-per-phase converter) is shown in the Fig 5.10. In this D_1, D_2, D_3, and D_4 are fast, freewheeling diodes and D_5, D_6, D_7, and D_8 are slow freewheeling diodes. The circuit operation can be explained as follows. Phase A is energized by turning on switches T_4 and T_1. If the current exceeds the reference current i_a^* (say) by the current window Δi (say), switchesT_4 and T_1 are turned off. This will enable the diodes D_1 and D_4 to carry the A phase current. The voltage across the winding becomes $-V_{dc}$ which indicates that the energy is being transferred from the winding to the dc link. This will reduce the phase A current rapidly to zero. An alternative strategy is to turn off only one switch to reduce the current between switching cycles. Consider T_4 is on while T_1 is turned off for one switching cycle and vice versa for the next switching cycle to reduce the rms rating of the switches T_1 and T_4 and for their equality during this operation we use two diodes and one switch are in series with the winding. With the current in phase A winding, if

phase B current is to be built up, then switches T_2 and T_1 have to be turned on. Turning on T_1 will turn off the diode D_1, which implies that the decaying phase-A current will circulate through the A-phase winding, diode D_5, switch T_1, and freewheeling diode D_4. This reduces the voltage across the A phase winding to zero. Further, this will increase the time for the phase-A current to decay to zero. During overlapping currents in the succeeding winding phases, independent control of the currents is lost which is undesirable in high-performance applications. Because of its higher current rating per switch, this configuration may not be better than other configurations. Moreover, this configuration requires an even number of machine phases, which restricts its applicability in practice.

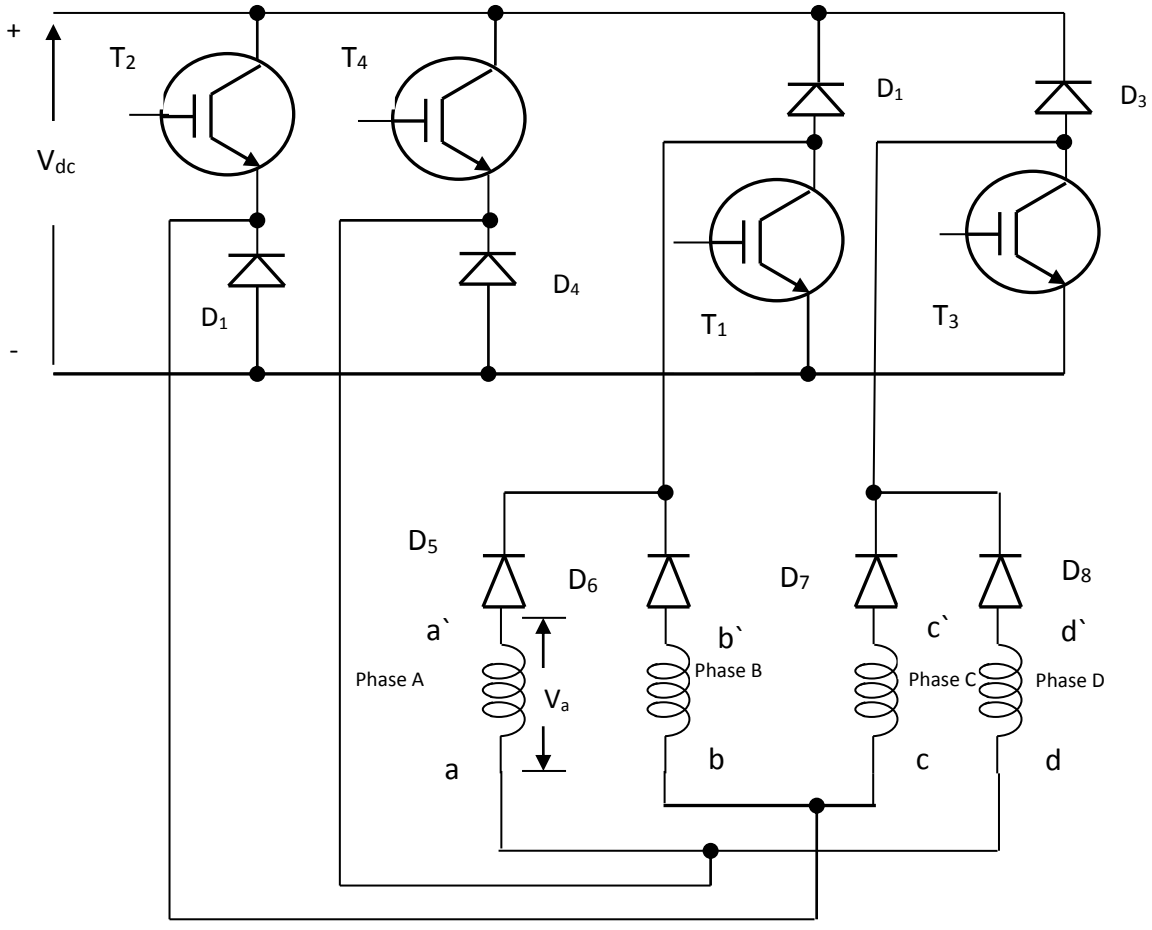

Fig.5.10 Modified single-switch-per-phase converters (The q -Switches and 2q- Diodes Converter)

5.6.3.5 q-Switch and 2q-Diode Configuration with independent phase current control

Single-switch-per-phase converter topologies presented in the above sections so far required modified/special bifilar windings and reduced DC link voltage to half for feeding a machine phase and involved higher losses and lower efficiency. A converter topology overcoming all the special requirements and drawbacks is shown in Fig.5.11. It requires additional q diodes and DC link capacitors. The diodes D_a, D_b, and D_c can be a slow type and their function is to create a separate dc link source voltage for each phase.

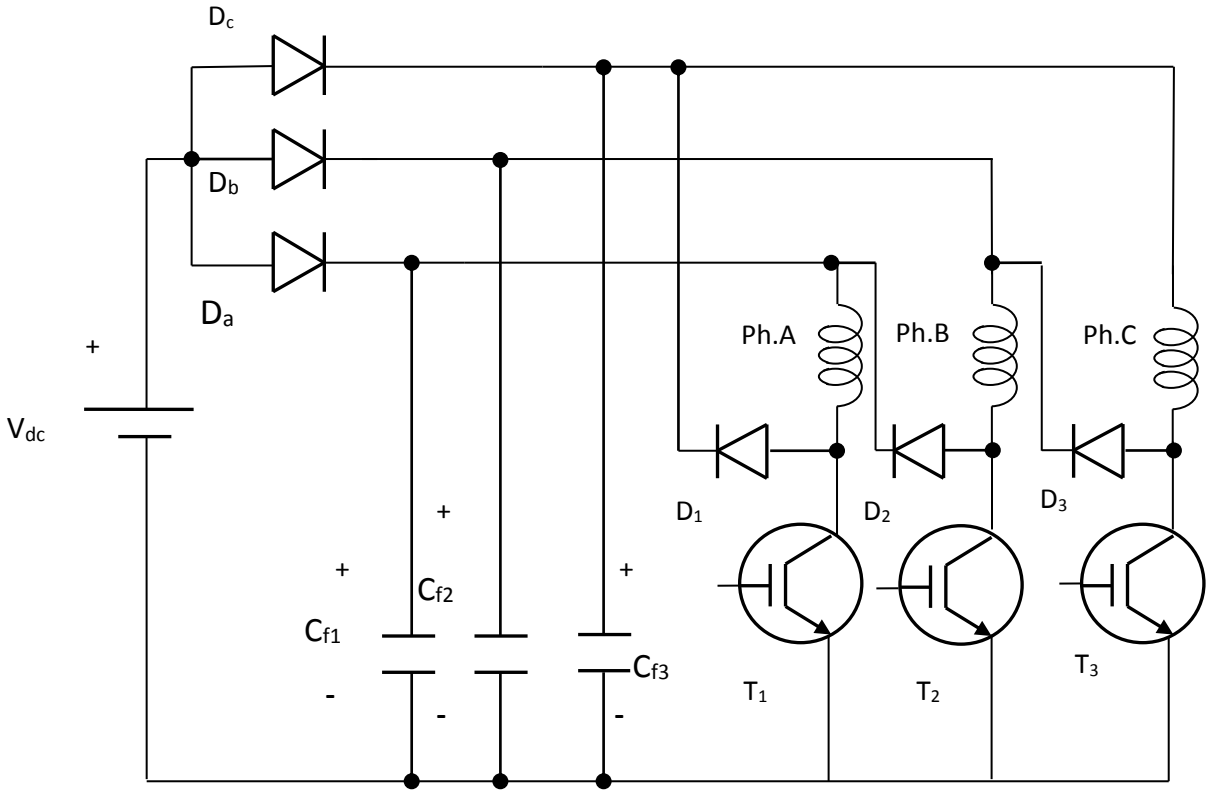

Fig.5.11 Single-switch and two-diodes-per-phase SRM converter

The operation of the circuit is as follows. Consider phase A operation. To energise phase A, T_1 is turned on. When phase-A current exceeds its reference by hysteresis window Δi (say), T_1 is turned off. The current in phase A takes the path via diode D_1 and capacitor C_{f3} connected between phase C and the dc source (equal to the voltage across C_{f1}) negative rail of the DC source voltage. Energy from phase A is partially transferred to C_{f3}, increasing its voltage beyond V_{dc}, which can rise to a maximum value of 2Vdc. The voltage across phase A during T_1 turn-off is the difference

between the source voltage and voltage across C_{f3}, which is negative. When A-phase current drops below the reference, T_1 is turned on to keep the A-phase current around its reference value. For final commutation of phase-A current, T_1 is turned off. In this the energy stored in C_{f3} will be depleted during phase C energisation. This happens because voltage across C_{f3} is much greater than V_{dc}, thus DC is reverse biased, resulting in an energy transfer from C_{f3} to phase C. Since the voltage acrossC_{f3} is higher than V_{dc}, this will allow a faster current rise in phase C. Further, it implies smaller advance angle for phase C and higher efficiency of the machine. When voltage across C_{f3} becomes less than the source voltage, phase C draws energy.

The advantages of the power converter circuit can be summarized in the following:

1. This circuit uses only one switch per phase with none of the disadvantages of other single-switch-per-phase topologies.
2. This topology endows independent phase current control in the SRM.
3. Energy transferred to dc link capacitors during current control and commutation of machine phases is utilised to provide a faster current response, resulting in faster dynamic torque and speed control of the SRM.

The disadvantages of this power converter are:

1. It requires additional q diodes and (q − 1) DC link capacitors, which maybe obtained by splitting the single dc link capacitor into q capacitors of equal value.
2. This converter provides only a positive or a negative voltage but is not capable of zero voltage, resulting in higher losses due to the circulating energy and higher acoustic noise.
3. The voltage rating of all the switches and diodes D1, D2, and D3 is 2Vdc which increases the volt–ampere (VA) rating of the converter.
4. The number of terminals required by the SRM is 2q for connection to the converter, whereas for most single-switch-per-phase topologies, it is (q + 1). This will increase the cost of the machine and will increase the labour involved in the assembly of the motor converter set.
5. This converter is not suitable for purely generator applications of the SRM as there are q capacitors from which energy has to be recovered. This increases the rating and component count of the energy recovery circuits.

5.6.4 Converters with auxiliary voltage supply: (q + 1) Switch and diode configurations

5.6.4.1 C-dump Converters:

The de-magnetization energy of a phase is fed in an auxiliary voltage supply with this converter type in order to restore the intermediate circuit or for directly energizing the succeeding phase. With the C-Dump-converter in Fig.5.12, the phase current is controlled by only one switch per phase. The stored magnetic energy is partially diverted to the capacitor C_d and recovered from it by the single quadrant chopper comprising of T_r, L_r, and D_r and sent to the DC source. Assume that T_1 is turned on to energize phase A and when the A-phase current exceeds the reference, T_1 is turned off. This enables the diode D_1 to be forward biased, and the current path is closed through C_d which increases the voltage across it. This has the effect of reducing the A-phase current and when the current falls below the reference by Δi (i.e., current window), T_1 is turned on to maintain the current close to its reference. When current has to be turned off completely in phase A, T_1 is turned off, and partially stored magnetic energy in phase A is transferred to energy dump capacitor C_d. The remaining magnetic energy in the machine phase has been converted to mechanical energy.

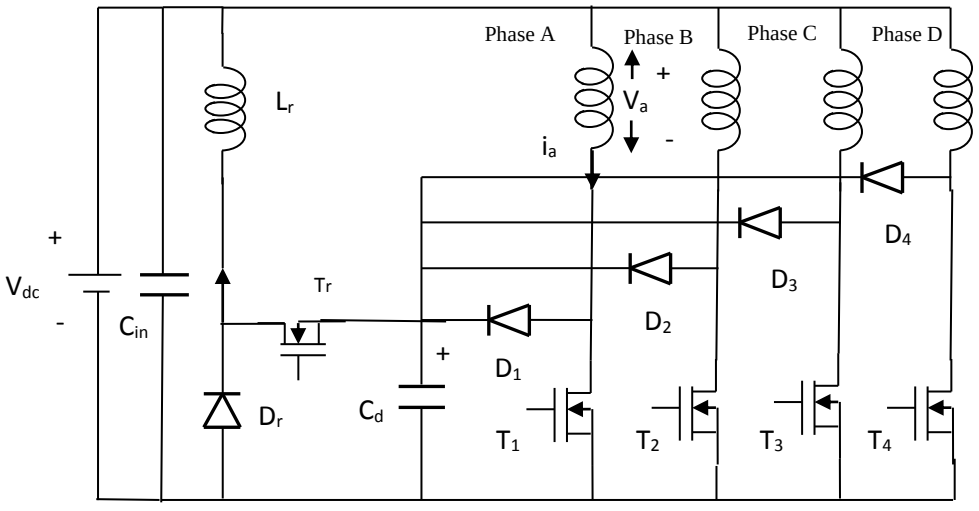

Fig.5.12 C-dump Converters

This converter has the advantage of minimum switches allowing independent phase current control. The main disadvantage of this circuit is that the current commutation is limited by the difference between voltage across C_d, V_o and the dc link voltage.

quick commutation of current requires larger V_o which results in increasing the voltage rating of the power devices.

5.6.4.2 Minimum switch topology with variable DC link

Two (q + 1) switch configurations for switched reluctance motor drives have been advocated due to their simple power converter topology having a minimum number of power switches and attractive control features, in spite of their operational limitations. These topologies have full four-quadrant operational capacity and endow the same voltage rating on all the devices as that of the dc source but have no independent energisation and commutation of the machine phases for overlapping conduction of the phases. The account with a C-dump has independent energisation and commutation control of phases but a higher voltage rating for the devices compared to the topologies already discussed. It also has a greater circulating energy through the machine windings and attendant losses. These disadvantages have restricted the use of many of these converters in practice.

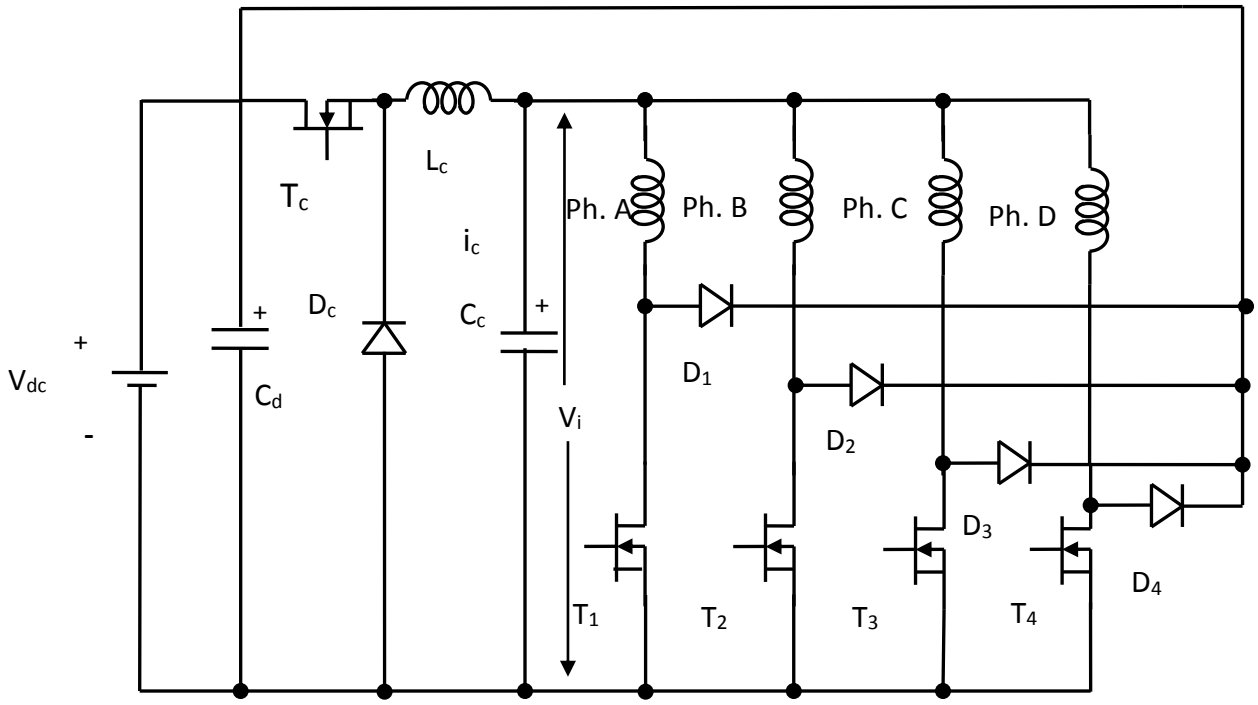

Fig.5.13 Variable DC link converter topology for SRM drives.

As shown in Fig.5.13, a three-phase SRM is an original power circuit topology overcoming the restriction on the independent control of energisation and commutation of the phase currents while maintaining the same number of power switching devices. The switch T_c, diode D_c, inductor L_c, and capacitor C_c forms the

step-down chopper power stage. This stage varies the input DC source voltage V_{dc} to V_i to obtain the desirable input voltage to the machine windings such as for single-pulse voltage switching, to minimize switching and reduce the associated losses both in the phase switches of the SRM converter and the core losses in the machine windings. Further, this stage provides the isolation required for faster commutation of the current while limiting the voltage rating of all the power devices to the DC source voltage. Unlike the case of the C-dump topology which requires a switch voltage rating twice that of the dc source bus. A step-down front-end chopper stage has been advocated for use with an asymmetric converter, but requires (2q + 1) switching devices and diodes.

The energisation mode is initiated by switching on the phase switch (say T_1) which applies the voltage V_i to the machine phase A, assuming an ideal diode and switch. To regulate the current in the winding, switch T_1 is turned off, which initiates the routing of the current through the freewheeling diode D_1, the source voltage V_{dc} and capacitor C_c, assuming that the chopper switch T_c is turned off during that time. Which would apply a negative voltage equal to the difference between V_{dc} and V_i across the machine phase. The energy in the capacitor C_c will be able to cater to the oncoming phase (say, B) during the time that the switch T_c is turned off. In this manner, the independence between various machine phases is maintained.

Merits and Demerits of the Converter

The merits of the topology are summarized as follows:

1. For an q-phase SRM, only (q + 1) switches and diodes are required for full four-quadrant operation.
2. Independent operation of the machine phases is guaranteed.
3. The commutation voltage is $(V_i - V_{dc})$, where as the applied voltage is v_i, which is less than the source voltage, V_{dc} and a faster current turn-off in the machine phases is obtained by reducing V_i during the commutation phase only.
4. Single-pulse voltage operation of the machine phases is made possible by varying the input voltage v_i to provide the required current, thus minimizing the switching losses in the power devices and machine core losses, resulting in enhancement of the efficiency of the SRM drive system.

5. The advantages of the minimum logic power supplies requirement of then other (q + 1) switch topologies which are preserved due to the fact that all the machine phase switch emitters are tied together.
6. Control and operation are very much similar to the C-dump topology without its disadvantages. For example, the link capacitor is rated for the same voltage as that of the dc source voltage with a margin unlike that of the capacitor ratings of the C-dump topology.

The disadvantages of the proposed topology are

1. The commutation voltage is lower compared to the two-switch-per-phase configuration.
2. The step-down chopper circuit has to be rated for the SRM power rating which may preclude its use in integral horsepower drives, thus making it suitable only for fractional horse power drive systems.
3. Coordinated control of the input voltage to the converter, V_i, during commutation to provide faster turn-off of current in the machine phases and to minimize machine and switch losses is quite new and has not been attempted with other topologies. Thus it must yet be developed for this drive.
4. Due to the additional stage of power processing in the chopper, the overall system efficiency of the SRM drive system is lower than that of the other schemes without the chopper stage. The reduction in system efficiency could be offset by resorting to single-pulse switching of the machine phases, thus boosting the efficiency of the machine converter stage and the machine.
5. This topology is unsuitable for continuous operation as a generator, as the oncoming phase has maximum (aligned) inductance and the outgoing phase has minimum (unaligned) inductance, which is contrary to the motoring operational mode. This phenomenon requires maximum voltage during commutation at the machine input. This will increase the commutation time and reduce the duration possible for generation, thus affecting the effectiveness of this operation.

5.6.4.3 Variable DC Link Voltage with Buck-Boost Converter Topology

An alternate variable dc link voltage converter circuit with four switches and diodes is shown Fig.5.14. There is only one switch per machine phase and it is

connected in series with the phase winding which prevents a shoot-through fault. The switch T_c, diode D_c, inductor L and output capacitor C form the buck-boost, front end power stage. The machine DC link voltage V_i can be varied from zero to greater than (say, two times) the dc source voltage V_{dc} to obtain the desirable input voltage to the machine windings. Further, this stage provides the isolation required for faster commutation of the current with the constant source voltage V_{dc}. The energisation mode is initiated by turning on the phase switch (say, T_1) and thereby applying the voltage V_i to machine phase A. To regulate the winding, switch T_1 is turned off which initiates the routing of the current through the freewheeling diode D_1, the DC source voltage V_{dc}, and phase A winding, regardless of the on or off condition of the chopper switch T_c which would apply a fixed negative DC source voltage V_{dc} across the machine phase winding. The energy in the output capacitor C will be able to cater to the oncoming phase (say, B) during the time that the switch T_c is turned off. In this manner, the independence between various machine phases is maintained in this converter topology.

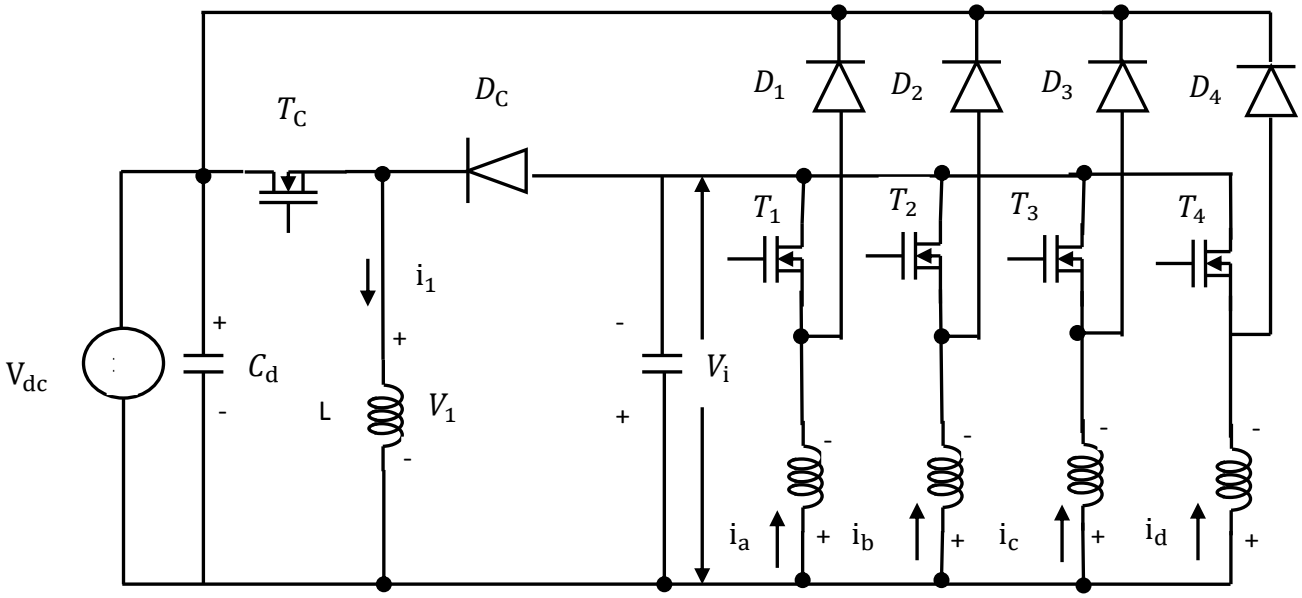

Fig.5.14 Variable DC link with buck-boost converter topology for SRMs

The distinct advantage of this power converter compared to the converter with a buck converter front end is that the input voltage to the machine phases could be increased over and above the DC source voltage to accelerate the buildup of the current in the machine phases. But a much greater advantage is found in the generation mode of the machine because the phase energisation instance coincides with the rotor and stator

pole alignment where the inductance is many times greater than the unaligned inductance encountered initially in the motoring mode of operation.

5.6.5 Resonant converter circuits

The power converter topologies either to discussed are known as hard-switched topologies because during turn-on and turn-off the power switch and diode voltages and/or currents are non zero, thus causing significant power loss in these devices. During the switching instant, if the current or voltage is zero, then the device loss is zero and topologies enabling such a condition are known as resonant circuits because the switching losses are theoretically zero in the resonant circuits, the circuit efficiency and hence the overall system efficiency is increased in the motor drive. The main disadvantage is that the device voltage ratings have to be multiple times that of the source voltage due to the action of the resonant circuit. This increases the volt–ampere rating of the converter to multiple times that of the conventional hard-switched topologies, restricting its industrial use in switched reluctance motor drive systems. Its advantage is that the quality of the current waveform can be made superior as the circuit can be operated at a higher frequency as the device switching losses are very small.

The resonant converter shown in Fig.5.15 circuit consists of inductor L_r, capacitor C_r, power switch T_r and diode D_r. The machine windings are connected in series with power devices T_1, T_2, and T_3 and diodes D_1, D_2, and D_3 steer the current of the machine phases during commutation and the excess current from the resonant circuit to the DC source, V_{dc}. In mode 1, energisation of the phase winding is achieved by switching the phase switch (say, T_1). When the machine current exceeds the desired level, we wish to turn-off the phase switch and reduce the energy transfer from the source to the machine. In mode 2, turn-off of the phase switch results in the machine current being diverted via D_r, C_r, D_a and the phase-A winding. This charges the resonant capacitor C_r, thus reducing the current in the machine winding. When the current reaches the acceptable lower limit, the phase switch T_1 is turned on to keep the winding current fairly a constant. Mode 3 is the resonant mode, with turn-on of the resonant switch, the resonant capacitor and inductor are connected in series, and the current fed to the source current is the excess current that is over and above that of the load current. During the resonant oscillation, the voltage across the capacitor has

reversed and is negative which is conductive for the takeover of current from the phase switch when it is being turned off. Note that turn-off of the main switches is achieved with zero voltage because its anti parallel diode D_1 is conducting during the energy recovery period, thus eliminating the turn-off switching loss in the phase switch.

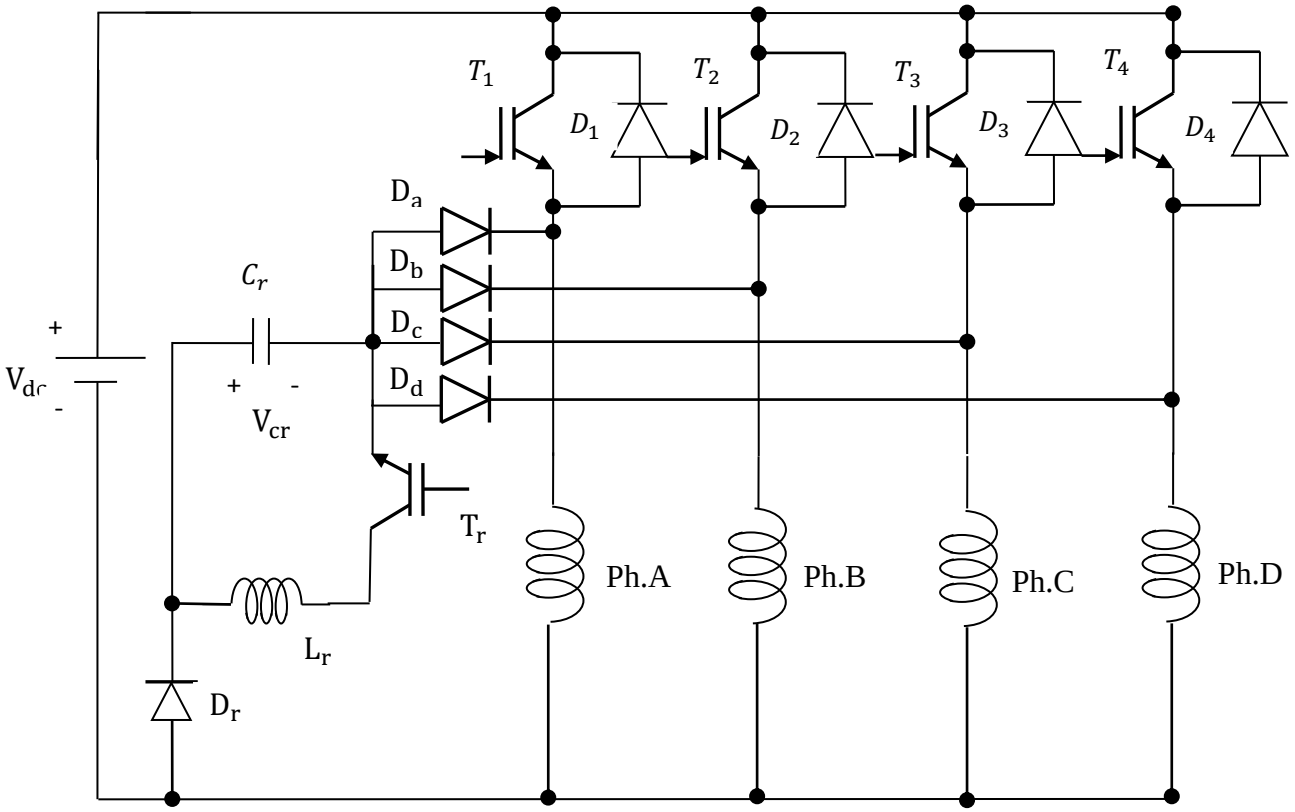

Fig.5.15.Resonant topology of a C-dump converter variant for SRM drives.

5.7 Controller Design

SRM drives are controlled by synchronizing the excitation of the motor phases with rotor position. From equation (2.16) in chapter 2 it is obvious that positive (or motoring) torque is produced when a phase is excited at rotor positions with positive $\frac{\partial L}{\partial \theta} > 0$ for that phase, and negative (or braking) torque is produced at rotor positions with negative $\frac{\partial L}{\partial \theta} < 0$. Hence a control system is required that determines rotor position and applies the phase-winding excitations at the appropriate instant. Therefore, the rotor position information is essential for the control system in order to generate the commutation signals. The commonly used position sensors are

phototransistors and photodiodes, Hall elements, magnetic sensors, pulse encoders and variable differential transformers. The SRM commutation strategy may use the rotor position feedback (ie., signal from opto-interrupters) to derive the commutating signals for the converter switches

The voltage applied to the motor phases is modulated with a duty cycle to reach the desired current in the excited phase. The instant of commutating the phase currents is synchronized to the rotor position. The current flowing through the SRM winding is regulated by switching on or off power devices, such as MOSFETs or IGBTs, which connect each SRM phase to a DC bus. The power converter topology is an important issue in SRM control because it largely dictates how the motor can be controlled. There are several converter topologies which are discussed in the previous section can be used with the controller. The use of converters depends on the application and the complexity in the converter design.

Error in rotor position detection could have a direct impact on the commutation positions, and may result in shifts of the phase conduction periods. The accuracy of position information determines the efficiency and torque capability as well as the torque pulsation of the drive. Therefore controller plays a vital role in SRM drive.

The control objective is to provide each phase with current over complete or part of the torque producing period, and to adjust the amplitude of the current such that the desired level of torque is obtained. In general current control scheme in order to acquire rapid motor torque response. The current control scheme uses the chopping speed controller. Design of the speed and current controllers for the SRM is quite a challenging problem which has attracted new interests in the control community. The details analysis of the proposed novel controller is discussed in the next chapter .The hardware design and testing the novel controller with 1 KW SRM is also discussed in the next chapter. The position sensor devices and auxiliary arrangements used to identify the location of the rotor is discussed in brief in the next section.

5.7.1 Phototransistor Sensors

The phototransistor sensor is based on the photoelectric principle. Fig.5.16 shows the basic structure of the phototransistor sensor. As shown in the Fig.5.16, a revolving shutter with a 120° electric angle gap is installed on the rotor shaft, rotating with the rotor of the SRM. Phototransistors of the same number as the motor phases (three

phases in the Fig 5.16 are fixed on the stator. When the gap is aligned with the phototransistor PT_1, the phototransistor will generate a current due to the light, while phototransistor PT_2 and PT_3 have only a very small leakage currents because the light is blocked by the revolving shutter. In this case, the stator phase associate with PT_1 should be turned on. Similar situation will occur when the gap of revolving shutter is aligned with PT_2 or PT_3.

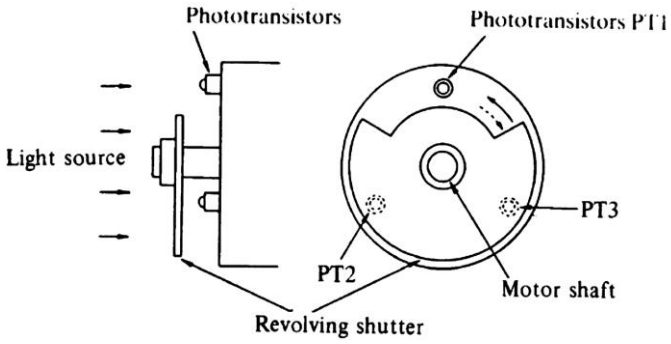

Fig 5.16 Phototransistor sensors

5.7.2 Hall Position Sensors

The function of a Hall sensor is based on the physical principle of the Hall effect named after its discoverer E. H. Hall: It means that a voltage is generated transversely to the current flow direction in an electric conductor (the Hall voltage), if a magnetic field is applied perpendicularly to the conductor

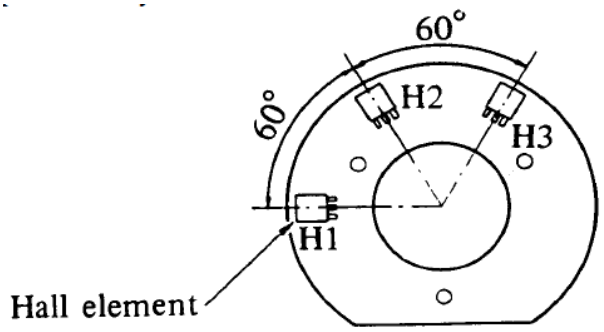

Fig.5.17 Hall position sensor

A typical structure of Hall position sensor for three phase motor is illustrated in Fig.5.17. It is made up of three Hall components and a rotating plate with permanent magnet fixed on the rotor shaft. Similar to the gap of the phototransistor sensors, the permanent magnet on the rotating plate is installed suitably so that the output of the Hall components can indicate the proper rotor position for the phase current control.

5.7.3 Slotted disc

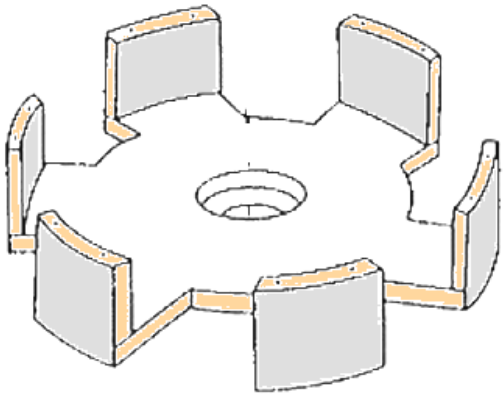

Fig.5.18 Slotted Discs

A slotted disc Shown in Fig.5.18 is mounted on rear end of the rotor with similar number of slots to that of the rotor so that the slots appear in between the space of the IR diode and the photo diode.

5.8 Selection of the Proper Converter Topology

However the selection of the proper converter for a certain application depends on many factors the designer has to compromise between them,, such as;

1. The hp capability:-For which hp capability the converter is suitable. This the main considerations taken into account for choosing a particular converter topology for a particular requirements.
2. Size and Volume requirement- The power converter having small sixe and less volume requirement is preferable in most of the applications
3. Economic Consideration: The cost of power converter is important factor taken into consideration while selecting a power converter. A low cost power converter is usually suitable
4. Speed requirements- The power converter suitable for high speed range is generally preferable
5. Switching frequency's range requirement
6. Whether the machine is used for motoring or for generation

5.9 Conclusions

The SR motor drive circuits have been critically reviewed in this chapter. Comparison of the most common drive circuit's topologies has been held showing the major

advantages and disadvantages of each topology together with its major field of applications**.** The most widely acceptable converter for SRM is the asymmetric bridge design. The asymmetric bridge begins with an ac supply fed into a bridge rectifier connected to a DC link. This is then fed to the bridge, which consists of two transistor switches and two diodes. This topology provide much faster rate of fall for the phase current which permits the motor to operate at higher speeds in comparison to other types of converters. This topology is more suitable for the high power drives than the other types of circuits. But this majorly suffers from the disadvantage that, it requires more number of switching devices, which will increases the converter cost and overall cost and also the complexity of the converter circuit. Other configurations are single switch converter like R-dump, split supply converter and the C-dump converter etc.

A C- Dump converter acts as both a power factor correction as well as phase de-fluxing component, reducing the device count. Better current regulations is achieved which makes it suitable for low voltage dc application such as automotive circuits. The improved power factor achievement without the use-of any voltage or current sensors can be utilized in AC applications

The split DC topology provides fast suppression of the tail current (during switch off wingind) in the phase winding and hence resulting in minimization of negative torque using doubly boosted voltage in the demagnetizing mode. This topology has higher efficiency and more output power than the other counterpart in the heavy load conditions and in high speed operations. From this topology we can use more positive torque region and enable to get more power from it. It has advantage over asymmetric bridge converter in the viewpoint of efficiency and output power varying the load and dwell angle. The simplicity and reduced count with compact packing of the topology makes make it an attractive low-cost for many variable speed drives application; hence in the present thesis a split dc converter is used along with SRM for designing and testing a novel controller circuit.

Chapter 6 Description of Experimental set up, Hardware and Software

This chapter introduces the novel combined control strategy of the S R motor drive. The equation of the average electromagnetic torque is presented. The hardware of the drive, such as the structure of the motor, the rotor position estimator with the slotted disk , the position sensors, the main circuit of the power converter and the scheme of the control strategy are proposed by taking a 4-phase 8/6 structure motor with the four-phase split supply converter power converter for example. The scheme of the turn-on angle and the turn-off angle in the power converter at the different range of the rotor speed are presented. The prototype adopted the novel combined control strategy is tested experimentally and compared with the know sensorless method of finding initial rotor estimation. The obtained values have been validated with the sensorless method. The sensorless method is carried out to prove the correctness of the methodology proposed. The tested results are given while the drive is operated at the different condition. The control for the system is implemented in a single low cost microcontroller. The experimental results validate the successful implementation of proposed alogirthm.

6.1 Necessity of Rotor Position

The rotor position information is an essential part of the SRM drive. It is used to generate precise firing command for the power switches in the power converter ensuring drive circuit stability, direction of rotation, and fast dynamic response. There are so many options for choosing position sensing scheme for the SRM drive including absolute or incremental encoder, Hall Effect sensors or even many sensorless methods. Various methods have been published in literature using different techniques (Lyons, J.P., MacMinn, S.R. and Preston, M.A 1991; Ehsani, M., Husain, I., and Kulkarni, A. B. 1992) and moreover in most of the sensorless methods, rotor position is estimated, either by measuring the inductance or the flux linkages .

The inductance profile of the SRM is triangular shaped for having equal stator and rotor pole arc combinations, with maximum inductance when it is in an aligned position and minimum inductance when it is in an unaligned position. One such profile for unequal stator and rotor pole arc combinations of a 8/6 pole SRM is given in Fig.6.1

The instantaneous torque (T) produced in the SRM is given by

$$T_d = \frac{1}{2} i^2 \frac{dL}{d\theta} \quad (6.1)$$

From equation (6.1) the positive torque is produced when the phase is switched on during the rising inductance, i.e., $(\frac{dL}{d\theta}) > 0$, negative torque is produced when the phase is switched on during the falling inductance, i.e., $(\frac{dL}{d\theta}) < 0$, and zero torque is produced when the phase is switched on during the constant inductance, i.e., $(\frac{dL}{d\theta}) = 0$. In order to have the motoring operation and proper control over the motor, therefore, rotor position is very important in SRM control.

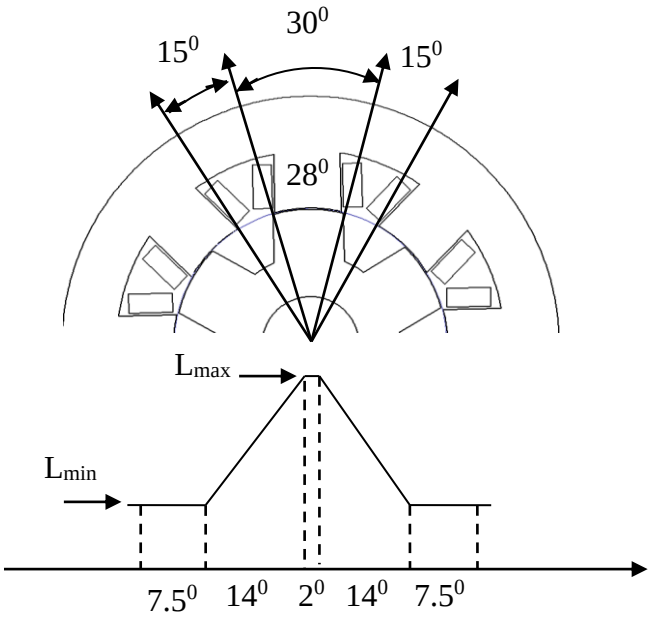

Fig. 6.1 Inductance profile for one rotor pole pitch

6. 2 Conventional rotor position estimation methods

In general, there are two types of rotor position sensing in SRM, namely direct sensing and indirect sensing techniques. In the direct sensing scheme, discrete sensors such as Hall-effect devices or optical encoders mounted on the back of the motor are used to produce necessary pulses in relation to rotor position (Perl, T., Husain, I. & Elbuluk, M. 1995). In the indirect sensing method, many different sensing techniques for the SRM drive have been proposed and presented by different researchers,

including in (Krishnan, R. 2001). In all of the methods utilized; the instantaneous phase inductance variation information has been used in some way to detect the rotor position indirectly and also, can be obtained from terminal measurements of the voltages and currents and associated derivatives, or by injecting low level high frequency signals into the non-energized phase inductance and then measuring the related outcomes (Perl, T., Husain, I. & Elbuluk, M. 1995). A comprehensive review of the existing indirect position detection methods in SRMs was discussed in the reference (A. Cheok and N. Ertugrul 1995). It has been shown in the reference that the indirect position determination methods can be classified into two major groups: inserting the low amplitude signals to the motor windings (major papers in this group include (P. P. Acarnley, R. J. Hill, and C.W. Hooper 1985), and monitoring the actual motor excitation waveforms (major papers in this group include (Gallegos-Lopez, P. C. Kjaer, and T. J. E. Miller 1999).Some of the indirect positions sensing methods are as follows:

a) Flux-current method

One of the simplest schemes is to measure the flux-linkage (λ) together with the phase current of the motor. Using these and also the non-linear static magnetization curve (λ, i, θ) of the motor, the rotor position (θ) can be estimated. Flux can be obtained by the following integration

$$\lambda = \int (\mathrm{V_{ph}} - \mathrm{R_s}\, \mathrm{i_{ph}})\mathrm{dt} \tag{6.2}$$

Where λ is the flux-linkage; i_{ph} is the phase current; V_{ph} is the phase voltage and R_s is the sensing resistor. Since the current goes to zero in every cycle, λ_0=0 can be used (Krishnan, R. (2001); Lyons, J. P., MacMinn, S. R. & Preston, M. A. (1999))

b) Current magnitude and current waveform detection methods

As the motor turns, the inductance of each phase varies with the rotor position. Voltage pulses are placed on the non-energized phase windings and the resulting current magnitudes are measured and compared to detect the rotor position. As in the current waveform detection, the shape of the current, or in other words the gradient of the current is monitored to determine the rotor position (Lyons, J. P., MacMinn, S. R. & Preston, M. A. 1991)

c) Frequency modulation

In this technique a high frequency carrier signal is injected into the non-energized phase. The signal containing the phase inductance information has a smaller frequency variation compared to the carrier signal and can be decoded using a demodulation technique to yield the rotor position (Panda, S. K. & Amaratunga, G. A. J. 1993)

d) Amplitude modulation

A low level alternating voltage is applied to an un-energized phase and the amplitude of the resulting current is mapped to the coil inductance. The inductance can be expressed as:

$$L = \frac{1}{\omega}\sqrt{\left(\frac{V_m^2}{I_m^2} - R\right)} \tag{6.3}$$

Where V_m is the voltage amplitude of the input voltage; I_m is the current amplitude and R is the resistance of the circuit (Ehsani, M. Husain, I. & Kulkarni A. 1992)

e) Phase modulation

A low alternating voltage is applied to an un-energized phase of the motor and the phase angle difference between the input voltage and the resulting current is detected. The inductance is given by

$$L = \frac{R\tan\theta}{\omega} \tag{6.4}$$

Where θ is the phase angle and ω is the angular velocity in rad/s (Ehsani, M., Husain, I., & Ramani, K. R. 1991)

f) Mutual voltage scheme

The principle of this technique is based on measuring the mutually induced voltage in an un-energized phase winding either adjacent or opposite to the energized phase. The magnitude of the induced voltage varies significantly as the rotor belonging to the energized phase moves from un-aligned position to the full alignment. The mutually induced voltage in an adjacent pole is given by

$$V_m = \frac{d\lambda_m}{dt} = \frac{d(M(\theta)i)}{dt} = M(\theta)\frac{di}{dt} + i\frac{dM}{d\theta} \tag{6.5}$$

Where M (θ) is the mutual inductance and i is the phase current (Ehsani, M., Husain, I., Mahajan, S. & Ramani, K. R. 1994; Husain, I. & Ehsani, M. 1994).There are different ways in intelligent control methods such as artificial neural networks (ANN) (Bellini, A., Filippetti, F., Franceschini, G., Tassoni, C. & Vas, P. 1998) and fuzzy control (Mese, E. & Torrey, D. A. 1997; Wang, Z., Cheok, A. D. & Wee, L. K. 2001) that found applications in the detection of rotor position in switched reluctance motor. Neural networks have the inherent capability for identification. Rotor position estimation can be viewed as an identification process given the set of current and flux linkages from the three dimensional relationships that exist between them. Such an approach is used in the ANN-based rotor position estimator. Fuzzy control uses a linguistic-based, approximated human reasoning to provide a solution to the problem of identification. The inputs are the estimated flux linkages and measured currents, and the output is the rotor position from which the speed is derived.

6.3 Proposed Rotor Position Estimation Method

A pair of IR transmitting and receiving sensors placed on the stator and an external rotor disc is used to estimate the rotor position. Based on the over-lapping of the rotor pole face with stator pole face, position sensors generate four states as shown in Fig.6.2. If the position sensor 1 output is low and the other position sensor output is also low, i.e both were low, then there is no overlapping of rotor pole face with stator pole face (Completely Unaligned (Fig.6.2 (a)), rotor pole is about to overlap with stator pole). If both position sensor signals output were high, rotor pole completely overlaps with the stator pole face (Fig.6.2 (c)), i.e. completely aligned position.Fig.6.2(b) and Fig.6.2(d) shows mis-aligned positions(one is increasing inductance and other is decreasing inductance). The output signal of the rotor position sensors is used as the basic triggering signals of the four phase main switches of the power converter. Based on information from the position sensors, initial rotor position is initially estimated and later on respective phases are being excited based on the information from the position sensors to rotate the motor (rotor) in clock-wise direction as well as in anti-clock wise direction. The step-by-step procedure for rotor position estimation at standstill and during running condition is explained with the

help of Fig 6.3 and Fig 6.4 .The truth tables for clock wise and anti clock wise directions are shown in Table 6.1 and Table 6.2

Table 6.1: Truth Table for backward direction (Anti Clock-Wise direction)

Position Sensor 1	Position Sensor 2	State	Phase to be excited
1	0	0	B
1	1	1	C
0	1	2	D
0	0	3	A

Table 6.2: Truth Table for forward direction (Clock-Wise direction)

Position Sensor 1	Position Sensor 2	State	Phase to be excited
1	0	0	A
1	1	1	B
0	1	2	C
0	0	3	D

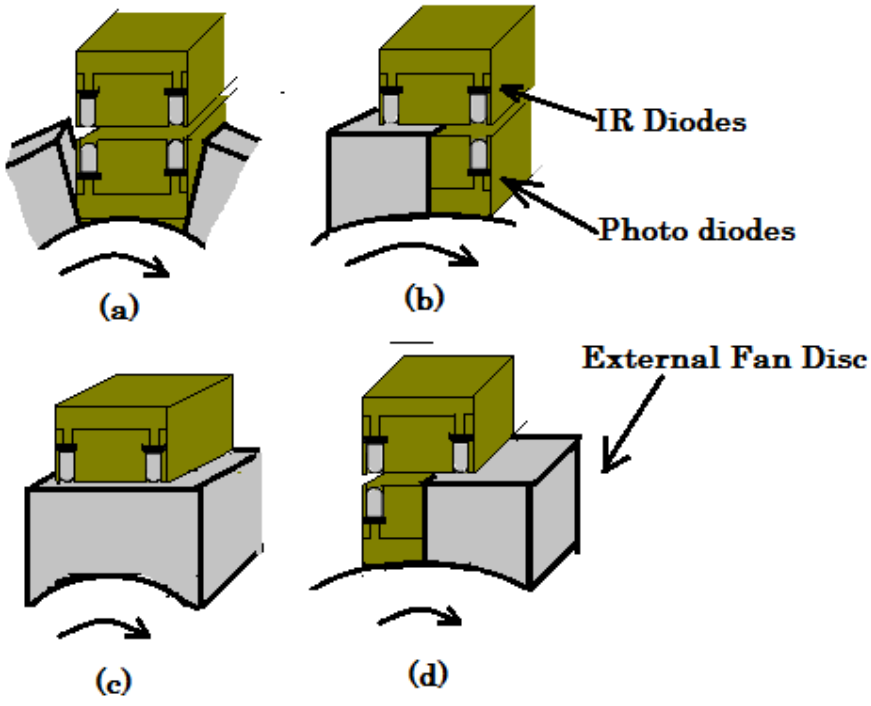

Fig.6.2 Rotor position states
(a) State: 3 (b) State: 0 (c) State: 1 (d) State: 2

6.3.1 Rotor position estimation at Stand-Still condition

Rotor position estimation at standstill condition is very important to indentify which phase has to be excited and to start the motor in proper direction without any difficulties. In order to predict the rotor position at standstill, information from position sensors is used. Say at starting, If both the position sensors output is low, then rotor poles are unaligned with Phase A, and Phase A has to be excited, and the sequence to be followed for a particular direction is based on the truth tables. The rotor position at standstill is obtained simply without magnetic characteristics of the motor and additional hardware

6.3.2 Rotor position estimation at running condition

In order to get a smooth and ripple free operation, it is necessary to monitor the rotor position when the machine is running. Once active phase is found, at stand still then the proposed algorithm based on the truth tables (Table 6.1 and Table 6.2) are used to give the triggering signals to the gate of the electronic switches of power converter to rotate the rotor in clockwise and anti clock wise direction. The details of the proposed algorithm is as follows

In a magnetic circuit, the rotating part prefers to come to the minimum reluctance position at the instance of excitation. While two rotor poles are aligned to the two stator poles, another set of rotor poles is out of alignment (unaligned) with respect to a different set of stator poles. Then, this set of stator poles is excited to bring the rotor poles into alignment. From Fig. 6.3 (i), it is clear that, with respect to phase "A" (stator poles A and A') the rotor poles R_1 and R_2 are at unaligned position. From equation (6.1) the, positive torque is developed when a particular phase (as it is at unaligned position) is excited, during its rising inductance. As the phase "A" inductance is rising, if a excitation is given to phase "A" (as per the truth table State 0) a flux is established through stator poles A and A' and rotor poles R_1 and R_2 tends to pull the rotor poles R_1 and R_2 towards the stator poles A and A'. The rotor poles R_1 and R_2 which were in unaligned position now will turn in anti clockwise direction to the intermediate position as shown in Fig.6.3 (ii) because this is the nearest position; Then , If the excitation to the phase "A" is switched off so that the current in phase a is $I_a = 0$ and parallel if phase "D" is switched on (i.e. if the excitation is given to phase "D") , the rotor continue to rotate in anti clock wise

direction, and rotor position will be changed from intermediate position to aligned position with respect to phase "A" as shown in Fig .6.3 (iii) ,Then ,if the excitation to the phase "D" is switched off so that the current in phase "D" is $I_d = 0$ and at the same time if phase "C" is switched on (i.e. if the excitation is given to phase "C") the rotor will keep its anti clockwise rotation, and with respect to phase "A" the position of the rotor poles is as shown in Fig. 6.3 (iv). Therefore, the stator exciting sequence a, d, c, b, a... generates anti clockwise rotation. For the same reason, the sequence d, a, b, c, d….yields clockwise rotation as shown in Fig 6.4. The truth table for the anti clock wise direction is shown in the table 6.1.

6.4 Verification of the proposed method to find out rotor initial position.

In this section, an estimation method of rotor position for SRM based on comparing the amplitude among 4-phase current to select the appropriate phase at standstill is described to compare and validate the proposed new algorithm discussed in section 6.3. The rotor position estimation method is applying the small testing signal and measuring the phase current of the motor (H.Gao, F.R. Salmasi., and M. Ehsani 2001; X. Kai, Z. ionghua, and L. Jianwu 2005). At stand still condition, the voltage and current equation can be expressed by the following equations. Based on the assumptions that the resistive voltage drop is negligible and there is no mutual coupling between any two phases, the voltage equation of one SRM phase can be simplified as

$$V = L\frac{di}{dt} \tag{6.5}$$

where L is the non-saturated phase self-inductance, v and i are the terminal voltage and winding phase current, respectively. From equation at the starting, the winding current can be rearranged as

$$i = \frac{V}{L}t \tag{6.6}$$

by injecting the short duration of gate drive signal to each phase simultaneously, each phase winding current will increase as a straight line from zero and have peak value at the end of excitation . That means the relation in Equation (6.6) is valid and the slope of the current waveforms directly depends on the value of $\frac{V_{dc}}{L}$ where V_{dc} is the supply voltage and L is the phase inductance, respectively. The phase inductance increases as the rotor pole approaches the stator

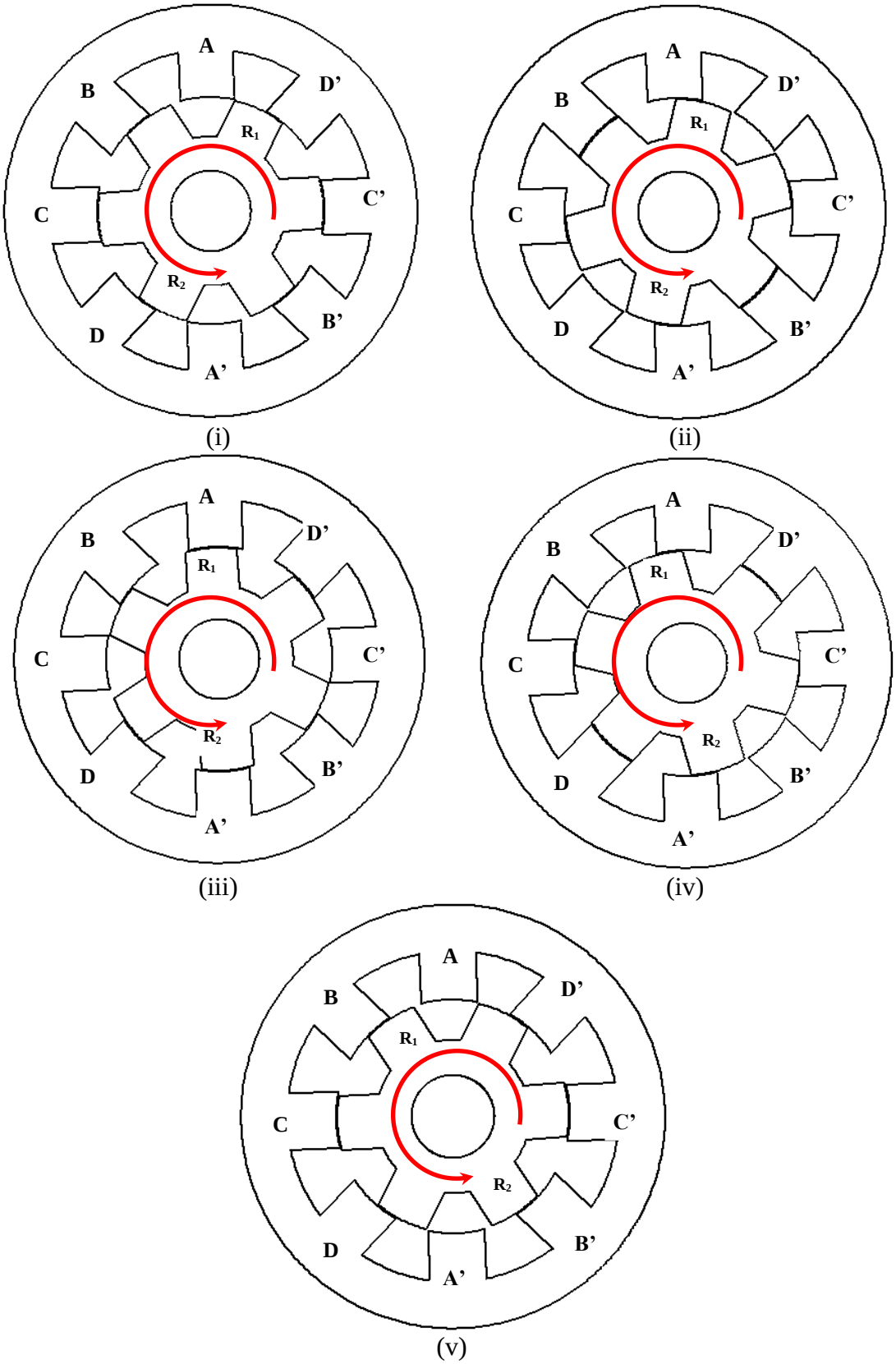

Fig.6.3 : Exciting Sequence A,D,C,B,A…. generates anti Anti clockwise Rotation

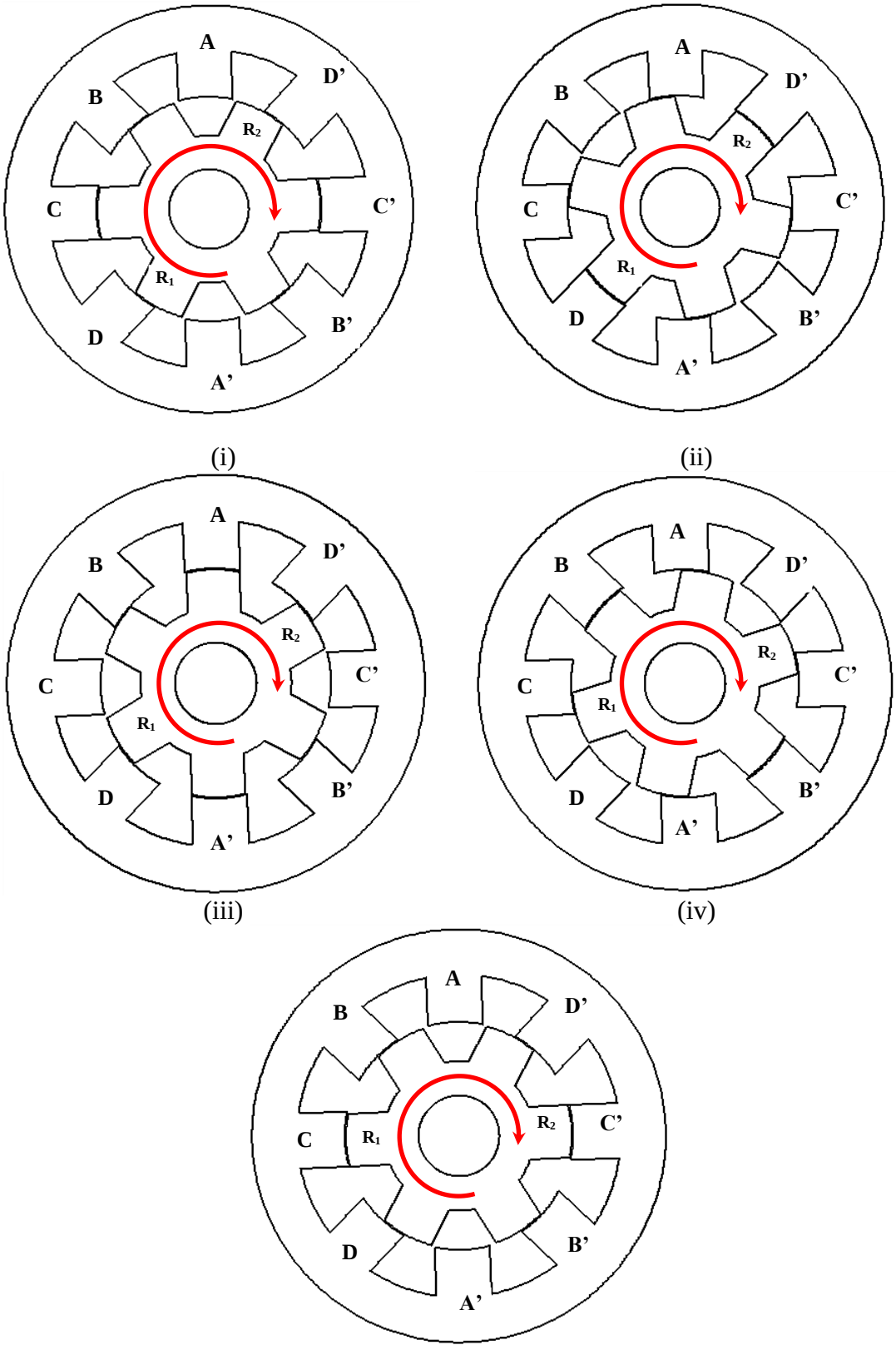

Fig.6.4 : Exciting Sequence D,A,B,C,D…. generates anti Clockwise Rotation

pole. When the stator and rotor poles are aligned, the phase inductance shows the maximum value, and thereafter the phase inductance decreases. Therefore, the rotor position is obtained by observing the value of the phase currents of all phases. The minimum current peak value occurs at the aligned position (maximum inductance) and maximum current peak occurs at the position near the unaligned positions

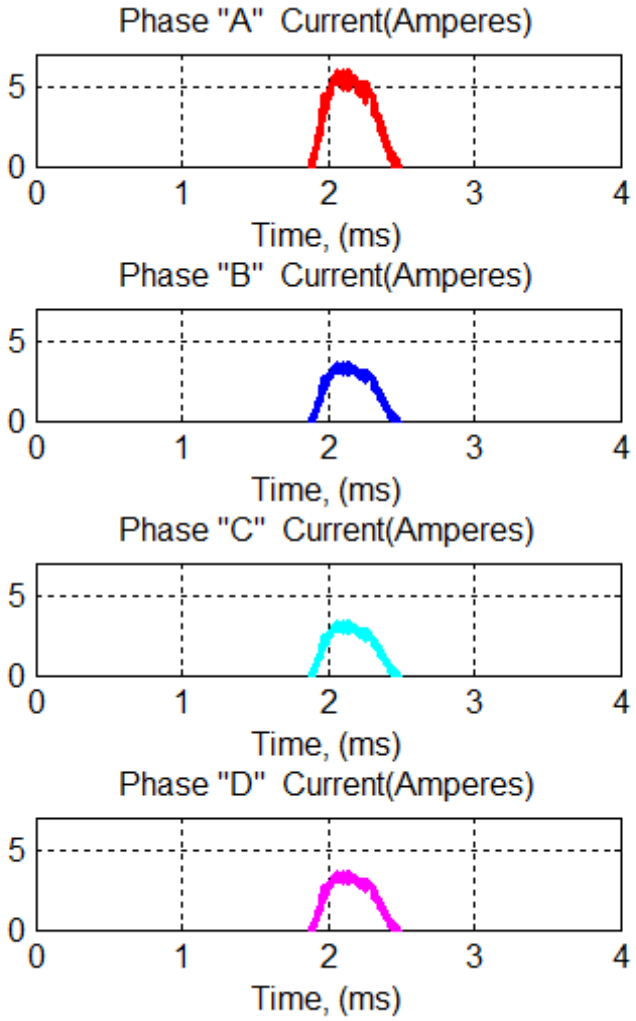

Fig.6.5 Phase current during estimation of initial rotor position
(Initial position is 00 deg)

Fig 6.5 shows Phase current during estimation of initial rotor position. At starting of the SRM, the initial phase excited is determined based on the magnitude of the phase currents to move the rotor toward the desired direction , and the initial rotor position is detected.

Table 6.3 Estimation of Initial Rotor Position

State	According to proposed algorithm, rotor is unaligned with	Phase with highest current, from experimental verification	According to experimental verification, rotor is unaligned w.r.t
0	Phase B	Phase B	Phase B
1	Phase C	Phase C	Phase C
2	Phase D	Phase D	Phase D
3	Phase A	Phase A	Phase A

Table 6.3 shows the experimental results of the estimation of the initial rotor position using the proposed method at various rotor positions. The experimental results show that the validity of the proposed method is verified.

6.5 Description of the complete drive – Hardware

Taking a four-phase Switched Reluctance motor drive prototype for example, the prototype consists of the four-phase 8/6 structure Switched Reluctance motor, the four-phase split dc power converter and the controller and power supply unit as shown in Fig.6.6. Position sensors are used for rotor position sensing. The details of power and controller circuits and various circuits are discussed in the next section.

6.5.1 Description of power circuit

The converter topology used in this thesis for testing the designed controller along with SRM is split dc converter. It consists of one switch per phase. Further the supply unit consists of six sealed maintenance free (SMF) Lead-Acid batteries each rated for 12 V, 18 Ah and a variable voltage source. A set of two capacitors in series provides three wire DC supply. Equal value resistances are connected across each capacitor to balance the voltage. The basic converter circuit is shown in the Fig.6.7. IGBTs are used as switching devices in all four phases. Each phase windings is energized by turning on the respective phase IGBTs. If phase A is to be energized, the IGBT T_1 has to be turned on, and then the current circulate through T_1, phase "A" and the capacitor C_1. When T_1 is turned on DC voltage is connected to the phase "A" winding and current flows through the phase winding. The flux is generated by the current flowing in the phase winding. Rotor is pulled into the direction of the reluctance minimum and to the direction of the phase inductance maximum. To provide continuous torque, the

driving IGBTs should be controlled successively. To prevent excessive production of negative torque, the exciting current is rapidly reduced to zero at the aligned position and when T_1 is turned off, the current continues to flow through winding, D_2 and C_2 .The energy stored in the phase "A" winding during on period is dumped to C_2. The phase "A" during off period is subjected to negative supply through C_2 which helps in quick demagnetization of the motor phase A and reducing the effect of negative torque. Similar process is followed for other phases. Fig.6.8 shows modes of operation of split DC converter.

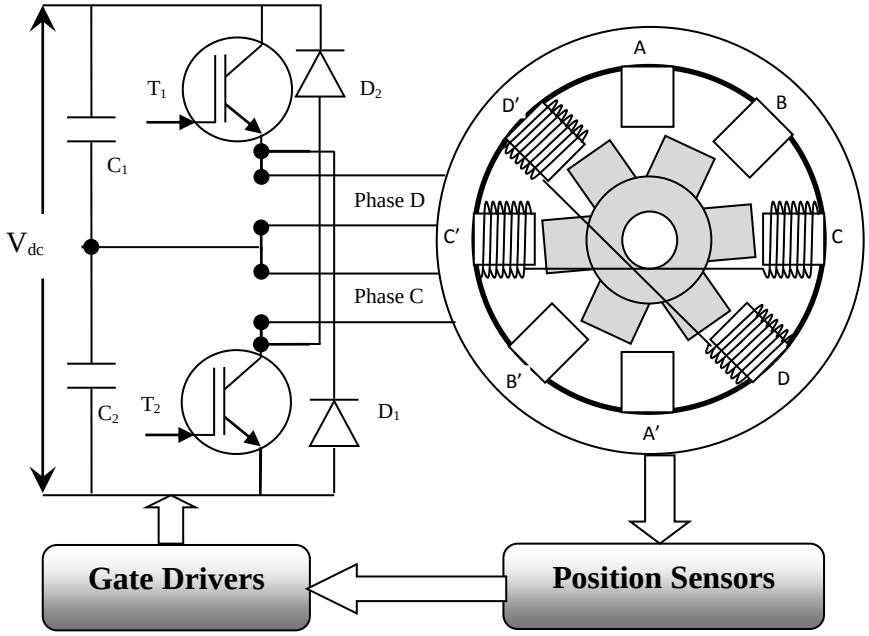

Fig.6.6 Configuration of SRM drive

The phase voltage is V_{dc} /2 when T_1 is on, and when it is turned off with a current established in phase A, the phase voltage is $-V_{dc}/2$. The voltage across the transistor T_1 during the on time is negligible, and it is V_{dc} when the current is turned off. That makes the switch voltage rating at least equal to the dc link voltage. When the winding current becomes zero, the voltage across T1 drops to 0.5 V_{dc} and so also does the voltage across D_2 Here main aim is to obtain performance characteristics of 1 kW SRM with 72 V DC source. Assume that there is no magnetic saturation that means

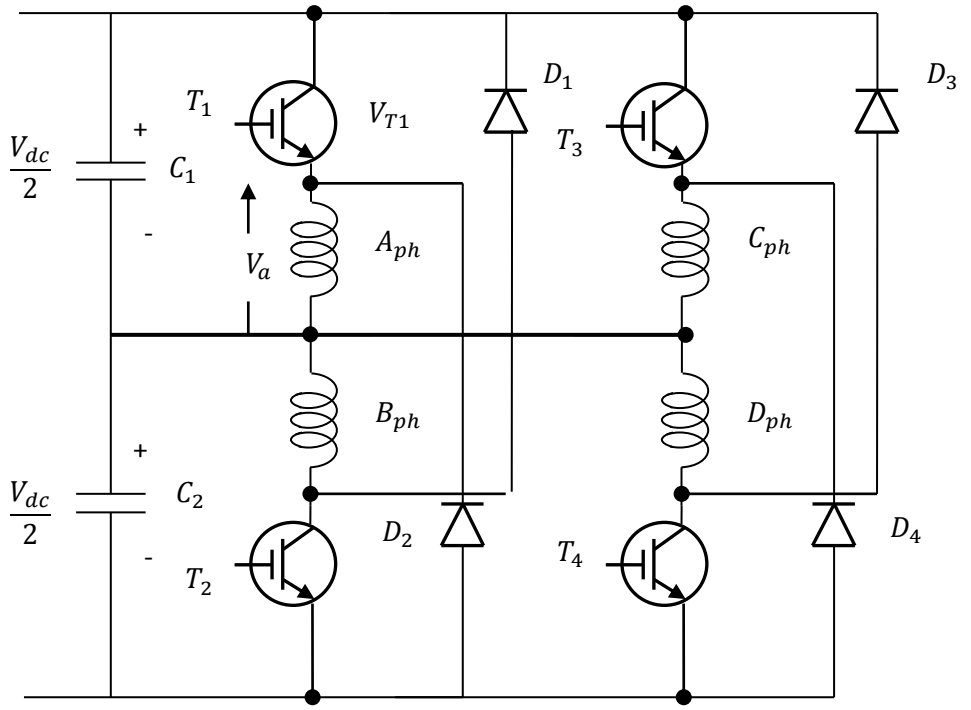

Fig.6.7 One switched per phase split DC converter

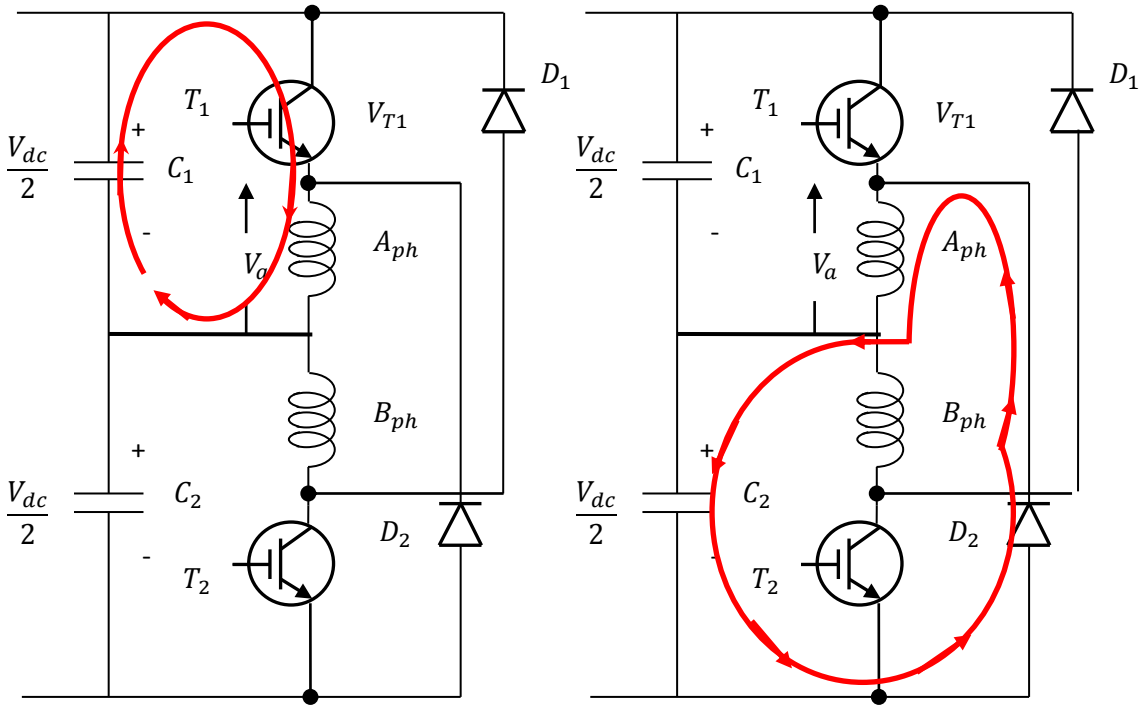

Fig.6.8 Mode of operation of split DC converter

inductance is unaffected by the current. Also neglecting the mutual inductance for the simplicity voltage equation of the one phase is

$$V_{ph}=R_{ph}i_{ph}+\frac{d\varphi_{ph}}{dt}=R_{ph}i_{ph}+\omega_m\frac{d\omega_{ph}}{dt}$$

Where V_{ph} is the phase voltage equal to $\frac{V_{dc}}{2}$

Fig.6.9 (a) and Fig.6.9 (b) shows the calculated phase "A" current and voltage. Note that this converter configuration has the disadvantage of de-rating the supply dc voltage, V_{dc}, by utilizing only half its value at any time. Moreover, care has to be

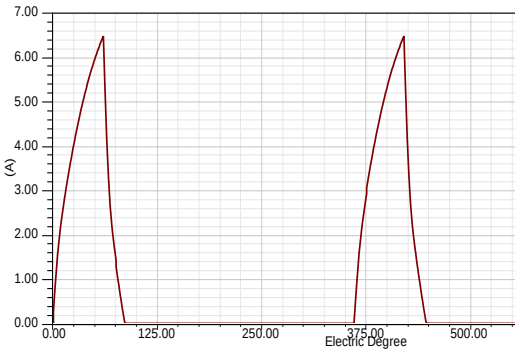

Fig.6.9 (a) Calculated Phase A current profile at 15000 RPM

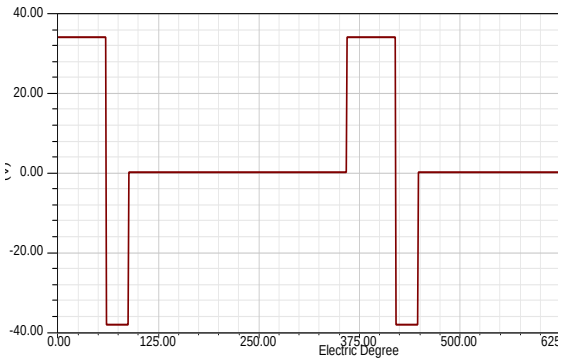

Fig.6.9(b) Calculated Phase A Voltage profile at 15000 RPM

exercised in balancing the charge of C_1 and C_2 by proper design measures. For balancing the charge across the dc link capacitors, the number of machine phases has to be even and not odd .In order to improve the cost-competitive edge of the SRM drive, this converter was chosen in earlier integral horse power (hp) product developments, but its use in fractional hp SRM drives supplied by a single phase 72V dc supply is much more justifiable; thus minimizing the cost of the converter. The number of switches used per phase in split dc supply converter is one. The number of diodes used per phase in split dc supply converter is one (Hong-Je Ryoo, Won-Ho Kim, Geun- Hie Rim, Wook Kang, Ji-Ho Park and Ching-Yuen Won 1998; Do-Hyun Jang 2001)

The advantages of a split dc supply converter are described as follows:

1. Compactness of converter package.
2. Lower cost due to minimum number of switches and diodes.
3. Capability of regeneration of stored energy.

The disadvantages of a split dc supply converter are enlisted below:

1. De-rating of the supply voltage.
2. Suitable only for motors with an even number of phases.

Application of split dc supply converter is in fractional hp motors with even number of phases.

6.5.2 Position Sensor Conditioning Circuit

Fig .6.10 shows the position sensing circuit of SRM. Two photo diodes and two infra –red (IR) diodes are used as sensors. Two number of IR diodes are directly connected in series to the in built dc supply of regulated 5V through a current limiting resistor in order to ensure constant current. The photo diodes are individually reversed biased from 5 volts dc regulated source. The photo diodes and the IR diodes are placed facing each other mounted on the stator in specific position so that, the infra-red light emitted by the IR diode directly fall on the photo diode. A slotted disc is mounted on rear end of the rotor with similar number of slots to that of the rotor so that the slots appear in between the space of the IR diode and the photo diode. Thus while the rotor makes a rotation the IR light which falls on the photo diode is interrupted through the slots of the disc. While the light is interrupted the photo diode resistance falls sharply to a low value. This fall of resistance forms a difference in potential to a comparator made out of Op-Amp, thus the output of the comparator is either 0 or 1 .Two comparators are used to get states such as 01, 11, 10, 00, which fall in synchronization with rotor position. For the starting purpose the corresponding state decides triggering of appropriate stator pole phase winding and while running it follows the sequence from there onwards

6.5.3 Location of Position Sensors and Exciting Sequence.

A pair of IR transmitting and receiving sensors which are placed on the stator and an external rotor disc is used to sense the rotor position .Based on the over-lapping of the rotor pole face with stator pole face, sensors generate four states as shown in Fig.6.2. When the sensor signals were both low there is no overlapping of rotor pole face with stator pole face. If both signals were high, rotor pole face completely overlaps with the stator pole face. These states are shown in the truth tables. Based on this the respective phases are being excited to rotate the motor in clock-wise direction as well as in anti-clock wise direction.

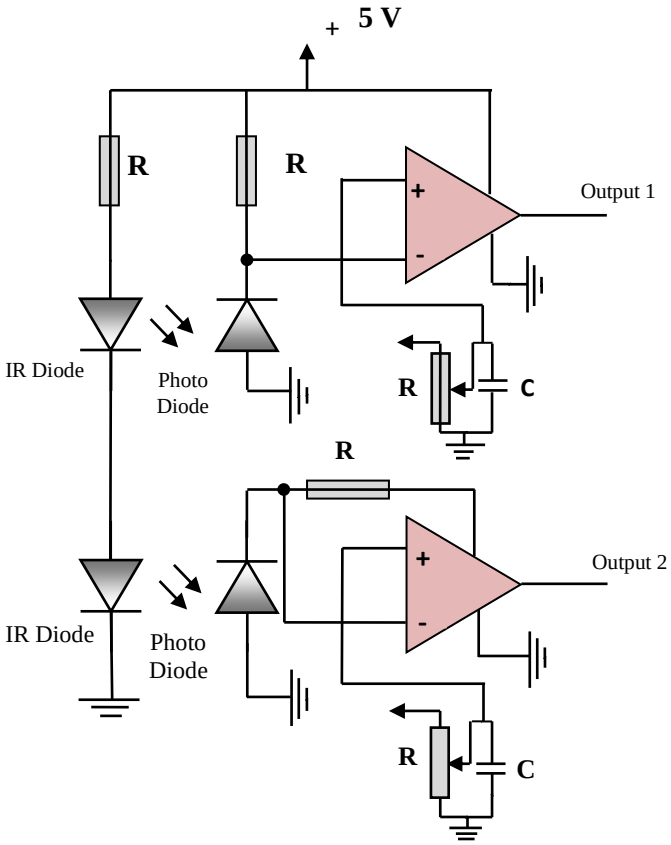

Fig.6.10 Position sensor Circuit

6.5.4 Basic Controller and Gate Drive circuit

The block diagram of the basic controller and gate driver circuit is shown in the Fig.6.11. The position sensor circuit receives the rotor position information through the position sensors and gives the information to the micro controller. The micro controller receives two separate input signals from the position sensor conditioning circuit as shown in the Fig.6.10 which are read, stored, and processed to determine the pulse-width modulated output signals that excites proper phase and to control the motor. The output of the micro-controller is fed to the input buffer circuit. A quad operational amplifier is used as four comparators and the output of which is used for driving the IGBT's through gate driving circuits. The inverting output of each comparator is given to a reference voltage through a potential divider from inbuilt regulated 5Volts D.C. The non-inverting inputs of the four comparators are driven from the micro controller output. As per the algorithm, output generated from the

micro-controller drives respective comparators to generate trigger pulses to respective gates of the IGBT's.

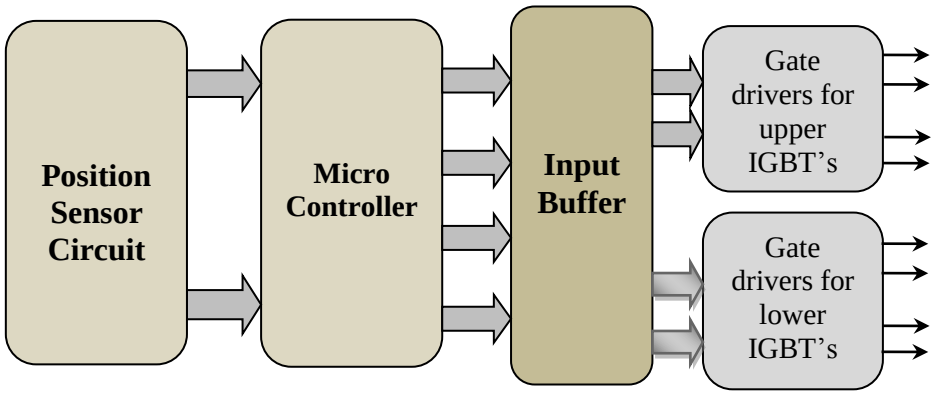

Fig.6.11 Basic Controllers and Gate Drive Circuit of SRM

6.6 Hardware Implementation

The overall setup of this system consists of the controller board, the gate drivers for the converter switches, the converter power-stage, the SRM and the interconnections is shown in the Fig.6.12

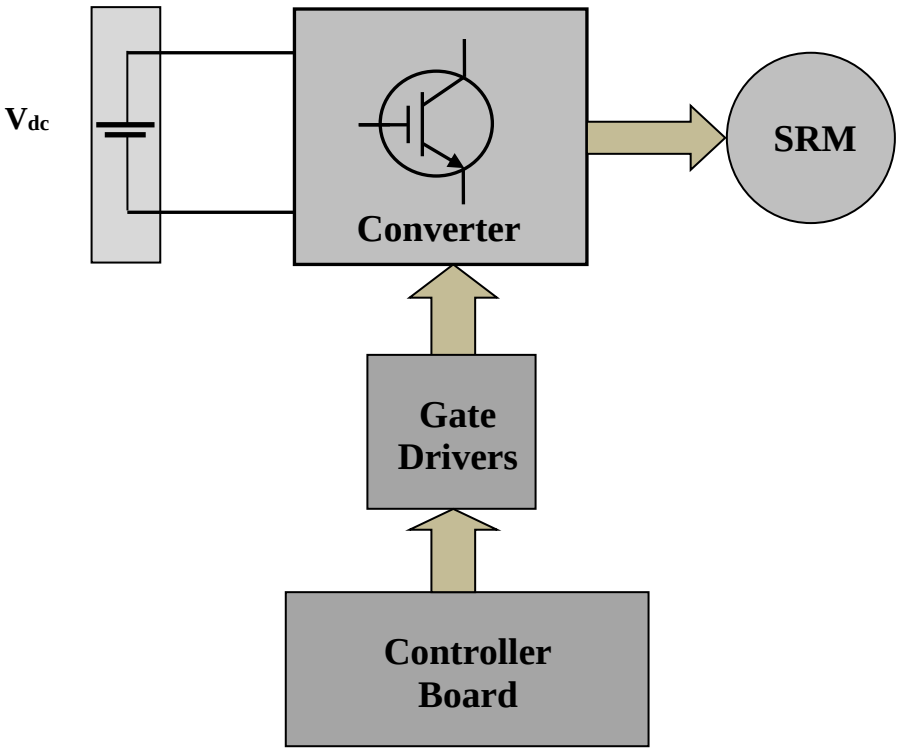

Fig.6.12 Proposed SRM Drive system

6.6.1 Power Stage

The first step in designing the power stage is to select the power semiconductor devices. This converter consists of four main switches and four freewheeling diodes. The input to the system is fixed at 72V DC and system is to be designed for an average load current of 12A. CT60AM-18F, a 900V and 60A power IGBT was chosen as the main switching device for the converter. To realize the freewheeling diode, a 600V, 30A, hyper fast diode, MUR1560, is chosen.LM324 IC is used in the position sensor conditioning circuit along with LM339 IC in buffer circuit. Further the supply unit consists of six sealed maintenance free (SMF) Lead-Acid batteries each rated for 12V, 18A and a variable voltage source. All the devices are connected on the heat sink and the interconnections are made on a PCB.

6.6.2 Controller Board

The control board gets the input from the position sensors as shown in Fig 6.13. A pair of IR transmitting and receiving sensors placed on the stator and an external rotor disc is used to sense the rotor positions .Based on the over-lapping of the rotor pole face with stator pole face, sensors generate four states as discussed in the previous section. The rotor position information as received from the position sensor circuit is fed to the micro controller .The micro controller reads, stores, and process to determine the pulse-width modulated output signals as per controlled algorithm that excites and controls the motor. The output of the micro-controller is fed to the input buffer circuit. LM 324 IC is used for implementing position sensing, while LM 339 IC is used as buffer circuit. Fig.6.14 shows the connection diagram for LM 324

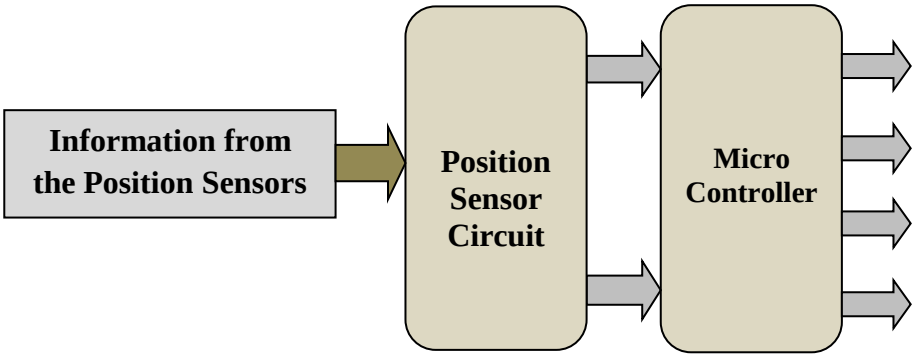

Fig.6.13 Block diagram of the Controller board

Two comparators of LM324 are used to get states such as 01, 11, 10, 00, which fall in synchronization with rotor position. LM 324 consists of four independent high-gain frequency-compensated operational amplifiers that are designed specifically to operate from a single supply over a wide range of voltages. Fig.6.15 shows the connection diagram for AT89C51 micro controller.

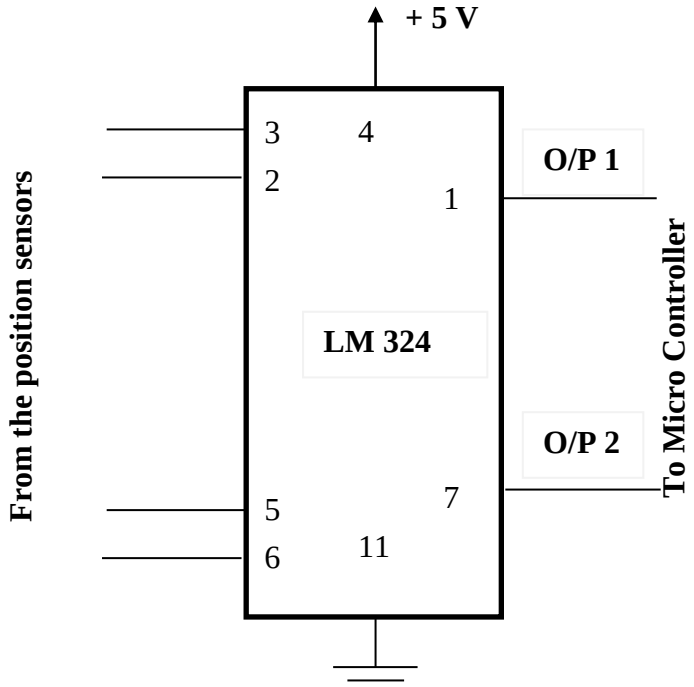

Fig.6.14 Connection diagram for LM 324

6.6.3 Gate Drivers

The gate drivers get the signal pulses from the control board and amplify them to the required level for switching the power IGBTs. The IGBTs used in this setup have an input capacitance of 4nF and thus the driving capability required from the gate drivers is not too large. The designed gate driver board consists of two parts. The first one being the input buffer and the second one being the gate driver. The input buffer is required to provide high impedance for the input control signal. It is also used to boost the current so that sufficient current is available to the gate driver circuit.

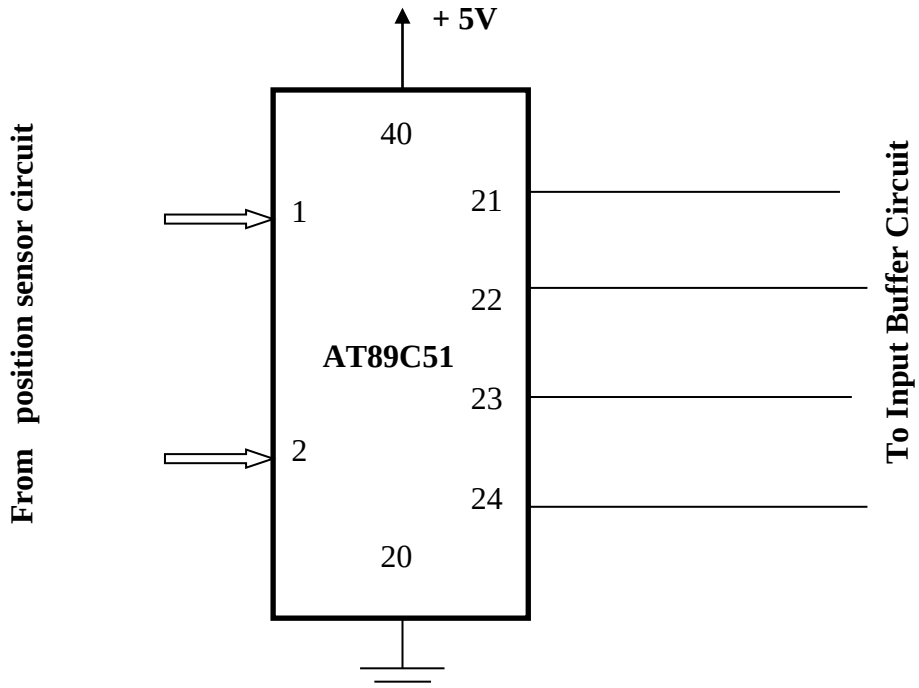

Fig.6.15 Connection diagram AT89C51 micro controller

Fig.6.16 shows the block diagram of the gate driver board. Fig.6.17 shows connection diagram for buffer circuit (LM 339) and Fig.6.19 shows the connection diagram for the gate driver circuit (IR2110).

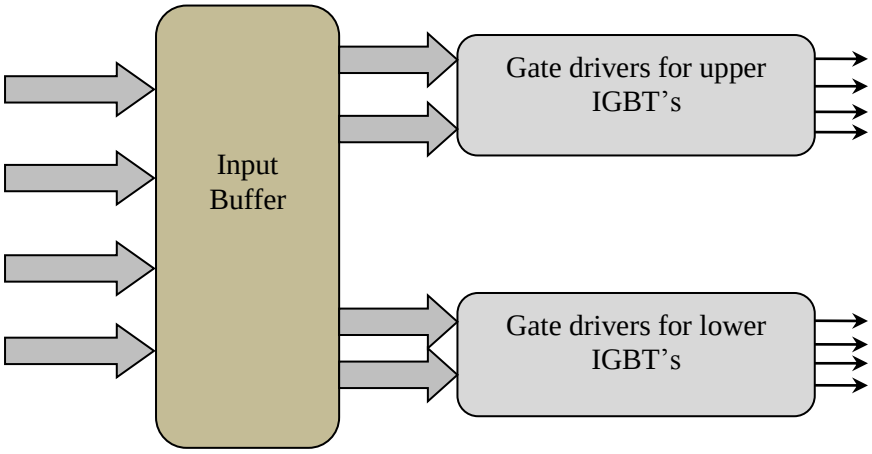

Fig.6.16 Block diagram of the gate driver board

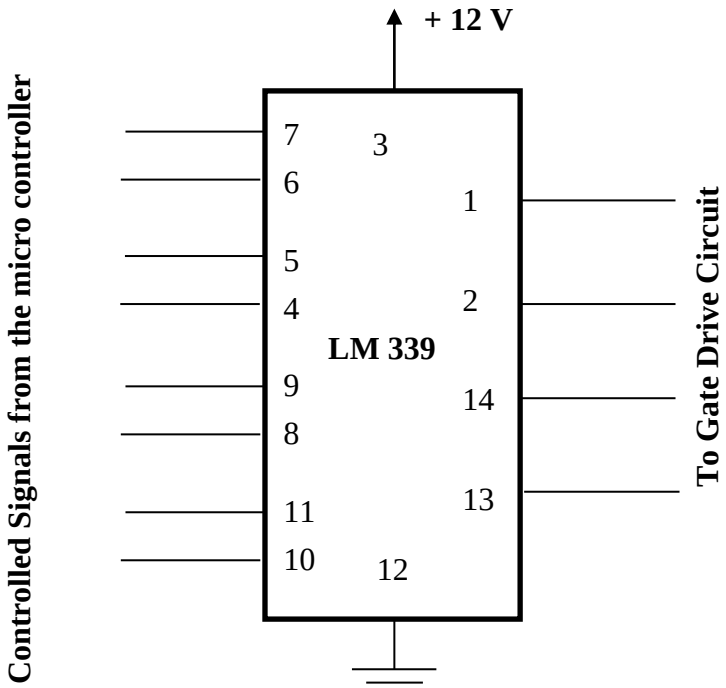

Fig.6.17 Connection diagram for buffer circuit (LM 339)

The LM339 series consists of four independent precision voltage comparators with an offset voltage specification as low as 2 m V_{max} for all four comparators. These comparators also have a unique characteristic so that the input common-mode voltage range includes ground, even though operated from a single power supply voltage.

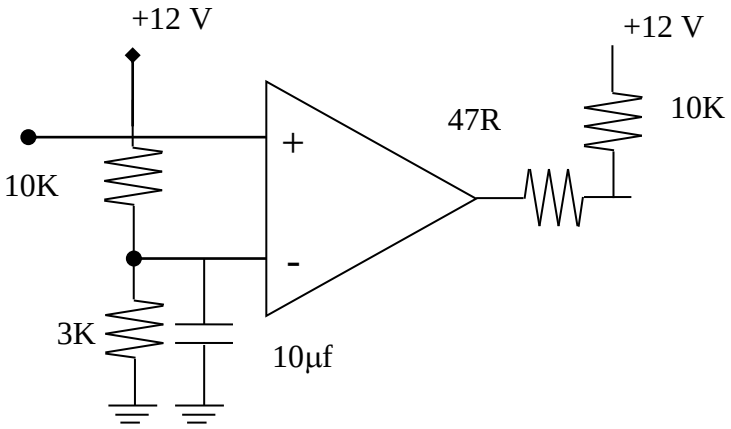

Fig. 6.18 A Comparator (LM 339)

The buffer circuit receives four signals from the micro controller and these inputs are given to the four comparators of LM339. A comparator shown in Fig. 6.18 is a circuit which compares a signal voltage applied at one input of an op-amp with output +/- V_{sat}(0V or 12V). The changes in the output state takes place with an increment in input V_i of only 2mV. A fixed reference voltage V_{ref} is applied to (-) input and the output from the micro-controller is applied to (+) input. The voltage is at $-V_{sat}$ (OV) for $V_i < V_{ref}$ and V_O goes to $+V_{sat}$ (12V) for $V_i > V_{ref}$.

In a practical circuit V_{ref} is obtained by using a 1kilo ohm potentiometer which forms to voltage divider with the supply voltages V+ and V- with the wiper connected to (-) input terminal as shown in the Fig.6.18 thus a V_{ref} of desired amplitude and polarity can be obtained by simply adjusting the 1kilo ohm potentiometer.

The outputs of the input buffer circuit are fed to the IR 2110. The outputs of IR 2110 IC are given to the gating terminals of the switching devices. The pin connection for the IR2110 is as shown in the Fig.6.19

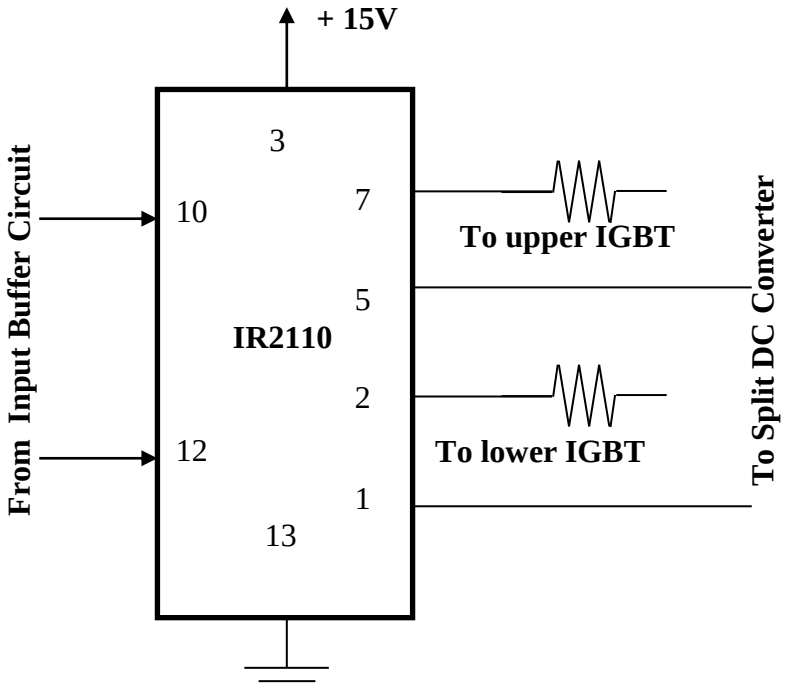

Fig.6.19 Connection diagram for IR 2110

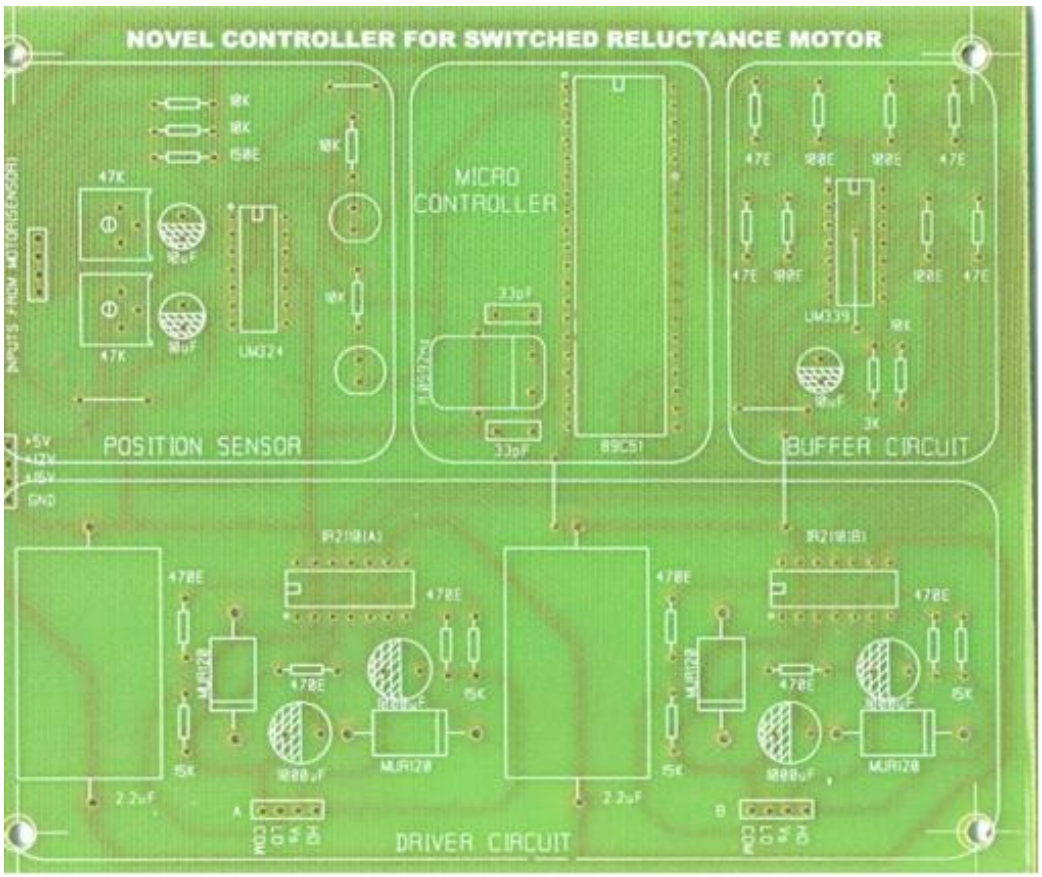

(a) PCB –Controller Circuit

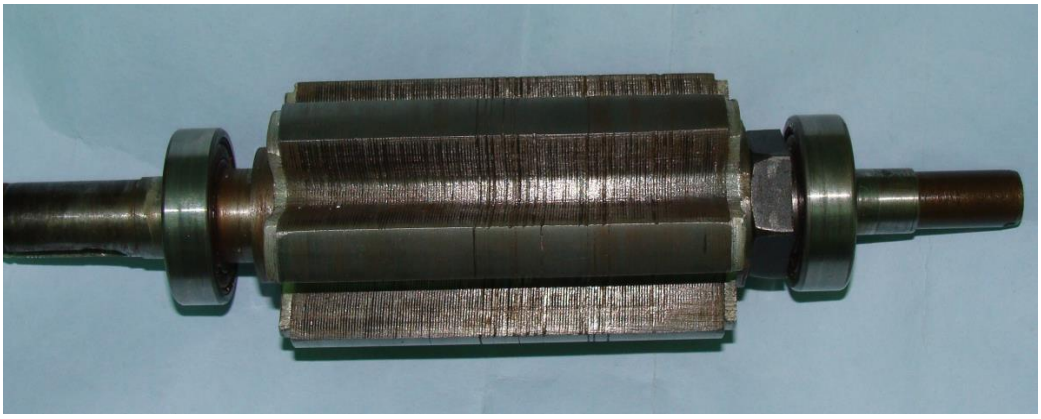

(b) 6-Pole Rotor

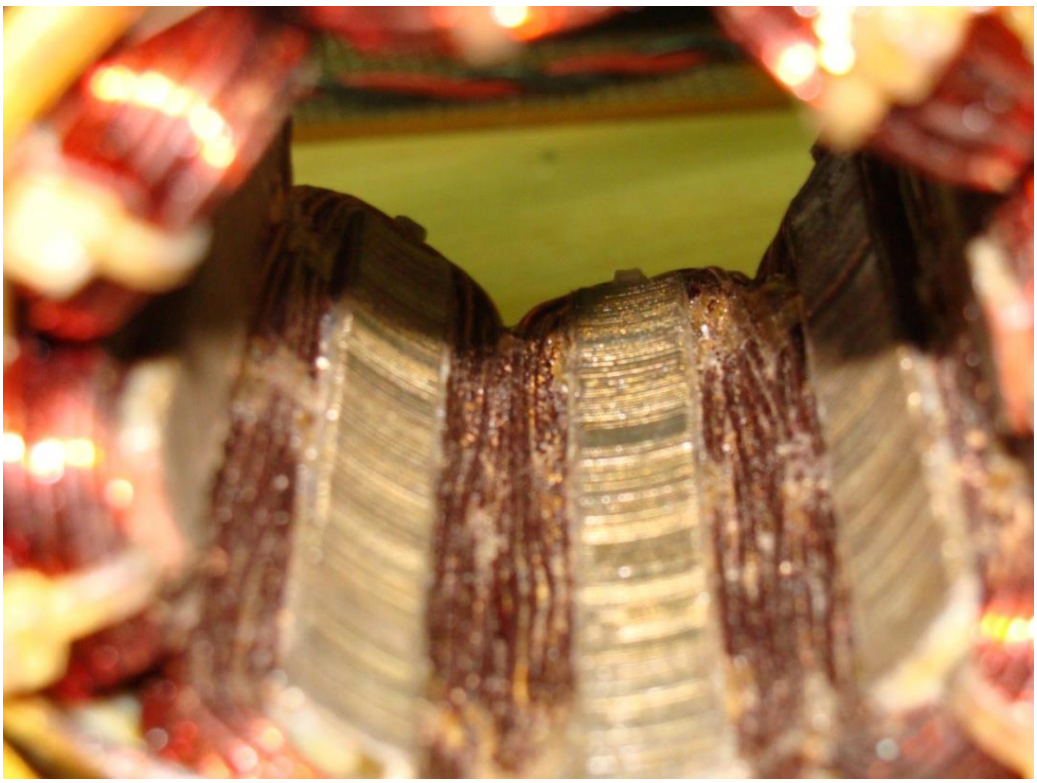

(c) Stator Inner View

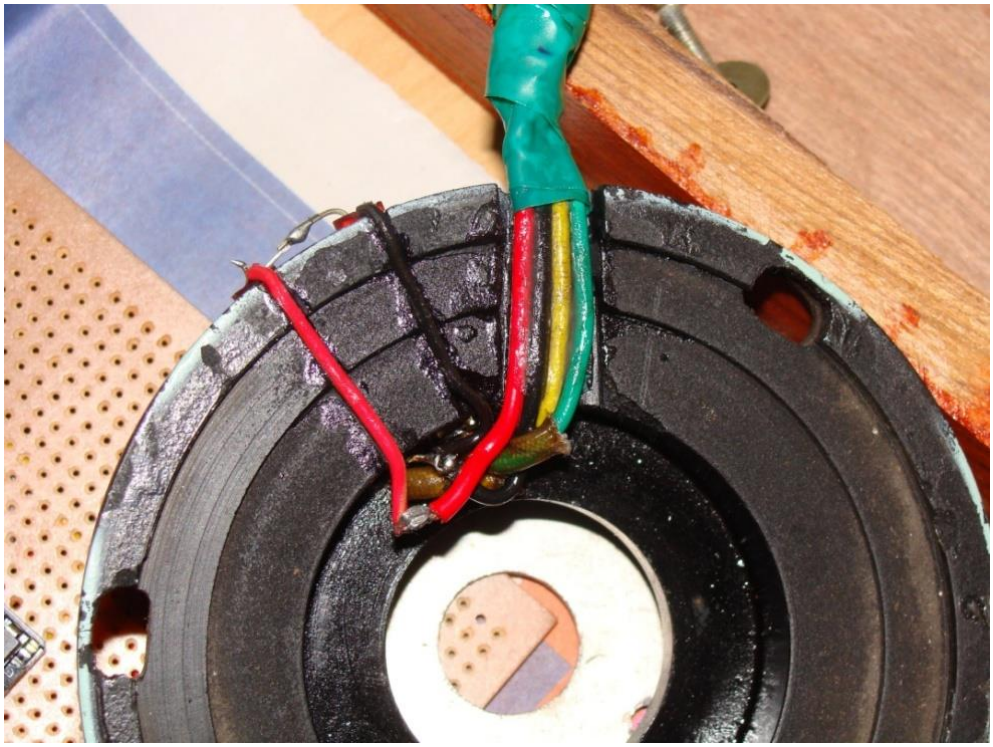

(d) Position Sensor Arrangements

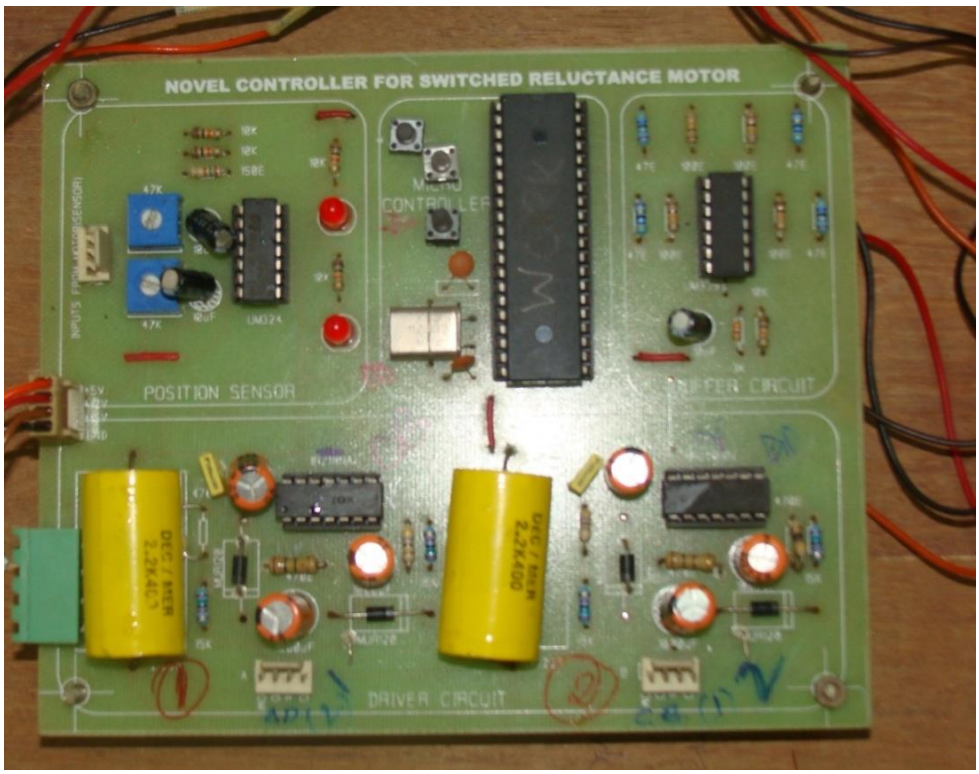

(e) Controller Circuit

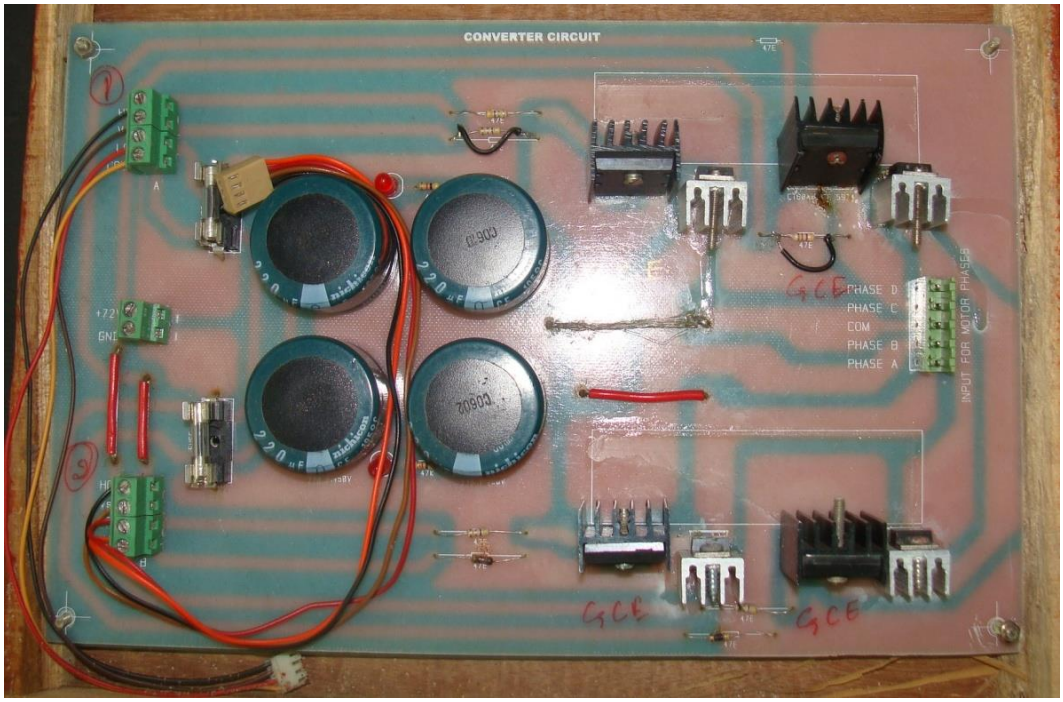

(f) Converter Circuit

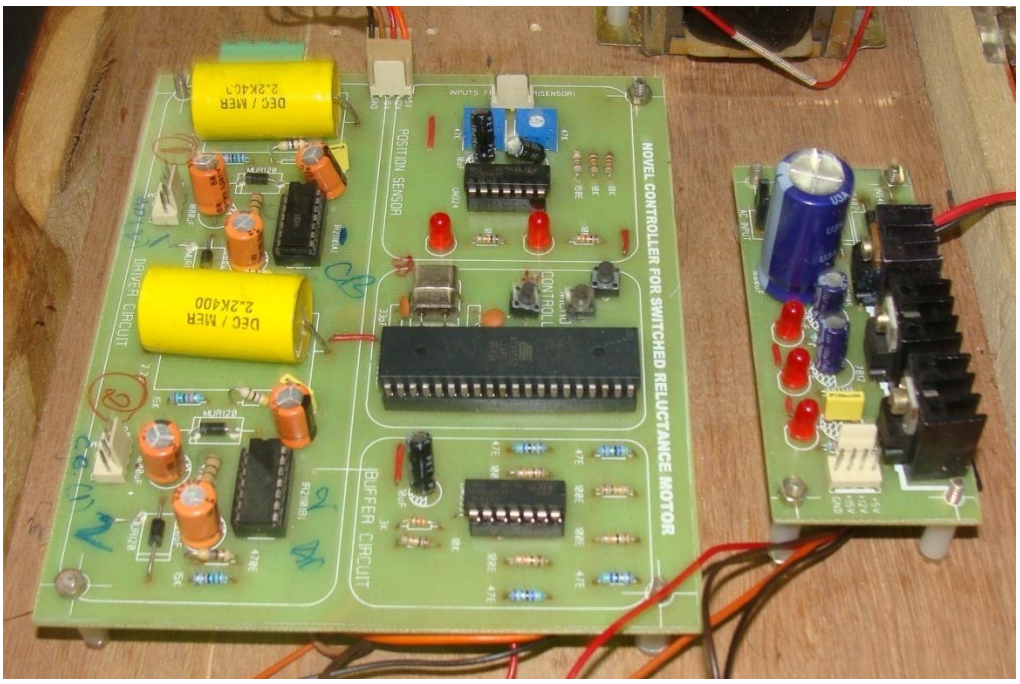

(g) Controller Board and Power Supply

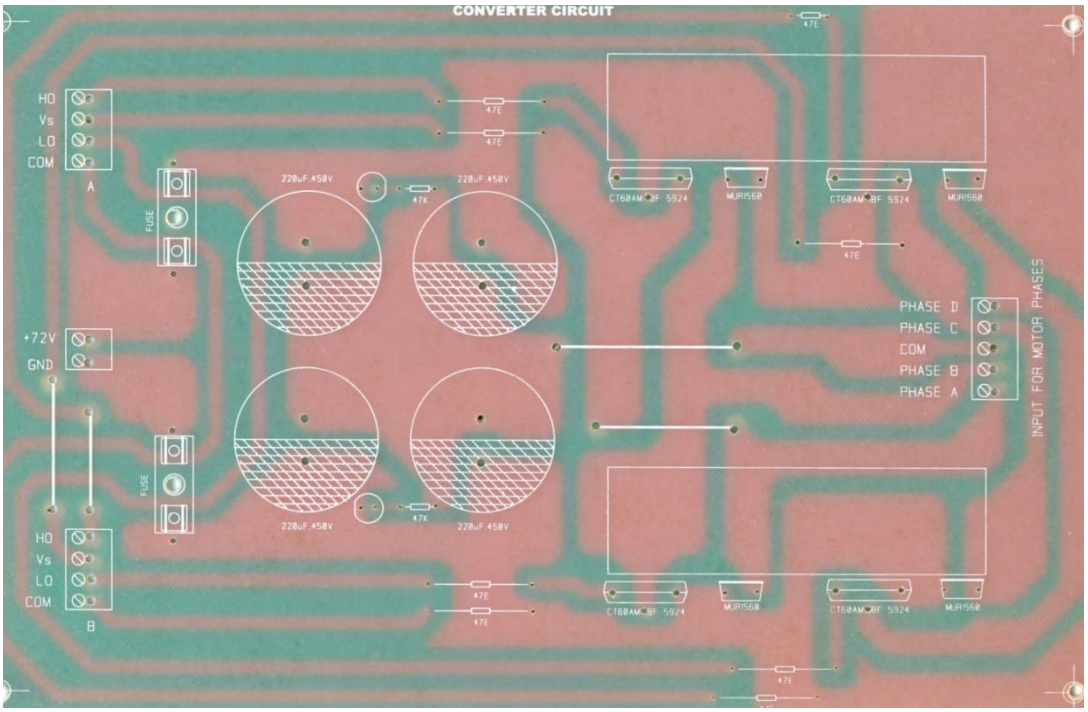

(h) Converter Circuit

Fig. 6.20 (a)-(h) Complete Hard ware

6.7 Testing of SRM Drive System

The hardware consisting of position sensing circuit, control circuit and gate drive circuit are tested individually using linear lamp load and inductive load prior to using SRM. After successful testing with linear load and inductive loads, first the SRM position sensor circuit is tested for getting appropriate logic four different states. There after the unit was tested with different DC supply from 12 to 72V with SRM as load and the response is experimentally recorded evaluating the performance of the drive. The testing is repeated for different operating conditions such as starting, starting in either direction, speed reversal and variable speed response. Experimental results are recorded to evaluate the performance of the drive. These are discussed in the next section. Before explaining the drive operation for different operating conditions, the generation of firing pulses for Phase A & C and Phase B & C in clock wise for different speeds are shown in Fig.6.21(a),6.21(b) and 6.21 (c)

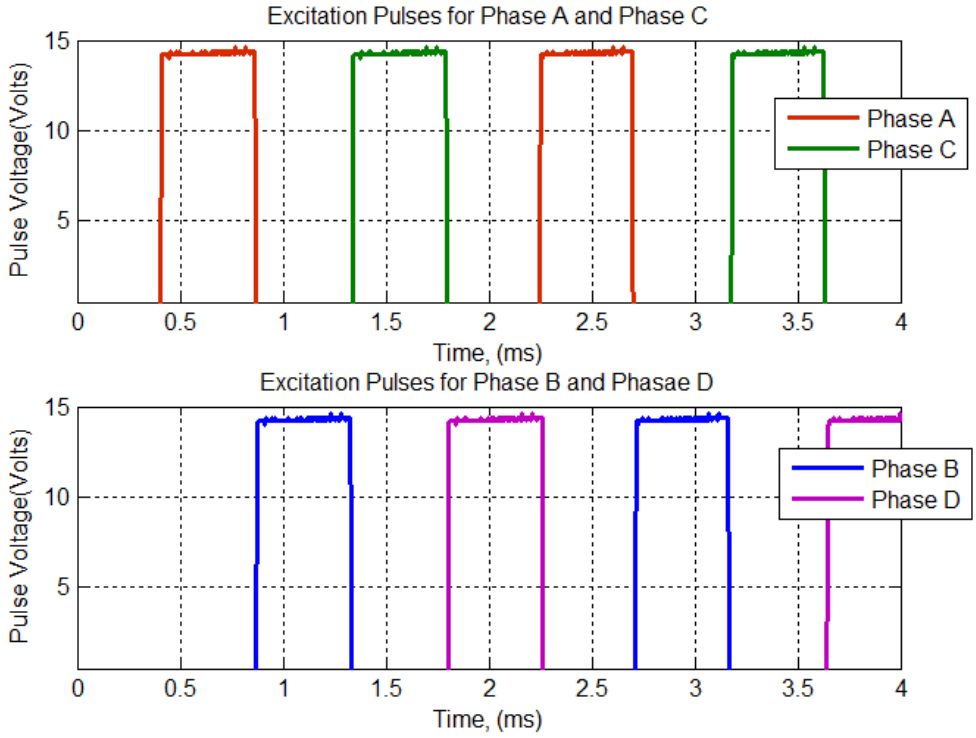

Fig.6.21 (a) Firing pulses for phase A & C, Phase B& D in Clock -Wise direction Speed=7500 RPM

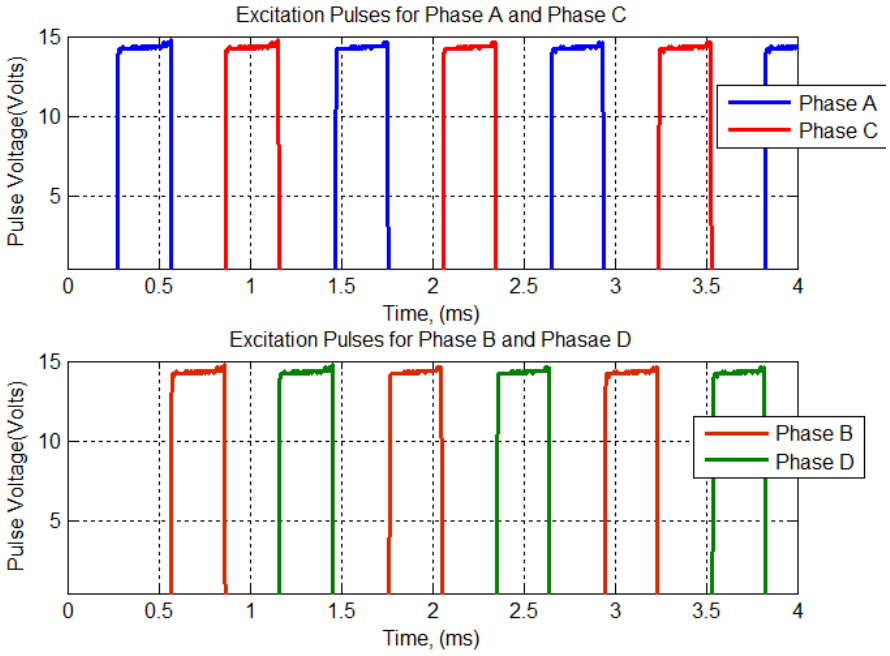

Fig.6.21 (b) Firing pulses for phase A &C , Phase B& D in Clock -Wise direction Speed=8500 RPM

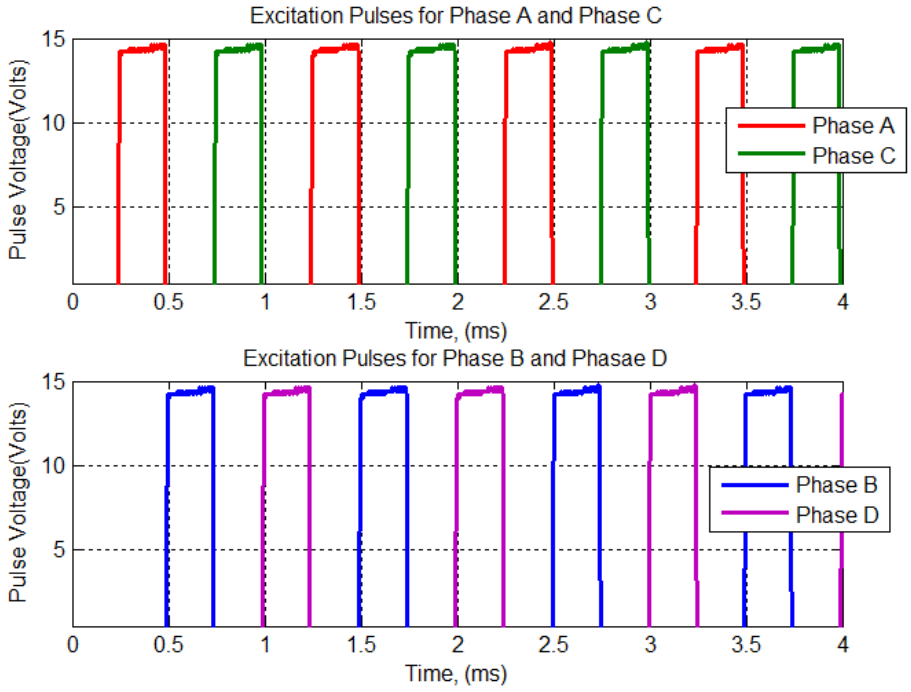

Fig.6.21 (c) Firing pulses for phase A& C, phase B & D in Clock -Wise direction Speed=10500 RPM

6.8 Test Results and Discussions

The excitation pulse for a particular phase is decided from the information received from position sensors. The IR position sensor continuously monitors the rotor position with respect to the arrangement of IR receiving sensors on the stator pole surface and gives the signals to micro-controller I/ O port which generate necessary gating signals. As per the algorithm, some other I/O ports to feed to the driver circuit comprising of OP-Amp to excite the correct phase accordingly through IGBT'S gate switching .The steady state current recording of all phases (Phase A&C and Phase B & C) for different speeds are shown in Fig. 6.22 (a) and Fig. 6.22 (b), when the motor is running in clock wise direction. Fig.6.22 (c) shows the voltage across and current through Phase A in clock -wise direction with V=68Voltsv at 10500 RPM and 6.21 (d) shows the voltage across and current through Phase D in Clock -Wise direction with V=68 volts and speed=10500 RPM and Fig 6.22 (e) shows the voltage across input capacitor in clock -wise direction with V=48 Volts and speed=8500 RPM.

6.8.1 Variable Speed Response

The motor is started initially with a voltage of 24 Volts. The motor attained nearly an initial speed of 7500 RPM in 3 sec. The no load current under steady state condition is observed to be 0.5 A (Average). The speed of the motor can be controlled by controlling the magnitude of input voltage. Different speeds can be obtained with different voltages and speed of the motor can be varied in either directions. Fig.6.23(a) and Fig.6.23 (b) shows the performance curves in anti-clock wise direction. From the experimental results it is observed that for an input voltage of 72V the voltage across the capacitor is not exceeding more than 40Volt. Fig. 6.24 shows the input voltage and the speed response under no load conditions

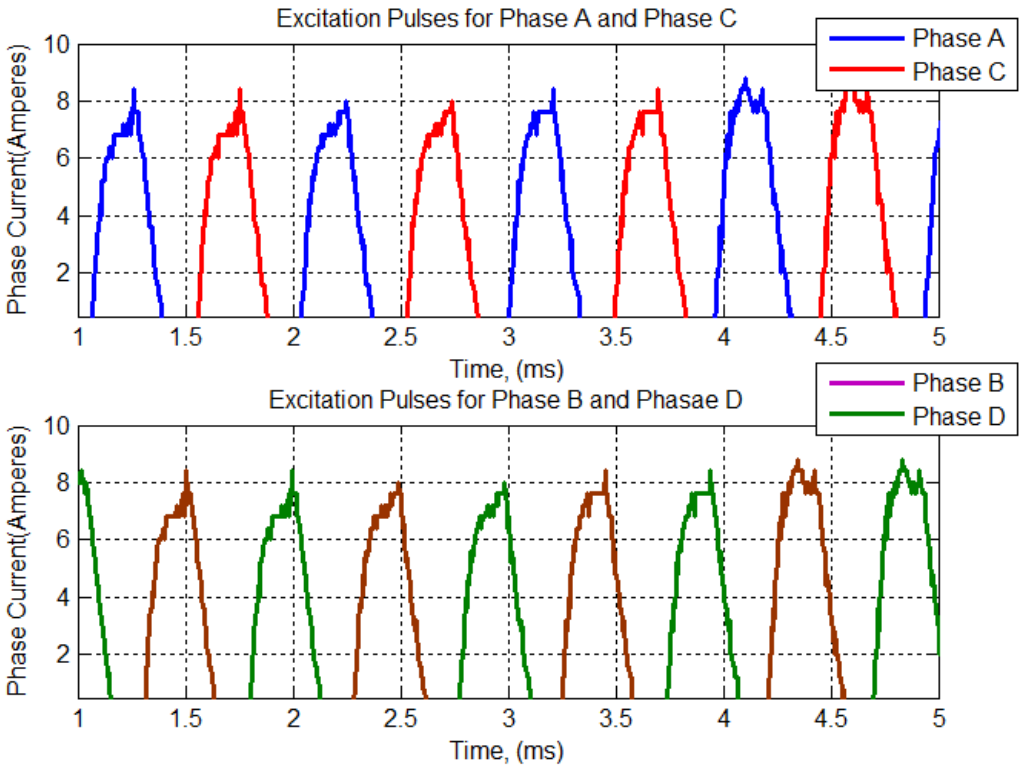

Fig.6.22 (a) Steady State Currents of Phase A & C and Phase B & D in Clock wise direction at 10500 RPM, V=68Volts

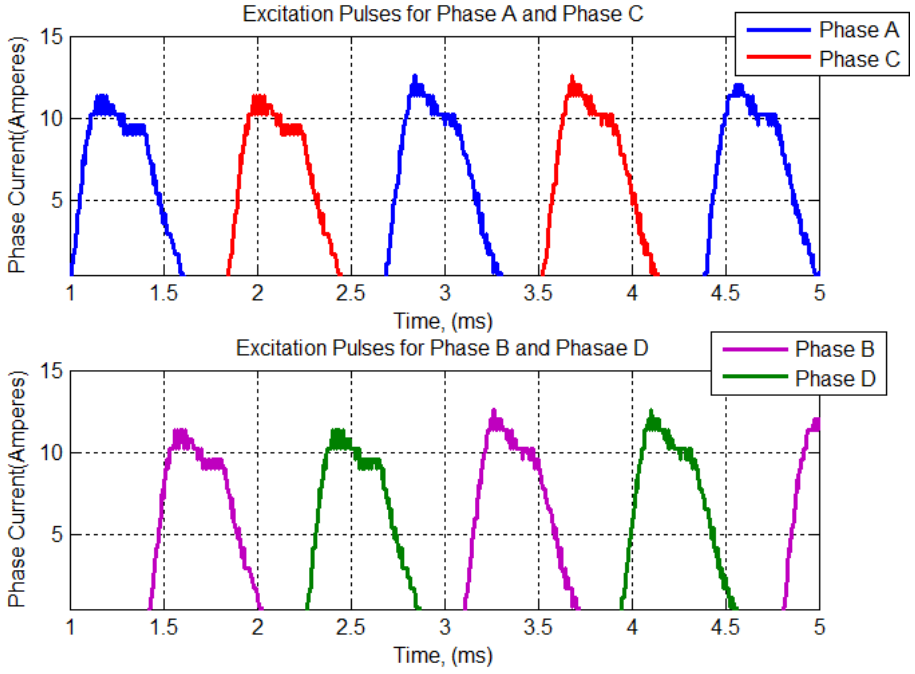

Fig.6.22 (b) Steady State Currents of Phase A and Phase C in Clock wise directions at 7500 RPM,V=24Volts

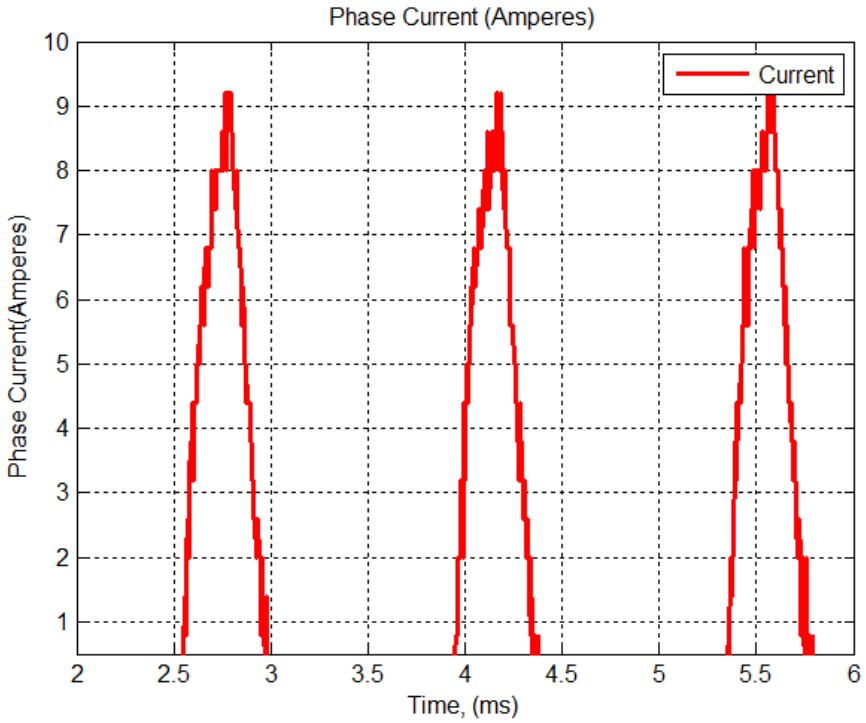

Fig.6.22 (c) Current through Phase A in Clock -Wise direction
V=48 Volts, Speed=8500 RPM

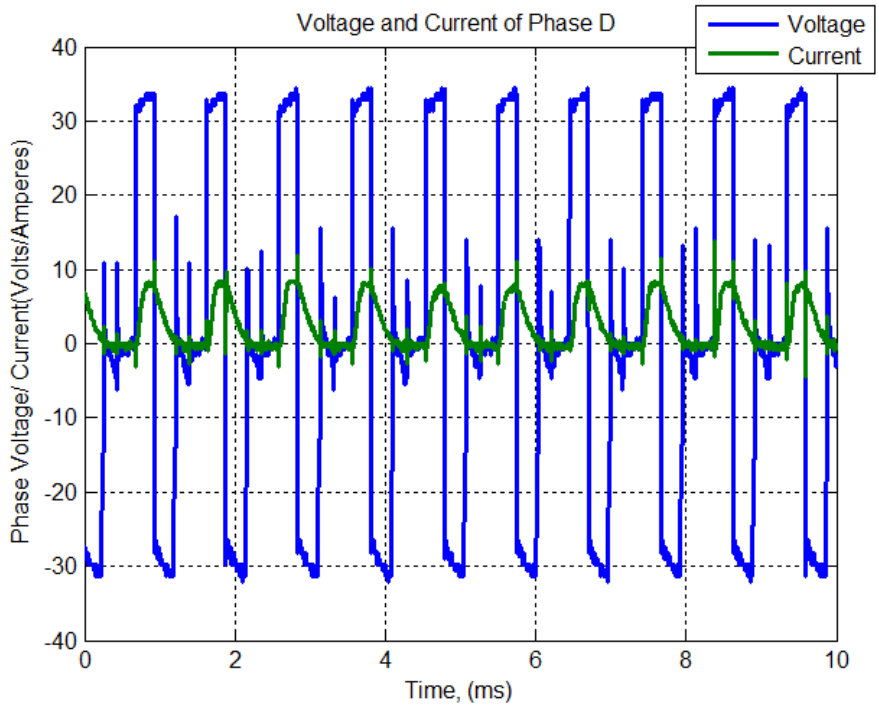

Fig.6.22 (d) Voltage across and current through Phase D in Clock -Wise direction
V=68 Volts, Speed=10500 RPM

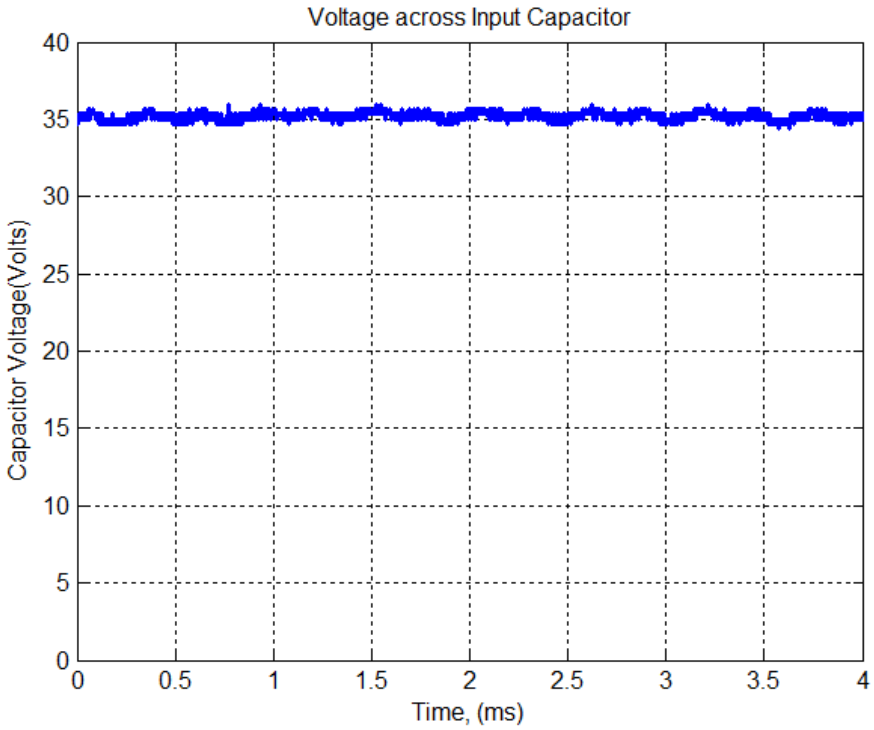

Fig.6.22 (e) Voltage across input capacitor in Clock -Wise direction
V=48 Volts, Speed=8500 RPM

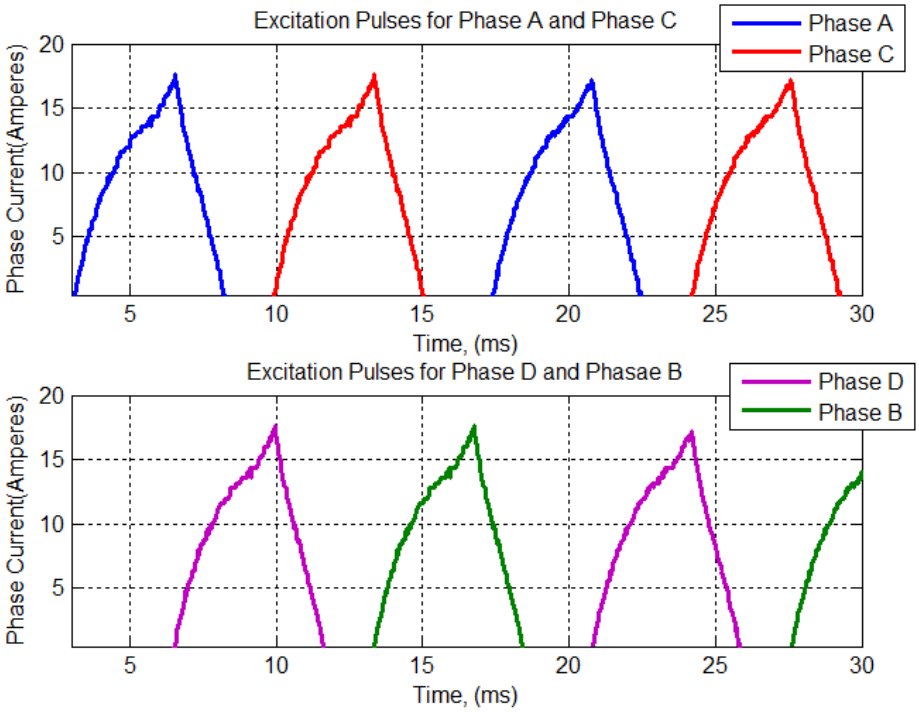

Fig.6.23 (a) Currents in all phases in Anti Clock -Wise direction
Speed=1500RPM

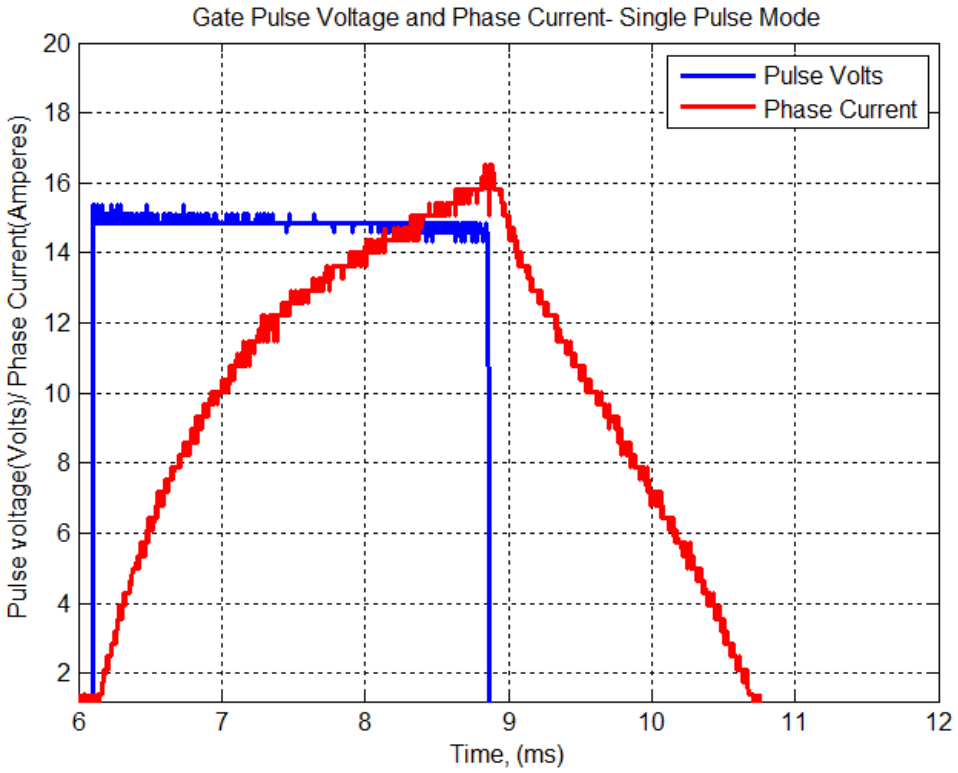

Fig.6.23 (b) Gate Pulse Voltage and Phase Current of phase "A" in Anti Clock wise direction at 2000 RPM

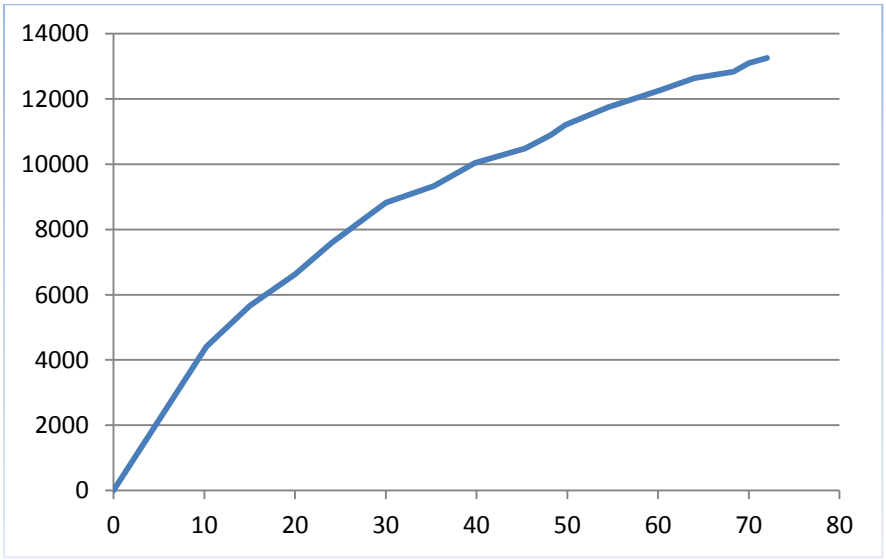

Fig.6.24 Speed versus Input Voltage

Table 6.4 Input Voltage Versus Speed (RPM)

Input Voltage(Volts)	Speed (RPM)
12	4700
24	7500
36	9300
48	8500
60	12200
72	13256

The raising characteristics of the speed curve show that, the drive can be suitable for automobile application and also for low cost application such as washing machines and other high speed application

6.9 Conclusions

This chapter presents a new approach of finding the rotor position of an SRM based on motor construction symmetry with minimum number of sensors and a simple micro-controlled based controller for control of switched reluctance motor in both the directions.

Motor offer maintenance free robust performance with low manufacturing cost and low material cost. Rotor inertia is very low because of salient pole type construction lead to low weight and small size compare to conventional AC and DC motor. Stator is simple to winding; end turns are short and robust and have no phase-phase crossovers support low cast easy manufacturing steps and also easy to repair. In most applications the bulk of the losses appear on the stator which is relatively easier to cool. Because there is no any costly permanent magnet on rotor permissible rotor temperature is high compare to permanent magnet motor in cost effective way. Motor provide higher torque compare to commutator motor and induction motor at all speed. Furthermore starting torque can be very high without the problem of excessive inrush currents and extremely high speed is possible. Motor is fully resistant to environment contrast to the permanent magnet motor.

SRM converter adds to the benefits, since they do not need a bipolar (reversed) device because torque is independent of direction of current. One switched per phase IGBT converter is cost effective compare to inverter particularly for brushless permanent magnet machines. It offers fault tolerant operation with one or more faulty phase or even with shorted IGBT. It is found experimentally that with one phase open motor is running with 80% of its full capacity and with one IGBT shorted motor is running with less efficiency and capacity because one phase is always remains on irrelative of rotor position which generate negative torque and required more starting current.

Furthermore digital controller and IGBT driver add to the benefit of low cost in simplest way. IGBT driver circuit required only three isolated power supply while mostly used asymmetric bridge converter of SRM requires five. Body mounted infrared positioning scheme add the benefits of cost with compare to costly encoders with reliable performance with CMOS and TTL logics for very high speed performance.

The controller is capable of implementing voltage-fed and current fed operation during high speed and low speed region respectively. The hardware developed for starting and speed control of SRM is implementation and cost of the designed controller is less than 1500 Indian rupees. The results demonstrate that the motor works satisfactorily over a wide range of speed and operating conditions. Experimental results validate the practical design of controller and prove the attractive features of such a control for industrial applications. The split dc converter is found to be more attractive when compared to R-dump or any other inverters. Based on the experimental results, it can be concluded that the proposed controller is suitable for low cost applications and high speed applications. Result dictates that the cost versus performance ratio of the proposed SRM drive is quite low.

Chapter 7 Conclusions and Future Work

The major contributions of this thesis are summarized as follows.

- This thesis covers the design procedure of an 8/6 SRM for automobile from the first principles and basic output equation. Extensive background knowledge of switched reluctance motors is not required to use the design procedure outlined. Certain references such as (Krishnan 2001) do have a design procedure outlined but this does require a lot of background knowledge to implement. The procedure outlined in this thesis requires only basic dimension data for Switched Reluctance motor.
- Since it is difficult to accurately incorporate the saturation effect and the detailed geometrical information in the empirical formulas, the finite element method was used for fine-tuning and validating the design. Torque characteristics, flux and flux linkages of SRMs are calculated by FEM for various stator current excitations and rotor position angles. Inductance of a stator winding was also evaluated by FEM. Incorporating the FEM-calculated parameters and the analytical model enables the study into the dynamic performance of an SRM under the converter control
- Based on this methodological approach an 8/6 4-phase 1kW SRM prototype is designed and fabricated.
- The procedure for calculating the flux linkages and inductances analytically for various rotor positions has been discussed in detail. The selection of the various flux tracks and their areas are intuitive with many approximations. The results do show some variation when compared with the finite element analysis. Better accuracy can probably be achieved by defining more regions of variations but is not required. This procedure has been described in (Krishnan 2001).
- The analytical calculation of the unaligned inductance in this chapter follows the basic principles of electromagnetic and does not rely on any previous sources whose documentation is hard to verify.
- The design verification using analytical procedure and experimental methods are also explained in detail. The experimental setup for determining the motor winding inductance at different rotor positions is discussed in detailed.

Moreover, it is observed that verification of the design either using analytical procedure or experimental method gave slightly similar results.

- Different measurement techniques of flux-linkage characteristics have been described (Krishnan, R. (2001)) in this chapter. A simplified experimental set for the determination of flux linkage characteristics of SR motor has been presented.This method involves in applying a step voltage application to one SRM phase and the rate of rise of current is measured. The new 3-D FEM analysis is carried out prove the correctness of the methodology. The experimental results values matches with the ANSOFT 3-D FEM Method.
- The SRM drive circuits have been critically reviewed in this thesis. These converter configurations was first described in literature in (Krishnan 2001) Comparison of the most common drive circuit's topologies has been held showing the major advantages and disadvantages of each topology together with its major field of applications. The most widely acceptable converter for SRM is the asymmetric bridge design. But this majorly suffers from the disadvantage that, it requires more number of switching devices, which will increases the converter cost and overall cost and also the complexity of the converter circuit.

The other converter such as split DC topology provides fast suppression of the tail current in the phase winding and hence resulting in minimization of negative torque using doubly boosted voltage in the demagnetizing mode. This topology has higher efficiency and more output power than the other counterpart in the heavy load conditions and in high speed operations. From this topology we can use more positive torque region and enable to get more power from it. It has advantage over asymmetric bridge converter in the viewpoint of efficiency and output power varying the load and dwell angle. The simplicity and reduced count with compact packing of the topology makes make it an attractive low-cost for many variable speed drives application; hence in the present thesis a split dc converter is used along with SRM for designing and testing a novel controller circuit. The different modes of operation are described in detail along with the various advantages and disadvantages

- The SRM drive consists of a power converter section that sequentially connects the motor phases independently and a control section that processes rotor position information form a position sensor and generates the phase excitation pulses. A new method to estimate the initial rotor position of the SRM at stand still and during running condition is proposed without the need of magnetisation curves. A pair of position sensors is used to detect the rotor positions and the output signals of the sensors are used as the basic triggering pulses for main switches.
- The proposed method was implemented by the simple microcontroller based novel controller. The controller has been tested under different conditions and some of the experimental results have been included. The proposed method is implemented with the 8/6, 1 kW 4-ph prototype SRM. This is a major contribution of the dissertation
- A known sensorless method of finding the rotor position is used to validate the correctness of the proposed method.

Chapter 7 Conclusions and Future Work

The future work following this thesis could be outlined as follows:

- Researches about SRM's noise generation and noise reducing are very complex and require a lot of mechanical investigations. That would go beyond the scope of this thesis.
- Future researches will deal with the measurement of core losses and copper losses for SRM prototype and acoustic noise reduction and thermal problems.

A. Consoli, A. Testa, N. Aiello, F. Gennaro, and M. Lo Presti (2001) ‘ Unipolar converter for switched reluctance motor drives with power factor Improvement’, Sixteenth annual IEEE applied power electronics conference and exposition, Vol. 2,pp .1102-1108

A. Cheok and N. Ertugrul (1995) ‘ Sensorless rotor position detection techniques in switched reluctance motor drives’, in Proc. Australasian Universities Power Eng. Conf., Perth, Australia, pp. 27–29

Acarnley, P. P. ,R. J. Hill, and C. W. Hooper (1985) ‘ Detection of rotor position in stepping and switched reluctance motors by monitoring of current waveforms’, IEEE Trans. Industrial Electronics, Vol. IE-32, No. 3, pp. 215-222.

A. D. Cheok, and Z. Wang (2005), ‘Fuzzy Logic Rotor Position Estimation Based Switched Reluctance Motor DSP Drive With Accuracy Enhancement’, IEEE Trans. on Power Electronics, vol. 20, no. 4, pp. 908-921

Ahn, J.W., Park, S.J., and Lee, D.H (2004) ‘Hybrid excitation of SRM for reduction of vibration and acoustic noise’, IEEE Trans. Ind. Electron., 51, (2), pp. 374–380

Arumugam, R., Lowther, D.A., Krishnan, R. and Lindsay, J.F.(1985) ‘Magnetic field analysis of switched reluctance motor using 2-dimensional finite element model’, IEEE Transactions on Magnetics, Vol. MAG-21, No. 5, pp. 1883-1885.

Arthur V. Radun (1985) ‘Design Considerations for the Switched Reluctance Motor’, IEEE Transactions on Industrial Applications’, Vol. 31, No. 5, pp .1079-1087.

Ansoft Maxwell User Manual

A. R. Miles (1991) ‘Design of A 5MW, 900V Switched Reluctance Motor’, IEEE Transactions on Energy Conversion, Vol. 6, No. 3, pp .484-491.

Bellini, A., Filippetti, F., Franceschini, G., Tassoni, C. & Vas, P. (1998) ' Position sensorless control of a SRM drive using ANN techniques' , Conf. Rec. IEEE Ind. Appl. Soc., pp. 709-714

B. Ge, X. Wang, P. Su, and J. Jiang (2002) 'Nonlinear internal-model control for switched reluctance drives', IEEE Trans. on Power Electronics, vol. 17, no. 3, pp. 379–388

B. K. Bose, T. J. E. Miller, P. M. Szczesny and W. H. Bicknell (1986) ' Microcomputer control of switched reluctance motor', IEEE Transactions on Industrial Applications, Vol. IA-22, No. 4, pp. 708-715.

Blaabjerg, F., and Pedersen, J.K (1993) 'Digital implemented random modulation strategies for AC and switched reluctance drives', Proc. IEEE IECON Conf., Vol. 2, pp. 676–682

Boukhobza, T., Gabsi, M., and Grioni, B (2001) ' Random variation of control angles, reduction of SRM vibrations' , Proc. IEEE IEMD Conf., Vol. 3, pp. 640–643

Cameron, D.E., Lang, J.H., and Umans, S.D (1992) ' The origin and reduction of acoustic noise in doubly salient variable-reluctance motors', IEEE Trans. Ind. Appl , 28, (1), pp. 1250–1255

Cailleux, H., Pioufle, B.L., Multon, B., and Sol, C (1993) 'A precise analysis of the phase commutation for the torque nonlinear control of a switched reluctance motor – torque ripples minimization' , Proc. IEEE IECON Conf., Vol. 3, pp. 1985–1990

Cai, W., Pillay, P., Tang, Z., and Omekanda, A (2001) ' Experimental study of vibrations in the switched reluctance motor', Proc. IEEE IEMD Conf., Vol. 1, pp. 576–581

Chapman, P.L., and Sudhoff, S.D.(2001) 'Optimized waveform control for an 8/6 switched reluctance motor drive' , Proc. IEEE APEC Conf., Vol. 2, pp. 1096–1102

Colby, R.S., Mottier, F.M., and Miller, T.J.E (1996) 'Vibration modes and acoustic noise in a four-phase switched reluctance motor', IEEE Trans. Ind. Appl.,32, (2), pp. 1357–1364.

Corda, J. and Stephenson, J.M. (1979) 'An Analytical Estimation of the Minimum and Maximum Inductances of a Double-Salient Motor', Proc. of the International Conf. On Stepping Motors and Systems, pp. 50-59.

David A. Torrey (2002) 'Switched reluctance generators and their control', IEEE Transactions on Industrial Electronics, Vol.49, No. 1, pp. 3-14

Do-Hyun Jang (2001) 'The Converter Topology with Half-Bridge Inverter for Switched Reluctance Motor Drives', IEEE International Symposium on Industrial Electronics Proceedings, Vol. 2,pp. 1387-1392

Ehsani, M., Husain, I., Mahajan, S. & Ramani, K. R. (1994) ' New modulation techniques for rotor position sensing in switched reluctance motors', IEEE Trans. on Industry Applications, Vol. 30, No. 1, pp. 85-91

Ehsani, M., Husain, I., and Kulkarni, A. B. (1992) ' Elimination of discrete position sensor and current sensor in switched reluctance motor drives', IEEE Transactions on Industry Applications, Vol 28, No.1, pp. 128-135.

Ehsani, M., Husain, I., & Ramani, K. R. (1991) ' An analysis of the error in indirect rotor position sensing ofswitched reluctance motors', Industrial Electronics, Control and Instrumentation, Proceedings IECON '91, pp. 295- 300

Ehsani, M., and Ramani, K. R. (1996) 'Direct control strategies based on sensing inductance in switched reluctance motors', IEEE Transactions on Power Electronics, Vol .11,No.1, pp.74-82

Fahimi, B., Suresh, G., Rahman, K.M., and Ehsani, M (1998) 'Mitigation of acoustic noise and vibration in switched reluctance motor drive using neural network based current profiling' , Proc. IEEE IAS Conf., Vol. 1, pp. 715–722

Ferrero A., Raciti A (1990) 'A Digital Method for Determination of Magnetic Characteristic of Variable Reluctance Motor', IEEE Transactions on Instrumentation & Measurement. Vol.39. No.4, pp. 604-608

Gabsi, M., Camus, F., Loyau, T., and Barbry, J.L (1999) 'Noise reduction of switched reluctance machine', Proc. IEEE IEMD Conf.,pp. 263–265

G.S,Buja, M.I.Valla (1994) ' Control characteristics of the SRM drives. Part II: operation in the saturated region', IEEE Transactions on Industrial Electronics, Vol.41, No. 3, pp. 316-325

Gallegos-Lopez, P. C. Kjaer, and T. J. E. Miller (1999) 'High-grade position estimation for SRM drives using flux linkage/current correction model', IEEE Trans. Ind. Applications., vol. 35, pp. 859–869

Ha, K.H., Kim, Y.K., Lee, G.H., and Hong, J.P (2004) 'Vibration reduction of switched reluctance motor by experimental transfer function and response surface methodology', IEEE Trans. Ind. Electron., 40, (2), pp. 577–580

Harris, W. D., and Lang, J. H. (1990) 'A simple motion estimator for variable-reluctance motors', IEEE Transactions on Industry Applications , Vol 26, No .2, pp. 237-243

Hong-Je Ryoo, Won-Ho Kim, Geun- Hie Rim, Wook Kang, Ji-Ho Park and Ching-Yuen Won (1998) 'A new split source type converter for SRM drive', 29th annual IEEE power electronics specialists conference, record, Vol.2 pp.1290-1294

H.Gao, F.R. Salmasi., and M. Ehsani (2001) 'Sensorless control of SRM at standstill", Applied Power Electronics Conference and Exposition', Sixteenth Annual IEEE, vol. 2

Husain, I., and Ehsani, M. (1994) 'Rotor position sensing in switched reluctance motor drives by measuring mutually induced voltages', IEEE Transactions on Industry Applications, Vol 30, No. 3, pp. 665-672

Im, Y.C., Kim, K.H., Na, S.H., Kim, H.D., and An, J.H (1998) 'Reduce acoustic noise in SRM using RPWM', Proc. Annual KIPE Conf., Korea, pp. 189–192

J. Corda and J. M. Stephenson (1979) 'Analytical estimation of the minimum and maximum inductances of a double-salient motor', Proc. Inf. Conf. on Stemming Motors and Systems, keds, England, pp. 50-59.

J. W. Finch, M. R. Harris, A. Musoke, and H. M. B. Metwally (1984) 'Variable speed drives using multi-tooth per pole switched reluctance motors', Proc. Thirteenth Ann. Symp. on Incremental Motion Control Systems and Devices, pp. 293-301.

J. Faiz and J.W. Finch (1993) 'Aspects of design optimisation for switched reluctance motors', IEEE Trans. on Energy Conversion, Vol. 8,No. 4, pp.704-13.

Krishnan, R., Arumugam, R., Lindsay, F.F (1998) 'Design Procedure for Switched-Reluctance Motors', IEEE Transactions on Industry Applications, Vol.24, No. 3

Krishnan, R. (2001) 'Switched Reluctance Motor Drives: Modeling, Simulation, Analysis, Design, and Applications', CRC Press.

Krishnan, R. and Materu, P.N. (1993) 'Analysis and Design of a Low-Cost Converter for Switched Reluctance Motor Drives', IEEE Transactions on Industry Applications, vol. 29, No. 2, pp. 320-327.

Krishnan, R. and Materu, P.N. (1990) 'Design of a Single-Switch-per-Phase Converter for Switched Reluctance Motor Drives', IEEE Transactions on Industrial Electronics, vol. 37, No. 6, pp. 469-476.

Krishnan, R., and Vijayraghavan, P (1998), 'State of the art: acoustic noise in switched reluctance motor drives'. Proc. IEEE IECON Conf., Vol. 2, pp. 929–934

Krishnan, R. (2001) 'Electric motor drives: modeling, analysis, and control', Prentice Hall.

Krishnan, R., and Vijayraghavan, P (1998) 'State of the art: acoustic noise in switched reluctance motor drives' , Proc. IEEE IECON Conf., Vol. 2, pp. 929–934

Lawrenson, P.J., Stephenson, J.M., Blenkinsop, P.T., Corda, J. and Fulton, N.N (1980) 'Variable-speed Switched Reluctance Motors', Proc. IEE Vol. 127, Pt B, No. 4, pp. 253-265.

L. Chang, G.E. Dawson and A. R. Eastham (1994) 'Finite element analysis of electric machines: Post-processing methods', Int. J. of Applied Electro-magnetic in Materials, NOS, pp.321-330.

L. Chen and Y. Zhou (1993) 'Design formulas and methods of the switched reluctance motor', J of Xi' An Jiaotong University, Vol. 27,110.6, pp.57-64

Lumsdaine, A, and Lang, J. H. (1990) 'State observers for variable-reluctance motors', IEEE Transactions on Industrial Electronics, Vol. 37, No. 2. pp 132-144.

Lovatt, H.C., and Stephenson, J.M. (1997) 'Computer-optimised smooth torque current waveforms for switched-reluctance motors', IEE Proc., Electr. Power Appl., 144, (5), pp. 310–316

Lumsdaine, A. and J. H. Lang (1990) 'State observers for variable reluctance motors', IEEE Trans. Ind. Elect., Vol. IE-37, no. 2, pp. 133-142.

Lyons, J. P., MacMinn, S. R. & Preston, M. A (1999) 'Flux/current methods for SRM rotor position estimation', IEEE – IAS Conference Record of the 1999, pp. 482-487

Lyons, J. P., MacMinn, S. R. & Preston, M. A. (1991) 'Rotor position estimator for a switched reluctance machine using a lumped parameter flux/current model', US patent # 5107195.

Lovatt, H.C., and Stephenson, J.M (1997) 'Computer-optimised smooth torque current waveforms for switched-reluctance motors', IEE Proc. Electr. Power Appl., 144,(5), pp. 310- 316

MacMinn, S. R., Rzesos, W. J., Szczesny, P. M., and Jahns, T. M. (1992) 'Application of sensor integration techniques to switched reluctance motor drives', IEEE Transactions on Industry Applications, Vol 28, No. 6, pp. 1339-1344

Matlab and Simulink User Manual (2003)

M. Ehsani, I. Husain, S. Mahajan, and K. R. Ramani (1994) 'New modulation encoding techniques for indirect rotor position sensing in switched reluctance motors', IEEE Trans. Ind. Applicat., Vol. 30, pp. 85–91.

Mese, E. & Torrey, D. A. (1997) 'Sensorless position estimation for VR machine using artificial neural networks. Conf. Rec', IEEE Ind. Appl. Soc., pp. 540-547

Michaelides, A., and Pollock, C (1996) 'Reduction of noise and vibration in switched reluctance motors: new aspects', IEEE Rec. IAS, Vol. 2, pp. 771–778.

Miller, T.J.E (1993) 'Switched Reluctance Motors and their Control', Magna Physics Publishing and Clarendon Press

Miller, T.J.E., McGilp, M. (1990) 'Nonlinear theory of the switched reluctance motor for rapid computer-aided design', IEE Proceedings, Vol. 137, Pt. B, No. 6, pp. 337-347

Miller, T.J.E (2002) 'Optimal design of switched reluctance motors', IEEE Trans. Ind. Electron., Vol. 49, (1), pp. 15–27

Mvungi, N.H. and Stephenson, J.M (1991) 'Accurate sensor less rotor position detection in an SR motor', EPE Conf. Proc.,Vol. I, pp. 390-393.

N.N. Fulton and J.M. Stephenson (1988) 'A review of switched reluctance motor design', Proc. of Int. Conf. OB Elec. Machines (ICEM), Pica, Vol. 1, pp. 423-28

Omekanda, A.M., C. Broche and M. Renglet (1997) 'Calculation of the Electromagnetic Parameters of a Switched Reluctance Motor Using an Improved FEM-BIEM-Application to Different Models for the Torque Calculation', IEEE Trans. Ind. Appl., Vol. 33, No.4, pp. 914-918

Panda, S.K., and Amaratunga, G.A.J (1991) ' Analysis of the waveform detection technique for indirect rotor position sensing of switched reluctance motor drives', IEEE Trans. on Energy Conversion, Vol. 6, No. 3, pp. 476-483

Panda, S. K. & Amaratunga, G. A. J. (1993) ' Waveform detection techniques for indirect rotor position sensing of switched reluctance motor drives Part I Analysis and Part II Experimental Results', IEEE Proc., Vol. 140, No.1, pp. 80-96

Parreira, B., S. Rafael, A.J. Pires and P.J. Costa Branco (2005) 'Obtaining the Magnetic Characteristics of an 8/6 Switched Reluctance Machine: from FEM Analysis to the Experimental Tests', IEEE Trans. On Ind. Electronics, Vol. 52, No. 6 pp 1635 – 1643

P. Andrada, E. Martinez, J.I. Perat, J.A. Sanchez, M. Torrent (2000) 'Experimental determination of magnetization curves of switched reluctance motor', ICEM 2000, Espoo Finland, pp. 761-765

Perl, T., Husain, I. & Elbuluk, M. (1995) 'Design trends and trade-offs for sensorless operation of switched reluctance motor drives', Industry Applications Conference. Thirteenth IAS Annual Meeting, IAS '95, Conference Record of the 1995 IEEE Akron Univ., OH, USA, pp. 278-285

P. P. Acarnley, R. J. Hill, and C.W. Hooper (1985) 'Detection of rotor position in stepping and switched reluctance motors by monitoring of current waveforms', IEEE Trans. Ind. Electron., vol. IE-32, pp. 215–222

P. J. Lawrenson, J. M. Stephenson, P. T. Blenkinsop, J. Corda, and N. N. Fulton (1980) 'Variable-speed switched reluctance motors', IEE Proc., Vol. 127, pt. B, No. 4, pp. 253-265.

P.J. Lawrenson (1983) 'Switched Reluctance Motor Drives', Electronics and Power, pp.144-147

Pillay, P., and Cai, M 'An investigation into vibration in switched reluctance motors', IEEE Trans. Ind. Appl., 1999, 35, (3), pp. 589–596

P. Jitkreeyarn, S. Kachapornkul, P.Somsiri, K. Tungpimolrut (2007)' An Initial Rotor Position Estimation Method for Switched Reluctance Motor without Using Machine Parameter', Proc of Int. Conf. on Electrical Machines and Systems, pp. 1686- 1689

P. Lobato, A. J. Pires, J.A. Dente (2003) 'A new control strategy based on optimized smooth-torque current waveforms for switched reluctance motors', Electro motion, International Journal of Electromechanical Energy Converters, Actuators and Transducers, Vol.10, No.4, pp. 579-583

Pollock, C., and Wu, C.Y (1997) 'Acoustic noise cancellation techniques for switched reluctance drives', IEEE Trans. Ind. Appl., 33, (1), pp. 477–484

Radun, A. (1999) 'Analytical calculation of the switched reluctance motor's unaligned inductance', IEEE Transactions on Magnetics, Vol. MAG-35, No. 6, pp. 4473-4481

Radun, A. (2000) 'Analytically computing the flux linked by a switched reluctance motor phase when the stator and rotor poles overlap', IEEE Transactions on Magnetics, Vol. MAG-36, No. 4, pt. 2

Rahman M.F. et al (2002) ‘ Dynamic modeling of four phase 8/6 switched reluctance motor using current and torque look-up tables’, Proc. IEEE Industrial Electronics Society, Vol.1, No. 1, pp. 491-496

R. Belmans (1994) ‘Recent Major Developments in CAE and Vibrations and Audible Noise Analysis of Rotating Electrical Machines’, Leuven/Apeldoorn GARANT

R. Krishnan, R. Arumugam, James F. Lindsay (1988) ‘Design Procedure for Switched-Reluctance Motors’, IEEE Transaction on Industry Applications, Vol. 24, No. 3, pp. 456-461.

R. Krishnan and P.N. Materu (1993) ‘ Analysis and design of a low cost converter for switched reluctance motor drives’, IEEE transactions on industrial application, Vol.29,pp 320-327.

S.A. Nasar (1996) ‘DC Switched Reluctance Motor’, Proceedings of the Institution of Electrical Engineers, vol.166, no.6 pp.1048-1049

Sharma, V.K., Murthy, S.S., and Singh, B (1999) ‘An Improved Method for the Determination of Saturation Characteristics of Switched Reluctance Motors’, IEEE Transactions on Instrumentation and Measurement, Vol. 48, No. 5,pp. 995-1000

S.K Panda, and P.K Dash ‘Application of nonlinear control to switched reluctance motors: a feedback linearisation approach’, IEE Proceedings. Electr. Power Appl. Vol. 143, No. 5. pp. 371-379, September 1996.

S. K. Panda and P. K. Dash (1996), ‘Application of nonlinear control to switched reluctance motors: A feedback linearization approach’, IEE Proc.-Electric Power App, vo1. 43, no. 5, pp. 371–379

Stephenson, J.M., Hughes, A., and Mann, R.(2002) ‘Online torque-ripple minimization in a switched reluctance motor over a wide speed range’, IEE Proc., Electr. Power Appl. 149, (4), pp. 261–267.

Stephenson, J.M., Hughes, A., and Mann, R. (2001) 'Torque ripple minimization in a switched reluctance motor by optimum harmonic current injection', IEE Proc., Electr. Power Appl., 148, (4), pp. 322–328

T. J. E. Miller, M. I. McGilp, and M. Olaru (2000) 'Finite element applied to synchronous and switched reluctance motors,' in IEE Seminar on Current Trends in the Use of Finite Elements in Electromechanical Analysis and Design, , pp. 3/1–3/4.

T. S. Chuang, and C. Pollock (1997) 'Robust speed control of a switched reluctance vector drive using variable structure approach', IEEE Trans. on Industrial Electronics, vol. 44, no. 6, pp. 800–808

Vujicic, V., and Vukosavic, S.N. (2000) 'A simple nonlinear model of the switched reluctance motor', IEEE Transactions On Energy Conversion, Vol. 15, No. 4, pp. 395-400

V.Ramanarayanan, L.Venkatesha, and D.P.Panda (1996) 'Flux-linkage Characteristics of Switched Reluctance Motor', PEDES '96 Conf. Rec., pp 281- 285

Vukosavic, S., Stefanovic, V.R (1991) 'SRM inverter topologies: a comparative evaluation', IEEE Transactions on Industry Applications, vol. 27, no. 6.

Wang, Z., Cheok, A. D. & Wee, L. K. (2001) ' Sensorless rotor position estimation algorithm for switched reluctance motors using fuzzy logic', Proc. Power Electronics Specialist Conf., Vol. 3, Cairns, Austrialia, pp. 1701-1706

Xiang-Dang Xue, K. W. E. Cheng, and S. L. Ho (2002) ' Simulation of Switched Reluctance Motor Drives Using Two-Dimensional Bicubic Spline', IEEE Transactions on Energy Conversion, vol.17, no. 4, pp. 471-477

X. Kai, Z. ionghua, and L. Jianwu (2005) 'A New Simple Sensorless Control Method for Switched Reluctance Motor Drives ', ICEMS 2005. Proceedings of the Eighth International Conference on vol. 1

Zhang, Y., X. Wei, and E. Li (2004), ‘ Electromagnetic scattering from three-dimensional isotropic objects using hybrid finite element-boundary integral method’, Journal of Electromagnetic Waves and Applications, Vol. 18, No. 11, 1549- 1563.

Appendix -A

BIODATA

Mr. Abdul Ahad Shaik is in teaching profession for the last 12 years. He is a graduate in B. Tech (Electrical and Electronics Engineering) from Kakatiya University. A.P and Post Graduate in M. Tech (Power & Energy Systems) from National Institute of Technology Karnataka (NITK). His fields of Interests are Electrical Circuits, Electrical Machines, Power Electronics and Electric Drives, Power Systems and Special Machines. Presently he is Associate Professor and Head in Electrical and Electronics Engineering Department , Nimra College of Engineering and Technology ,Vijayawada-A.P

Contact Address:
Abdul Ahad Shaik, Associate Professor and Head
Department of Electrical and Electronics Engineering
Nimra College of Engineering and Technology, Jupudi, Ibrahimpatnam, VIJAYAWADA-521456
Email: abuahad@rediffmail.com , abuahad786@yahoo.com
Phone: 0866-2882910 (207) or 0866-2882010

Appendix B

Refereed Journals

1. Dr. Uday Kumar R.Y, Abdul Ahad Shaik, Shaik Nisar Ahmed K.S.R Deepika," Analysis Design and Performance Characteristics of Switched Reluctance Motor", International journal of Multidisciplinary research and advances in engineering(IJMRAE), Vol.3, No. II, April 2011.

Conference Proceedings

1. Dr. Uday Kumar R.Y, Abdul Ahad Shaik, K.S.R Deepika, "Rotor position estimation and design of low cost controller circuit for switched reluctance motor based on machine design parameter" fifth international conference on industrial and information systems (ICIIS2010) p. 568-573

2. Dr. Uday Kumar R.Y, Abdul Ahad Shaik, K.S.R Deepika, "Design analysis and performance characteristics of switched reluctance motor" fifth international conference on industrial and information systems (ICIIS2010) p. 574-579